University of Warsaw
Faculty of Mathematics, Informatics and Mechanics

Magdalena U. Bogdańska

Mathematical models for the dynamics of low-grade gliomas and their response to therapies

PhD dissertation

Supervisor:
dr hab. Marek Bodnar
Institute of Applied Mathematics and Mechanics
Faculty of Mathematics, Informatics, and Mechanics
University of Warsaw

Co-supervisor:
Dr D. Víctor M. Pérez-García
Institute of Applied Mathematics in Science and Engineering
University of Castilla-La Mancha

Auxiliary supervisor:
dr hab. Monika J. Piotrowska
Institute of Applied Mathematics and Mechanics
Faculty of Mathematics, Informatics, and Mechanics
University of Warsaw

November 2018

Author's declaration:
I hereby declare that this dissertation is my own work.

November 28, 2018 .....
date *Magdalena Bogdańska*

Supervisor's declaration:
The dissertation is ready to be reviewed.

November 28, 2018 .....
date *dr hab. Marek Bodnar*

Co-supervisor's declaration:
The dissertation is ready to be reviewed.

November 28, 2018 .....
date *Dr D. Víctor M. Pérez-García*

Auxiliary supervisor's declaration:
The dissertation is ready to be reviewed.

November 28, 2018 .....
date *dr hab. Monika J. Piotrowska*

Abstract

In this dissertation, mathematical models and methods were used to study the evolution and the response to treatments of low-grade gliomas. Low-grade gliomas are brain tumours usually growing slowly but causing death due to their progression to more malignant counterparts.

We constructed macroscopic models of low-grade gliomas' growth in such a way that they were accurate enough to reflect available clinical observations and simple enough so that they could be analysed analytically. The models presented in this thesis were designed in the form of systems of either ordinary differential equations or reaction-diffusion equations complemented with expressions accounting for the response to treatments.

We studied the proposed models both analytically and numerically. We also showed that the solutions of the developed mathematical models fit well to the dynamics of low-grade gliomas of individual patients. On the basis of our validated models, we addressed some problems of clinical practice. Finally, we derived analytical estimates which could be potentially useful in assessing tumours aggressiveness and selecting the best therapies.

Streszczenie

W tej rozprawie modele i metody matematyczne zostały wykorzystane do badania wzrostu i odpowiedzi na leczenie glejaków niskiego stopnia. Glejaki niskiego stopnia są to guzy mózgu, które zazwyczaj rosną powoli, ale są nieuleczalne. Śmierć następuje zwykle w konsekwencji przekształcenia się tych nowotworów w bardziej złośliwe formy.

Skonstruowaliśmy makroskopowe modele wzrostu glejaków niskiego stopnia, które wystarczająco dokładnie odzwierciedlają dostępne obserwacje kliniczne i jednocześnie są na tyle proste, że mogły być analizowane analitycznie. Modele przedstawione w tej pracy zostały sformułowane w postaci układów równań różniczkowych zwyczajnych lub równań reakcji-dyfuzji uzupełnionych wyrażeniami opisującymi wpływ leczenia.

Zbadaliśmy proponowane modele zarówno analitycznie, jak i numerycznie. Pokazaliśmy również, że ich rozwiązania dobrze dopasowują się do dynamiki glejaków niskiego stopnia poszczególnych pacjentów. Na podstawie naszych zwalidowanych modeli zajęliśmy się pewnymi problemami praktyki klinicznej. Uzyskaliśmy analityczne oszacowania, które mogą być potencjalnie wykorzystane w ocenie agresywności nowotworów i wyborze najlepszych terapii.

Resumen

En esta tesis se han desarrollado modelos y utilizado metodología matemática para estudiar la evolución de gliomas de bajo grado y su respuesta a los tratamientos. Este tipo de cáncer crece lentamente pero causa la muerte debido a su transformación en formas más agresivas del tumor.

Se han construido modelos macroscópicos de crecimiento de estos tumores lo suficientemente precisos como para reflejar las observaciones clínicas disponibles y al mismo tiempo sencillos para que su estudio analítico fuera viable. Los modelos presentados en esta tesis son bien sistemas de ecuaciones diferenciales ordinarias o bien ecuaciones de reacción-difusión complementadas con expresiones que representan la respuesta a los tratamientos.

Los modelos propuestos se han estudiado tanto analíticamente como numéricamente en esta tesis. También se ha demostrado que las soluciones de estos modelos describe correctamente la dinámica de gliomas de bajo grado de pacientes reales. Sobre la base de nuestros modelos validados, he discutido algunos problemas relacionados con la práctica clínica. Por último, se han encontrado estimaciones analíticas potencialmente útiles para evaluar la agresividad de los tumores y elegir las mejores terapias.

Contents

Chapter 1

Introduction

1.1 Motivation

The idea for this dissertation arose thanks to a collaboration with Prof. Víctor M. Pérez-García, the Head of the Mathematical Oncology Laboratory (University of Castilla-La Mancha, Spain) that began during an Erasmus internship of the author of this thesis. That internship resulted in the publication of a research article, which focused on mathematical modelling of the growth of low-grade gliomas and their response to radiotherapy [1]. Low-grade gliomas (LGGs) are slowly growing brain tumours that mostly affect young patients and usually become fatal, mostly due to their infiltration and transformation into more malignant types, known as high-grade gliomas (HGGs), for detailed information see Section 1.5. Each year around six out of 100 000 citizens suffer from gliomas worldwide [6]. However, the social impact of these tumours is highly disproportional to their incidence. Median untreated survival time for HGGs patients' ranges from 6 months to 1 year and the average years of life lost* for each patient with HGG is high (20.1 years). Thus, HGG was ranked as the most malignant tumour out of 17 types of cancer [7]. Even low-grade gliomas, frequently mistagged as benign tumours due to their very slow proliferation indexes [8, 9], have very poor prognosis† as they can rarely be cured. The median survival of treated LGG patients is between five and ten years [10], compared with one to two years for treated HGG patients [11]. LGGs have a tremendous impact on the society also because of the fact that they usually occur in young patients [12], therefore being the object of strong clinical interest.

In Section 1.5 we explain some of the challenges in making treatment decisions for LGGs. Unfortunately, it is extremely difficult to verify an arbitrary number of possible therapy schemes *in vivo* as, apart from ethical reasons, it is very time-consuming. Due to the long time of disease evolution in some of LGGs patients, clinical trials on LGGs require many years to test a single hypothesis. To give an example, a European clinical trial designed to test the efficacy of early versus delayed radiotherapy for LGGs started in 1986 and long-term results were presented in 2005 [13]. Moreover, as Byrne [14] suggested, hypotheses on physical processes sometimes are even impossible to verify in the biological experiments with the use of existing technology. All biomedical research is based on the use of experimental models. Unfortunately, so far, no one has been able to establish cell line which reproduces in mice or rats the behaviour of human

*The average years of life lost is a sum of the differences between the actual age at death and the expected age at death for each person who died of cancer divided by the actual number of deaths for a cancer type studied.

†Patient prognosis refers in general to the likely outcome or course of a disease, the chance of recovery or recurrence.

LGGs. These are some of the reasons why research on this type of tumours has been very slow during decades.

In fact, the potential of mathematical models to help in managing medical problems was the first motivation behind the research presented here. Mathematical models may be used to simulate the tumour growth, drug kinetics, effects of different therapies *etc*. for cohorts of hypothetical patients, which helps in saving money and time in comparison to "blind" biological experiments. Obviously, mathematical models alone cannot replace biomedical models (*i.e.* cell lines, research animals or clinical trials), but they allow for extrapolation beyond the situations that were studied originally. It gives a broader picture which might aid in finding answers for some cancer-related open questions. Using the mathematical models allows basic researchers to make an inference of possible mechanisms, falsification of underlying biological processes and quantitative description of relationships between different components of a system, see *e.g.* [14, 15, 16] for a review. Clearly, mathematical models are simplified descriptions of reality, which allow reproducing the behaviour of the original system, but can also provide ways to raise new hypotheses. To give an example, in [17] the authors exploited a mathematical model to predict that brain tumours could be labelled as either nodular or infiltrative due to the size of tumour bulk and the extent of infiltrative part (estimated from patients imaging data obtained with the use of two different imaging modalities). Interestingly, their mathematical model led to a prediction which group of a tumour (the nodular ones) would benefit more from radical surgery.

If the effect of therapy is included in a mathematical model, it can give qualitative and sometimes even quantitative predictions of tumours' response to therapies and patients' survival. The results can help in making individual patients' treatment decisions, finding appropriate therapeutical timings and/or fractionations or even the development of new therapies [18]. Properly constructed mathematical models could assist in personalising medicine, which represents another hallmark of contemporary medicine. This kind of approach has been already proven to be successful in few cases, *e.g.* in predicting and monitoring chemotherapy-induced myelosuppresion [19], and is an emergent field of applied mathematics that is expected to develop further in the future.

Basic researchers working in the area of mathematical oncology (or mathematical biology in general) usually have one of the following approaches: either they use biological and medical knowledge only as a source of mathematical problems and do not look for any applications, or they search for issues of major biomedical importance and open-minded physicians in order to ensure that theoretical results obtained might be exploited for practical, therapeutic purposes [15]. We are in favour of the second approach, agreeing completely that collaboration between mathematicians and biologists or medical doctors can enhance both areas of science. As Cohen said "Mathematics is biology's next microscope, only better. Biology is mathematics' next physics, only better" [20]. These are interdisciplinary collaborations that enable performing mathematical studies which could be beneficial in solving cancer-related problems. Sadly, they are difficult to establish and maintain because of several obstacles. An obvious reason for difficulties faced during interdisciplinary work in mathematical biology, in particular in the so-called "mathematical oncology" [16], is the completely different type of knowledge in mathematics in comparison to biology or medicine. Even when both basic and clinical scientists are willing to translational research, they do not necessarily speak the same language due to different training and experience. Furthermore, the role of mathematics in generating mechanistic insight into biomedical problems is, in general, less well known than *e.g.* in physics and engineering. Mathematical models might seem as esoteric, mysterious

scientific instruments to most biologists and physicians [21]. They have been unintelligible to most biomedical researchers, therefore it is usually a mathematician who has to acquire an understanding of main biological processes. Another difficulty is related to different scientific goals. Most biologists and physicians do not consider mathematicians as possible contributors as, instead of theorems, they look forward to studies designed for therapeutic improvements [21]. Moreover, in the case of low-grade gliomas, to be analysed here, one has to face the limitation of data available and the general lack of large cohorts of patients treated in the same way, see Section 1.5.

Mathematical modelling of LGG growth started roughly 10 years ago and has received strong attention in the last few years, see *e.g.* [22, 23, 24, 25, 1, 26, 27]. Unfortunately, from the clinical point of view, up to now there were very few applicable results derived from mathematical models of these tumours. Thus, many questions coming from medicine which could be potentially addressed using mathematical frameworks, still remain without answers. For instance, timing and dosing of chemotherapy to LGG patients requires a careful planning that may benefit from — now absent — rational design based on mathematical modelling.

Furthermore, many mathematical models presented so far to describe gliomas evolution includes tens or even hundreds of unknown parameters, see *e.g.* the reviews [15, 18, 16] and the references therein. Thus, a problem of overfitting appears as excessively complicated models may fit whatever kind of behaviour is observed. Interestingly, up to now, it has been possible to extract conclusions useful for clinicians only from simple models , as in *e.g.* [28, 29], see also Section 1.6. Still, there is a need for models accounting for the fundamental features of low-grade gliomas' dynamics and their response to therapies without involving excessive details on the often unknown specific processes but enabling the qualitative understanding of the phenomena involved.

In this thesis, mathematical models and methods are used to provide insight into low-grade gliomas and their response to therapies. We construct models that are accurate enough to reflect available clinical observations and simple enough so that they can be analysed mathematically. We build the models from the bottom up, adding new components only as they become necessary, starting with the definition of a glioma as a mass proliferating without control, invading locally. Such models of growth are complemented with expressions accounting for the response of tumours to therapies used nowadays. We formulate macroscopic models as such models describe the local tumour cell densities or tumour size and may be more easily adapted to specific patient data from our collaborators. We investigate mathematical properties of the models and derive clinically-relevant suggestions, that can be later tested by clinicians and/or biologists.

1.2 Structure of the dissertation

The outline of this dissertation is the following. In this chapter we first list papers in which the majority of the results of this thesis were published. Next, we present some introductory information about characteristics and diagnosis of cancer, focusing on brain tumours. We describe low-grade gliomas and their typical treatments. We use this information to design our mathematical models. We also discuss in this chapter the most relevant mathematical models that have been developed to describe gliomas growth. Finally, we outline the methodology used in the presented research and describe medical data used to validate our mathematical models and hypotheses. As an addendum to this introductory chapter we present the mathematical

notation and acronyms used throughout this thesis. The broader meaning of each abbreviated term is given at its first occurrence within the text.

In the dissertation, we present three different mathematical models. First, in **Chapter 2** a macroscopic model of LGG growth and response to chemotherapy is developed. In **Chapter 3** we derive in detail a model to analyse the process of malignant transformation. Both Chapters 2 and 3 include mathematical analysis of the proposed models. These chapters explore a wide range of patient-specific parameters and they also study their role. We also fit the models to patients data and estimate values of practical interest. We discuss potential therapeutical implications from the formulated models and obtained estimates. In **Chapter 4** we develop and analyse a model of LGG growth including a spatial component and response to chemotherapy. Later on, we proceed to estimate the time when malignant transformation begins for tumours treated with chemotherapy and consider some novel chemotherapy fractionations. **Chapter 5** includes a brief summary of the results obtained.

In **Appendix A** we add an article describing a model of LGG growth and response to radiotherapy. Finally, we complement dissertation with **Appendix B** which includes the most relevant numerical procedures used to perform numerical simulations of presented mathematical models and to fit them to patients data.

1.3 List of publications derived from this thesis

The results presented in this dissertation gave rise to the following publications in international peer-reviewed journals:

[1] V. Pérez-García, M. Bogdańska, A. Martínez-González, J. Belmonte-Beitia, P. Schucht, L. Pérez-Romasanta. Delay effects in the response of low-grade gliomas to radiotherapy: a mathematical model and its therapeutical implications. *Mathematical Medicine and Biology.* 2015; 32:307–29.

[2] M. U. Bogdańska, M. Bodnar, J. Belmonte-Beitia, M. Murek, P. Schucht, J. Beck, V. M. Pérez-García. A mathematical model of low grade gliomas treated with temozolomide and its therapeutical implications. *Mathematical Biosciences.* 2017; 288:1–13.

[3] M. U. Bogdańska, M. Bodnar, M. J. Piotrowska, M. Murek, P. Schucht, J. Beck, A. Martínez-González, V. M. Pérez-García. A mathematical model describes the malignant transformation of low grade gliomas: Prognostic implications. *PLoS One.* 2017; 12(8):e0179999.

[4] M. Bodnar, M. J. Piotrowska, M. U. Bogdańska. Mathematical analysis of generalised model of chemotherapy for low grade gliomas. *Discrete & Continuous Dynamical Systems - B.* 2018 (accepted).

Results presented in [2, 3] are fully included in Chapters 2-3. Publication [1] is included as Appendix A since it contains the results obtained before the beginning of doctoral studies of the dissertation author. However, the mathematical modelling approach, together with numerical methods used in this publication, are similar to those presented in Chapters 2 and 3.

Thus, the techniques used in [1] were explained in more detail in the context of other models described here.

1.4 Cancer - a brief characterisation

Cancer is a general term describing a very heterogeneous group of diseases. Each cancer is formed by anomalous cells that impair tissue homeostasis, affecting the proper functioning of the human body. It can originate almost anywhere in the body. Thus, there are more than 100 cancer types, usually named after the organs or tissues where they form or by the type of cells that formed them.

There are several key processes occurring in most cancer types, see Figure 1.1. All cancers are characterised by unchecked growth that progresses toward limitless expansion. Normally, the rates of new cell growth and old cell death are kept in balance. Old, unneeded and damaged cells are removed from the human body through a process known as programmed cell death or **apoptosis**. In cancer, however, this balance is disrupted as a result of uncontrolled cell growth or loss of cell's ability to undergo cell suicide. Cancer cells are able to ignore signals that tell cells to stop dividing or to begin apoptosis.

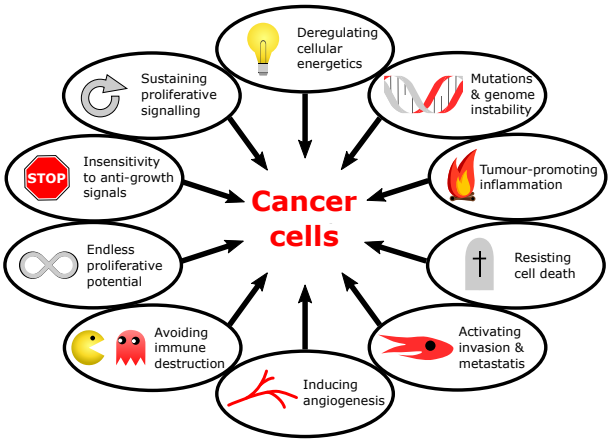

Figure 1.1: Hallmarks of cancer. Figure adapted from Hanahan and Weinberg [30].

Cancer cells are capable of spreading by two mechanisms: **invasion** and **metastasis**. The first term refers to the direct migration and penetration of cancer cells into neighbouring tissues. The term "metastasis" describes the ability of cancer cells to penetrate into lymphatic and/or blood vessels, circulate through them, and then invade other tissues elsewhere in the body. Gliomas are likely to invade the nearby healthy brain tissue and spread to other parts of the brain or to the spinal cord, however, they rarely spread to other parts of the body.

Cancer cells might also evade the immune system. Though the immune system normally removes damaged or abnormal cells, some cancer cells are able to "hide" from it.

Another characteristic of cancer cells is that they may influence the normal cells, molecules, and blood vessels that surround and feed a tumour – an area known as the microenvironment. For instance, they can induce nearby normal cells to form blood vessels that supply a tumour with oxygen and nutrients, allowing for tumour expansion. Such a process through which new blood vessels are formed from pre-existing vessels is called **angiogenesis**. It occurs in grade III and IV gliomas and is associated with poor prognosis.

1.5 Gliomas - an overview with focus on low-grade gliomas

In this dissertation we focus on modelling the growth of gliomas, which are the most frequent brain tumours. They represent approximately 30% of all central nervous system tumours and about 80% of all malignant brain tumours [31]. The term "**gliomas**" refers to astrocytomas and oligodendrogliomas, which are tumours originating from precursors of supporting glial cells in the brain (mainly from astrocytes and oligodendrocytes*). These tumours usually arise in the cerebrum.

In this dissertation, we use gliomas patients' data, described precisely in Section 1.7. We use mainly two kinds of information concerning individual patients: tumour size measured from imaging scans and the microscopic results confirming both the initial diagnosis and later the transformation into a more malignant tumour. Thus, we introduce here main facts considering the whole process of diagnosis for brain tumours. Subsequently, we describe LGGs in detail. We present some of the most important findings concerning their response to chemotherapy and malignant transformation, which are modelled in the dissertation.

Brain tumours imaging. Microscopic examination. Classification

Gliomas are usually diagnosed with the use of imaging techniques coupled with the analysis of lesion samples extracted from a biopsy. Currently, the main radiological technique used for brain imaging is **magnetic resonance imaging (MRI)**, which can produce three-dimensional images of sections of the body. There are many different types of MRI, see *e.g.* [32] for review. T1-weighted MRI (T1), T2-weighted MRI (T2) and Fluid Attenuation Inversion Recovery (FLAIR) are most common for the purpose of detecting and diagnosing brain tumours. On T2 and FLAIR scans one can observe peritumoral oedema†, if present, while T1 shows also regions of necrosis‡. T1 is sometimes used with intravenous contrast gadolinium (T1+Gd), which can show the region of unstable vasculature or hypoxia in white/light grey ("**contrast enhancement**"). We show examples of T1 and T2 MRI scans of LGG in Figure 1.2. Later on, in Figure 1.5 we also present the results of FLAIR and T1+Gd scans made for glioma before and after its malignant transformation, see detailed description in Section 1.5.

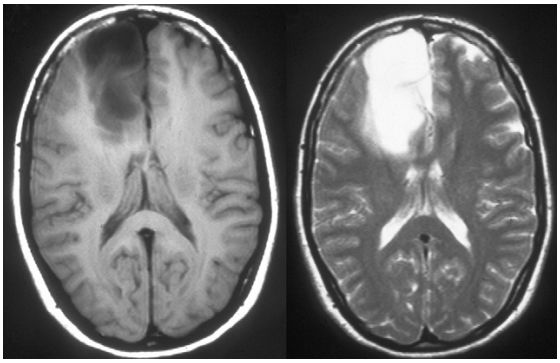

Figure 1.2: T1 (left) and T2 (right) MRI scan of LGG in the frontal lobe. Figure reprinted from [33].§

*Oligodendocytes are responsible mainly for providing a support and insulation to axons, while astrocytes are providing support to cells forming the blood–brain barrier and providing nutrients to the nervous tissue, among others.

†Oedema (am. edema) is an abnormal accumulation of fluid causing the affected tissue to become swollen.

‡Necrosis is a type of cell death induced by pathological factors external to the cell or tissue. Regions of necrotic tissue, indicating a poor prognosis, are present in many aggressive cancers (such as grade IV glioma).

§Reprinted from The Lancet Neurology, 2(7), P. H. Wessels *et al.*, Supratentorial grade II astrocytoma: biological features and clinical course, 395–403, Copyright (2003), with permission from Elsevier.

In clinical routine, a sequential follow-up of the tumour evolution and response to therapies is performed. By comparing imaging scans done over time, medical doctors can observe a tumour response to a given treatment or find out if cancer has relapsed after treatment. In LGGs database used in this dissertation, two imaging techniques were used to follow LGGs development: T2 and FLAIR.

If a brain scan suggests the presence of a tumour, a biopsy shall be performed for a proper diagnosis. It may be done as a separate procedure or at the time the tumour is removed if surgery is a treatment option. Then, **histopathology**, *i.e.* a microscopic examination of a biopsy or surgical specimen, is carried out. Figure 1.3 presents a histopathological section of LGG tissue. Under the microscope, cancer tissues have a distinctive appearance (*e.g.* there is a large number of irregularly shaped dividing cells). Based on such characteristic traits, a pathologist determines whether a tumour is benign or malignant and assigns the tumour's grade. To put it simply, **tumour grade** tells how abnormal the tumour cells are when compared to normal, healthy cells. Generally, a low number grade (grade I or II) refers to cancers with fewer cell abnormalities than those with higher numbers (grade III or IV) and indicates a better prognosis. Higher-grade cancer may grow and spread more quickly and may require immediate or more aggressive treatment.

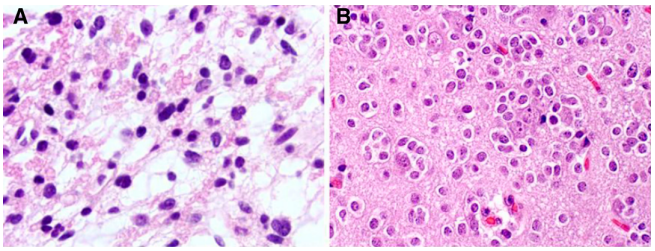

Figure 1.3: Histopathology images of LGGs: astrocytoma (A) and oligodendroglioma (B). Figure reprinted from [34].*

The most widely accepted system for classifying central nervous system tumours is the World Health Organisation (WHO) classification [35]. According to the 2007 WHO classification, valid at the beginning of PhD studies of the author, grade I gliomas (pilocytic astrocytomas) are very rare, non-infiltrating and curable. They will not be addressed here. WHO grade II gliomas (oligodendroglioma, astrocytoma) are usually referred to as **low-grade gliomas (LGGs)**, while WHO grade III gliomas (anaplastic astrocytoma, anaplastic oligodendroglioma, anaplastic oligoastrocytoma) and IV (glioblastoma)– as **high-grade gliomas (HGGs)**, see [12] for the detailed classification.

After identifying the tissue as cancerous, the pathologist may perform additional tests to get more information about a tumour. To give an example, an antigen Ki-67 is a marker used to determine the growth fraction of a given cell population. The fraction of Ki-67-positive tumour cells (the Ki-67 labelling index, Ki-67 LI) is often correlated with the clinical course of cancer. In the case of brain tumours, the prognostic value of Ki-67 LI for survival and tumour recurrence have been proven in uni- and multivariate analysis [36, 37]. In the dataset of our collaborators, values of Ki-67 LI has been measured for some patients. We compare values of Ki-67 LI obtained for LGGs patients before and after malignant transformation in Table 3.3 in Section 3.3.2.

*Reprinted with permission. © (2016) American Society of Clinical Oncology. All rights reserved.

Finally, a pathologist may examine molecules within organs, tissues or body fluids. Such examination is called **molecular pathology**. Its use for cancer patients aids in more accurate diagnosis, selection of specific treatments that are most likely to be effective for them and determining biomarkers with a prognostic value. In the case of brain tumours, status of IDH 1/2 mutations, TP53 mutations, 1p/19q loss and MGMT promoter methylation have been found to have prognostic value, *cf.* [38, 39, 40]. It should be noted that from 2016, increased importance has been given to molecular markers for gliomas, both in terms of determining a detailed diagnosis and in prognosis [35, 6, 34]. To be specific, the status of IDH and 1p/19q have been included in a new WHO classification of low-grade gliomas. IDH wildtype tumours (*i.e.* without IDH 1 or 2 mutations) are known to have a poorer prognosis compared to IDH mutated tumours. Gliomas with 1p and 19q loss generally have a better prognosis, related to therapy [41] or not [42]. At the beginning of the presented research, it was not a gold standard to verify those characteristics, thus, we did not analyse them.

Low-grade gliomas and their treatment

LGGs are rare primary tumours*, usually occurring in frontal and temporal lobes. They usually grow very slowly, see Figure 1.4 showing proliferating cells in a LGG sample. Nevertheless, they are almost invariably incurable due to their diffusive infiltrative nature and often lead to patient death due to a transformation of a tumour into more aggressive anaplastic form, for details see Section 1.5.

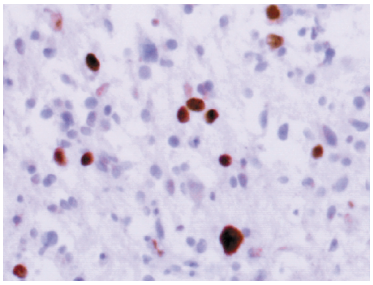

Figure 1.4: Ki-67 immunostaining in a LGG of a 26-year-old patient. Taking into account that normal brain cells do not proliferate, those cells that are marked in red are probably the tumour cells. A labelling index of 4.4% was associated with a survival of 35 months. Figure reprinted from [33].†

Treatment of patients with LGGs brings many controversies to clinicians due to the fact that these tumours usually affect patients between 30 and 45 years old, who, besides seizures, appear neurologically asymptomatic. Other symptoms (headaches, lethargy, mental changes) are less common. Thus, the treatment goal is not only to prolong the time of survival, but also to minimise the side effects of aggressive therapies in such a way that these otherwise healthy and mostly young patients maintain a good quality of life for the longest possible time. Treatment planning for individual LGG patients is troublesome also because of the diverse prognoses for patients facing this disease. Some LGGs grow very slowly for years causing easily-controlled seizures, while others progress rapidly causing major neurological deficits and subsequent death. Because of the unpredictable clinical course, there are various treatment strategies for LGG. On one hand, for some patients a "wait and see" approach is preferred, *i.e.* a patient is regularly monitored with imaging MRI while other treatment options are applied

*Primary tumour is a tumour located at the site of origin.

†Reprinted from The Lancet Neurology, 2(7), P. H. Wessels *et al.*, Supratentorial grade II astrocytoma: biological features and clinical course, 395–403, Copyright (2003), with permission from Elsevier.

when there occur some changes suggesting tumour progression. On the other hand, some patients undergo gross total resection* followed by immediate radiotherapy or chemotherapy. Such management decisions for those tumours (whether and when a patient should receive resection, radiation therapy or chemotherapy) are usually based on many factors including age, performance status, the location of a tumour and patient preference [9].

The current standard of care is first to perform a maximal resection as it was demonstrated that the extent of resection is a prognostic factor for LGG patients, see *e.g.* [10, 43, 44, 39, 45]. At the same time quality of life following surgery has to be taken into account. Thus, the European Federation of Neurological Societies and European Association for Neuro-oncology recommended that "surgical resection is the first treatment option, with the goal to maximally resect the tumour mass whenever possible, whilst minimizing post-operative morbidity" [46].

Sadly, due to the infiltrative nature of gliomas, surgery alone is able to eradicate only the tumour bulk and consequently, other therapeutic treatments are necessary to control the disease. There is a trend to use more active treatments and various alternative approaches have been considered. Post-operative radiotherapy could be a therapeutic option for LGGs, but it causes long-term neurocognitive toxicity and shows only a moderate impact on patients overall survival [47, 48, 49]. In this context, there is an increasing interest in the use of chemotherapeutic agents which could influence tumour evolution and at the same time allow the delay of more aggressive treatments. Chemotherapy tends to be performed early, especially in the case of clinical and/or radiological progression. Radiation therapy is usually deferred in LGG patients and proposed usually only for inoperable tumours progressing after chemotherapy and/or with significant enhancement on post-contrast T1 MRI scans, see for instance [9].

Chemotherapy for LGGs

We now focus on only one type of treatment considered for LGGs – chemotherapy, as we directly model its therapeutic effect in Chapters 2 and 4. Currently, there are two chemotherapeutic drugs effective for the treatment of LGG patients: temozolomide (TMZ) and a combination of procarbazine, lomustine and vincristine (PCV). About 25-50% of LGGs show chemotherapeutic responses to treatment with either TMZ or PCV. PCV has been used from the 1970's and has been suggested as a clinically relevant option especially for some subtypes of anaplastic gliomas with the 1p/19q codeletion [50, 51]. Unfortunately, it causes significant side effects [52, 53]. On the other hand, temozolomide has a better toxicity profile than PCV, being well tolerated by most patients [54, 55, 56], see *e.g.* [2] for a detailed description. Moreover, in contrast to PCV, TMZ is administered orally, which is another reason why this drug is a drug of choice for most LGG patients.

TMZ is a cell-cycle non-specific prodrug†, absorbed with almost 100% bioavailability [57]. Details of the mechanism of TMZ action can be found in [58, 59]. A clinical trial by Stupp *et al.* showed the efficacy of TMZ for high-grade gliomas [60]. Other clinical studies have demonstrated its effectivity against both previously irradiated and unirradiated LGGs [61, 62, 56]. In addition, there are reports of cases where neoadjuvant chemotherapy‡ given to surgically unresectable tumours has allowed subsequent gross total resection [63, 64], which is of great importance especially when a tumour is highly infiltrative or located in eloquent areas. It

*A brain tumour resection is called a "gross total resection" when there is no obvious tumour tissue visible on a brain scan performed soon after surgery.

†Prodrug – a medication or compound that, after administration, undergoes chemical conversion by metabolic processes before becoming an active pharmacological agent.

‡Neoadjuvant therapy is the administration of therapeutic agents before a main radical treatment intervention.

has also been reported that TMZ treatment may lead to an important reduction in seizure frequency in LGG patients [65]. Thus, a prolonged TMZ treatment until evidence of resistance is a clinically interesting option for selected patients as an up-front or adjuvant treatment. Clinical trials are on the way to study the effect of this treatment on overall survival.

The response of LGGs to chemotherapy has been the subject of many clinical and biological studies. In some LGG patients, a response to TMZ therapy is observed three months after the end of the treatment [66, 67]. Moreover, dynamic volumetric studies have shown that a treatment-related volume decrease can be observed for many months after the chemotherapy is discontinued [68, 69]. The time to maximum tumour response was reported to be larger than two years in some cases [70]. Other researchers investigated relations between some molecular characteristics of LGGs and response to TMZ [71, 62, 69, 72]. However, the crucial question of the correct timing of chemotherapy remains unanswered, namely whether it should be given as a first-line therapy or when progression has been observed. Another issue to be addressed is the optimal fractionation of TMZ.

Chemotherapy schedulings. Chemotherapeutic drugs are usually given in sequences called "cycles" in the oncological terminology [73]. Such a sequence consists of a treatment-period followed by a rest period. The typical plan of TMZ treatment is to give doses of 150–200 mg per m^2 of patient body surface once per day for 5 days every 28 consecutive days, *i.e.* five days of doses administration are followed by 23 days of break before the next cycle. The number of such cycles in clinical practice is usually between 12 and 30 [69, 22, 70], however, it depends on patient-related characteristics and sometimes the treatment can be stopped earlier due to the haematological toxicity observed. Such a fractionation scheme was proven to be effective in HGGs and has been subsequently transferred to the management of LGGs [60]. There have been a few clinical studies on alternative treatment regimens for LGGs. Among others, in [61] patients were treated in cycles with doses of 75 mg/m^2 given daily for 7 weeks followed by four-week breaks. Some trials on dose escalation [74, 75, 76] intended to overcome the DNA-repair activity [38, 77]. However, these TMZ regimes were either not effective or had to be rejected because of a high toxicity [78]. Many clinicians conclude that the chemotherapy fractionation scheme providing the best tumour response and acceptable haematologic toxicity is still to be determined.

Malignant transformation

The process known as malignant transformation, anaplastic transformation or malignant progression of LGGs is a transformation of a grade II tumour into a grade III or IV tumour. As a consequence, it is the main process leading to LGG patients death.

The time of occurrence of malignant transformation differs among patients. The results vary among clinical studies with a 5-year malignancy-free survival rate (that is the period of time when malignant transformation does not occur) ranging from 30 to 70% [79, 80, 81, 82, 83]. There are reports claiming that all LGGs undergo malignant transformation during their clinical course, *e.g.* [33, 84].

In order to confirm malignant transformation, both data from imaging and pathology report are usually required, *cf.* Section 1.5. Radiologically, malignant transformation is usually defined based on the appearance of contrast enhancement on MRI scans and/or a histopathologically proven malignant degeneration in tissue acquired during biopsy or resection [82]. It was reported that LGGs displaying preoperative contrast enhancement had a significant in-

creased risk of recurrence [82], thus the complete resection of contrast enhancement areas of a tumour significantly increases the time to phenotypic change [85]. Medical doctors believe that early detection of malignant transformation could improve the prognosis. Some indicators of malignant transformation have been suggested, *cf.* [85, 86, 87, 88], nonetheless, their significance is still under study. In Figure 1.5 we show the representative slices of MRI scans of a glioma before and after its malignant transformation. Upper figures were made for LGG, lower figures – for HGG. In the lower panel with images for HGGs, one can observe a contrast enhancement ring corresponding to part of tumour with increased proliferation and a dark region being necrotic core. These structures are not present in LGGs. In Figure 1.6 we additionally show histopathology imaging of both LGG and HGG together with the simplified illustration of changes leading to malignant transformation.

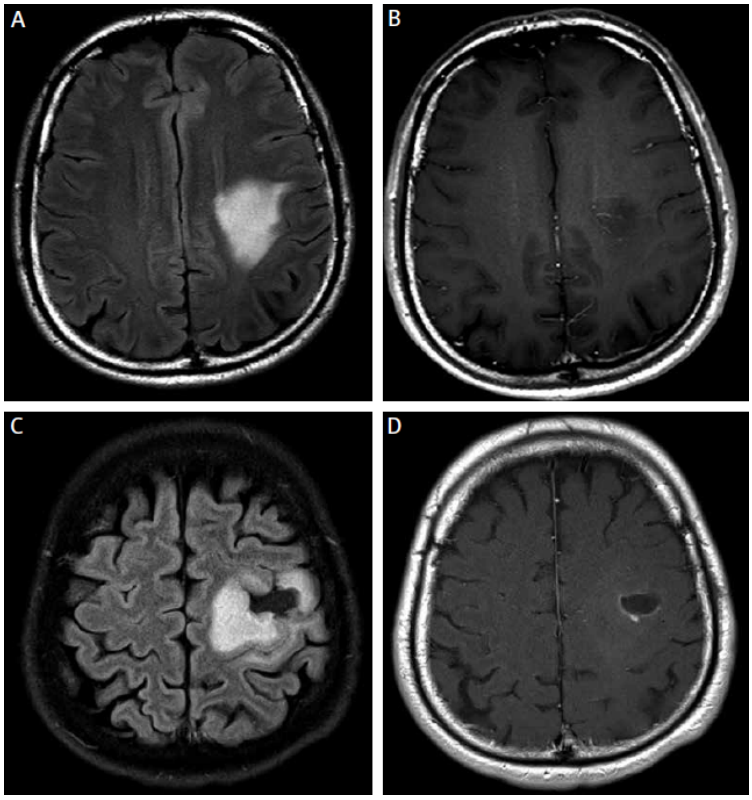

Figure 1.5: MRI scan of glioma. The initial MRI: FLAIR (A) and T1+Gd (B); the final MRI after malignant transformation: FLAIR (C) and T1+Gd (D). Reprinted from [85].*

1.6 Mathematical models of gliomas

Historical overview. First models for HGGs.

Macroscopic mathematical modelling of tumour growth began with the early simple hypothesis that the tumour mass increases by a constant fraction in equal time intervals, see [89] for a review. Such assumption was supported by major experimental and human studies, which indicated that cancer cells divided at rates that, though varying widely among different cancer types, were relatively constant over long periods of time in individual cases, see *e.g.* pioneering

*Reprinted, courtesy of the Mossakowski Medical Research Centre Polish Academy of Sciences and the Polish Association of Neuropathologists under a CC BY-NC-SA 4.0 license (http://creativecommons.org/licenses/by-nc-sa/4.0/).

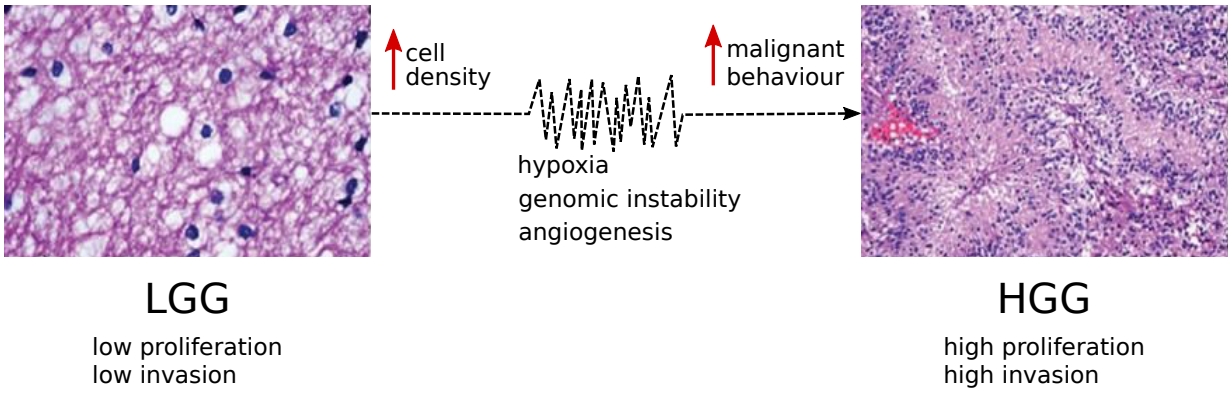

Figure 1.6: Schematic representation of the process of malignant transformation of LGGs. Left and right images are histopathological sections of tumour tissue, see Section 1.5. Adapted from [37].

work by Collins *et al.* in [90] and review in [91]. Those observations led to the assumption of the exponentially growing total number of tumour cells G according to the Malthus model [92]: $\mathrm{d}G/\mathrm{d}t = \rho G$. The parameter ρ governs the effective cell cycle time and its inverse gives an estimate of the typical tumour cells doubling time. Indeed, if all cells were dividing, the cell cycle time would equal $\ln(2)/\rho$ (which is also the volumetric doubling time, that is the time when the tumour double its total volume). However, the Malthusian model usually overestimates the tumour growth in a long-term horizon as it represents a theoretical situation in which there are no intrinsic limitations on the growth of tumour cells.

The introduction of logistic and Gompertzian growth [93, 94] into the cancer development models [95, 96, 97] enabled to model the slower growth in the later stages due to the limitation in nutrient supply in avascular tumours. In such models, the rate of growth slows down as the cell density increases toward the tissue carrying capacity (understood usually as a maximum number of cells that can fit in $1\mathrm{mm}^3$ of tissue). On the other hand, such models describing the evolution of the total number of tumour cells, or equivalently its total size, do not take into account the spatial arrangement of the cells or their infiltration in the surrounding tissue. Thus, especially in modelling more malignant gliomas which do not stay as a compact mass, terms describing their motility became relevant.

Most of the first mathematical models of gliomas accounting for tumour motility were studied for high-grade gliomas due to their remarkably fast invasion. As far as we know, the first general model describing cellular kinetics was formulated by Murray in the early 1990s, see Chapter 11 in [98]. This model is based on a mass-balance law, stating that in any given location, the number of tumour cells increases only by new cells produced by tumour proliferation or new cells which move into the region. Murray and co-workers [98] proposed the reaction-diffusion formalism as:

$$\frac{\partial G(t,x)}{\partial t} = -\mathrm{div}\,(J(t,x)) + S(G(t,x)) - T(G(t,x)),$$

where $G(t,x)$ denotes the glioma cell concentration in position x at time t, $J(t,x)$ is the diffusion flux of the cell that follows Fick's law (that is $J = -D\nabla G$), $S(G)$ denotes the source factor, representing the cancerous cell reproduction and finally $T(G)$ is the treatment factor accounting for the glioma cell loss due to treatment if present. The initial state of the model $G(0,x)$ is defined as the initial distribution of glioma cells.

In 1995 Tracqui *et al.* [99] formulated a reaction-diffusion model based on the understanding of cancer as an uncontrolled proliferation of cells with the capacity to invade and metastasise.

This model was simplified by taking into account that in practice gliomas do not metastasise outside the brain, as already stated in Section 1.4. Tracqui proposed that the cells proliferate at exponential rate, which resulted in the following model:

$$\frac{\partial G}{\partial t} = \nabla (D \nabla G) + \rho G.$$

In many models describing gliomas evolution, a constant rate of diffusion was considered giving rise to the following model referred to as Skellam equation [100]:

$$\frac{\partial G}{\partial t} = D \Delta G + \rho G. \tag{1.1}$$

From the very beginning of diffusive models, finding approximate values of parameters was a crucial task. One of the first estimation of parameters ρ and D from biological data was done by Silbergeld *et al.* in [101], where the glioma diffusion coefficient D was estimated to be between $10^{-3}\text{cm}^2/\text{day}$ and $10^{-2}\text{cm}^2/\text{day}$ and the glioma proliferation rate ρ was estimated to be around 10^{-2} day.

The Murray's group made subsequent improvements in the original model. For instance, in [102] the original model was modified to mimic the effects of resection and the postoperative glioma dynamics. It successfully represents two major clinical observations. First, it shows that gliomas infiltrate so much that it is not possible to cure them by resection alone, independently of its extent. Second, the extent of surgery is positively correlated with the life expectancy, see Section 1.5.

A significant contribution to the development of mathematical models for gliomas was made by Swanson (former PhD student of Murray) and co-workers. Let us comment on some of her main results. In 2000 Swanson *et al.* [103] considered diffusion to be a function of the spatial variable in order to account for brain anatomy and heterogeneity, which was also addressed in [104, 105, 106]. However, to consider specific processes related to migration of cancerous cells in real patients, one would need detailed imaging data, preferably acquired using several different imaging modalities.

In [107] Swanson *et al.* tackled the first time an issue of tumour growth beyond the limits of current medical imaging with mathematical modelling approach. We follow those results in Chapter 3, where we also introduce an analogue of detection threshold in our model of LGG growth and transformation based on reaction-diffusion equations.

All those models of gliomas developed before 2008 were based on the assumption that glioma cells can reproduce in an exponential manner. In our models for LGGs, we take into account that LGGs may evolve slowly for many years (see Section 1.5) and thus, we describe tumour proliferation using logistic law. However, we use exponential growth to derive analytical approximations for short time-horizons. In Section 3.4 we use a modification of model (1.1) to determine analytical estimate of tumour growth before malignant transformation, while in Sections 2.4.3 and 2.4.6 we use an ODE with exponential growth term to estimate time of response to chemotherapy and change in tumour volume caused by chemotherapy.

Fisher-Kolmogorov equation

In 2008 Swanson and colleagues [28, 108] took into account the limits on the tumour growth in the longer time-frame. It was assumed that tumour cell concentration changes over time due to net proliferation and net diffusion of cancer cells. The net proliferation rate ρ is the difference between proliferation and apoptosis of tumour cells. Cell migration was assumed

to be a random walk, corresponding to Fickian diffusion characterised by a constant diffusion coefficient D, what leads to the so-called Fisher-Kolmogorov equation (FKE):

$$\frac{\partial G}{\partial t} = D\Delta G + \rho G(1 - G). \tag{1.2}$$

In Eq. (1.2) $G(t, x)$ describes the tumour cell density as a function of time t and the spatial position x. It is measured in units of the maximal cell density allowed in the tissue. The model formulation is completed by zero flux boundary conditions which impose no migration of cells beyond the brain boundary [99] and initial conditions $G(0, x) = G_0(x)$ where $G_0(x)$ is a nonnegative function defining the initial spatial distribution of cancerous cells.

This equation was first derived in 1937 to describe the spread of an advantageous gene in a spatially extended population [109, 110]. This model is already well-described in the literature and has been used in a variety of contexts: to study flame propagation and nuclear reactors, autocatalytic chemical reactions, problems in neurophysiology, ecology, and in general phase transition problems [111]. FKE is a simple example of non-linear reaction-diffusion equation. Owing to its nonlinearity, explicit solutions cannot be found in general. Even for the simplest version of the FKEs only a limited number of solutions are known for specific parameter values [112, 113]. However, the problem of existence, form and stability of travelling waves have been well-studied. Kolmogorov, Petrovsky and Piscounov in [110] considered a one-dimensional case and proved that if the initial function G_0 is monotone and continuous with $G_0(x) = 1$ for $x < a$ and $G_0(x) = 0$ for $x > b$, where $-\infty < a < b < \infty$, then the solution evolves into a travelling wave with minimum speed $c_{min} = 2\sqrt{D\rho}$. The travelling wave solution means that the solution switches from the equilibrium state $G = 0$ to the equilibrium state $G = 1$. In fact, in [110] the authors considered the model after scaling, or, equivalently, the case of $\rho = D = 1$. In general for any $c > 0$, there exists a unique right-going traveling wave with speed c connecting the state $G_0(x) = 1, G_0'(x) = 0$ for $x \to -\infty$ to the state $G_0(x) = 0, G_0'(x) = 0$ for $x \to \infty$. For $c \geqslant 2\sqrt{D\rho}$, the wave is a monotonically decreasing function of x, while for $c < 2\sqrt{D\rho}$ it is oscillatory. McKean [114], using probabilistic methods, showed that under appropriate assumptions these travelling waves are stable with respect to small perturbations. In Chapter 4 we study the existence of travelling wave solutions in a system of two coupled Fisher-Kolmogorov-type equations.

It was verified that the use of FKE for modelling gliomas can have major practical implications. FKE is a very simple model but its usefulness comes from the fact that it enables to obtain quantities of medical interest. As already stated, the typical tumour cells doubling time can be estimated as the inverse of the proliferation rate ρ. Parameters of FKE given by Eq. (1.2) quantify the overall biological aggressiveness of gliomas and are known to be highly correlated to patients' survival and response to therapies, see *e.g.* [115]. Interestingly, in [29] authors measure model-defined parameters based on pretreatment MRIs of 32 HGG patients. The results indicate that dynamic insight from routinely obtained pretreatment imaging may be quantitatively useful in characterizing the survival of individual patients with glioblastoma, the most malignant type of glioma.

Some authors even believe that the values of those kinetic parameters may be correlated with genetic indicators of tumour response to treatments, *cf.* [17] for HGGs. Moreover, the ratio D/ρ has been suggested to have the potential to estimate the mass of glioma undetectable on MRI scans [106]. A very interesting feature of FKE is also the well-known fact that there arise a front propagating at the asymptotic (constant) speed of $v_* = 2\sqrt{D\rho}$. This property of a model' solutions is in a very good agreement with the observed fact that the mean

glioma diameter grows at an approximately constant speed (before the onset of malignant transformation), see [116, 117, 69] and Figure 1.7. The median LGG growth speed was estimated in various studies to be around 4 mm per year, *cf.* [118] and the table in [116].

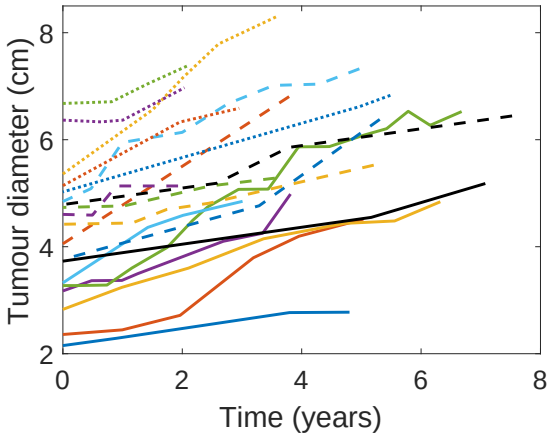

Figure 1.7: Evolution of mean tumour diameter for 19 LGG patients from the diagnostic MRI till the last follow-up MRI (or the last MRI before malignant transformation). Figure adapted from [117].

Fisher–Kolmogorov equation became the classical model for modelling glioma growth. To give an example, in [28] a model based on FKE was used to describe HGGs evolution after surgical resection. In order to validate proposed concept, they used a data from a single pre-treatment MRI scan and overall survival for 70 patients. Note that having data from only one MRI scan, authors were not able to estimate two main parameters (D and ρ). Thus, they verified the outcomes for a large cohort of virtual patients. They concluded that the concordance between survivals for real and virtual patients suggested that the mathematical model was realistic enough to allow for a precise definition of the effectiveness of individualised treatments.

In the last decade, the simple FKE model has been extended to describe many different phenomena, *e.g.* [119, 120, 121]. For instance, in [23] Swanson *et al.* introduce proliferation-invasion-hypoxia-necrosis-angiogenesis model to include the effects of angiogenic factors and lack of oxygen observed in HGGs. In a very recent report [122] authors allow additionally the model parameters to depend on the oxygen concentration. Importantly, the model results can be directly compared to *in vivo* data obtained using anatomic and molecular imaging modalities.

However, most of the mathematical studies of glioma growth apply only to HGGs and some specific processes characteristic for that kind of tumours. Let us recall that LGGs have less phenotypic and genotypic variability than HGGs. They neither display phenomena such as angiogenesis, hypoxia or necrosis, because their low cellular density does not lead to oxygen deficits. Consequently, there is no need to incorporate the evolution of vasculature and concentration of nutrients into their dynamics. Thus, a simple Eq. (1.2) may be expected to successfully describe the growth of this kind of tumours. Indeed, it has been extensively used also to describe LGGs dynamics, see *e.g.* [106, 25, 123, 1, 124]. We describe two of those studies in the following subsection and treat FKE as a base for modelling LGG growth in Chapters 3 and 4.

Models for LGGs

To our knowledge, the first study containing quantitative data of LGGs evolution in time, opening the door to macroscopic mathematical modeling of this kind of tumours was done in 2003 by Mandonnet *et al.* in [117]. The authors performed careful measurements of tumour sizes at subsequent MRI scans made for 27 untreated LGG patients. They investigated the evolution of estimated tumours diameters in time to verify whether there was any pattern in their growth. It turned out that the growth of tumours diameter could be accurately fitted using linear mixed-effects regression*. It was concluded that untreated LGGs often appear to be "stable" on crude visual analysis, however they grow continuously and at a relatively predictable rate, see Figure 1.7. These results were confirmed using the same conditions on a larger group of 143 patients. The analysis of serial MRIs of those patients showed individual velocities of diametric expansion ranging from 1 up to 36 mm/year with an average rate of 4.4 mm/year [115].

Based on the above results, in 2008 the members of the same research group built a model based on Skellam equation (1.1) [106]. Such a simple model shows that the velocity of diametric expansion is constant [125, 102], thus, it allowed characterising LGGs dynamics from serial MRIs. The product of model parameters $D\rho$ is related to tumour kinetics and enables the prediction of tumour growth in its premalignant phase. Mandonnet *et al.* claimed that the ratio D/ρ determined the tumour spatial extent, as discussed also in [126]. Thus, it could be potentially used to determine the non-visible part of the tumour, however a validation of this idea and specific methodology is still missing. Nonetheless, that work was of great significance as it showed that tumour dynamics can be predicted using information derived from non-invasive imaging techniques coupled with mathematical model.

An interesting question that arises is how long LGGs take to reach a clinically detectable size. The answer can be useful to develop screening strategies for early detection.

Interestingly, Gerin *et al.* in [25] used FKE to study the possible time of "tumour birth". They considered the possible time frame between tumour biological onset (time when first tumour cells began to proliferate and migrate) and time of tumour radiological discovery (corresponding to time when the tumour was diagnosed and was visible on imaging scans). Their modelling approach assumed saturated tumour growth described by logistic growth and initial tumour distribution described by Gaussian function. We use similar basic assumptions on LGGs growth in our model presented in Chapter 3.

Gerin *et al.* used analytical solution of Skellam equation (that is neglected saturation term) to provide estimates on the time of tumour genesis from MRI data of patients diagnosed with low-grade gliomas. Based on the patients' age at time of first MRI examination, two types of tumours were identified: very slowly growing tumours that appear during adolescence and slowly growing tumours that appear later, during early adulthood. Further, the model results suggest that low-grade gliomas become visible on MRI without clinical revelation at a mean patient age of 25–30 years. Although this model provided a description of genesis and growth of low-grade gliomas, predictions on the appearance of malignancy that commonly occur in gliomas were not possible. That is the problem we address in Chapter 3.

Another interesting model of LGGs growth was developed by Badoual *et al.* in [123]. That model consists of reaction-diffusion equation describing the tumour growth and an ODE governing the evolution of tumour-associated oedema. In that paper the authors consider also

*A mixed-effects regression model consists of two parts: fixed-effects, that are usually the conventional linear regression part, and the random effects associated with individual experimental units drawn at random from a population. In [117] the random effects were included to account for a different tumour size at the time of diagnosis.

the effect of radiotherapy. They make a simplifying assumption that radiotherapy acts once at a given time point (corresponding to the onset of actual treatment) instead of considering it in the whole time-frame of treatment. With such a mathematical description it turned out to be possible to obtain a satisfactory fit to patients data and explain quantitatively the delay in tumour regrowth after radiotherapy. That model predicts strong correlation between high proliferation indexes and low gain in survival attained with the use of radiotherapy. It is a similar conclusion to our obtained earlier in [1], where we claimed that tumours with lower proliferation indexes have longer time of response to radiotherapy than those with higher proliferation rates.

Models of chemotherapy for LGGs

In general, for solid tumours, mathematical models have considered different chemotherapy-related factors such as drug diffusion, uptake/binding, clearance and their effect on cell cycle progression (see *e.g.* [127, 128, 129, 130]). Many mechanistic mathematical models have been developed to improve the design of chemotherapy regimes (see *e.g.* [131] for a summary). However, only few models have considered chemotherapy of LGGs.

To our knowledge, one of the first models addressing the response of LGGs to chemotherapy was proposed by Ribba *et al.* in [22]. In that model the tumour before the onset of treatment is considered to be a mixture of two types of cells: proliferating cells P (growing in a logistic manner with a constant rate) λ_P, and non-proliferating quiescent cells Q. Ribba *et al.* assume that a chemotherapeutic drug has a homogeneous distribution in brain and that its concentration C decays with a constant rate KDE. The authors assert that chemotherapy treatment directly kills proliferating cells, but only damages quiescent cells which, in a consequence, become damaged quiescent cells Q_P. Those damaged quiescent cells can either repair their damage and become proliferative glioma cells P or die due to irreparable DNA damage. The model in [22] was developed in the form of the following system of four ODEs:

$$\begin{cases} \dfrac{\mathrm{d}C}{\mathrm{d}t} = -\mathrm{KDE} \cdot C, \\ \dfrac{\mathrm{d}P}{\mathrm{d}t} = \lambda_P \cdot P \left(1 - \dfrac{P+Q+Q_P}{K}\right) + k_{Q_P P} \cdot Q_P - k_{PQ} \cdot P - \gamma_P \mathrm{KDE} \cdot CP, \\ \dfrac{\mathrm{d}Q}{\mathrm{d}t} = k_{PQ} \cdot P - k_{PQ} \cdot P - \gamma_Q \mathrm{KDE} \cdot CQ, \\ \dfrac{\mathrm{d}Q_P}{\mathrm{d}t} = \gamma_Q \mathrm{KDE} \cdot CQ - k_{Q_P P} \cdot Q_P - \delta_{QP} \cdot Q_P. \end{cases} \tag{1.3}$$

Parameters γ_P, γ_Q denote rates of DNA damages in proliferative and quiescent tissue, respectively. The parameter δ_{QP} describes death of damaged quiescent cells, whereas $k_{Q_P P}$ refers to the rate of repairment of damaged quiescent cells and their phenotype switching to proliferative state.

System (1.3) is quite complex and includes ten parameters. Some of them are very difficult (if possible) to measure or to estimate based on available data, *cf.* [15], which is a strong limitation for possible application of this model. In contrast, our model, developed in [2] and described in Chapter 2, is constructed with a minimal number of parameters allowing for a potential future use in practice. Still, using a model simpler from mathematical perspective and with a smaller number of parameters we were able to effectively fit the evolution of real-patients' tumours and their response to chemotherapy.

Another drawback of the model constructed by Ribba *et al.* is that it does not represent realistically the administration of chemotherapy drug. Constant level of drug present in treated tumour seem not to be the most appropriate mathematical description of chemotherapy administered orally in cycles, see Section 1.5 for details.

Moreover, the model proposed in [22] was intended to reflect LGGs response not only to chemotherapy with TMZ, but also to chemotherapy with PCV and radiotherapy. This seems to be a small oversimplification as radiotherapy is well-known to act differently from chemotherapy and, moreover, there are clinical recognised mathematical models capable of describing tumours' response to radiotherapy sufficiently well, see *e.g.* [132, 1]. In [1] we developed mathematical model of LGGs response to radiotherapy modifying the mathematical framework already used for describing radiotherapy effect on other tumours.

The model of Ribba *et al.* was later extended by Mazzocco *et al.* in [133] where the authors took into account the possibility of acquired resistance to drug. That model was also used to find more efficient schemes for LGG chemotherapy with PCV in [134], however the authors raised their conclusions based solely on the results of simulations of that model.

Models of malignant transformation of LGGs

As far as we know, the only mathematical model accounting for the malignant transformation of LGGs was formulated by Swanson *et al.* in [23]. In that work a system of differential equations was proposed to describe the evolution of three types of glioma cells (normoxic C, hypoxic h and necrotic n) with a vascular component v and an antiangiogenic factor a:

$$\begin{cases} \dfrac{\partial C}{\mathrm{d}t} = \nabla\left(D(1-T)\nabla c\right) + \rho c(1-T) + \gamma hV - \beta c(1-V) + \alpha_n nc, \\ \dfrac{\partial h}{\mathrm{d}t} = \nabla\left(D(1-T)\nabla h\right) - \gamma hV + \beta c(1-V) - \left(\alpha_h h(1-V) + \alpha_n nh\right), \\ \dfrac{\partial n}{\mathrm{d}t} = \alpha_h h(1-V) + \alpha_n n(c+h+v), \\ \dfrac{\partial v}{\mathrm{d}t} = \nabla\left(D_v(1-T)\nabla v\right) + \mu\dfrac{a}{K_m+a}v(1-T) - \alpha_n nv, \\ \dfrac{\partial a}{\mathrm{d}t} = \nabla\left(D_a\nabla a\right) + \delta_c c + \delta_h h - q\mu\dfrac{a}{K_m+a}v(1-T) - \omega av - \lambda a, \\ V = \dfrac{v}{c+h+v}, \\ T = \dfrac{c+h+v+n}{k}. \end{cases} \tag{1.4}$$

Interestingly, the authors argued that the accumulation of genetic mutations is not necessary for malignant progression and the growth kinetics parameters alone can drive the glioma transformation. This conclusion seems to be related to the one stated by us in [3], where we assumed that it may be a tumour growth beyond some critical level that triggers significant changes in tumour tissue and malignant transformation visible as phenotypic switch (that is transition to different tumour subpopulation described by increased growth kinetics parameters), see Chapter 3.

The main drawbacks of the model in [23] are its complexity and the fact that some of the underlying biological assumptions are not completely realistic. For instance, according to Swanson *et al.* model, normoxic cells convert directly not only to hypoxic, but also to necrotic ones, which, according to our knowledge, is not in a full agreement with biological observations.

1.7 Methodology

In this dissertation, we formulate macroscopic mathematical models that mimic the growth of LGGs, their response to chemotherapy and the process of malignant transformation into their higher-grade counterparts. In order to do so, we assume that tumours belonging to that class share similar patterns of growth and similar qualitative response to chemotherapy. We base our models on existing mathematical models proposed for these brain tumours. In each chapter, we also specify biological and medical facts which were used to develop each of our models separately, apart of the ones described in Sections 1.4 and 1.5.

Mathematical models constructed in this thesis are single- or multi-phenotype using either reaction-diffusion or ordinary differential equations (ODEs). Due to nonlinear terms and complex dependencies, explicit solutions are impossible to find in a general case. Thus, we study their mathematical properties, we use numerical methods to simulate models solutions, and we observe dependencies on models' parameters. We validate models with patients data and perform models simplifications to formulate clinically-interesting hypotheses.

Mathematical analysis of models

Mathematical analysis of the proposed models is a relevant task in this dissertation. We verify various mathematical properties of the models, starting from the existence and uniqueness of solutions. We investigate the models' dynamics in the asymptotic case. We study how the long-time behaviours of the models' solutions depend on the parameters' values. We use Hartman-Grobman theorem [135] and Lyapunov theorem [136] to verify the local asymptotic stability of steady states. In Chapter 2 we use Dulac criterion [135] to exclude the existence of periodic solutions in the case of constant chemotherapy function. Poincare-Bendixson theorem [135] is used to prove the global stability of tumour-free steady state when additional conditions are satisfied (see Theorem 2.11). We also use Brouwer theorem [137] to justify the existence of periodic solutions for some specific cases of periodic treatment function. We also prove that diffusion-driven instability does not appear in the reaction-diffusion model described in Chapter 3. In Chapter 4 we study the modification of the ODE system described in Chapter 2. We analyse fast and slow system and study the existence of a heteroclinic solution in the case of two saddle steady states. Using Fredholm alternative theorem, we prove the existence of so-called travelling wave solution.

As already stated, models formulated in the dissertation, though simple, in general do not have known analytical solutions allowing for the direct calculation of the clinically relevant quantities. Hence, using analytical methods, the original model equations are simplified in such a way that behaviour is similar quantitatively, but the computation of an explicit solution is possible. Consequently, we derive estimations which could be potentially useful in assessing tumours aggressiveness or selecting the best therapies.

Models validation

An extremely significant part of this dissertation is the validation of proposed models. There are few studies containing systematic and quantitative measurements of LGG growth rates which provide key information for the development and validation of macroscopic mathematical models, see [115]. Here we validate formulated models using patients data.

Patients data. For the conduction of this research, we had an access to the glioma patients database* of Bern University Hospital provided by medical doctors from the Department of Neurosurgery, due to a courtesy of Prof. Dr. med. Philippe Schucht, Prof. Dr. med. Jürgen Beck, Dr. med. Michael Murek. This database contained volumetric longitudinal data of patients diagnosed with gliomas and followed at the Bern University Hospital between 1990 and 2013. Patients were followed using MRI T2 or FLAIR, see Section 1.5 for details.

Radiological glioma growth was quantified there by manual measurements of tumour diameters on successive MRI scans. The three largest tumour diameters (D_1, D_2, D_3) according to three reference orthogonal planes (axial, coronal and sagittal planes) were measured and tumour volumes were estimated using the ellipsoidal approximation: $V = (D_1 \cdot D_2 \cdot D_3)/2$, following the standard clinical practice at the time when this data has been collected [138, 106].

For some patients, additional data were available (Ki-67 LI, per cent of tumour cells showing overexpression of p53-protein, IDH-1-Mutation, MGMT-Promoter Methylation Status), as such measurements were found to be associated with either prognosis or response to some treatments, *cf.* Section 1.5. Nevertheless, in order to be able to prepare specific models for different molecular subtypes, one should dispose of data of a large cohort of patients with distinct molecular characteristics. Clearly, in this dissertation we treat LGGs as one disease entity as they all share similar pattern of growth and have similar qualitative response to therapies.

As mentioned before, there is a lack of large cohorts of LGG patients treated in the same way. The total number of LGGs patients in the mentioned database is 82. Among those cases 32 patients had confirmed malignant transformation, see Section 1.5 for criteria, and 18 patients were treated with chemotherapeutic agent TMZ, modelled in Chapter 2. Moreover, for fitting mathematical models, some additional conditions need to be satisfied, see Sections 2.3.2 and 3.3.2.

We believe that mathematical models which may be useful in practice should be constructed in such a way that all parameters have biological interpretations. Thus, values of some of them can be taken from the literature, but some should certainly be patient-specific and need to be estimated using proper experimental or clinical data. For that purpose, we exploit volumetric patients data from the database described above. We use numerical methods to calculate and minimise the error between the model simulations' outcome and the data.

Model fitting to patients data. To compare the results of model simulations with patients' data, first we need to choose how to assess the model fit and calculate the difference between the model output and measured tumour size. Let us recall the well-known method of least squares, credited to Gauss and Legendre [139]. Formally, it is assumed that a given dataset consists of n points (data pairs) (x_i, y_i) with $i \in \{1, \dots, n\}$, where x_i is an independent variable and y_i is a dependent variable whose value is found by observation. While fitting our patients' data, an independent variable is the time of MRI, while a dependent variable – tumour size (mean diameter or volume) estimated from the respective MRI scan. The mathematical model is assumed to have a general form $f(x, \beta)$, where m adjustable parameters are held in the vector β. In our case β would contain some patient- or treatment-specific parameters. For each data point, the corresponding residual r_i is computed as:

$$r_i = y_i - f(x_i, \beta).$$

*A clinical study no. 2039 was developed to provide data. The study was approved by Kantonale Ethikkommission Bern (Bern, Switzerland), the approval number: 07.09.72. The patients' data was anonymised.

The standard least-squares method finds the most appropriate parameter values by minimising the sum S of squared residuals:

$$S = \sum_{i=1}^{n} {r_i}^2.$$

However, that procedure results in outlying points being given disproportionately large weighting. Thus, in many practical applications, the relative residuals are considered and the value to be minimised is, therefore, the following:

$$S = \sum_{i=1}^{n} \left(\frac{y_i - f(x_i, \beta)}{y_i} \right)^2. \tag{1.5}$$

The resulting method is called "relative least squares". Throughout this thesis, while performing model fitting to patients data, we use relative least squares method taking also into account additional constraints. To be specific, we typically assume that the parameters values fall into ranges determined from appropriate literature.

In order to find parameters values minimising the sum of squared residuals we use two methods. In Chapter 2, where at most two parameters are fitted at once, we use built-in Matlab function "lsqnonlin" [140]. In Chapter 3 where we need to fit four parameters at once we use a particle swarm optimisation (PSO) algorithm. The latter algorithm was created by Kennedy, Eberhart and Shi [141, 142] and implemented in Matlab with a constriction factor introduced by Clerc and Kennedy [143]. In short, PSO is a computational method for optimising a problem by iteratively improving a candidate solution with respect to a certain measure of quality. PSO solves a problem by having a population of particles (solutions) that moves around in the search space influenced by their own best past location and the best past location of the whole swarm or a close neighbour. Taking a swarm of particles enables to avoid being trapped in a local optimum. This technique has an immense scope of applications, see *e.g.* [144] for a review, among others in parameter estimation, solving optimisation problems and feature selection problems.

Numerical analysis of models

To solve systems of reaction-diffusion equations numerically we use the standard Matlab PDE solver *pedpe*, see [145], while for simulating ODEs we use solver *ode45* based on the Runge-Kutta 4th-order method [146].

We analyse numerous simulations of our mathematical models for different possible values of parameters. The dependence between model output and parameters values is verified on the base of thorough analysis of model behaviour for a broad range of parameter values. We also study which parameters have the largest effect on the dynamics of tumours growth and virtual patients' prognosis.

In Chapter 3 we perform **sensitivity analysis**. This method allows testing robustness of models solutions with respect to all uncertainties. In order to use this method, first we assure the proper distribution of all parameters of the model and subsequently, we study their impact on the time when malignant transformation begins and the predicted time left to death. Sensitivity analysis is performed using the SaSAT package, implemented in Matlab by Hoare *et al.* [147].

Numerical methods are used not only for the fitting our mathematical models to patients data. We also present the results of models' simulations that do not correspond to any patient case. In such situations, we follow *e.g.* [148, 126] and write **"virtual patients"**. We also refer

to **virtual tumours** as tumours evolving according to the simulations of a mathematical model for specific values of parameters, such as initial tumour size, proliferation rate, motility rate, rate of response to therapy, similarly as done by many authors, see *e.g.* [107, 126, 98, 149]. Summing up, a virtual tumour is a solution of a mathematical model which does not describe any specific patient from our database but describe a hypothetical patient, called a virtual patient.

Based on cohorts of virtual patients we formulate hypotheses, concerning LGGs treatment, that could be verified in clinical studies in the future. Thus, we address questions such as: "What are the quantitative indicators reflecting tumour intrinsic behaviour that can be observed and measured in clinical practise?" or: "Which quantities have prognostic values for response to treatment?". Based on obtained formulas, see Section 1.7, as well as numerical studies of virtual patients cohorts we propose new ideas (*e.g.* alternative treatment schemes) to be considered for LGGs.

1.8 Notation and acronyms

We introduce the following notation:

- $\mathbb{R}^+ = (0, +\infty)$,
- $\mathbb{R}_0^+ = [0, +\infty)$,
- $(\mathbb{R}_0^+)^2 = [0, +\infty) \times [0, +\infty)$,
- $F(a^-) = \lim_{x \to a^-} F(x)$, $F(a^+) = \lim_{x \to a^+} F(x)$ for any function $F \colon \mathbb{R} \to \mathbb{R}$ and $a \in \mathbb{R}$,
- $\{a\}$ – fractional part of a non-negative real number a.

Throughout the thesis we also use the following abbreviations:

- ODE – ordinary differential equation,
- PDE – partial differential equation,
- FKE – Fisher-Kolmogorov equation,

- LGG – low-grade glioma,
- HGG – high-grade glioma,
- WHO – World Health Organisation,
- MRI – magnetic resonance imaging,
- MTD – mean tumour diameter,
- FTB – fatal tumour burden,
- OS – overall survival,
- TMZ – a chemotherapy drug temozolomide,
- PCV – a chemotherapy drug combination including procarbazine, lomustine and vincristine,
- CSF – cerebrospinal fluid,
- Ki-67 LI – Ki-67 labelling index,
- t_{RP} – time to radiological progression,
- t_{OMT} – time of the onset of malignant transformation.

They are described at the time of first occurrence.

Chapter 2

Mathematical model of response to chemotherapy

In this part of thesis we develop a simple mathematical model for LGG growth and response to chemotherapy that fits very well with longitudinal volumetric data of patients diagnosed with LGGs. We also verify the mathematical properties of the model proposed. Interestingly, the model suggests that the response of the tumour to chemotherapy may be related to its aggressiveness. We also provide an approximate explicit formula for the time of maximal tumour response to chemotherapy. This equation may be helpful to clinicians in selecting patients who will benefit most from early treatment and finding the best personalised therapy.

2.1 Formulation of mathematical model

2.1.1 Dynamics of tumour cells

In order to keep our description as simple as possible we build a continuous macroscopic model assuming that the tumour grows due to net cell division with coefficient ρ such that its inverse gives an estimate of the typical cell doubling time. In general the rate of growth is described by $\rho f(P/K)$, where P is a mean tumour cell number, K is carrying capacity and f represents the space available for tumour cells to proliferate. The simplest choice for the proliferative term is to assume that the evolution of tumour mean cell number $P(t)$ is governed by a logistic growth [94]. In such a case function f takes the following form:

$$f\left(\frac{P}{K}\right) = 1 - \frac{P}{K}. \tag{2.1}$$

We take into account a fact that the specific form of LGGs' growth function remains unknown. Thus, for the purpose of mathematical analysis we consider a broader class of possible functions f describing tumour growth and we impose the following assumptions:

(A1) $f\colon \mathbb{R}_0^+ \to \mathbb{R}$ of class C^1 on $(0, +\infty)$,

(A2) $f(1) = 0$, f strictly decreasing,

(A3) either

- (a) $f(0) = 1$ or
- (b) $\lim_{v\to 0^+} f(v) = +\infty, \lim_{v\to 0^+} vf(v) = 0$ and $f(0) = 0$.

Note that if tumour growth is modelled by logistic term (2.1), then assumptions (A1), (A2) and (A3a) are fulfilled. On the other hand, if one consider Gompertzian law of growth [93] with $f(P/K) = -\ln(P/K)$, then the assumptions (A1), (A2) and (A3b) are fulfilled.

We complement the equation for the mean number of functionally alive tumour cells $P(t)$ with an equation for the evolution of the mean number of cells irreversibly damaged by chemotherapy $D(t)$. This type of model has been used successfully to describe the effect of radiotherapy on LGGs [1, 150], see also Appendix A. We model the response to chemotherapy in a similar way since a key feature of glioma response to both chemo- and radiotherapy is delayed cell death. In many studies it has been observed that TMZ-induced damage leads to cell death long after the end of therapy [68, 151, 69, 70]. It has been verified *in vitro* that the glioma cells death after administration of TMZ is induced most typically in one of the post-treatment cell cycles [152] due to futile mismatch repair cycles (see *e.g.* [58] for a detailed description of this mechanism). Thus, in line with this biological evidence we assume that irreversibly damaged tumour cells try to enter mitosis with the same probability as those active, but die after a mean value of k such attempts, which results in the growth rate $\rho f\left(\frac{P+D}{K}\right)$ for proliferative cells and the death rate $-\frac{\rho}{k} f\left(\frac{P+D}{K}\right)$ for damaged cells. Of note, due to our assumptions on function f, *per capita* growth of proliferating cells P in our model decreases with the increase of the total tumour mass $P + D$. The mean number of cells damaged by the drug in a time unit is considered to be proportional to the concentration of the drug in the tumour tissue C multiplied by the average number of proliferating tumour cells with the rate α, measuring the influence of TMZ on cells. The above assumptions lead to the following set of equations

$$\begin{aligned} \dot{P} &= \rho P \cdot f\left(\frac{P+D}{K}\right) - \alpha P C, \\ \dot{D} &= -\frac{\rho}{k} D \cdot f\left(\frac{P+D}{K}\right) + \alpha P C, \end{aligned} \tag{2.2}$$

where $t \in \mathbb{R}_0^+$. We assume that initially (at time $t = 0$, taken to be the start of the tumour observation) the tumour has a certain mass P_0 and before $t = 0$ no treatment was administered, thus, there are no damaged cells. Those assumptions imply the following initial conditions of system (2.2):

$$P(0) = P_0, \quad D(0) = 0. \tag{2.3}$$

2.1.2 Kinetics of chemotherapy drug

The systemic pharmacokinetic and pharmacodynamic properties of TMZ has been studied in detail in several studies [153, 154]. Baker *et al.* [153] described the concentrations of TMZ, MTIC and AIC in plasma in detail. Ostermann *et al.* [154] collected data on TMZ concentration from blood and cerebrospinal fluid (CSF) obtained via lumbar puncture in patients with malignant gliomas.

However due to the physiological separation of brain and tumour from both blood and CSF (through blood-brain, blood-tumour, blood-CSF and CSF-tumour barriers) the amount of drug reaching the tumour differs from the amount of drug circulating in blood and CSF [155, 156]. Therefore, instead of describing a complicated mechanism with many unknown parameters based on data collected from blood or CSF, we choose a simpler dynamics based directly on the brain tissue data. Thus, we base our model on data from the study by Portnow *et al.* [157] who examined TMZ concentration in intracerebral microdialysis samples from peritumoural brain interstitium obtained from patients with central nervous system tumours.

With regard to chemotherapy pharmacokinetics, we assume, as usual [158, 22], that the concentration C of TMZ measured in units of days, decays exponentially due to the drug clearance with a constant rate λ. It is consistent with the fact that TMZ has linear pharmacokinetics [57].

TMZ reaches a maximal drug concentration in the brain about two hours after administration [78, 157, 153], what is very short in comparison to the time scale of tumour evolution in the model (of the order of years). Thus, we may treat the whole time of oral drug administration, absorption and transport to the brain as a discontinuous change in the drug concentration that occurs at given administration times. Such a formulation of the problem enables also the following mathematical analysis and estimations.

Here we assume that in general chemotherapy consists of a sequence of doses $d_1, d_2, \ldots, d_n$ given at times $0 \leq t_1 < t_2 < \ldots < t_n$, which we model as impulses due to assumptions given above. As a consequence, we obtain an impulsive ODE for C:

$$\begin{aligned} \dot{C}(t) &= -\lambda C, \\ C(0) &= C_0, \\ C(t_j) &= C(t_j^-) + C_j, \end{aligned} \tag{2.4}$$

where $t \in \mathbb{R}_0^+$ and C_j is the fraction of the dose d_j which reaches the tumour tissue, accounting for drug loss during transport to the brain. Note that such a model allows to represent the situation in which after the start of observation at time 0 chemotherapy is deferred (then $t_1 > 0$ and $C_0 = 0$) or it begins at time 0 (then $t_1 = 0$ and $C_0 = C_1$).

Typically TMZ treatment for LGGs' patients is planned in such a way that doses of 150–200 mg per m^2 of patient body surface are given once per day for 5 days every 28 consecutive days, a sequence that it is called "cycle" in the oncological terminology, see Section 1.5. Let us consider a general chemotherapy fractionation scheme such that p equal doses are given every r days in cycles of length T. We intend to compute the value of chemotherapy concentration for every time $t \in \mathbb{R}_0^+$.

In order to do so, first we solve system (2.4) assuming that $C_j = C_0$ and $t_j = jT$ with $j \in \{1, 2, \ldots\}$. Such a system describes a chemotherapy concentration when constant drug doses C_0 are given in equal time intervals T. Moreover, we assume that the concentration of chemotherapy between subsequent cycles of length T is described by an auxiliary function h to be defined in what follows. Function C solving system (2.4) just before the cycle number m attains the value:

$$C(jT^-) = C_0 h(T)\left(1 + \mathrm{e}^{-T\lambda} + \ldots + \mathrm{e}^{-(j-1)T\lambda}\right) = C_0 h(T)\frac{1 - \mathrm{e}^{-jT\lambda}}{1 - \mathrm{e}^{-T\lambda}}.$$

Using a recursive procedure we get

$$\begin{aligned} C(t) &= C_0 h(t - jT) + C(jT^-)\mathrm{e}^{-(t-jT)\lambda} = C_0\left(h(t - jT) + h(T)\frac{1 - \mathrm{e}^{-jT\lambda}}{1 - \mathrm{e}^{-T\lambda}}\mathrm{e}^{-(t-jT)\lambda}\right) \\ &= C_0\left(h(t - jT) + h(T)\frac{\mathrm{e}^{-(t-jT)\lambda}}{1 - \mathrm{e}^{-T\lambda}}\right) - C_0 h(T)\frac{\mathrm{e}^{-t\lambda}}{1 - \mathrm{e}^{-T\lambda}}, \end{aligned}$$

for $t \in [jT, (j+1)T)$. From the definition of fractional part of a non-negative real number, we have

$$t - jT = \left(\frac{t}{T} - \left\lfloor \frac{t}{T} \right\rfloor\right) T = \left\{\frac{t}{T}\right\} T.$$

If the number of chemotherapy cycles is infinite we can represent C in the following way:

$$C(t) = C_0 \left(h(\{t/T\}T) + h(T)\frac{e^{-\{t/T\}T\lambda}}{1-e^{-T\lambda}} \right) - C_0 h(T)\frac{e^{-t\lambda}}{1-e^{-T\lambda}}. \tag{2.5}$$

Now let us derive the explicit formula of the function h describing the concentration of drug in the first cycle assuming that unit doses are given. Thus, h is a solution of system:

$$\begin{aligned} \dot{h}(t) &= -\lambda h, \\ h(0) &= 1, \\ h(t_i) &= 1 + h(t_i^-), \end{aligned} \tag{2.6}$$

where $t \in [0, T]$, $t_i = ir$ with $i \in \{0, \ldots, (p-1)r\}$. At times of discontinuity we have:

$$h(ir^-) = e^{-r\lambda}\left(1 + e^{-r\lambda} + \ldots + e^{-(i-1)r\lambda}\right) = e^{-r\lambda}\frac{1-e^{-ir\lambda}}{1-e^{-r\lambda}}.$$

Solving system (2.6) we obtain

$$h(t) = \begin{cases} e^{-t\lambda}\frac{e^{(\lfloor t/r \rfloor + 1)r\lambda}-1}{e^{r\lambda}-1}, & \text{for } t \in [0, (p-1)r), \\ e^{-t\lambda}\frac{e^{pr\lambda}-1}{e^{r\lambda}-1}, & \text{for } t \in [(p-1)r, T], \end{cases} \tag{2.7}$$

what gives us the explicit form of function (2.5). Note that, due to the fact that h given by Eq. (2.7) is bounded, function given by Eq. (2.5) tends to a periodic function:

$$C_0 \left(h(\{t/T\}T) + h(T)\frac{e^{-\{t/T\}T\lambda}}{1-e^{-T\lambda}} \right)$$

for $t \to +\infty$. Following [159] let us recall the subsequent definition.

Definition 2.1. *We say that a function $C\colon \mathbb{R}_0^+ \to \mathbb{R}$ is an asymptotically periodic function with a period T if there exist functions $C_{\text{per}}, C_{\text{rest}}\colon \mathbb{R}_0^+ \to \mathbb{R}$ such that C_{per} is periodic with a period T, $C_{\text{rest}} \xrightarrow{t\to+\infty} 0$ and*

$$C(t) = C_{\text{per}}(t) + C_{\text{rest}}(t).$$

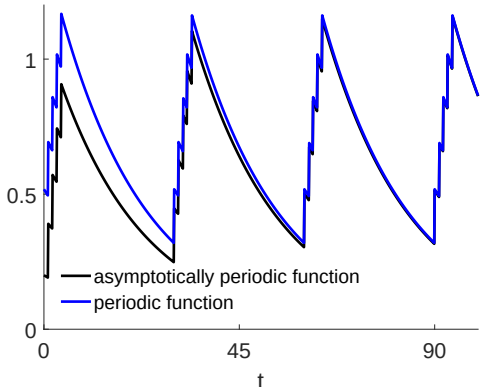

Figure 2.1: Examples of periodic and asymptotically periodic functions given by Eqs. (2.5) and (2.8), respectively with function h given by Eqs. (2.7).

Thus, function given by Eq. (2.5) with h as in Eq. (2.7) is an asymptotically periodic function with period T with

$$C_{\text{rest}}(t) = -C_0 h(T)\frac{e^{-t\lambda}}{1-e^{-T\lambda}} = -C_0 e^{-T\lambda+(p-1)r\lambda-t\lambda}\frac{1-e^{-pr\lambda}}{(1-e^{-r\lambda})(1-e^{-T\lambda})}$$

and

$$C_{\text{per}}(t) = \begin{cases} C_0 h(t) + C_0 h(T)\frac{\mathrm{e}^{-t\lambda}}{1-\mathrm{e}^{-T\lambda}}, & t \in [0,T), \\ C_{\text{per}}\left(\{t/T\}T\right), & t \geq T. \end{cases} \tag{2.8}$$

We also compute the mean value of C_{per} to be used later in proving the convergence of model solutions. We have

$$\begin{aligned} \bar{C} =& \frac{1}{T}\int_0^T C_{\text{per}}(t)\mathrm{d}t = \frac{C_0}{T}\left(\sum_{j=0}^{p-2}\int_{jr}^{(j+1)r} e^{-t\lambda}\frac{\mathrm{e}^{(j+1)r\lambda}-1}{\mathrm{e}^{r\lambda}-1}\mathrm{d}t + \int_{(p-1)r}^{T} e^{-t\lambda}\frac{\mathrm{e}^{pr\lambda}-1}{\mathrm{e}^{r\lambda}-1}\mathrm{d}t\right) \\ &+\frac{C_0}{T}\int_0^T h(T)\frac{\mathrm{e}^{-t\lambda}}{1-\mathrm{e}^{-T\lambda}}\mathrm{d}t = \frac{C_0 p}{\lambda T}. \end{aligned} \tag{2.9}$$

Figure 2.1 presents an example of asymptotically periodic function given by Eq. (2.5) and periodic function given by Eq. (2.8) with h as in Eqs. (2.7). Note that asymptotically periodic functions can represent many different chemotherapy schedules, among others the typical one described and considered in Section 2.1.2.

To sum up, we present two alternative mathematical models for the description of chemotherapy: (i) a system of impulsive ordinary differential equations (2.4) for finite number of chemotherapy doses $t_1, \ldots, t_n$ and (ii) asymptotically periodic function (2.5) describing the drug concentration when infinite number of chemotherapy cycles are given.

It is important to emphasise that system (2.2) intends to describe the effect of first-line chemotherapy, since after the treatment resistant phenotypes arise leading to the acquisition of drug resistance. Thus, a detailed analysis of second-line chemotherapy would require the introduction of more phenotypes in the model and is beyond the scope of this research.

2.2 Mathematical analysis of the chemotherapy model

For the purpose of mathematical analysis, without loss of generality we assume that the drug administration starts at time $t_1 = 0$. We discuss the behaviour of system (2.2) for the following cases of chemotherapy administration:

(a) constant infinite chemotherapy,

(b) chemotherapy administered periodically:
- with finite number of cycles,
- with infinite number of cycles.

Let us rescale the variables of system (2.2) by taking

$$x = \frac{P}{K}, \quad y = \frac{D}{K}, \quad z = \frac{\alpha}{\rho}C, \quad s = \rho t \tag{2.10}$$

to get the system:

$$\begin{aligned} \dot{x}(s) =& \quad xf(x+y) - xz, \\ \dot{y}(s) =& \quad -\frac{1}{k}yf(x+y) + xz, \end{aligned} \tag{2.11}$$

with initial conditions:

$$x(0) = x_0, \quad y(0) = 0. \tag{2.12}$$

The system governing evolution of rescaled concentration of chemotherapy (2.4) is now of the form:

$$\begin{aligned} \dot{z}(s) &= -\mu z, \\ z(0) &= z_0, \\ z(s_j) &= z(s_j^-) + z_0, \end{aligned} \tag{2.13}$$

where

$$z_0 = \frac{\alpha}{\rho} C_0, \quad \mu = \frac{\lambda}{\rho}. \tag{2.14}$$

In this section we study system (2.11) with the general form of the function f satisfying the assumptions (A1)–(A3). We study the dynamics of resulting general model, showing that this dynamics is in some sense similar independently of the choice of the specific growth function. Moreover, we take into account the possibility that one of the tumour cells populations makes better use of the resources. Thus, we consider the more general term describing the proliferation of glioma cells, that is instead of term $xf(x+y)$ we consider $xf(x+\gamma y)$ with $\gamma > 0$ describing competition between cells x and y. Values of $\gamma \in (0,1)$ are used to represent the case when LGG proliferative cells are less competetive than the damaged cells, while $\gamma > 1$ describes the opposite case. Thus, we study the following generalisation of system (2.11):

$$\begin{aligned} \dot{x}(s) &= xf(x+\gamma y) - z(s)x, \\ \dot{y}(s) &= -\frac{1}{k} yf(x+\gamma y) + z(s)x, \end{aligned} \tag{2.15}$$

with initial conditions:

$$x(0) = x_0, \quad y(0) = 0,$$

where f satisfies assumptions (A1)-(A3).

Proposition 2.1. *Let f satisfy (A1)-(A2) and $z\colon \mathbb{R}_0^+ \to \mathbb{R}_0^+$ be continuous, bounded and non-negative function. Then, for any non-negative initial condition $\big(x(0), y(0)\big)$ solutions to system (2.15) exist for all $t \geq 0$. Moreover, if f additionally satisfies (A3a) or $x(0) > 0$ or $y(0) > 0$, then the solution is unique.*

Proof. The local existence of solutions of system (2.15) for every initial data from $(\mathbb{R}_0^+)^2$ follows from the continuity of the function of the right-hand side of the system in $(\mathbb{R}_0^+)^2$. Moreover, the right-hand side of system (2.15) is a C^1 function in $(\mathbb{R}_0^+)^2$ or in $(\mathbb{R}_0^+)^2 \setminus \{(0,0)\}$ or, if assumption (A3a) holds, even in a whole $(\mathbb{R}_0^+)^2$. This fact implies uniqueness of solutions in the respective set. □

Note that in the case of function satisfying condition (A3b) we may loose uniqueness of solutions if $x(0) = 0$ and $y(0) = 0$ (*e.g.* if we take $f(v) = 1/\sqrt{v}$ and $z = 0$).

It is straightforward to find out that

Lemma 2.2. *Function $z\colon \mathbb{R}_0^+ \to \mathbb{R}_0^+$ solving system (2.13) is continuous on $\mathbb{R}_0^+$.*

The asymptotic behaviour of system (2.15) under the effect of a finite number of chemotherapy doses is easy to obtain.

Theorem 2.3. *If z is continuous on $\mathbb{R}_0^+$ and $z(s) \to 0$ for $s \to +\infty$, then the solutions of system (2.15) tend to point $(1,0)$.*

Proof. As function x is bounded and $z(s) \to 0$ for $s \to +\infty$, then $x(s)z(s) \to 0$ for $s \to +\infty$. As a consequence $\dot{y}(s) < 0$ for sufficiently large time. Thus, it is easily seen that $y(s) \to 0$ and $x(s) \to 1$ as $s \to +\infty$. □

As a consequence we arrive at

Proposition 2.4. *The solutions of system (2.11),(2.13) after the end of a treatment tend to $(1,0)$.*

Proof. When no drug is given for time $s \geq s_n$ (with n being the index of the last dose), then

$$z(s) = z(s_n)\exp(-\mu(s - s_n)) \to 0 \text{ as } s \to +\infty.$$

Using Theorem 2.3 we obtain the assertion of the theorem. □

This behaviour is not surprising and can be interpreted as patient death due to drug clearance and tumour regrowth.

Theorem 2.5. *For $\gamma > 1$ set $\Omega = (\mathbb{R}^+)^2$ is a positively invariant set for system (2.15) with f fulfilling conditions (A1)-(A3) and non-negative initial conditions.*

Proof. Notice that the right-hand side of system (2.15) is a continuous function of x and y for both assumptions (A3a) and (A3b).
Let then $(x_0, y_0) \in \Omega$ be the initial point for $t_0 = 0$. We know that the unique solution exists on some time interval $[0, t^*)$. If Ω is not an invariant set, then there exists such initial condition and time $t_1 > 0$ for which the solution reaches the boundary of Ω. Therefore, either $\lim_{t\to t_1} x(t) = 0$ or $\lim_{t\to t_1} y(t) = 0$. However, the function of the right-hand side of system (2.15) show that if $x(t_1) = 0$, then $\dot{x}(t_1) = 0$ and if $y(t_1) = 0$, then $\dot{y}(t_1) \geq 0$. When assumption (A3a) holds, this would compromise the uniqueness of solutions. When assumption (A3b) holds, from the fact that points $(0, y)$ with $y \leq 0$ are repelling we deduce that none of the solutions starting from the inside of Ω_1 reaches the boundary of this set. Therefore, the solution of system (2.15) cannot leave the set Ω. □

If $\gamma \leq 1$, then there exists a bounded invariant set of system (2.15).

Theorem 2.6. *For $\gamma \leq 1$ set $\Omega_1 = \{(x, y) \in \mathbb{R}^2 : x > 0, y > 0, x + \gamma y < 1\}$ is a positively invariant set for system (2.15) with f fulfilling conditions (A1)-(A3) and non-negative initial conditions.*

Proof. One shows the non-negativity of x and y in a similar way as in the proof of Theorem 2.5. Thus, here we need only to show that solutions do not cross the line $x + \gamma y = 1$ for $\gamma < 1$. For

$$u = x + \gamma y, \tag{2.16}$$

we have

$$\dot{u}(s) = \frac{f(u)}{k}\left((k + 1)x - u\right) + (\gamma - 1)zx. \tag{2.17}$$

Clearly, Eq. (2.17) is a non-autonomous differential equation with x being a non-negative function of time, and it has unique solutions. Moreover, $u \equiv f^{-1}(0)$ is a solution of Eq. (2.17) for $\gamma = 1$. For $\gamma < 1$ we have $\dot{u}\Big|_{u=1} = (\gamma - 1)zx < 0$ and the solutions tend towards the interior of Ω_1. As a consequence, for all $(x_0, y_0) \in \Omega_1$, solutions of system (2.15) stay in Ω_1 when $\gamma \leq 1$. □

Proposition 2.7. *Consider the solutions of system (2.15) such that initial data (x_0, y_0) fulfils $x_0 + \gamma y_0 = 1$. For $\gamma < 1$ they tend toward the interior of set Ω_1, for $\gamma = 1$ they stay on the line $x + \gamma y = 1$, for $\gamma > 1$ they repel from set Ω_1.*

Proof. The assertion of the theorem follows immediately from the proof of Theorem 2.6. □

2.2.1 Existence and stability of the steady states for constant chemotherapy function

Now, before we study the dynamics of system (2.15) in the case when the function z is asymptotically periodic, we consider the case when the function z is constant. With some abuse of the notation we write $z(s) \equiv z$. Although this case seems to be an oversimplification of the real process, it is a preliminary step needed for the latter analysis. In order to find steady states $(\bar{x}, \bar{y})$ of system (2.15) with $z(s) \equiv z$, we solve a system of equations:

$$\bar{x} f(\bar{x} + \gamma\bar{y}) - z\bar{x} = 0, \tag{2.18a}$$

$$-\frac{1}{k}\bar{y} f(\bar{x} + \gamma\bar{y}) + z\bar{x} = 0. \tag{2.18b}$$

From Eq. (2.18a) we get that either $\bar{x} = 0$ or $f(\bar{x} + \gamma\bar{y}) = z$. Clearly, assumption (A2) allows to invert function f. Thus, for $\bar{x} = 0$ $\bar{y}$ equals 0 or $f^{-1}(0)/\gamma = 1/\gamma$. For $f(\bar{x} + \gamma\bar{y}) = z$ Eq. (2.18b) implies that $\bar{y} = k\bar{x}$. As a result, system (2.15) with $z(s) \equiv z$ has at most three steady states:

$$P_1 = (0, 0), \quad P_2 = (0, 1/\gamma), \quad P_3 = (\tilde{x}, k\tilde{x}),$$

with $\tilde{x} = f^{-1}(z)/(1 + k\gamma)$. Clearly, steady state P_3 exists if and only if $f^{-1}(z) > 0$, that is $z < f(0^+)$ (see assumptions (A2) and (A3)). It should be stressed that assumption (A3b) implies the existence of steady state P_3 for all $z > 0$. Otherwise, that is when (A3a) holds, steady state P_3 exists only if $z < 1$. Let us denote

$$\delta = f^{-1}(z)|f'(f^{-1}(z))|. \tag{2.19}$$

Clearly the existence of P_3 implies positivity of δ.

Theorem 2.8. *Consider system (2.15) with f fulfilling conditions (A1)-(A3) and $z(s) \equiv z$. Then the steady state*

(i) P_1 is locally stable for $z \geq f(0+)$ and unstable for $0 < z < f(0+)$,

(ii) P_2 is locally unstable,

(iii) P_3 (if it exists) is locally

- *stable for $z \geq \delta$ or $\gamma < 1 + \frac{k+1}{k}\frac{z}{\delta - z}$,*
- *unstable for $z < \delta$ and $\gamma > 1 + \frac{k+1}{k}\frac{z}{\delta - z}$,*

where δ is given by Eq. (2.19).

Proof. The Jacobi matrix of right-hand side function of system (2.15) with $z(s) \equiv z$ calculated at arbitrary steady state $P = (\bar{x}, \bar{y})$ reads

$$J(P) = \begin{bmatrix} f(\bar{x} + \gamma\bar{y}) + \bar{x} f'(\bar{x} + \gamma\bar{y}) - z & \gamma\bar{x} f'(\bar{x} + \gamma\bar{y}) \\ -\frac{1}{k}\bar{y} f'(\bar{x} + \gamma\bar{y}) + z & -\frac{1}{k}\left(f(\bar{x} + \gamma\bar{y}) + \gamma\bar{y} f'(\bar{x} + \gamma\bar{y})\right) \end{bmatrix}.$$

Assume first, that assumption (A3b) holds. Then for $x + \gamma y < f^{-1}(z)$ we have $\dot{x} > 0$. Thus, the solution to (2.15) leaves the set $\left\{(x, y) : x + \gamma y < f^{-1}(z)\right\}$ which implies that P_1 and P_2 are unstable.

On the other hand, if assumption (A3a) holds, the Jacobi matrix at P_1 equals

$$J(P_1) = \begin{bmatrix} f(0) - z & 0 \\ z & -\frac{1}{k} f(0) \end{bmatrix} = \begin{bmatrix} 1 - z & 0 \\ z & -\frac{1}{k} \end{bmatrix}.$$

Clearly in that case for $z > 1$ both eigenvalues of $J(P_1)$ are real and negative, thus, P_1 is a stable node. On the contrary, for $z < 1$ one of the eigenvalues becomes positive, thus, P_1 is

a saddle. Now, we prove that P_1 is locally stable if $z = 1$. Because $z = 1$, f is decreasing and $f(0) = 1$ (see (A2)-(A3a)), thus, $\dot{x}(s) \leq 0$. The function x is non-increasing and bounded from below, thus, it has a limit $\hat{x}$ as $s \to +\infty$. We have $\hat{x} = 0$ or $\hat{x} + \gamma y = 1$. However, the latter case is impossible if $x(0)$ is sufficiently close to 0. In fact, if $x(0) = x_0$ is close to zero, then derivative $\dot{y} \leq x_0 - yf(x_0 + \gamma y)$ is negative for sufficiently large y. Thus, P_1 is locally stable for $z = 1$. In Figure 2.2 we present examples of phase portraits for that case.

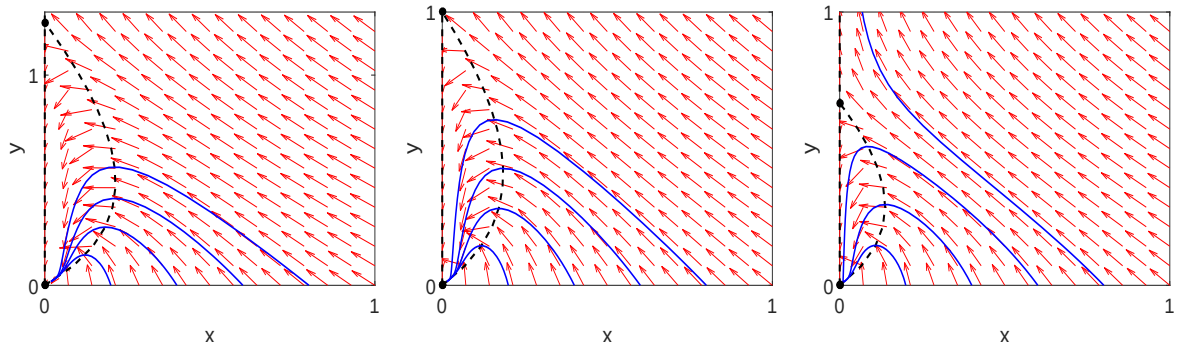

Figure 2.2: Phase portrait of system (2.15) with $z(s) \equiv 1$ and $f(x + \gamma y) = 1 - x - \gamma y$ in case when: (left) $\gamma < 1$, (centre) $\gamma = 1$, (right) $\gamma > 1$. Dashed curves represent null-clines.

If assumption (A3a) holds, assumption (A2) implies that for steady state P_2 we have:

$$J(P_2) = \begin{bmatrix} f(1) - z & 0 \\ -\frac{1}{k\gamma} f'(f^{-1}(0)) + z & -\frac{1}{k}(f(1) + f'(f^{-1}(0))) \end{bmatrix} = \begin{bmatrix} -z & 0 \\ -\frac{f'(1)}{k\gamma} + z & -\frac{1}{k} f'(1) \end{bmatrix}.$$

The eigenvalues of $J(P_2)$ are $-z$ and $-\frac{1}{k} f'(1)$. As f is strictly decreasing (see assumption (A2)), P_2 is a saddle independently of the model parameters.

As far as P_3 is considered assumptions (A2) and (A3) imply:

$$J(P_3) = \begin{bmatrix} \tilde{x} f'(f^{-1}(z)) & \gamma \tilde{x} f'(f^{-1}(z)) \\ z - \tilde{x} f'(f^{-1}(z)) & -\frac{z}{k} - \gamma \tilde{x} f'(f^{-1}(z)) \end{bmatrix} = \begin{bmatrix} -\frac{\delta}{1+k\gamma} & -\gamma \frac{\delta}{1+k\gamma} \\ z + \frac{\delta}{1+k\gamma} & -\frac{z}{k} + \gamma \frac{\delta}{1+k\gamma} \end{bmatrix}.$$

Stability of steady state P_3 depends on the value of trace and determinant of Jacobi matrix:

$$\operatorname{tr}(J(P_3)) = -\left(\frac{z}{k} + (1 - \gamma) \frac{\delta}{1 + k\gamma} \right),$$

$$\det(J(P_3)) = \frac{z}{k} \frac{\delta}{1 + k\gamma} + \gamma z \frac{\delta}{1 + k\gamma} = \frac{z\delta}{1 + k\gamma} \left(\gamma + \frac{1}{k} \right) = \frac{z\delta}{k}.$$

Consequently, the characteristic polynomial of the matrix $J(P_3)$ equals

$$\lambda^2 + \left(\frac{z}{k} + (1 - \gamma) \frac{\delta}{1 + k\gamma} \right) \lambda + \frac{z\delta}{k}. \tag{2.20}$$

The steady state P_3 is asymptotically stable if conditions

$$\frac{z}{k} > (\gamma - 1) \frac{\delta}{1 + k\gamma}, \tag{2.21a}$$

$$\frac{z\delta}{k} > 0, \tag{2.21b}$$

hold. Clearly condition (2.21b) is always fulfilledand condition (2.21a) is equivalent to condition $\gamma k(\delta - z) < k\delta + z$. Hence, for $z \geq \delta$ steady state P_3 is asymptotically stable, as in that case we have $k\delta + z > 0$. On the other hand, if $z < \delta$ steady state P_3 is asymptotically stable provided that $\gamma < 1 + \frac{k+1}{k} \frac{z}{\delta - z}$. This completes the proof. □

We now determine conditions under which the type of steady state P_3 changes. Steady state P_3 can be either a node or a focus depending on the relation between the model parameters. Let us denote

$$k_1 = \frac{(z-\delta)^2}{4z\delta}, \tag{2.22}$$

$$\gamma_1 = \frac{-z^2 + 3kz\delta + z\delta + k\delta^2 - 2\delta(1+k)\sqrt{kz\delta}}{k\left((z-\delta)^2 - 4kz\delta\right)}, \tag{2.23}$$

$$\gamma_2 = \frac{-z^2 + 3kz\delta + z\delta + k\delta^2 + 2\delta(1+k)\sqrt{kz\delta}}{k\left((z-\delta)^2 - 4kz\delta\right)}. \tag{2.24}$$

Theorem 2.9. *Let f satisfy assumptions (A1)-(A3), $z(s) \equiv z$, and the steady state P_3 of system (2.15) exists. Then the steady state P_3 is a node in the following cases:*

(i) $z > \delta$ and

- *$k < k_1$ or $0 < \gamma < \gamma_1$,*

(ii) $z < \delta$,

- *$0 < \gamma < \gamma_1$ or ($\gamma > \gamma_2$ and $0 < k < k_1$).*

P_3 is a focus if:

(i) $z > \delta$, $k > k_1$ and $\gamma > \gamma_1$ or

(ii) $z < \delta$,

- *$k > k_1$ and $\gamma > \gamma_1$ or*
- *$0 < k < k_1$ and $\gamma_1 < \gamma < \gamma_2$,*

where k_1, γ_1, γ_2 are given by Eqs. (2.22)–(2.24).

Proof. We study the determinant Δ of quadratic equation (2.20). We have:

$$\Delta = \left(\frac{z}{k} + \frac{1-\gamma}{1+k\gamma}\delta\right)^2 - 4\frac{z\delta}{k} = \left(\frac{z}{k}\right)^2 + \left(\frac{\gamma-1}{1+k\gamma}\delta\right)^2 + 2\frac{1-\gamma}{k(1+k\gamma)}z\delta - 4\frac{z\delta}{k}.$$

To determine the sign of Δ we determine the sign of $\tilde{\Delta} = k^2(1+k\gamma)^2\Delta$, which equals:

$$\begin{aligned}
\tilde{\Delta} &= ((1+k\gamma)z)^2 + ((\gamma-1)k\delta)^2 + 2(1-\gamma)(1+k\gamma)kz\delta - 4(1+k\gamma)^2kz\delta = \\
&= (1+k^2\gamma^2+2k\gamma)z^2 + (1+\gamma^2-2\gamma)k^2\delta^2 - 2\left(1+\gamma+3k\gamma+k\gamma^2+2k^2\gamma^2\right)kz\delta \\
&= (z^2+\delta^2-2z\delta-4kz\delta)k^2\gamma^2 + 2(z^2-3kz\delta-z\delta-k\delta^2)k\gamma + \left(z^2+k^2\delta^2-2kz\delta\right) \\
&= \left((z-\delta)^2-4kz\delta\right)k^2\gamma^2 + 2\left(z^2-3kz\delta-z\delta-k\delta^2\right)k\gamma + (z-k\delta)^2.
\end{aligned}$$

We obtain quadratic function of γ with a discriminant equal to:

$$\begin{aligned}
\Delta_\gamma &= 4k^2\Big[(z(z-\delta)-k\delta(3z+\delta))^2 - \left((z-\delta)^2-4kz\delta\right)(z-k\delta)^2\Big] \\
&= 4k^2\Big[(z-\delta)^2\left(z^2-(z-k\delta)^2\right) - 2kz\delta(z-\delta)(3z+\delta) + k^2\delta^2(3z+\delta)^2 + 4kz\delta\,(z-k\delta)^2\Big] \\
&= 4k^3\delta\Big[(z-\delta)^2(2z-k\delta) + 2z\left(2\,(z-k\delta)^2 - (z-\delta)(3z+\delta)\right) + k\delta(3z+\delta)^2\Big].
\end{aligned}$$

Combining terms with $2z$ and $k\delta$ we arrive at

$$\begin{aligned}
\Delta_\gamma &= 4k^3\delta\Big[2z\left(2\delta^2-4kz\delta+2k^2\delta^2\right) + k\delta\left(8z^2+8z\delta\right)\Big] = 16k^3z\delta^3(2k+1+k^2) \\
&= 16k^3z\delta^3(1+k)^2.
\end{aligned}$$

Note that Δ_γ is always positive as all parameters are positive, thus, $\Delta_\gamma(\gamma)$ has two real square roots given by Eqs. (2.23) and (2.24).

We introduce notation:

$$a = \left((z-\delta)^2 - 4kz\delta\right)k^2, \quad b = 2\left(z^2 - 3kz\delta - z\delta - k\delta^2\right)k, \quad c = (z-k\delta)^2 > 0.$$

Clearly, if $a > 0$ then $\gamma_1 < \gamma_2$, otherwise $\gamma_2 \leq \gamma_1$. We use Vieta's formulas to verify the sign of γ_1 and γ_2. We see that

$$a > 0 \iff k < k_1,$$
$$b > 0 \iff k < \frac{z(z-\delta)}{\delta(3z+\delta)} := k_2.$$

Note that k_1 is positive for all positive values of z and δ, while k_2 is negative for $z < \delta$. Thus, we consider two cases: $z \geq \delta$ and $z < \delta$.

First for $z \geq \delta$ we have $k_1 \leq k_2$. Indeed, using definition of k_1 and k_2 we have

$$k_1 \leq k_2 \iff (z-\delta)^2(3z+\delta) \leq 4z^2(z-\delta) \iff 0 \leq z^2 + 2z\delta + \delta^2 = (z+\delta)^2.$$

For $0 < k < k_1$ both expressions a and b are positive, thus, both square roots of Δ_γ are negative. As a consequence, for all positive values of γ and $0 < k < k_1$ determinant $\tilde{\Delta}(\gamma)$ is positive and steady state P_3 is a node. For $k > k_1$ coefficient a is negative and $\gamma_2 < 0 < \gamma_1$. Thus, for $\gamma > \gamma_1$ determinant $\tilde{\Delta}(\gamma)$ is negative and steady state P_3 is a focus, while if $0 < \gamma < \gamma_1$ steady state P_3 is a node.

Second for $z < \delta$ we consider two cases: $k > k_1$ or $0 < k < k_1$ (as $k_2 < 0 < k_1$ and we assumed that k is positive). If $k > k_1$ and $z < \delta$ we arrive at the same conclusion as for $k > k_1$ and $z \leq \delta$. If $0 < k < k_1$ we have that $a > 0, b < 0$ and consequently both square roots of Δ_γ are positive. Determinant $\tilde{\Delta}(\gamma)$ is negative when $\gamma \in (\gamma_1, \gamma_2)$, thus, P_3 is a focus. When $0 < \gamma < \gamma_1$ or $\gamma > \gamma_2$, steady state P_3 is a node. □

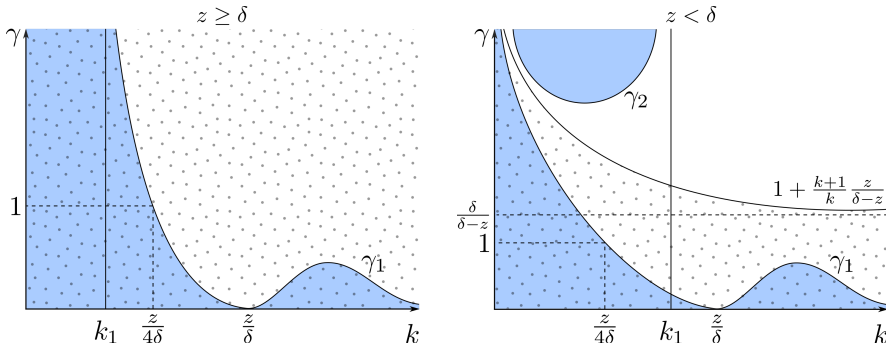

Figure 2.3: Sketch presenting the character of steady state P_3 depending on considered cases: (left) $z \geq \delta$; (right) $z < \delta$. Blue and white areas represent sets of parameters for which P_3 is a node or focus, respectively. Dots denote region where P_3 is stable, no pattern — region where P_3 is unstable.

In Figure 2.3 we graphically illustrated the assertion of Theorem 2.9 presenting the character and stability of steady state P_3 depending on parameters k and γ. Note that for $k = z/\delta$ we have $\gamma_1 = 0$, while for $k = z/(4\delta)$ equality $\gamma_1 = 1$ holds. In addition, condition $\gamma \leq 1$ yields stability of steady state P_3 (if it exists).

Additionally, in Figure 2.4 we present exemplary phase portraits with null-clines represented by dashed curves for $\gamma = 1$ and $f(x+y) = 1 - x - y$, which results in a logistic model. In that case steady state P_1 is either stable node if $z > 1$ or saddle if $z < 1$. P_2 is a saddle independently of model parameters. P_3 is locally stable as both conditions (2.21a) and (2.21b)

hold (as $\gamma = 1$). To be specific, P_3 is a stable node when $k < \frac{z}{4(1-z)}$ and a stable focus when $k > \frac{z}{4(1-z)}$. In Figures 2.5 and 2.6 we present exemplary phase portraits with null-clines for $f(x+\gamma y) = 1 - x - \gamma y$ in a case when $z < 1$ and $z > 1$, respectively. The phase portraits drawn numerically agrees with the analytical results presented in Theorems 2.8 and 2.9.

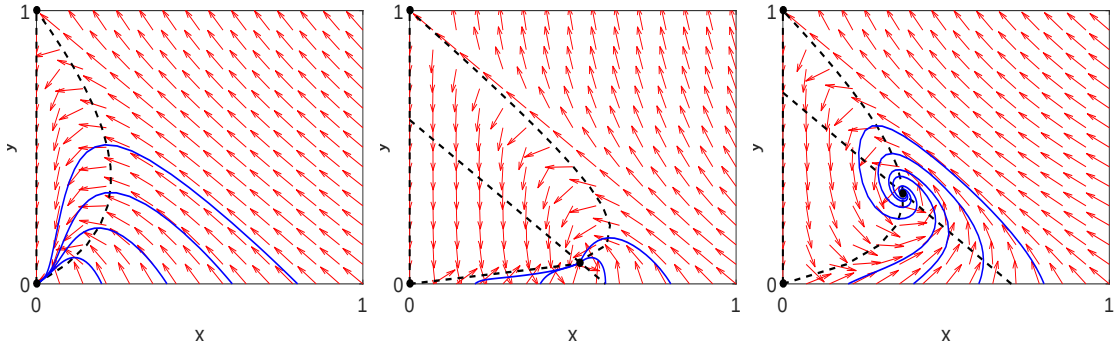

Figure 2.4: Phase portrait of system (2.15) with $z(s) \equiv z$, $f(x+\gamma y) = 1 - x - \gamma y$ and $\gamma = 1$ in case when: (left) the positive steady state P_3 does not exist, $z = 1.3, k = 0.5$, (centre) P_3 is a stable node, $z = 0.4, k = 0.15$, (right) P_3 is a stable focus, $z = 0.3, k = 0.9$. Dashed curves represent null-clines.

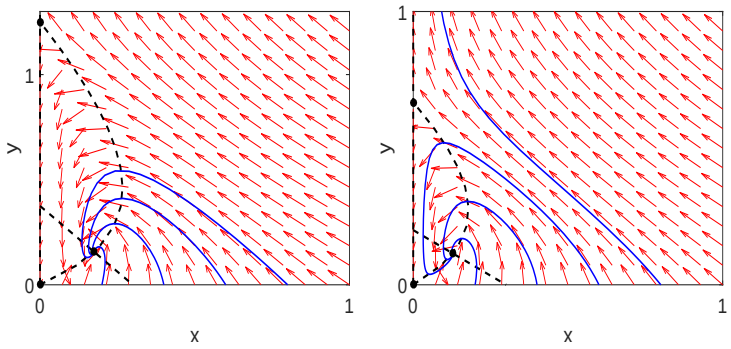

Figure 2.5: Phase portrait of system (2.15) with $z(s) \equiv z < 1$, $f(x+\gamma y) = 1 - x - \gamma y$ and either $\gamma < 1$ (left) or $\gamma > 1$ (right). Dashed curves represent null-clines.

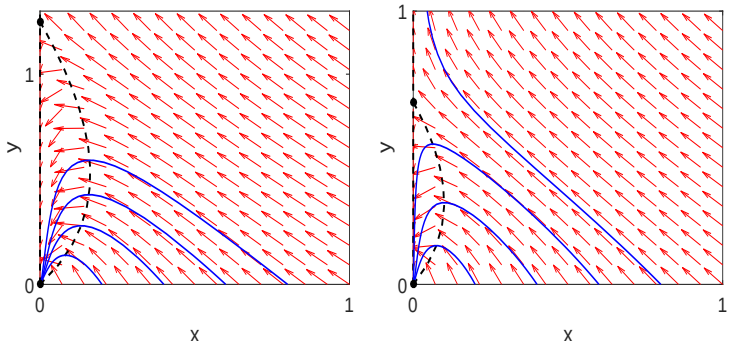

Figure 2.6: Phase portrait of system (2.15) with $z(s) \equiv z > 1$, $f(x+\gamma y) = 1 - x - \gamma y$ and either $\gamma < 1$ (left) or $\gamma > 1$ (right). Dashed curves represent null-clines.

Lemma 2.10. *Let f satisfy assumptions (A1)-(A3), $z(s) \equiv z$, and the steady state P_3 exists. If $\gamma \leq 1$ then there is no periodic solution to system (2.15) in the interior of a set $\Omega_2 = \{(x, y) : x \geq 0, y \geq 0, x + \gamma y \leq 1\}$.*

Proof. To prove that system (2.15) has no periodic solutions we use Dulac criterion [135]. We consider a variable u defined by Eq. (2.16). Then system (2.15) with $z(s) \equiv z$ has the following form:

$$\begin{aligned} \dot{x}(t) &= x(f(u) - z), \\ \dot{u}(t) &= \frac{f(u)}{k}\left((k+1)x - u\right) + (\gamma - 1)zx. \end{aligned} \tag{2.25}$$

Let us denote by F the right-hand side function of system (2.25) and let us take the function $\psi(x,u) = \frac{1}{xf(u)}$ as a Dulac function [160]. We calculate:

$$\begin{aligned} \operatorname{div}(\psi F) &= \frac{\partial}{\partial x}\left[\frac{1}{xf(u)}x(u-z)\right] + \frac{\partial}{\partial u}\left[\frac{1}{xf(u)}\left(\frac{f(u)}{k}\left((k+1)x-u\right) + (\gamma-1)zx\right)\right] \\ &= -\frac{1}{xk} + \frac{z(1-\gamma)}{f^2(u)}f'(u). \end{aligned}$$

The expression above for $\gamma \leq 1$ has the same sign (negative and non-zero) almost everywhere in Ω. As a consequence, system (2.25) does not have closed orbits. □

Theorem 2.11. *Let f satisfy assumptions (A1)-(A2), $z(s) \equiv z$, and $\gamma \leq 1$.*

(i) If f satisfy additionally (A3a) and $z \geq 1$ all trajectories of system (2.15) starting in $\{(x,y) : x \geq 0,\ y \geq 0,\ x + \gamma y < 1\}$ converge to P_1.

(ii) If $z < 1$ or f satisfies (A3b), all trajectories of system (2.15) starting in $\{(x,y) : x > 0,\ y \geq 0,\ x + \gamma y < 1\}$ converge to P_3.

Proof. The assertion of the theorem follows from Lemma 2.10, the Poincare-Bendixson theorem [135] together with the analysis of the phase portraits. □

2.2.2 The case of asymptotically periodic chemotherapy function

Now let us study the asymptotic behaviour of system (2.15) when function z is not constant and is given by

$$z(s) = z_{\text{per}}(s) + z_{\text{rest}}(s), \tag{2.26}$$

following Definition 2.1, being asymptotically periodic with period $\widetilde{T}$. We show that for any asymptotically periodic function z such that mean value of this function converges to a value not smaller than 1, the solutions of system (2.15) tend to steady state P_1.

Theorem 2.12. *Let f satisfy assumptions (A1)–(A2), (A3a) and z be an asymptotically periodic function with period $\widetilde{T}$ in the sense of Definition 2.1. If*

$$\bar{z} = \frac{1}{\widetilde{T}}\int_0^{\widetilde{T}} z_{\text{per}}(s)\mathrm{d}s \geq 1,$$

and the integral $\int_0^{+\infty} z_{\text{rest}}(s)\mathrm{d}s$ is convergent, then the solution of system (2.15) converges to P_1.

Proof. Due to the fact that f is decreasing, $\gamma > 0$, x and y are non-negative we have $xf(x+\gamma y) \leq xf(x)$ and as a consequence

$$\dot{x} = x\left(f(x+\gamma y) - z(s)\right) \leq x\left(f(x) - z(s)\right)$$

holds. The Gronwall inequality implies

$$\begin{aligned} x(s) &\le x(0)\exp\left(\int_0^s (f(x(v)) - z(v))\,\mathrm{d}v\right) \\ &= x(0)\exp\left(\int_0^s ((f(x(v)) - 1) + (1 - z_{\mathrm{per}}(v)) - z_{\mathrm{rest}}(v))\,\mathrm{d}v\right). \end{aligned}$$

We divide the integrand into three components. First includes function depending only on x, second – periodic function on the interval which length is a multiplication of period and in the last component we group the remaining terms. To this end for any $s \ge 0$ we find $m \in \mathbb{N} \cup \{0\}$ and $\tilde{s} \in [0, \widetilde{T})$ such that $s = m\widetilde{T} + \tilde{s}$ and we rewrite the last inequality in the following manner

$$x(s) \le x(0) A(s) B_m E(s),$$

where

$$\begin{aligned} A(s) &= \exp\left(-\int_0^s (1 - f(x(v)))\,\mathrm{d}v\right), \\ B_m &= \exp\left(\int_{\tilde{s}}^{\tilde{s}+m\widetilde{T}} (1 - z_{\mathrm{per}}(v))\,\mathrm{d}v\right) = \exp\Big(m\widetilde{T}\,(1 - \bar{z})\Big), \\ E(s) &= \exp\left(\int_0^{\tilde{s}} (1 - z_{\mathrm{per}}(v))\,\mathrm{d}v\right)\exp\left(-\int_0^s z_{\mathrm{rest}}(v)\mathrm{d}v\right). \end{aligned}$$

Note that $E(s)$ is uniformly bounded because $\tilde{s} \in [0, \widetilde{T})$ and the integral $\int_0^{+\infty} z_{\mathrm{rest}}(s)\mathrm{d}s$ is convergent.

First, consider $\bar{z} > 1$. Then $A(s) \le 1$ as f is decreasing and $x(s) \ge 0$ for all times s. Moreover,

$$B_m = \exp\Big(-m\widetilde{T}\,(\bar{z} - 1)\Big)0 \quad \text{as } s \to +\infty.$$

Thus, $x(s) \to 0$ as $s \to +\infty$.

Now, assume that $\bar{z} = 1$. Then $B_m = 1$. As $x(s) \ge 0$ for all s and f is decreasing, we have $\int_0^{+\infty} (1 - f(x(v)))\,\mathrm{d}v \le +\infty$. If this integral is convergent, then due to the boundedness of derivative of $f(x(s))$, $(1 - f(x(s))) \to 0$ holds for $s \to +\infty$. As a consequence, $x(s) \to 0$ as $s \to +\infty$ due to the continuity of f. On the other hand, the divergence of the integral implies $A(s) \to 0$ as $s \to +\infty$. This proves that $x(s) \to 0$ as $s \to +\infty$ because $E(s)$ is uniformly bounded, as stated before.

We have proved that $x(s) \to 0$ and consequently $y(s) \to 0$ as $s \to +\infty$. □

The model behaviour for $\bar{z} < 1$ is more complex. Numerical simulations suggest that the steady state P_1 is repulsive in that case, see an example in Figure 2.7. However, if $z(s)$ is a periodic function and its values remain inside the interval $(0, 1)$, then we can prove the existence of a periodic solution.

Theorem 2.13. *Let f satisfy assumptions (A1)–(A2), (A3a), z be a periodic function with period T, and $\gamma \le 1$. If there exist z_m and z_M such that $0 < z_m \le z(t) \le z_M < 1$ for all positive t, then there exists a periodic solution to system (2.15) with a period $\widetilde{T}$.*

Proof. For convenience we consider system (2.15) in variables x and u, which has the following form:

$$\begin{aligned} \dot{x}(s) &= x(f(u) - z(s)), \\ \dot{u}(s) &= \frac{f(u)}{k}\left((k+1)x - u\right) + (\gamma - 1)\,xz(s). \end{aligned} \tag{2.27}$$

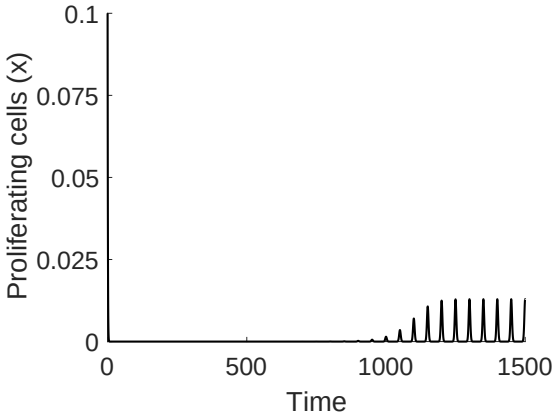

Figure 2.7: Evolution of x in time due to system (2.15) for $\bar{z} < 1$. The parameters values were: $\gamma = 1, k = 10$ and $z(s) = 0.98(1 + \sin\left(2\Pi s/\widetilde{T}\right))$ with $\widetilde{T} = 50$.

Moreover, Theorem 2.6 allows us to limit our considerations to the set:

$$\Omega_u = \{(x, u) \in \mathbb{R}^2 : 0 < x \leq u \leq 1\}.$$

For any $(x_0, u_0) \in \Omega_u$ we define the operator

$$\Phi(s, x, u) = \Big(x(s; x_0, u_0), u(s; x_0, u_0)\Big), \quad \Phi_{\widetilde{T}}(x, u) = \Phi(\widetilde{T}, x, u),$$

where $\Big(x(s; x_0, u_0), u(s; x_0, u_0)\Big)$ is a solution of system (2.27) with initial condition $x(0) = x_0$, $u(0) = u_0$. Note that if some $(x_0, u_0) \in \Omega_u$ is a fixed point for the operator $\Phi_{\widetilde{T}} \colon \Omega_u \to \Omega_u$ then, due to the assumption of periodicity of z, solution of system (2.27) with initial condition (x_0, u_0) is periodic.

We use the Brouwer theorem [137] to show that such fixed point of the operator $\Phi_{\widetilde{T}}$ exists. To this end, we show that there exists a convex compact subset $K \subset \Omega_u$ such that $\Phi_T(K) \subset K$. Note that a closure of Ω_u is not a good choice because it contains steady states of system (2.27).

Vector field corresponding to system (2.27) is the following one:

$$F_z(s) = \left[x(f(u) - z(t)), \frac{f(u)}{k}\Big((k+1)x - u\Big) + (\gamma - 1)xz(s)\right].$$

Let us divide the set Ω_u in four sets

$$\Omega^1 = \left\{(x, u) \in \mathbb{R}^2 : \frac{u}{1+\gamma k} \leq x \leq u,\ 1 - z_m \leq u \leq 1\right\},$$
$$\Omega^2 = \left\{(x, u) \in \mathbb{R}^2 : 0 \leq x \leq \frac{u}{1+\gamma k},\ 1 - z_M \leq u \leq 1\right\},$$
$$\Omega^3 = \left\{(x, u) \in \mathbb{R}^2 : 0 \leq x \leq \frac{u}{1+\gamma k},\ 0 \leq u \leq 1 - z_M\right\},$$
$$\Omega^4 = \left\{(x, u) \in \mathbb{R}^2 : \frac{u}{1+\gamma k} \leq x \leq u,\ 0 \leq u \leq 1 - z_m\right\}.$$

Now, we define the border of the set K. Let φ_1 be a trajectory of system (2.15) with $z \equiv z_m$ and arbitrary chosen initial condition $(x_0, x_0) \in \Omega^1$ for time $[0, s^*]$, where s^* is the first point $t > 0$ at which this trajectory reaches the boundary of Ω^1. Because of the direction vector field

F_{z_m} (which is independent of time) in Ω^1, the trajectory φ_1 reaches the line $(\kappa+\gamma)x = \kappa u$ at s^*. Let us call this point (x_1, u_1). Let φ_2 be a trajectory of system (2.15) with $z \equiv z_M$ and initial condition (x_1, u_1) for time $[0, s^{**}]$, where s^{**} is the first point $t > 0$ such that the trajectory φ_2 reaches the boundary of Ω^2. Because of the direction vector field F_{z_M} (which is independent of time) in Ω^2, the trajectory φ_2 reaches the line $u = 1 - z_M$. Denote this point (x_2, u_2). As φ_3 we denote the line that connects points (x_2, u_2) with (x_2, u_3) lying on the line $u = (1+\gamma k)x$, thus, $u_3 = (1+\gamma k)x$. We denote by φ_4 the horizontal line between (x_2, u_3) and (u_3, u_3). Finally, we denote the line connecting points (u_3, u_3) and (x_0, x_0) by φ_5. Obviously, the curve $\Gamma = \varphi_1 \cup \varphi_2 \cup \varphi_3 \cup \varphi_4 \cup \varphi_5$ appoints a convex set in Ω_u. We denote the set bounded by this curve (with the boundary) by K, compare Figure 2.8.

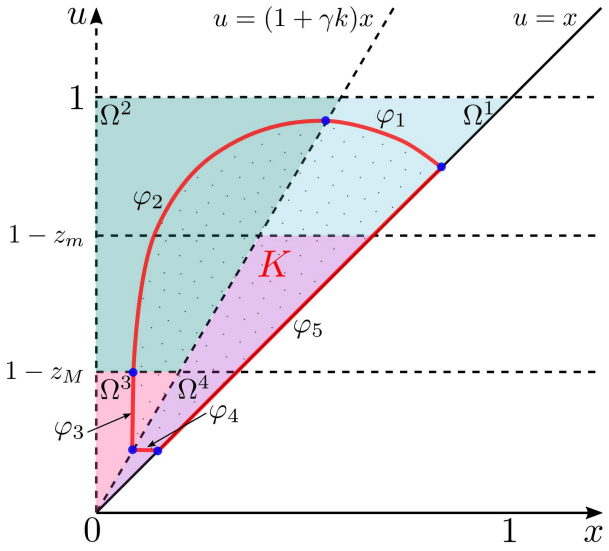

Figure 2.8: Sketch of set K (dotted region) defined in proof of Theorem 2.13. Blue points denote points (x_0, x_0), (x_1, u_1), (x_2, u_2), (x_2, u_3) and (u_3, u_3).

We show, that if $(x(0), u(0)) \in K$ then for all $s \geq 0$ $(x(s), u(s)) \in K$, where $(x(s), u(s))$ is a solution of system (2.15). Two parts of the boundary of K are the trajectories of system (2.15) with $z \equiv z^*$, where $z^* = z_m$ or $z^* = z_M$. The normal vector to such trajectory pointing towards the interior of K is

$$\vec{n}(z^*) = \left[-f(u)\Big((\kappa+1)x - \kappa u\Big) - (\gamma-1)xz^*, x(f(u) - z^*)\right].$$

Let $(x(s), u(s))$ be a solution of (2.15) and assume that for some s^* it reaches the set $\varphi_1 \cup \varphi_2$. Then, the scalar product of the vector tangent to the trajectory with the normal vector $\vec{n}$ is

$$\langle F_z(s), \vec{n}\rangle = xf(u)(z(s) - z^*)\Big((\kappa+1)x - \kappa u + (\gamma-1)x\Big).$$

Assume now, that $(x(s^*), u(s^*)) \in \varphi_1$. Then, $z^* = z_m$, hence, $z(s) \geq z_m$ and $(\kappa+\gamma)x - \kappa u \leq 0$ as $\varphi_1 \subset \Omega^1$. Thus, $\langle F_z(s), \vec{n}\rangle \geq 0$. Similarly, if $(x(s^*), u(s^*)) \in \varphi_2$ then $z^* = z_M$, hence, $z(s) \leq z_M$ and $(\kappa+\gamma)x - \kappa u \geq 0$ as $\varphi_2 \subset \Omega^2$. Thus, again $\langle F_z(s), \vec{n}\rangle \geq 0$. Note, that in Ω^3 we have $\dot{x}(s) > 0$. Similarly, in Ω^4 the derivative of u is positive. Thus, on the lines φ_3 and φ_4, the vectors of the vector field points towards the interior of K. Finally, it is easy to see that on φ_5 the vector field is also pointing towards the interior of K because as it was shown before, solutions $x(s)$, $y(s)$ are positive and $u(s) = x(s) + \gamma y(s) \leq 1$. This implies that solution of (2.15) that starts in K cannot leave this set. And therefore,

$\Phi_{\tilde{T}}(K) \subset K$. In Figure 2.8 we present the sketch of the set K, curves φ_i, $i = 1, \ldots, 5$, and sets Ω^j, $j = 1, 2, 3, 4$.

Thus, the Brouwer theorem yields existence of a fixed point of Φ_T, and thus, a periodic solution of (2.27). □

2.3 Numerical results

In this section we show that model (2.2) fits well to the patients data as well as study numerically how the model behaviour depends on parameters. For the purpose of model fitting to patients data and numerical analysis we will assume the logistic model of tumour growth as it is typically done for that kind of tumours, thus, we consider f to be as in Eq. (2.1). Note that taking an average cell volume, we can easily treat the tumour mass $P + D$ as the total tumour volume, which is easier to compare with results obtained from MRI scans, usually used in brain tumour diagnosis and follow-up observation.

2.3.1 Values of the model parameters

To work with system (2.2) and function f as in Eq. (2.1) we need to provide realistic values for the model parameters. All parameters of the model are assumed to be positive due to their biological interpretation.

The saturation coefficient K for LGG growth will be set to the volume of a sphere of diameter 10 cm reported to be the maximal mean tumour diameter observed in LGG patients [69]. In fact, patient death usually occurs when the tumour reaches a critical size called the fatal tumour burden considered to be in high-grade glioma models to be around 6 cm in diameter [108, 102] We will use this value subsequently in order to analyse different outcomes of virtual patients.

We can estimate the rate of drug decay λ using values of TMZ half-life clearance time $t_{1/2}$. From the definition of $t_{1/2}$ and assuming exponential decay as in system (2.2) we have

$$\frac{1}{2} = \mathrm{e}^{-\lambda t_{1/2}}.$$

To account also for the drug loss during transport to the brain we calculate value C_j of the maximal dose d_j reaching the tumour as

$$C_j = \beta \cdot d_j \cdot b, \tag{2.28}$$

where β is the fraction of TMZ getting to 1ml of brain interstitial fluid (from a unit dose) and b is a surface of a patient body with $j \in \{1, \ldots, n\}$ and n being the total number of doses d administered. Then C_j can be interpreted as an effective dose per fraction.

Standard dose per day is 150 mg per m^2 of patient body surface, which is usually around 1.6 m^2 for women and 1.9 m^2 for men [161] with an average of 1.7 m^2 [162]. Then in the case of the standard chemotherapy scheme we will fix dose $d_j = d = 150$ mg/m^2 and effective dose $C_j = C_0 = \beta \cdot d \cdot b$.

The parameter β can be calculated using the value of maximal TMZ concentration $C_{\max}$ for a dose of 150 mg/m^2 taken from the literature [78, 157]. Assuming that time to reach peak drug concentration in the brain is negligible (equals 0.85-2h) in comparison to the time scale of the model, we set the drug concentration C_0 in the moment of its administration to the value $C_{\max}$.

A summary of the biological parameter values is presented in Table 2.1.

Table 2.1: **Biological parameters describing TMZ concentration in brain.**

Parameter	Description	Value, references	
$t_{1/2}$	TMZ half-life clearance time	$\simeq$2h	[78]
C_{max}	mean peak TMZ concentration in brain interstitium	0.6 μg/ml	[157]
λ	rate of decay of TMZ	0.3466/h	Calculated from [78, 157]
β	fraction of TMZ getting to brain interstitium	$2.1 \cdot 10^{-6}$/ml (m) $2.5 \cdot 10^{-6}$/ml (w)	Estimated from [78, 157]

2.3.2 Model fitting to patients data

To test if our simple model given by system (2.2) with function f as in Eq. (2.1) is able to reflect the dynamics of LGG response to chemotherapy, we have used the model to describe volumetric longitudinal data of patients followed at the Bern University Hospital, see details in Section 1.7. In this study we selected data on 18 patients who had been treated with TMZ out of a total number of 82 LGGs patients, see Table 2.2. The inclusion criteria for patients for the purpose of model fitting in this study included:

(i) biopsy/surgery confirmed LGG (astrocytoma, oligoastrocytoma or oligodendroglioma), according to the WHO classification at the time of diagnosis,
(ii) availability of at least 2 MRI scans before the onset of TMZ treatment,
(iii) no other treatment given in the period of study,
(iv) availability of at least 4 MRI scans after TMZ onset with at least one after the end of the chemotherapy.

Seven patients satisfied these criteria. All patients in this group received more than 4 TMZ cycles and the mean duration of TMZ treatment was 6.26 months.

Table 2.2: **Characteristics of patients treated with TMZ**

Age at diagnosis, mean (st. deviation), yr	47.19 (7.54)
Sex, M/F	14/4
Histology at diagnosis	
Oligodendroglioma	7
Oligoastrocytoma	9
Astrocytoma	1
Unknown	1
Type of surgery	
Biopsy	10
Resection	9
Radiotherapy	8
Chemotheraphy (CT)	18
Age at CT onset, mean (st. deviation), yr	51.8 (8.35)
Time from surgery to CT, mean (st. deviation), yr	3.7 (4)
Second-line CT	8

The rate of tumour cell proliferation ρ, the coefficient k describing the delay in damaged cell death and the parameter of TMZ-cell kill strength α were considered to be tumour-specific and fitted for each patient. Thus, only three parameters are unknown and the others are taken as in Table 2.1.

Note that until the beginning of the treatment $D \equiv 0, C \equiv 0$, thus, the tumour growth is

governed by a simple logistic equation:

$$P(t) = \frac{K P_0 e^{\rho t}}{K - P_0 (1 - e^{\rho t})}. \tag{2.29}$$

Thus, to estimate the parameter ρ we used patient data before the start of TMZ administration since it is the only relevant parameter during that time. The initial tumour volume P_0 in this equation was fixed to be the volume from first MRI scan done after surgery. Then, having obtained the value of ρ, MRI data after the onset of chemotherapy was used to estimate parameters α and k in system (2.2). To simulate system (2.2), we have used the standard Matlab ODE solver based on the Runge-Kutta 4th-order method. Model fitting was done on the basis of a relative least squares method, *cf.* Section 1.7, using built-in MATLAB function *lsqnonlin* [140].

Figure 2.9 shows both the real tumour volume data obtained from the MRI scans (circles) together with the best fit (solid line) obtained with system (2.2), where function f was defined by Eq. (2.1). Parameters values obtained by model fitting to patient data and the number of TMZ cycles applied to each patient are listed in Table 2.3. The model dynamics fit the real volumetric tumour evolution well, showing an impressive agreement with a minimal number of parameters for patients with delayed response to chemotherapy. The minimal value of the fitted proliferation rate for some patients is one order of magnitude smaller than values $(1-5)\cdot 10^{-3}$ day^{-1} observed in other studies [25, 1, 26] as in these studies the model for tumour growth also considered a diffusive term. Some of the tumours were relatively large, however no formation of neoangiogenesis or necrotic core was observed.

Table 2.3: **Values of parameters fitted for each patient in the study and the number of TMZ cycles applied, together with the minimal doses d_{min} that should be applied according to Theorem 2.12**

Patient id	TMZ cycles	ρ (/day)	α (ml/μg/day)	k	$d_{\min}$ (mg/m^2)
10	13	0.00022	0.199094	0.075644	12.8999
25	4	0.002416	1.387798	0.272291	20.3232
57	10	0.000338	0.17367	0.019279	22.7203
108	5	0.001761	0.971918	0.555867	21.1520
151	12	0.000701	0.236439	0.257806	34.6115
159	11	0.000136	0.279911	0.025617	5.4218
170	15	0.001652	0.203217	0.002087	94.9012
mean	10	0.001032	0.49315	0.172656	24.4299
st. deviation	4.0852	0.00090228	0.485383	0.203174	—

2.3.3 Tumours with faster response have worse prognosis

We have also studied how the tumour response depends on parameters fitted, see Figures 2.11 and 2.12. We denote by "time to radiological progression" t_{RP} the time when the tumour attains its minimum volume after the chemotherapy onset and starts regrowing. We refer to "growth delay" as the time for which the tumour volume equals the initial one when regrowing after the therapy, see [1]. We refer to "early response" when t_{RP} is attained shortly after the end of chemotherapy and "no response" when there was no decrease in tumour volume.

In case of frequent MRI scans these times can be easily obtained from model simulations and compared with the values obtained from patient's MRI volumetry. It can be estimated

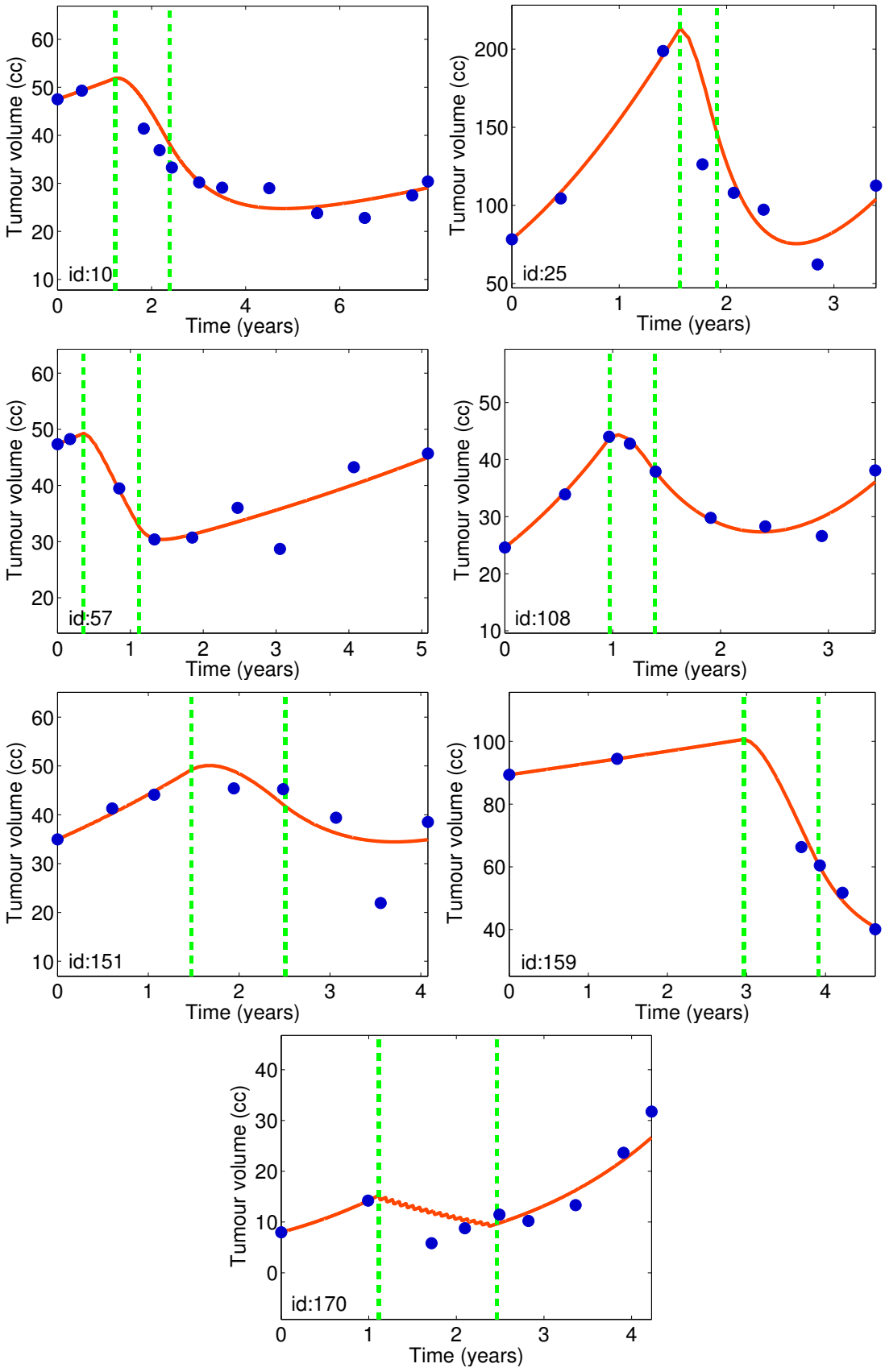

Figure 2.9: Tumour volume evolution for selected patients treated with TMZ. The beginning and the end of TMZ treatment are marked with vertical dashed lines. There are shown the volumes calculated from MRI scans (circles) and from the fitted mathematical model (solid lines). The number of TMZ cycles and the values of parameters were different for each patient as indicated in Table 2.3.

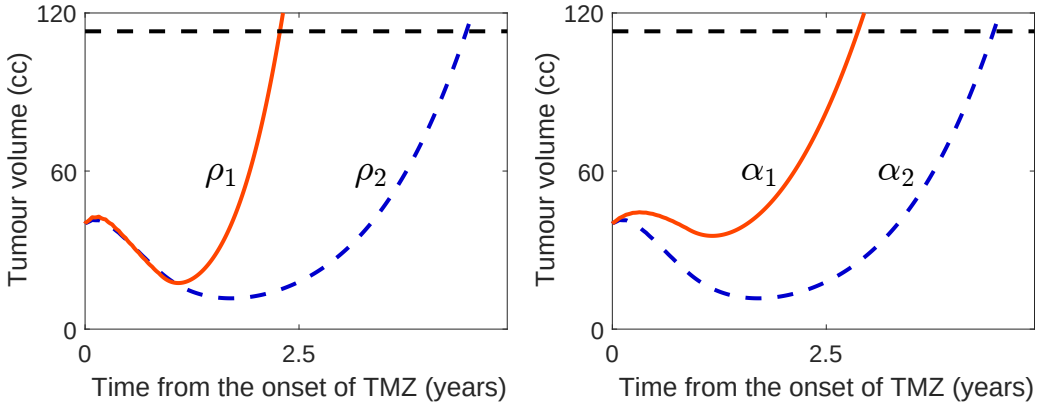

Figure 2.10: Virtual tumour volume evolution after the onset of TMZ treatment for different values of parameters. We considered 12 cycles of TMZ delivered using the standard procedure (see Section 2.1.2) for virtual patients with LGG of initial volume 40 cm^3 and with $k = 0.5$. (left) Parameter α was fixed to value 0.8ml/μg/day, $\rho_1 = 0.006$/day, $\rho_2 = 0.003$/day. (right) Parameter ρ was fixed to value 0.003/day, $\alpha_1 = 0.4$ml/μg/day, $\alpha_2 = 0.8$ml/μg/day. The horizontal dotted lines correspond to tumour sizes equal to the fatal tumour burden.

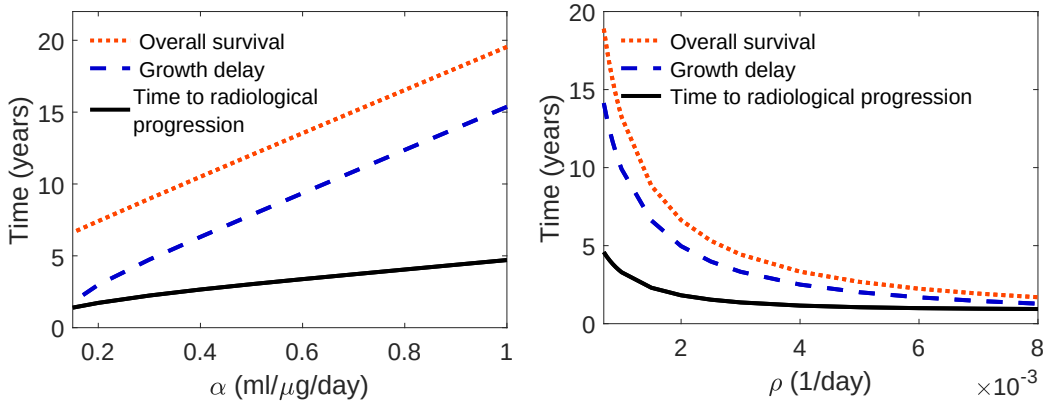

Figure 2.11: Characteristic times of tumour response for different proliferation rates ρ and different levels of TMZ cell kill strength α. We considered 12 cycles of TMZfor virtual patients with LGG of initial volume 40 cm^3. (left) Results for $\rho = 0.0008$/day, $k = 0.3$ and $\alpha \in [0.1, 1]$ml/μg/day. (right) Results for $\alpha = 0.8$ml/μg/day, $k = 0.3$ and $\rho \in [0.7, 8] \times 10^{-3}$/day.

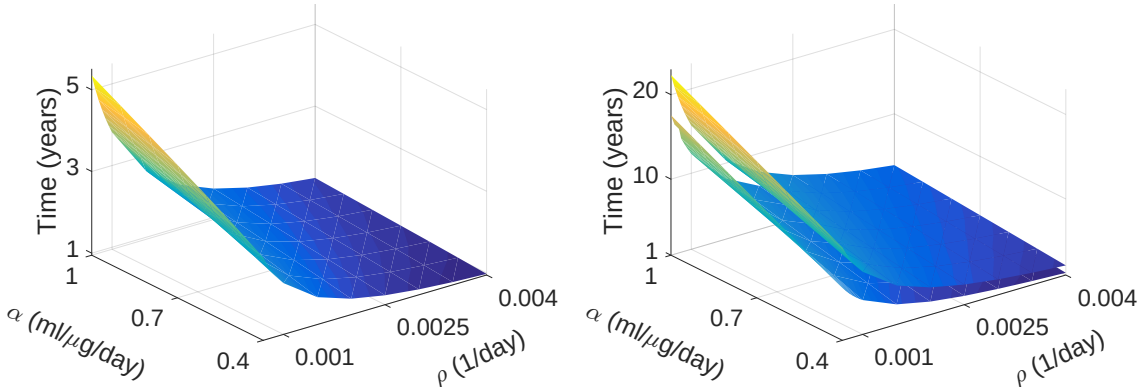

Figure 2.12: Characteristic times of tumour response for different proliferation rates ρ and different levels of TMZ cell kill strength α. We considered 12 cycles of TMZwith $k = 0.3$. Values of time to radiological progression (left), growth delay and overall survival (right) are shown for virtual patients with LGG of an initial volume of 40 cm^3.

with an error of an order of the time between two subsequent MRI scans. We have also

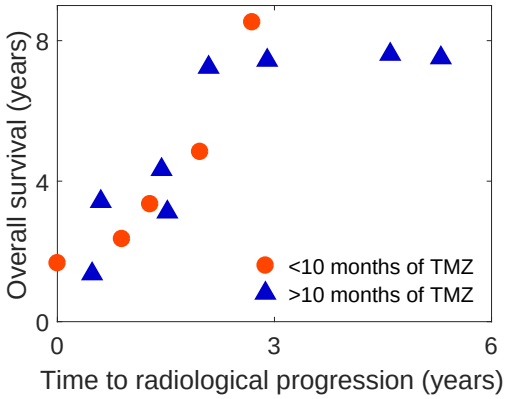

Figure 2.13: Time to radiological progression and overall survival of LGGs patients treated with TMZ. Patients were divided into two groups: in the first, denoted by circles, patients were treated with TMZ for less than 10 months (average: 5.72, st. deviation: 3.8), in the second group, denoted by triangles, patients were treated with TMZ for more than 10 months (average: 13.65, st. deviation: 3.14).

computed the estimate of overall survival (OS) as the time until reaching the fatal tumour burden defined in Section 2.3.1. We have considered only the cases of virtual tumours whose volumes decreased below the volume at TMZ onset. Note that for the purpose of analysis of response to TMZ, OS is computed for virtual tumours responding to TMZ and without any other treatment in the following course of disease. Therefore, in general, the obtained OS could be overestimated and thus should not be compared to the values of real-patients survival.

After performing many simulations for different initial values and chemotherapy schemes, we conclude that both larger proliferation rate ρ and smaller TMZ cell kill strength α, lead to an earlier response to TMZ treatment. A more systematic study is shown in Figure 2.10 for two specific parameter sets, providing representative examples. Virtual patients who responded earlier to TMZ (had smaller t_{RP}) had a faster regrowth and reached the fatal tumour burden earlier. Thus, a shorter t_{RP} is an indicator of worse prognosis.

Are these model features also present in the patient's data? Figure 2.13 shows how the overall survival rate correlates with the time to radiological progression. For the purpose of this analysis we also included patients with only one MRI scan before treatment with TMZ in the patient group indicated in Section 2.3.2. At the same time we excluded (i) two patients in which only two MRI scans were available after the end of chemotherapy showing no tumour regrowth and (ii) one patient treated with TMZ for only 1.5 month showing no response. For each patient t_{RP} was estimated as the time to the MRI scan in which tumour volume was the smallest after the onset of treatment. Due to the substantially different duration of TMZ treatments we divided patients into a group receiving less than 10 TMZ cycles and those receiving 10 or more cycles.

The Spearman rank correlation coefficient between t_{RP} and OS equals 1 for data of patients treated with TMZ for less than 10 months and 0.9047619 for those treated with TMZ for longer time. The exact Spearman coefficient test significance levels equal 0.008333 and 0.002282 for right-tailed tests for group of patients treated with less and more than 10 cycles of TMZ, respectively. This result indicates a positive correlation between t_{RP} and OS. The significance levels were calculated using R. Data on overall survival is right-censored, however the results suggest that the early regrowth of the tumour after chemotherapy is related to its aggressiveness. Despite therapies used after progression, those tumours that responded faster

to TMZ treatment progressed faster, suggesting either larger proliferation potential and/or smaller TMZ cell kill strength.

2.3.4 Tumours with smaller response have worse prognosis

We study whether change in tumour volume after chemotherapy can be also an indicator of prognosis. In order to do so, based on the results of simulations we estimate tumour volume decrease at time to radiological progression and verify whether it correlates with tumour aggressiveness. Let us define the relative tumour volume decrease ΔV as

$$\Delta V = \frac{P_1 - V_{\mathrm{RP}}}{P_1}, \tag{2.30}$$

where P_1 is tumour volume just before the onset of chemotherapy and V_{RP} is tumour volume at the time to radiological progression. We suggest using such a relative difference as it does not depend on initial tumour size.

Figure 2.14 shows how the tumour volume decrease ΔV depends on tumour-specific parameters: ρ and α. Based on numerous simulations of system (2.2) we deduce that a virtual patient with smaller volume decrease is more aggressive in terms of proliferation potency or resistance to chemotherapy, thus, its prognosis is worse.

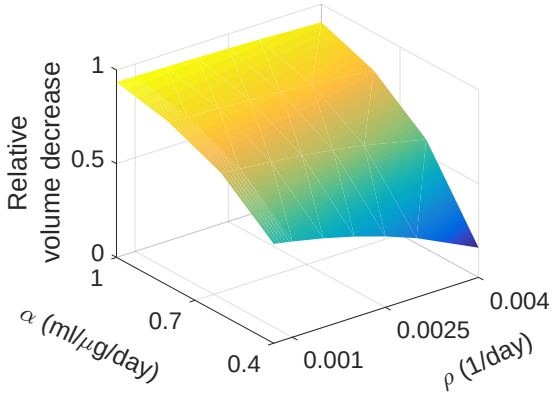

Figure 2.14: Relative tumour volume decrease for different proliferation rates ρ and different levels of TMZ cell kill strength α. We considered 12 cycles of TMZfor virtual patients with LGG of initial volume 40 cm^3.

We also try to verify whether such relation exists in a real life. In Figure 2.15 we present how the overall survival rate relates with the relative volume decrease for the same set of patients data as in Section 2.3.3. Correlation rate between tumour volume decrease and overall survival equals 0.6. Thus, in general, patients who had smaller response to chemotherapy (that is ΔV is smaller) have worse prognosis.

2.4 Analytical estimates of tumour response to chemotherapy

2.4.1 Survival fraction

Up to now our numerical analysis has been based on simulations of system (2.2) with function f as in Eq. (2.1). We can calculate the fraction of tumour cells eliminated by a single dose of chemotherapy, which in the context of radiotherapy is usually referred to as "survival fraction". To do so, we assume that the time of drug absorption, distribution and elimination from the

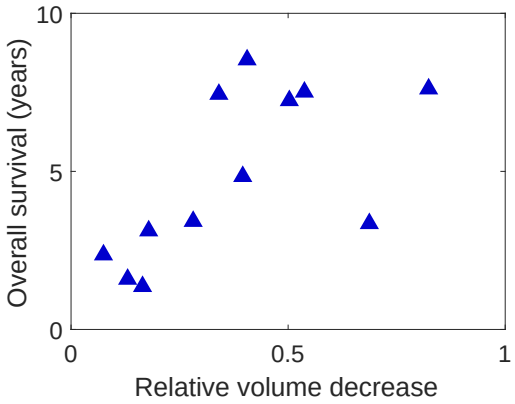

Figure 2.15: Relative volume decrease and overall survival of LGGs patients treated with TMZ.

human body is much shorter than the doubling time of the tumour cell population, what is true for LGGs. Therefore, focusing on short-term effects of the drug we may neglect the term describing tumour proliferation. Consequently the size of damaged cells population remains zero and we consider instead the simplified model

$$\dot{P}(t) = -\alpha P C,$$
$$\dot{C}(t) = -\lambda C$$

with initial condition:

$$P(0) = P_0, \quad C(0) = C_0.$$

For time before the second drug administration we have

$$C(t) = C_0 \mathrm{e}^{-\lambda t},$$
$$P(t) = P_0 \exp\left(\frac{\alpha}{\lambda} C_0 \left(\mathrm{e}^{-\lambda t} - 1\right)\right).$$

Then we define a function S_f describing the survival fraction as follows

$$S_f(t) = \frac{P(t)}{P_0} = \exp\left(\frac{\alpha}{\lambda} C_0 \left(\mathrm{e}^{-\lambda t} - 1\right)\right).$$

Thus, for long times $t \gg 1/\lambda$ we obtain the formula

$$S_f = \exp\left(-\frac{\alpha}{\lambda} C_0\right).$$

Survival fraction depends exponentially on the TMZ cell kill strength α, the effective dose C_0 and inversely on the time of exposure to chemotherapy λ. This formula is similar to the linear term in the linear-quadratic model describing the effect of a single dose of radiotherapy on cells [132].

2.4.2 Generalised chemotherapy fractionation scheme

In the following subsection we compute analytical estimates for the t_{RP} as a function of the model parameters. We study a broad range of chemotherapy fractionation schemes in which the interval between doses (typically 1 day) is larger than the time of whole dose elimination (reported to be around 7h [163]) and the typical damage repair times (of the order of a few hours [132]), so that one dose does not alter the effect of the next one.

Without loss of generality, we can assume that the drug administration starts at time $t_1 = 0$, as in Section 2.2. In agreement with clinical practise, we assume all drug doses to be equal. Thus, $d_j = d$ for $j \in \{1, \dots, n\}$ with n being the total number of doses. The effective dose per fraction C_0 is calculated as in Section 2.3.1. In order to obtain analytical estimates let us introduce the following notation. Each chemotherapy cycle is described by three parameters: the cycle duration T (measured in days), the number of doses per cycle p, and the interval between doses in each cycle r (measured in days). We assume that $pr \leq T$. The total number of TMZ cycles in such a general fractionation scheme equals $\left\lfloor \frac{n}{p} \right\rfloor$ and the times of drug administration are

$$t_j = (j-1)r + m\Big(T - pr\Big), \tag{2.31}$$

where $m = \left\lfloor \dfrac{j-1}{p} \right\rfloor$ is the number of completed chemotherapy cycles before dose given in time t_j, $j \in \{1, \dots, n\}$. Then $m \in \{0, \dots, \lfloor (n-1)/p \rfloor\}$ and

$$j = pm + i, \tag{2.32}$$

i being the index of a dose within each TMZ cycle, $i \in \{1, \dots, p\}$.

This definition allows for the description of many different chemotherapy schemes, including those in which administration of drug doses in a cycle is followed by some break (as T can be greater than pr). For instance, in the clinical trial described in [61] patients were treated with TMZ given daily for seven weeks followed by four-week breaks. For that study we would take $T = 77, r = 1, p = 49$ and the drug would be administered at days $t_1 = 0, t_2 = 1, t_3 = 2, \dots, t_{49} = 48, t_{50} = 77, t_{51} = 78$ *etc*. In order to characterise the standard fractionation scheme described in Section 2.1.2 we would take $T = 28, r = 1, p = 5$.

Let us recall that system (2.2) describing the growth of proliferative and damaged tumour cells after rescaling takes the following form (2.11):

$$\begin{aligned} \dot{x}(s) &= xf(x+y) - xz, \\ \dot{y}(s) &= -\frac{1}{k} yf(x+y) + xz, \end{aligned}$$

with initial conditions (2.12):

$$x(0) = x_0, \quad y(0) = 0.$$

The evolution of concentration of chemotherapy (2.4) after rescaling is of a form (2.13)

$$\begin{aligned} \dot{z}(s) &= -\mu z, \\ z(0) &= z_0, \\ z(s_j) &= z(s_j^-) + z_0, \end{aligned} \tag{2.34}$$

where

$$z_0 = \frac{\alpha}{\rho} C_0, \quad \mu = \frac{\lambda}{\rho}.$$

The rescaled dose z_0 is assumed to be given at times $s_1 = 0$, $s_2 = \rho t_2, \dots, s_n = \rho t_n$.

2.4.3 Time of response to chemotherapy

As already mentioned, one of the main observable characteristics of the tumour response to therapy is the time to radiological progression, *i.e.* the time until the tumour starts regrowing.

In our mathematical framework it is the time t_{RP} at which the total tumour mass attains its minimum, *i.e.* $P(t_{\mathrm{RP}}) + D(t_{\mathrm{RP}}) = \min_{t \geq t_n} \{P(t) + D(t)\}$. In terms of rescaled variables we look for s_{RP} such that

$$x(s_{\mathrm{RP}}) + y(s_{\mathrm{RP}}) = \min_{s \geq s_n} \{x(s) + y(s)\}.$$

We focus only on cases of tumours responding to chemotherapy with $\alpha > 0$, thus, showing a radiologically visible decrease in total volume. Therefore, in our approach, in which only first-line chemotherapy is described and resistant cells do not arise, tumour progression occurs after the end of chemotherapy ($s_{\mathrm{RP}} \gg s_n$) provided tumour growth is slow, as happens in the case of LGGs. Thus, we try to derive explicit formulae approximating x and y for $s \gg s_n$.

We assume that initial tumours sizes are small and, as a consequence, we approximate function f by its value $f(0) = 1$. Thus, Eq. (2.11) takes the simpler form

$$\begin{aligned} \dot{x}(s) &= x - xz, \\ \dot{y}(s) &= -\frac{1}{k} y + xz \end{aligned} \tag{2.35}$$

with initial conditions: $x(0) = x_0$, $y(0) = 0$. Then for rescaled time s_{RP} we have $\dot{x}(s_{\mathrm{RP}}) + \dot{y}(s_{\mathrm{RP}}) = 0$, therefore

$$x(s_{\mathrm{RP}}) = \frac{1}{k} y(s_{\mathrm{RP}}). \tag{2.36}$$

Clearly, system (2.35) with Eqs. (2.34) are a set of ODEs with impulses, the functions x and y being continuous, and z being discontinuous at times $s_2, \ldots, s_n$. Since dose clearance time is about two hours we may assume that each dose is cleared in one day, then, in the rescaled units $z((s_j + \rho)^-) \approx 0$ for $j \in \{1, \ldots, n\}$. Therefore, we approximate

$$z(s) \approx \begin{cases} z_0 \mathrm{e}^{-\mu(s - s_j)} & s \in (s_j, s_j + \rho), \\ 0 & \text{for other } s, \end{cases} \tag{2.37}$$

where $j = \max_{i \in \{1, \ldots, n\}} \{s_i \leq s\}$. Let us define

$$\begin{aligned} w(s) &= \int_0^s z(t) \mathrm{d}t, \\ w_0 &= w(\rho) = \int_0^\rho z(t) \mathrm{d}t = \frac{z_0}{\mu} \left(1 - \mathrm{e}^{-\mu\rho}\right). \end{aligned}$$

We should emphasise that for $s > s_2$, $w(s) \neq z_0 \left(1 - \mathrm{e}^{-\mu s}\right)/\mu$ due to the administration of the next drug dose. Furthermore, from Eq. (2.37) we have

$$\begin{aligned} w(s) &= \int_0^{s_\ell} z(t) \mathrm{d}t + \int_{s_\ell}^s z(t) \mathrm{d}t = w(s_\ell) + \int_0^{s - s_\ell} z(t) \mathrm{d}t \approx (\ell - 1) w_0 + w(s - s_\ell) \\ &\approx \begin{cases} (\ell - 1) w_0 + \frac{z_0}{\mu} \left(1 - \mathrm{e}^{-\mu(s - s_\ell)}\right) & s - s_\ell \leq \rho, \\ \ell w_0 & \text{otherwise}, \end{cases} \end{aligned} \tag{2.38}$$

where $\ell = \max_{i \in \{1, \ldots, n\}} \{s \geq s_i\}$. Hence, for $s > s_n + \rho$ we have that $w(s) \approx n w_0$ and the formulae for rescaled proliferating and the damaged part of tumour take the form

$$\begin{aligned} x(s) &= x_0 \mathrm{e}^s - w(s) = x_0 \mathrm{e}^s - n w_0, \\ y(s) &= \int_0^s \mathrm{e}^{-\frac{s - t}{k}} x(t) z(t) \mathrm{d}t. \end{aligned} \tag{2.39}$$

We look for s_{RP} which fulfils condition (2.36). Using Eqs. (2.39) we have

$$k\mathrm{e}^{\tilde{k}s_{\mathrm{RP}}} - nw_0 = \int_0^{s_{\mathrm{RP}}} \mathrm{e}^{\tilde{k}t - w(t)} z(t)\mathrm{d}t,$$

$$s_{\mathrm{RP}} = \frac{1}{\tilde{k}}\left[nw_0 + \ln\left(\frac{1}{k}\int_0^{s_{\mathrm{RP}}} \mathrm{e}^{\tilde{k}t - w(t)} z(t)\mathrm{d}t\right)\right], \tag{2.40}$$

where

$$\tilde{k} = 1 + \frac{1}{k}.$$

As a result of approximations (2.37) and (2.38) we conclude that the integral term in Eq. (2.40) for $s \geq s_n + \rho$ reads

$$\begin{aligned}
&\int_0^s \mathrm{e}^{\tilde{k}t - w(t)} z(t)\mathrm{d}t = \sum_{j=1}^{n} z_0 \int_{s_j}^{s_j+\rho} \mathrm{e}^{\tilde{k}t - w(t)} \mathrm{e}^{-\mu(t-s_j)}\mathrm{d}t \\
&= z_0 \sum_{j=1}^{n} \mathrm{e}^{-(j-1)w_0 + \tilde{k}s_j} \int_{s_j}^{s_j+\rho} \mathrm{e}^{(\tilde{k}-\mu)(t-s_j) + \frac{z_0}{\mu}\left(\mathrm{e}^{-\mu(t-s_j)} - 1\right)}\mathrm{d}t \\
&= z_0 \left(\sum_{j=1}^{n} \mathrm{e}^{-(j-1)w_0 + \tilde{k}s_j}\right) \int_0^{\rho} \mathrm{e}^{(\tilde{k}-\mu)t + \frac{z_0}{\mu}\left(\mathrm{e}^{-\mu t} - 1\right)}\mathrm{d}t.
\end{aligned} \tag{2.41}$$

Using Taylor expansion of an exponential function for $t < 1/\mu$ we approximate

$$\mathrm{e}^{-\mu t} - 1 \approx \begin{cases} -\mu t & 0 \leq t < 1/\mu, \\ -1 & t \geq 1/\mu, \end{cases}$$

and obtain

$$\begin{aligned}
&\int_0^{\rho} \mathrm{e}^{(\tilde{k}-\mu)t + \frac{z_0}{\mu}\left(\mathrm{e}^{-\mu t} - 1\right)}\mathrm{d}t \approx \int_0^{\frac{1}{\mu}} \mathrm{e}^{(\tilde{k}-\mu)t - z_0 t}\mathrm{d}t + \int_{\frac{1}{\mu}}^{\rho} \mathrm{e}^{(\tilde{k}-\mu)t - \frac{z_0}{\mu}}\mathrm{d}t \\
&= \frac{1}{\tilde{k}-\mu-z_0}\left(\mathrm{e}^{\frac{\tilde{k}-\mu-z_0}{\mu}} - 1\right) + \frac{1}{\tilde{k}-\mu}\left(\mathrm{e}^{(\tilde{k}-\mu)\rho - \frac{z_0}{\mu}} - \mathrm{e}^{\frac{\tilde{k}-\mu-z_0}{\mu}}\right) \\
&= \frac{1}{(\tilde{k}-\mu-z_0)(\tilde{k}-\mu)}\left[z_0\mathrm{e}^{\frac{\tilde{k}-\mu-z_0}{\mu}} - \tilde{k} + \mu + (\tilde{k}-\mu-z_0)\mathrm{e}^{(\tilde{k}-\mu)\rho - \frac{z_0}{\mu}}\right].
\end{aligned} \tag{2.42}$$

To compute the sum term in Eq. (2.41) we need the relation between dose indexes j and the times of their administration s_j. Taking into consideration assumptions from Section 2.4.2 and Eqs. (2.31)-(2.32) we get

$$s_j = \Big[(i-1)r + mT\Big]\rho,$$

where $m \in \{0, \ldots, \lfloor (n-1)/p \rfloor\}$ is the number of completed chemotherapy cycles before dose given in time s_j, $j \in \{1, \ldots, n\}$ and $i \in \{1, \ldots, p\}$ is an index of dose within the TMZ cycle. We now assume that chemotherapy treatment is not interrupted during the cycle, that is $\lfloor n/p \rfloor \in \mathbb{Z}$. As a result $m \in \{0, \ldots, \lfloor n/p \rfloor - 1\}$ and from now on, for simplicity, we omit the floor and obtain

$$\begin{aligned}
&\sum_{j=1}^{n} \exp\left(-(j-1)w_0 + \tilde{k}s_j\right) \\
&\qquad = \sum_{m=0}^{n/p-1} \sum_{i=1}^{p} \exp\left(m\left(-pw_0 + \tilde{k}\rho T\right) + (i-1)(-w_0 + \tilde{k}\rho r)\right) \\
&\qquad\qquad = \frac{1 - \mathrm{e}^{\left(-pw_0 + \tilde{k}\rho T\right)\frac{n}{p}}}{1 - \mathrm{e}^{-pw_0 + \tilde{k}\rho T}} \cdot \frac{1 - \mathrm{e}^{\left(-w_0 + \tilde{k}\rho r\right)p}}{1 - \mathrm{e}^{-w_0 + \tilde{k}\rho r}},
\end{aligned} \tag{2.43}$$

where n is the total number of doses and n/p is the total number of chemotherapy cycles as previously stated. Then using Eqs. (2.40), (2.41) and (2.42) we get

$$s_{\mathrm{RP}} = \frac{nw_0}{\widetilde{k}} + \frac{1}{\widetilde{k}} \ln \left\{ z_0 \mathrm{e}^{\frac{\widetilde{k}-\mu-z_0}{\mu}} - \widetilde{k} + \mu + \left(\widetilde{k} - \mu - z_0\right) \mathrm{e}^{\left(\widetilde{k}-\mu\right)\rho - \frac{z_0}{\mu}} \right\}$$
$$+ \frac{1}{\widetilde{k}} \ln \left\{ \frac{z_0 \left(1 - \mathrm{e}^{\left(-pw_0 + \widetilde{k}\rho T\right)\frac{n}{p}}\right)\left(1 - \mathrm{e}^{\left(-w_0 + \widetilde{k}\rho r\right)p}\right)}{k\left(1 - \mathrm{e}^{-pw_0 + \widetilde{k}\rho T}\right)\left(1 - \mathrm{e}^{-w_0 + \widetilde{k}\rho r}\right)\left(\widetilde{k} - \mu - z_0\right)\left(\widetilde{k} - \mu\right)} \right\}.$$

In terms of the initial time scale, the time to tumour progression can be estimated as $t_{\mathrm{RP}} = s_{\mathrm{RP}}/\rho$, giving the final result

$$t_{\mathrm{RP}} = \frac{nw_0}{\widetilde{k}\rho} + \frac{1}{\widetilde{k}\rho} \ln \frac{A_1 A_2}{A_3}, \tag{2.44}$$

where

$$A_1 = z_0 \mathrm{e}^{\left(\widetilde{k}-\mu-z_0\right)/\mu} - \widetilde{k} + \mu + \left(\widetilde{k} - \mu - z_0\right) \mathrm{e}^{\left(\widetilde{k}-\mu\right)\rho - z_0/\mu},$$
$$A_2 = z_0 \left(1 - \mathrm{e}^{\left(-w_0 + \widetilde{k}\rho r\right)p}\right)\left(1 - \mathrm{e}^{\left(-pw_0 + \widetilde{k}\rho T\right)n/p}\right),$$
$$A_3 = k\left(\widetilde{k} - \mu - z_0\right)\left(\widetilde{k} - \mu\right)\left(1 - \mathrm{e}^{-w_0 + \widetilde{k}\rho r}\right)\left(1 - \mathrm{e}^{-pw_0 + \widetilde{k}\rho T}\right)$$

and $\widetilde{k} = 1 + 1/k$, $\mu = \lambda/\rho$, $z_0 = \alpha C_0/\rho$, $w_0 = \alpha C_0\left(1 - \mathrm{e}^{-\lambda}\right)/\lambda$. Eq. (2.44) gives the time to radiological progression as a function of parameters with relevant biological and/or therapeutical meaning. Since t_{RP} is a metric of practical relevance, it is very interesting that it is possible to estimate its value analytically. Note that we have made only few assumptions and estimate (2.44) holds for any function f such that $f(0) = 1$.

Although formula (2.44) is an approximation of the exact explicit formula for t_{RP}, we can simplify it further to get the simplest possible version which preserves the properties of the original one and can be used to answer clinically relevant questions. In order to do so, we take the same parameters values as in Section 2.3.1. Taking $\lambda = \ln 2/2$ h ≈ 8.32 per day, we can assume that

$$\mathrm{e}^{-\mu\rho} = \mathrm{e}^{-\lambda} \approx 0.0003 \approx 0.$$

Thus, we have:

$$w_0 = \frac{\alpha C_0}{\lambda}\left(1 - \mathrm{e}^{-\lambda}\right) \approx \frac{\alpha C_0}{\lambda}, \tag{2.45}$$

and taking value $C_0 = 0.6\,\mu$g/ml we get:

$$\frac{z_0}{\mu} = \frac{\alpha}{\rho} C_0 \cdot \frac{\rho}{\lambda} = \frac{\alpha}{\lambda} \cdot 0.6\,\mu\mathrm{g/ml} \approx 0.$$

We assume that w_0 is relatively small in comparison to $\widetilde{k}\rho r$, thus,

$$1 - \mathrm{e}^{-\left(w_0 - \widetilde{k}\rho r\right)p} \approx 1 - \mathrm{e}^{\widetilde{k}\rho r p}.$$

Due to the fact that $\widetilde{k}\rho r p$, $\widetilde{k}\rho r$ are small and much smaller than 1 we may use the Taylor expansion with respect to variable r, obtaining:

$$1 - \mathrm{e}^{\widetilde{k}\rho r p} \approx -\widetilde{k}\rho r p, \quad 1 - \mathrm{e}^{\widetilde{k}\rho r} \approx -\widetilde{k}\rho r.$$

Moreover, we observe that $\widetilde{k}$ is small compared with μ, thus, we neglect this term obtaining:

$$\begin{aligned} A_1 &\approx z_0 \mathrm{e}^{\frac{1}{k\mu}-1} + \mu, \\ A_2 &\approx -z_0 \widetilde{k} \rho r p \left(1 - \mathrm{e}^{\left(-pw_0 + \widetilde{k}\rho T\right)\frac{n}{p}}\right), \\ A_3 &\approx k\mu^2 \widetilde{k} \rho r \left(1 - \mathrm{e}^{-pw_0 + \widetilde{k}\rho T}\right). \end{aligned}$$

As $\mu \gg 1$ and z_0 is small (as dose C_0 is small due to possible toxicity effects), then $z_0 \exp(1/k\mu - 1) \ll \mu$. Therefore, we omit the first term obtaining: $A_1 \approx \mu$ and

$$\frac{A_1 A_2}{A_3} \approx \frac{-\mu z_0 \widetilde{k} \rho r p \left(1 - \mathrm{e}^{\left(-pw_0 + \widetilde{k}\rho T\right)\frac{n}{p}}\right)}{k\mu^2 \widetilde{k} \rho r \left(1 - \mathrm{e}^{-pw_0 + \widetilde{k}\rho T}\right)} = -\frac{z_0 p}{\mu k} \frac{1 - \mathrm{e}^{\left(-pw_0 + \widetilde{k}\rho T\right)\frac{n}{p}}}{1 - \mathrm{e}^{-pw_0 + \widetilde{k}\rho T}}$$

In the latter simplifications we do not neglect terms nw_0 and pw_0 as they can be large. However, using Eq. (2.45) we obtain:

$$t_{\mathrm{RP}} \approx \frac{n\alpha C_0}{\widetilde{k}\lambda\rho} + \frac{1}{\widetilde{k}\rho} \ln \left\{ \frac{\alpha C_0 p \left(1 - \mathrm{e}^{-n\frac{\alpha C_0}{\lambda} + \widetilde{k}\rho T \frac{n}{p}}\right)}{\lambda k \left(1 - \mathrm{e}^{-p\frac{\alpha C_0}{\lambda} + \widetilde{k}\rho T}\right)} \right\}. \tag{2.46}$$

2.4.4 Validation for the standard chemotherapy protocol

Eqs. (2.44) and (2.46) have been obtained via a number of approximations, and thus, it is relevant to compare those predictions with the results of the original system (2.2) and real patient data.

To do the latter we first fix the treatment parameters to match those routinely used for TMZ therapeutic schedules. Since TMZ is given on 5 consecutive days in cycles consisting of 28 days, we get $p = 5$, $T = 28$, $r = 1$. Taking dose per fraction to be 150 mg/m^2 and the other parameters as in Section 2.3.1 we can then estimate the time to radiological progression for the individual patients studied previously (accounting for the number of cycles received by each patient), *cf.* Section 2.3.2.

Figure 2.16 shows how well formula (2.44) estimates the response to chemotherapy for three patients chosen from our database. The task of comparing simulation results with real patients MRI data requires a lot of caution. In particular, we need to take into account the limitations of calculations of tumour volume using the method of three largest diameters. The method is only an approximation of real tumour volume and its accuracy is limited by slice thickness, changes in head position [164] or even by perception of medical doctor who calculate these diameters. In the future we hope that MRI data will be analysed through automatic segmentation, *e.g.* with algorithm suggested by Porz *et al.* [165] and the real tumour volume will be calculated more accurately.

Moreover, we validate the obtained formulas by calculating the relative error with respect to results of simulations of system (2.2). Figure 2.17 presents relative differences between t_{RP} from estimated formulas (2.44,2.46) and simulations of system (2.2) for varying parameters, suggesting a very good approximation.

2.4.5 The study of response for other chemotherapy protocols

We have also verified that Eqs. (2.44) and (2.46) provide a good approximation of t_{RP} for system (2.2) for other fractionation schemes. Figure 2.18 shows some examples.

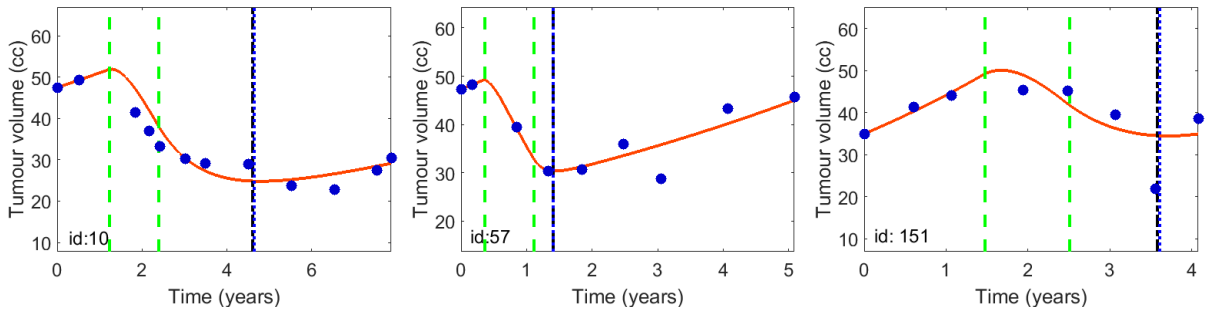

Figure 2.16: Tumour volume evolution for three patients treated with TMZ. Vertical dashed lines mark the start and the end of TMZ treatment. Circles denote the volumes obtained from MRI scans and solid lines the results of the best fit using system (2.2). The times to radiological progression computed using Eq. (2.44) and (2.46) are marked with vertical black dashed-dotted and blue dotted lines, respectively, showing a very good agreement with the data and the simulations of system (2.2).

2.4.6 Tumour volume decrease after chemotherapy

Motivated by the results of Section 2.3.4 we also estimate the relative tumour volume decrease. Using Eqs. (2.36), (2.39) and assuming that $s_{\mathrm{RP}} \gg s_n$ we arrive at:

$$(x+y)(s_{\mathrm{RP}}) = (k+1)x(s_{\mathrm{RP}}) = (k+1)x_0 \exp\left(s_{\mathrm{RP}} - nw_0\right). \tag{2.47}$$

Thus, tumour volume V_{RP} at time t_{RP} equals:

$$V_{\mathrm{RP}} = (P+D)(t_{\mathrm{RP}}) = K(x+y)(s_{\mathrm{RP}}) = (k+1)P_1 \exp\left(s_{\mathrm{RP}} - nw_0\right).$$

Using Eqs. (2.45) and (2.46) we approximate:

$$V_{\mathrm{RP}} \approx (k+1)P_1 \exp\left\{\frac{n\alpha C_0}{\widetilde{k}\lambda} + \frac{1}{\widetilde{k}} \ln\left(\frac{\alpha C_0 p\left(1-\mathrm{e}^{-n\frac{\alpha C_0}{\lambda}} + \widetilde{k}\rho T\frac{n}{p}\right)}{\lambda k\left(1-\mathrm{e}^{-p\frac{\alpha C_0}{\lambda}} + \widetilde{k}\rho T\right)}\right) - n\frac{\alpha C_0}{\lambda}\right\}$$

$$= (k+1)P_1 \exp\left(-\frac{n\alpha C_0}{(k+1)\lambda}\right)\left(\frac{\alpha C_0 p\left(1-\mathrm{e}^{-n\frac{\alpha C_0}{\lambda}} + \widetilde{k}\rho T\frac{n}{p}\right)}{\lambda k\left(1-\mathrm{e}^{-p\frac{\alpha C_0}{\lambda}} + \widetilde{k}\rho T\right)}\right)^{\frac{1}{\widetilde{k}}}.$$

Finally we obtain the following estimate of relative volume decrease defined in Eq. (2.30):

$$\Delta V \approx 1 - (k+1)\exp\left(-\frac{n\alpha C_0}{(k+1)\lambda}\right)\left(\frac{\alpha C_0 p\left(1-\mathrm{e}^{-n\frac{\alpha C_0}{\lambda}} + \widetilde{k}\rho T\frac{n}{p}\right)}{\lambda k\left(1-\mathrm{e}^{-p\frac{\alpha C_0}{\lambda}} + \widetilde{k}\rho T\right)}\right)^{\frac{1}{\widetilde{k}}}. \tag{2.48}$$

We verify goodness of this estimate, comparing it with the results of various simulations of original mathematical model (2.2). Figure 2.19 shows differences in tumour volume decrease estimated from simulations and formula (2.48).

2.5 Discussion

Up to now there have been a great deal of relevant research into the pharmacokinetic/pharmacodynamic properties of TMZ [153, 78, 154, 157], its specific mechanism of action [58, 152, 59,

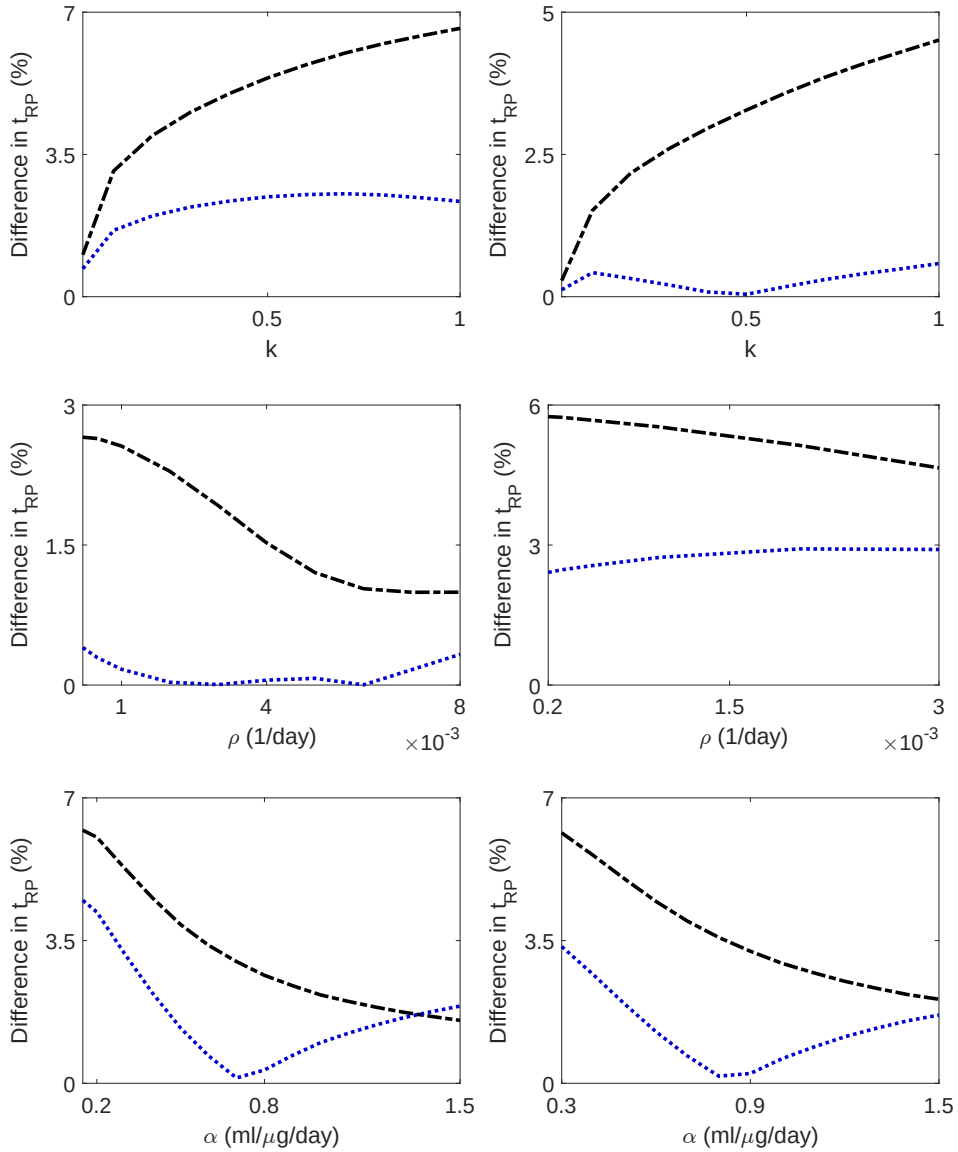

Figure 2.17: Relative percentage differences between t_{RP} calculated from simulations of system (2.2) and estimated formulas: (2.44) and (2.46) indicated by black dashed-dotted and blue dotted lines, respectively. We considered 12 cycles of TMZ as in standard fractionation scheme (see Section 2.3.1) for a virtual patient with LGG of initial volume 40 cm^3. (top) Results for $\rho = 0.0004$/day, $\alpha = 0.4$ml/μg/day, $k \in [0.02, 1]$ (left) and $\rho = 0.0008$/day, $\alpha = 0.8$ml/μg/day, $k \in [0.02, 1]$ (right). (centre) Results for $\alpha = 0.8$ml/μg/day, $k = 0.3$, $\rho \in [0.2, 8]\times 10^{-3}$/day (left) and $\alpha = 0.4$ml/μg/day, $k = 0.6$, $\rho \in [0.2, 3] \times 10^{-3}$/day (right). (bottom) Results for $\rho = 0.0004$/day, $k = 0.3$, $\alpha \in [0.15, 1.5]$ml/μg/day (left) and $\rho = 0.0008$/day, $k = 0.6$, $\alpha \in [0.3, 1.5]$ml/μg/day (right).

163] and modelling its concentration dynamics *in vitro* and *in vivo* [166, 167, 168]. However there are fewer mathematical studies of patient response to TMZ in LGGs, see our discussion in Section 1.6.

Here we intended to construct a mathematical model which would enable understanding of delayed response to chemotherapy observed in LGGs without using an excessive number of unknown parameters. Cells were assumed to grow logistically, chemotherapy drug kinetics and its effect on glioma cells was based on TMZ concentration in brain tissue [157] and clinical observations [151, 69, 70]. Note that even the authors of the very complicated model [168], constructed for the purpose of describing pharmacokinetics and pharmacodynamis of TMZ, validated their model for human cerebral tumours on the basis of data of Portnow *et al.* [157].

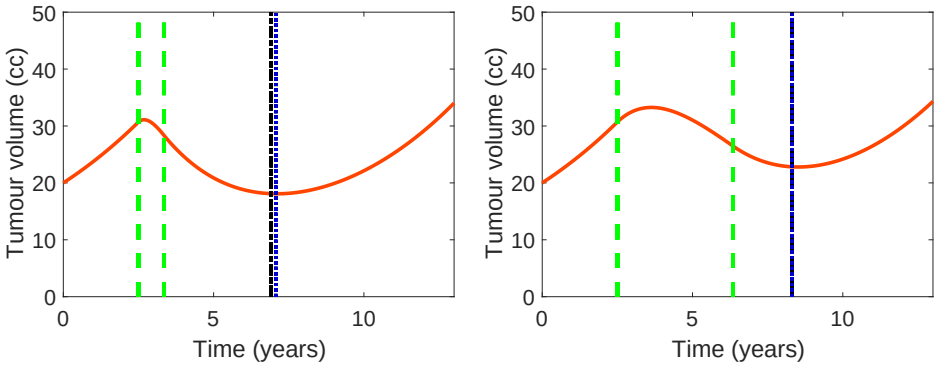

Figure 2.18: Tumour volume evolution for virtual patients simulated from system (2.2). Times to radiological progression estimated from Eq. (2.44) and (2.46) are marked with vertical black dashed-dotted and blue dotted lines, respectively. Values of parameters were $k = 0.5$, $\alpha = 0.4\text{ml}/\mu\text{g}/\text{day}$ and $\rho = 0.005/\text{day}$. The start and the end of TMZ treatment are marked with vertical dashed lines. (left) 9 TMZ cycles of 34 days with doses given every 2 days for a total of 10 doses per cycle. The dose per fraction was d=100 mg/m^2. (right) 18 TMZ cycles of 77 days with doses given every 7 days for a total of 10 doses per cycle. The dose per fraction was d=50 mg/m^2. Relative differences between times free of progression calculated from Eq. (2.44) and estimated from simulations were 0.026756 and 0.025303 years, respectively. Relative differences between times free of progression calculated from Eq. (2.46) and estimated from simulations were 0.0053011 and 0.024816 years, respectively.

It is remarkable that a simple model such as the one presented here with essentially only three unknown parameters (α, ρ, k) is able to describe the response of real patients to a variable number of cycles of TMZ.

The model also shows a correlation between a short time to radiological progression and a poor virtual patient outcome. We may conclude that time to radiological progression can be useful as a measure of tumour aggressiveness due to its dependence on tumour-specific parameters: proliferation rate ρ and TMZ cell kill strength α (see Figures 2.11, 2.12). Our data on patients treated with first-line TMZ suggests likewise that despite other therapies used in the follow-up, patients who had shorter estimated t_{RP} had worse prognosis. Such observation has been made for radiotherapy [169, 170], but so far no similar analysis of response to TMZ has been done. The velocity of tumour decrease after radiotherapy (or equivalently time to radiological progression) is strongly associated with the risk of rapid progression and poor overall survival. Here we suggest a similar result for the response to chemotherapy, namely that short time to radiological progression results in shorter overall survival.

This outcome makes us think of the possibility of using chemotherapy to probe tumours, hence providing estimates of tumour-specific parameters ρ and α. We could apply a small number of cycles of TMZ causing minimal toxicity and monitor the radiological tumour response to chemotherapy. At least two measurements before and three after TMZ onset would be necessary to assure the reasonable measurement error. We predict that the time horizon would be of around 2 years from the time of the first MRI scan. We believe it could be feasible as even up to now there were patients with MRI done three times a year. Based on our database we presume that there will be no progression at this time horizon. Such a procedure can be used as a novel way to assess tumour aggressiveness. Our mathematical model suggests that tumours attaining their minimal volume early after a short course of TMZ treatment (has shorter t_{RP}) may be more aggressive, therefore, in such cases the remaining TMZ doses have to be finished as soon as possible and other therapeutic options (further surgery if feasible or radiotherapy) should be considered. Such a concept can be supported also by the *in vitro* re-

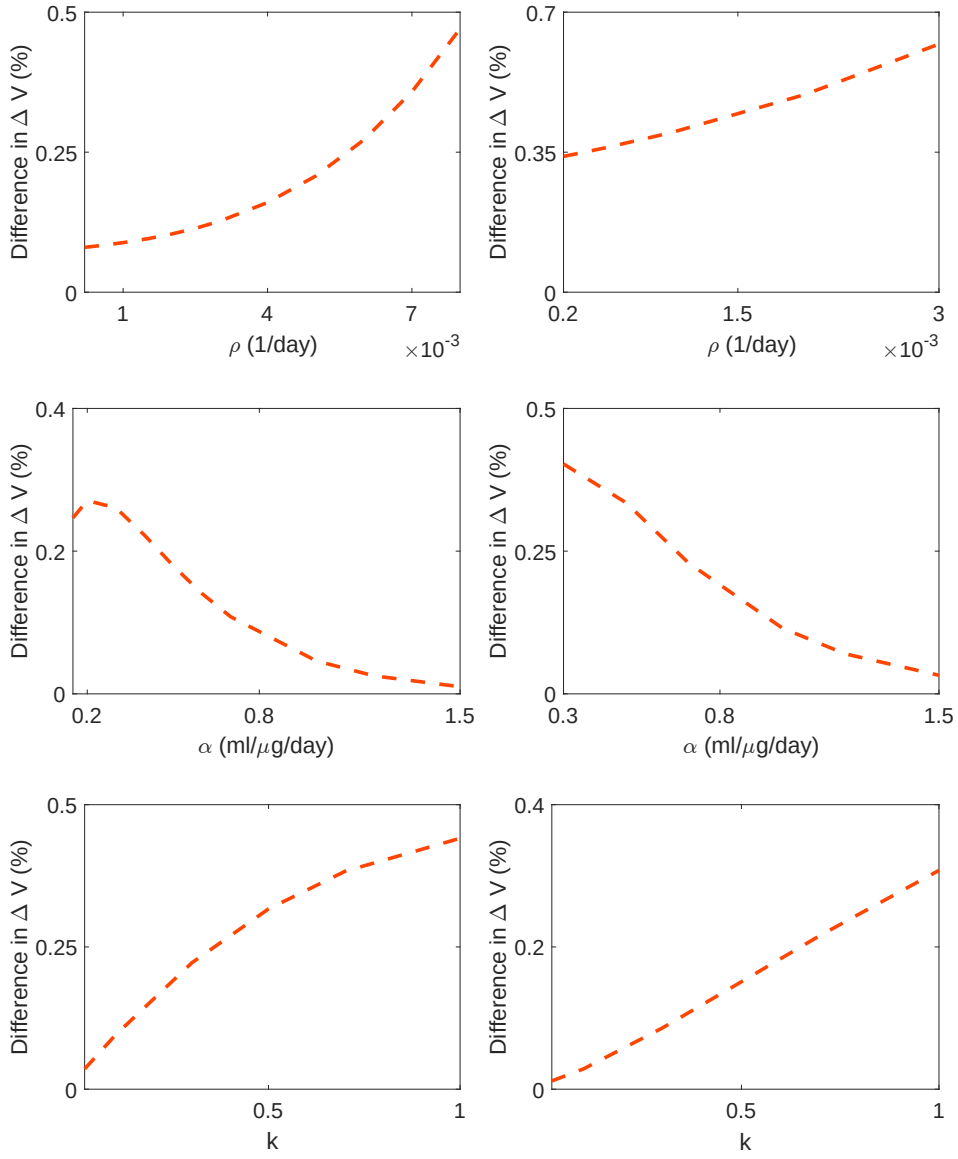

Figure 2.19: Relative percentage differences between ΔV calculated from simulations of system (2.2) and Eq. (2.48). We considered 12 cycles of TMZfor a virtual tumour of initial volume 40 cm^3. (top) Results for $\rho = 0.0004$/day, $\alpha = 0.4$ml/μg/day, $k \in [0.02, 1]$ (left) and $\rho = 0.0008$/day, $\alpha = 0.8$ml/μg/day, $k \in [0.02, 1]$ (right). (centre) Results for $\alpha = 0.8$ml/μg/day, $k = 0.3$, $\rho \in [0.2, 8] \times 10^{-3}$/day (left) and $\alpha = 0.4$ml/μg/day, $k = 0.6$, $\rho \in [0.2, 3] \times 10^{-3}$/day (right). (bottom) Results for $\rho = 0.0004$/day, $k = 0.3$, $\alpha \in [0.15, 1.5]$ml/μg/day (left) and $\rho = 0.0008$/day, $k = 0.6$, $\alpha \in [0.3, 1.5]$ml/μg/day (right).

sults of Roos *et al.* [152], who have showed that higher proliferation rates accelerated apoptosis after TMZ treatment, *i.e.* a shorter t_{RP}.

This idea resembles that described in [1], but with chemotherapy instead of radiotherapy. Although the modelling principles are similar, from the clinical point of view the use of TMZ is a much more interesting as a way to probe a tumour than the use of radiotherapy as its side-effects are larger, long-term and non-reversible. Moreover, radiotherapy is known to induce changes in the MRI scans due to inflammation which may distort the analysis of the tumour response. Finally, TMZ is easily managed because it is administered orally.

We have also performed a mathematical analysis of a more general model. We take into account the possibility that a more general tumour growth function may fit better to the

individual patients data. Thus, we only assume its general properties (determining its shape) and consequently consider a broader class of possible functions. In addition, we incorporate a new component to tumour growth term – a parameter describing the effectiveness of the competition between damaged cells and proliferating ones.

We prove the existence and uniqueness of solutions together with the existence of the invariant set. We study the long time behaviour of the model depending on its parameters, including the ones describing chemotherapy effect. We discus stability of the steady states for constant chemotherapy and we prove the condition under which the trivial steady state is asymptotically stable in the case of periodic treatment. We also show that there exist periodic solutions for some specific cases of periodic treatment function.

Our generalised model given by system (2.15) together with Theorem 2.12 make us think of possible therapeutical implications. Theorem 2.12 gives us the optimality condition, *i.e.* that the model solutions converge to the zero steady state for $\bar{z} \geq 1$. Such condition refers to the situation when some concentration of drug is present in the bloodstream and in the tissues and its mean influence on the tumour is greater or equal the proliferation rate. Note that in the chemotherapy scheme most frequently used for LGG patients equal doses of TMZ (namely 150 mg per m^2 of body surface area) are administered. However, it has been noted, both in clinical and mathematical studies [171, 61, 172, 74, 22, 173], that such a dose seems not to be the most appropriate for slowly-growing LGGs. Theorem 2.12 suggests the possibility of estimation of the minimal dose d allowing to eradicate tumour under assumption that drug doses are administered infinitely many times and that tumour cells do not acquire drug resistance. Clearly, in real life one should focus on treatment schemes with finite time horizons. However, a significantly prolonged chemotherapies could be considered such as therapies lasting until obtaining an expected response to treatment. In [174], Khasraw *et al.* report cases of LGGs patients for whom chemotherapy treatment administered for even 5-8 years did not cause serious side effects. Thus, on the basis of this clinical study we presume that prolonged chemotherapy could remain safe for LGG patients. In addition, Mannas *et al.* conclude that long-term chemotherapy with TMZ could be considered a therapeutic option as long as appropriately monitoring is assured [175].

Now, we use theory developed in this chapter to estimate minimal effective dose in the case of long time treatments. In order to do so, we use parameters values estimated in Table 2.1. Parameters α, that describes the effectiveness of the drug, and ρ providing the proliferation rate of LGG were assumed to be patient-specific, thus, we used ranges of parameters as in Table 2.3. Finally, considering model rescaling (2.10) and definition of fraction of drug dose acting on tumour tissue given by Eq. (2.28), we have

$$\bar{z} = \frac{p}{T\lambda} \cdot \frac{\alpha}{\rho} \beta b d \geq 1 \implies d \geq \frac{T\lambda\rho}{p\alpha\beta b}, \tag{2.49}$$

where $p = 5$ and $T = 28$ are the values mimicking the standard chemotherapy scheme. Hence, we estimate that minimal eradication dose is between 5.42 mg and 94.9 mg per m^2 of body surface area for pairs of patient-specific parameters (ρ, α) estimated for patients, *cf.* Table 2.3. Clearly, dose of 5.42 mg is significantly smaller than the dose that is administered in a clinical practice. This result suggests that metronomic therapy* could be a good option for successful treatment of selected patients. There have been already several studies analysing metronomic chemotherapy for HGGs, see *e.g.* [178, 179]. As for LGGs, Lashkari *et al.* in [172] studied

*Metronomic chemotherapy is a schedule consisting of many, equally spaced and generally low doses of chemotherapeutic drug without extended rest periods, see *e.g.* [176, 177].

two alternative treatments with smaller TMZ dose. The authors concluded that metronomic regimens of TMZ may result in better LGGs response comparing to the conventional regimen, however there is a need for randomised clinical trials to verify this result. Also recent observations of the benefits of metronomic chemotherapy with other drug (vinblastine) administered for a limited number of LGG patients may be related to our analysis [180]. Our result also indicates that more patient specific therapy schemes should be designed to obtain the best effectiveness. It also points out that the proper dosing should be decided on the basis of tumour-specific characteristics. We would also like to underline that doses smaller than those calculated from Eq. (2.49) could not be effective in treating LGGs in an infinite time horizon, consequently they should not be considered for the realistic, finite time schemes.

However, in reality one also need to take into account the possibility of drug resistance, that can be acquired by tumour, which is beyond the phenomena explored here. In the future we plan to extend the model in order to be able to broaden the possible applicability of this results and address other clinically-driven problems such as drug resistance or cytoxicity, being a strongly limiting factor of any chemotherapy. Such a task would require inclusion of more terms and variables in the model and more biomedical data in order to validate the model and estimate model' parameters. In particular, the main cytotoxic effects induced by TMZ are due to haematologic toxicity [56, 163, 181, 182]. In order to include them in considered model, one would require additional data from systematic blood morphological patients tests, preferably before and during the treatment with TMZ. Moreover, in [183, 184] it has been discussed that TMZ effectiveness in treating gliomas is limited not only due to cytotoxicity, but also due to the drug influence on endothelial cells. If we wish to include also that phenomenon in our model we would need to consider additional variable in the system. Consequently, the model should be calibrated with additional data. Having proper model of toxicity we would be able to find the minimal doses and minimal frequency of therapy such that the solution (namely tumour mass) stays below a given threshold and the chemotherapy does not cause too large side effects. Unfortunately, at the moment, we do not have an access to patients TMZ cytotoxicity data nor the quantitative data reporting this specific drug effect on endothelial cells.

On the other hand, it is known that the effect of acquiring resistance can be modelled in various ways, see *e.g.* [185, 186, 187, 188] and references therein. However the selection of suitable approach needs to be deeply investigated, mainly by taking into account available data and the possibility of verification of obtained results.

To conclude, we plan further studies aimed to find the best possible way to build and validate models describing the above phenomena in more detail which would also be used to address questions concerning LGG which remain open.

Chapter 3

Mathematical model of malignant transformation

In this chapter, we formulate a mathematical model describing the growth of LGG and the process of its transformation to a more malignant higher-grade counterpart, see Section 1.5 for the description of malignant transformation. We prove the existence, uniqueness and non-negativity of solutions of the proposed system of reaction-diffusion equations as well as study the stability of space homogeneous steady states and show that Turing instabilities do not arise. We fit the proposed model to patients data and discuss the important relations between model parameters and patient prognosis. Furthermore, we provide estimates of LGG radius and the time when malignant transformation could begin.

3.1 Formulation of mathematical model

Our mathematical model describes the change of the tumour cell density in time and space due to the interplay of net proliferation and net diffusion of cancer cells, as in some previous works [98, 29, 1, 124].

Various researchers have suggested that malignant transformation of LGGs may be induced by a high cell density focus [1, 23, 189, 120, 121]. As a result of elevated cellular density, tumour cells may start having a limited access to nutrients that causes major changes in the tumour microenvironment, including vessels damage, generation of hypoxic foci, stabilisation of hypoxia-dependent signalling molecules like hypoxia-inducible factor-1 (HIF-1) and increase of genomic instability [190, 191, 119, 120]. These changes lead to the appearance of more aggressive tumour cell phenotypes and/or additional mutations, see also Figure 1.6.

Thus, we base our model of malignant transformation on the assumption that the first step in this phenotypic transition is the growth of the tumour density beyond a certain critical level L_{crit} initiating a non-reversible damage to the microenvironment [121]. Beyond that point, hypoxia arises and angiogenesis is triggered. However, this microvasculature is aberrant and leads to both chronic and acute hypoxia events. This abnormal vasculature plays a key role in the development of more aggressive phenotypes [119, 192] and an enhanced genetic instability.

Malignant transformation cannot be reversed, once the transformation is triggered, cells cannot change their phenotype to a less aggressive one because of the accumulation of new mutations. We assume that after the onset of malignant transformation the process of acquiring a more aggressive high-grade behaviour by glioma cells requires some time τ.

The behaviour of cells before and after transformation differs from one another , which is reflected in the model by different proliferation and motility rates (ρ_L, D_L and ρ_H, D_H for LGG and HGG, respectively). The density of LGG cells is described by a non-negative function $L\colon \mathbb{R}_0^+ \times \Omega \to \mathbb{R}$, where Ω describes the brain domain under consideration. The spatiotemporal density of the more malignant (transformed) cells is described by a function $H\colon \mathbb{R}_0^+ \times \Omega \to \mathbb{R}$. Then, the full mathematical model for the evolution of both tumour cells populations is given by the following system of Fisher–Kolmogorov–type equations:

$$\frac{\partial L}{\partial t} = \rho_L L\left(1 - \tfrac{L+H}{K}\right) + D_L \Delta L - \tfrac{1}{\tau} S\left(\tfrac{L+H}{K}\right) L, \tag{3.1a}$$

$$\frac{\partial H}{\partial t} = \rho_H H\left(1 - \tfrac{L+H}{K}\right) + D_H \Delta H + \tfrac{1}{\tau} S\left(\tfrac{L+H}{K}\right) L \tag{3.1b}$$

with initial conditions:

$$L(0,x) = L_0(x) \in C^2\left(\bar{\Omega}\right), \quad H(0,x) = 0 \tag{3.1c}$$

and homogeneous von Neumann boundary conditions:

$$\left.\frac{\partial L}{\partial n}\right|_{\partial\Omega} = \left.\frac{\partial H}{\partial n}\right|_{\partial\Omega} = 0. \tag{3.1d}$$

All model parameters are assumed to be positive due to their possible biological interpretation. In this chapter we express critical glioma density triggering malignant transformation L_{crit} in terms of the maximal cellular density K, that is $L_{\text{crit}} = \beta K$ for some $\beta \in (0,1)$. Function $S\colon \mathbb{R} \to [0,1]$, used to describe the malignant transformation of LGG cells to HGG cells, is assumed to be a C^2 function of total glioma density measured in the units of maximal cell density K. We assume that that $S(T) = 0$ for $T < \beta - \Delta_{\text{crit}}$, $S(T)$ is increasing for $T \in \left[\beta - \Delta_{\text{crit}}, \beta + \Delta_{\text{crit}}\right]$ and $S(T) = 1$ for $T > \beta + \Delta_{\text{crit}}$, where Δ_{crit} is the width (or sensitivity) of the switch function. The specific forms of the initial function L_0 and the switch function S taken for numerical simulations are given in Section 3.3.

3.2 Mathematical analysis of the model

For the purpose of mathematical analysis of system (3.1) it is convenient to rescale time and space. Let us take

$$u(\tilde{t},\tilde{x}) = L(\tilde{t},\tilde{x})/K, \quad v(\tilde{t},\tilde{x}) = H(\tilde{t},\tilde{x})/K,$$

where

$$\tilde{t} = \rho_H t \quad \text{and} \quad \tilde{x} = \sqrt{\rho_H/D_H}\, x$$

are the rescaled time and space variables, respectively. In new variables system (3.1) reads

$$\frac{\partial u}{\partial t} = D\Delta u + \rho u\Big(1 - u - v\Big) - \gamma S(u+v)u, \tag{3.2a}$$

$$\frac{\partial v}{\partial t} = \Delta v + v\Big(1 - u - v\Big) + \gamma S(u+v)u, \tag{3.2b}$$

where we have omitted tildes to simplify notation, $(t,x) \in [0,+\infty) \times \Omega$, $D = D_L/D_H$, $\gamma = 1/(\tau\rho_H)$ and $\rho = \rho_L/\rho_H$. We consider von Neumann boundary condition

$$\left.\frac{\partial u}{\partial \vec{n}}\right|_{\partial\Omega} = \left.\frac{\partial v}{\partial \vec{n}}\right|_{\partial\Omega} = 0 \tag{3.2c}$$

and initial condition

$$u(0,x) = u_0(x) \in [0,1], \quad v(0,x) = 0. \tag{3.2d}$$

Note that $D \in (0,1)$ and $\rho \in (0,1)$ due to the assumption that proliferation rate and motility rate are higher for HGGs cells. The set Ω is an open subset of $\mathbb{R}^n$ with a smooth boundary. We also assume that initial function $u_0 \in C^2\left(\bar{\Omega}\right)$.

Theorem 3.1. *There exists local unique classical solution to system* (3.2).

Proof. The reaction term of system (3.2) and initial conditions are C^2 functions, thus, solution to system (3.2) exists locally and is unique due to general properties of reaction-diffusion systems, see *e.g.* Theorem 3.3.3. in [193]. □

Theorem 3.2. *For $(t,x) \in [0,+\infty) \times \Omega$ we have $u(t,x), v(t,x) \geq 0$, where (u,v) is the classical solution to system* (3.2). *Moreover, if initial condition $u_0(x) \leq 1$ we have $u(t,x) \leq 1$ for all $(t,x) \in [0,+\infty) \times \Omega$.*

Proof. First, notice that for $u \equiv 0$ Eq. (3.2b) takes the following form:

$$\frac{\partial v}{\partial t} = \Delta v + v(1-v),$$

which is a FKE. Together with non-negative initial condition and von Neumann boundary condition, a solution to this equations is non-negative. From non-negativity of function S we obtain the non-negativity of v.

Knowing that $v(t,x) \geq 0$ for $(t,x) \in [0,+\infty) \times \Omega$, we conclude that the solution of FKE

$$\frac{\partial u}{\partial t} = D\Delta u + u(1-u),$$

with von Neumann boundary condition is a sub-solution of Eq. (3.2a). Similarly, $u(t,x) \equiv 0$ is a super-solution. As a consequence, using the basic properties of FKE and invariant rectangle theorem (*cf.* [194]) we deduce that $u(t,x) \in [0,1]$ for all $(t,x) \in [0,+\infty) \times \Omega$. □

Note that the solution v of system (3.2) does not have to be bounded by 1.

Example. Let us assume that $\Omega = [-R,R]$ for some $R \in \mathbb{R}^+$ and consider new variable $w = u + v$. Then, system (3.2) is of a form:

$$\begin{aligned} \frac{\partial u}{\partial t} &= D\Delta u + \rho u(1-w) - \gamma S(w)u, \\ \frac{\partial w}{\partial t} &= \Delta w + (D-1)\Delta u + \Big((\rho-1)u + w\Big)(1-w), \end{aligned} \tag{3.3}$$

with boundary condition given by Eq. (3.2c). Let us consider initial condition given by:

$$u(0,x) = u_0(x), \quad w(0,x) \equiv 1, \tag{3.4}$$

where function $u_0(x)$ equals $a - x^2$ for some $a \in (0,1)$ and for $x \in (-\epsilon,\epsilon)$ and outside this set we extend function $a - x^2$ smoothly and monotonically. Thus, we have

$$\left.\frac{\partial w}{\partial t}\right|_{x=0} = 2(1-D),$$

which is positive due to assumption that $0 < D < 1$. As a consequence, the solution w of the system (3.3) increases above value 1.

This example shows the limit of possible use of system (3.2). Set $[0,1]\times[0,1]$ is not invariant for system (3.2) in the case of non-zero diffusion coefficient, *i.e.* even if initial functions are within the square $[0,1]\times[0,1]$, the model solutions could leave it. As a consequence, the model should not be used for some specific cases when the tumour cells' density is very close to its maximal possible value. However, as stated at page 58, the motivation behind the formulation of the original system (3.1) was to describe quantitatively the process of malignant transformation of LGGs and we do not focus here on the description of growth of already transformed HGG cells. The growth of the tumour composed mostly of HGG cells, which is significantly different from the behaviour of LGG, has been studied thoroughly in various research papers, see Section 1.6.

It is known that in the case of systems of two or more reaction-diffusion equations a much larger range of possible phenomena can occur than in the case of one reaction-diffusion equation. Alan Turing observed that a steady state that is stable for ODE system can become unstable with respect to small spatial perturbations in the presence of diffusion. Then diffusion is a driving force of the spatial pattern that occurs in the real world for instance in the form of fingerprints, strips on zebra and skin patterns on fishes. Such phenomenon is called Turing bifurcation or Turing instability, see for instance [98, 195].

Following [98], we determine the stability of spatially homogeneous steady states of system (3.2) and the equivalent space homogeneous model:

$$\begin{aligned}\frac{\partial u}{\partial t} &= \rho u\Big(1-u-v\Big) - \gamma S(u+v)u,\\ \frac{\partial v}{\partial t} &= v\Big(1-u-v\Big) + \gamma S(u+v)u\end{aligned} \tag{3.5}$$

together with initial condition (3.2d). System (3.5) has two steady states:

$$P_1 = (0,0) \text{ and } P_2 = (0,1).$$

Proposition 3.3. *Steady states P_1 and P_2 of system (3.5) are unstable and locally stable, respectively.*

Proof. In order to verify the stability of steady states P_1 and P_2, we study the behaviour of the linearisation of the system (3.5) near those equilibrium points. The Jacobi matrix of the right-hand side function of system (3.5) calculated at the steady state $P=(\bar u,\bar v)$ reads

$$J(P) = \begin{bmatrix} \rho\Big(1-2\bar u-\bar v\Big) - \gamma S(\bar u+\bar v) - \gamma S'(\bar u+\bar v)\bar u & -\rho\bar u \; - \gamma S'(\bar u+\bar v)\bar u \\ -\bar v + \gamma S(\bar u+\bar v) + \gamma S'(\bar u+\bar v)\bar u & 1-\bar u-2\bar v + \gamma S'(\bar u+\bar v)\bar u \end{bmatrix}.$$

Thus, Jacobi matrices at the steady states P_1 and P_2 are

$$J(P_1) = \begin{bmatrix} \rho & 0 \\ 0 & 1 \end{bmatrix}, \quad J(P_2) = \begin{bmatrix} -\gamma & 0 \\ \gamma-1 & -1 \end{bmatrix},$$

respectively. We establish the asymptotic stability of steady states using the Hartman–Grobman theorem. P_1 is an unstable node as both eigenvalues of $J(P_1)$ are real and positive. On the other hand, $J(P_2)$ has real negative eigenvalues, and hence, P_2 is a stable node. □

Proposition 3.4. *The local stability of spatially homogeneous steady states P_1 and P_2 of system (3.2) is the same as for system (3.5) with initial condition (3.2d).*

Proof. In order to verify the stability of spatially homogeneous steady states of system (3.2) we linearise it around the steady state, obtaining for $i \in \{1, 2\}$ system:

$$\frac{\partial z}{\partial t} = J(P_i)z + \tilde{D}\Delta z, \quad \tilde{D} = \begin{bmatrix} D & 0 \\ 0 & 1 \end{bmatrix}.$$

Thus, we need to study the following matrices:

$$J(P_i) - k^2 \begin{bmatrix} D & 0 \\ 0 & 1 \end{bmatrix}$$

for $i \in \{1, 2\}$ and any wave number k being eigenvalue of Laplacian, *i.e.* k is the eigenvalue of the problem

$$\Delta W + k^2 W = 0$$

with zero flux boundary condition on Ω, see *e.g.* [98, 196]. The values of k depend on the space Ω, however here we do not need to find the exact values of k. For the corresponding reaction-diffusion system (3.2) zero is always the eigenvalue of Laplacian, as we consider von Neumann boundary conditions. As a result, the stability of steady state P_1 is the same as in the case of system without diffusion. It is also true for P_2 which is locally stable for system (3.5), but also for system (3.2), as $k^2 \geq 0$. □

As a consequence of Proposition 3.4 we conclude that for both of spatially homogeneous steady states of system (3.2) the diffusion-driven instability is impossible.

Theorem 3.5. *Let $\Omega \subset \mathbb{R}^n$ be an open set with a smooth boundary. Then system (3.2) does not exhibit Turing instabilities.*

3.3 Numerical results

In what follows, we assume that the switch function S, describing the malignant transformation in system (3.1), have a form inspired by [119]:

$$S(T) = \begin{cases} 0 & \text{for } T < \beta - \Delta_{\text{crit}} \\ 0.5\left[1 + \coth(1)\tanh\left(\dfrac{T-\beta}{\Delta_{\text{crit}}}\right)\right] & \text{for } T \in \left[\beta - \Delta_{\text{crit}}, \beta + \Delta_{\text{crit}}\right] \\ 1 & \text{for } T > \beta + \Delta_{\text{crit}}, \end{cases} \tag{3.6}$$

where T is the total tumour density expressed in the units of maximal cellular density K, β is the fraction of maximal cellular density triggering malignant transformation and Δ_{crit} is the width (or sensitivity) of the switch function.

System (3.1) was simulated using the standard Matlab PDE solver *pdepe*. Since the bulk dynamics of FK-type equations does not depend much on the spatial dimensionality (see [192] for a similar example) we chose to simulate model equations in a one-dimensional domain. In order to avoid the boundary effects and focus on the dynamics of the tumour bulk, we took the computational domain Ω to be 10 cm which is much larger than the typical tumour sizes.

As in [98, 25] we assume that initial cells' density distribution is a Gaussian one with a mean cell density h_0 at the centre of the tumour $x = 0$, *i.e.*

$$L_0(x) = h_0 \exp\left(-\frac{x^2}{\sigma}\right), \tag{3.7}$$

where σ is a measure of the spread of LGG cells.

3.3.1 Values of the model parameters

System (3.1) with a function S defined by Eq. (3.6) and initial condition for LGG cells given by function (3.7) has nine parameters describing the dynamical properties of the two glioma cells compartments and the phenomenon of malignant transformation.

The maximal tumour density K is estimated by taking the typical astrocyte size to be about 10 μm in diameter leading to a value 10^8cells/mm^3 [197, 108].

The parameters ρ_L, D_L and ρ_H, D_H quantify the overall biological aggressiveness of gliomas growth, *e.g.* proliferation rates ρ_L and ρ_H are based on the observable values of tumour cells doubling times. We assume the LGG proliferation rate ρ_L to be larger than 0.0001/day, which is ten times smaller than the smallest proliferation rate observed in the study of Gerin *et al.* [25]. As an upper bound for ρ_L we take a value 0.008/day, which is the smallest value of proliferation rate estimated for HGGs [29]. The diffusion coefficient for LGGs is chosen in the range between 0.0003 and 0.008mm^2/day. These values are, respectively, around three times smaller than minimal and three times larger than the maximal values for LGG diffusion coefficients estimated in [25]. For HGG cells, we assume that they proliferate with a typical rate 0.042/day observed in this kind of tumours, see *e.g.* [198, 29] and move with diffusion coefficient between 0.0008 and 0.9mm^2/day. These values are close to minimal and maximal diffusion rates estimated in [29].

The value of critical density L_{crit} triggering microenvironment damage and the malignant transformation is taken to be around 60% of the carrying capacity K, in agreement with the previous estimates [1, 26]. The switch function sensitivity Δ_{crit} is arbitrarily chosen to be 5%.

The time τ needed for a high grade tumour to arise corresponds to the time required for the development of hypoxia in the presence of a high cellularity, the generation of transient hypoxic events leading to the development of more aggressive phenotypes and higher genetic instability leading to new mutations. We can estimate τ to be of the order of a few months (100–200 days) [3].

In order to estimate the tumours' sizes evolution in time on the basis of our reaction-diffusion system, we introduce the natural notion of "detection threshold", *i.e.* the minimal tumour cell density that can be detected as tumour tissue. In T2/FLAIR imaging sequences the delineated abnormality corresponds to the presence of oedema, see [199]. In LGGs, oedema correlates locally with the presence of glioma cells [189]. We assumed, in line with previous works [108, 23, 200], that the T2/FLAIR signal is detectable above a certain local cell-density threshold. The analysis of biopsies in LGG patients suggests that the detection threshold for gliomas should be fixed between 10 and 20% of the maximal local tissue density K [189]. In the following, similarly to [108, 124], we assume that the threshold of detection of gliomas d equals $0.16K$, what allows to calculate the diameter of the radiologically detectable part of the simulated tumour due to system (3.1).

The tumour cell density h_0 leading to relevant symptoms and disease detection is difficult to estimate as it can vary broadly depending on the tumour location. The normal physiological value of cellularity of brain tissue is around 10-15%. LGGs are characterised by an increased cellularity with respect to the healthy brain tissue. We assume that the minimal mean density leading to glioma diagnosis is around $0.3K$ as in [26]. Note that such value is bigger than the presumed value of the detection threshold d. This choice implies that the symptoms occur when the tumour cells density is 30% of the maximal tissue density. Thus, we impose the initial mean density h_0 to be no smaller than $0.3K$. On the other hand, as we consider only tumours before malignant transformation, h_0 should be smaller than $L_{\text{crit}} - \Delta_{\text{crit}}K = 0.57K$, which

corresponds to minimal density causing the onset of LGG cells transformation, as discussed previously.

Typical values together with units and the references used in this chapter are summarised in Tables 3.1 and 3.2.

Table 3.1: **Typical parameter values for system (3.1)**

Param.	Description	Value	Units	References
K	carrying capacity (maximal cellular density)	10^8	cells/mm^3	[197]
ρ_H	proliferation rate of HGG cells	0.042	1/day	[29, 198]
d	detection threshold	$0.16K$	cells/mm^3	[189, 108, 23]
L_{crit}	tumour cell density causing malignant transformation	$0.6K$	cells/mm^3	[26]
Δ_{crit}	switch function sensitivity	0.05	cells/mm^3	Assumed
τ	time of change to HGG phenotype	100	days	Estimated

Table 3.2: **Ranges of fitted parameters for system (3.1)**

Param.	Description	Range	Units	References
h_0	initial mean LGG cell density	$0.3K$–$0.57K$	cells/mm^3	[26]
ρ_L	proliferation rate of LGG cells	0.0001–0.008	1/day	[25, 29]
D_L	diffusion rate of LGG cells	0.0003–0.008	mm^2/day	[25]
D_H	diffusion rate of HGG cells	0.0008–0.9	mm^2/day	[29, 125, 108, 102]

3.3.2 Model fitting to patients data

A retrospective study of the volumetric growth of LGGs was developed to verify the potential of the mathematical model to describe the malignant transformation. Initially, for the presented study 82 patients diagnosed with LGG and followed with MRI scans were considered, see details in Section 1.7. The criteria for patient inclusion in this study were:

(i) first biopsy/surgery confirmed LGG (astrocytoma, oligoastrocytoma or oligodendroglioma), according to the WHO classification at the time of diagnosis,

(ii) second biopsy/surgery confirmed HGG (anaplastic oligodendroglioma, anaplastic astrocytoma, anaplastic oligoastrocytoma or glioblastoma),

(iii) availability of at least 5 MRI scans before the histological confirmation of the malignant transformation,

(iv) no treatment given in the period of study,

(v) no decrease of total tumour size observed in the absence of treatment.

Among all considered patients, 32 had confirmed malignant transformation and 8 satisfied all of the inclusion criteria of the study. Table 3.3 summarises the included patients data.

Radiological glioma growth was quantified by the measurements of the tumour diameter on successive T2 (or FLAIR) MRI scans as described in Chapter 1. Longitudinal data of mean tumour diameter evolution was used to fit the parameters of system (3.1). We fixed the initial condition (3.7) on the basis of the first MRI scan for each patient. Namely, for each patient the variance of LGG cells distribution was computed through

$$\sigma = -r_0^2 / \ln\left(\frac{d}{h_0}\right), \tag{3.8}$$

Table 3.3: **Characteristics of patients selected in the study**

Age at diagnosis, mean (st. deviation),	37.89 (13.66)
Sex, M/F	3/5
Histology at diagnosis	
Oligodendroglioma	2
Oligoastrocytoma	2
Astrocytoma	4
Ki-67 LI at diagnosis, mean (st. deviation)	4.71% (1.72%)
Histology after malignant transformation	
Anaplastic oligodendroglioma	4
Anaplastic astrocytoma	4
Ki-67 LI after malignant transformation, mean (st. deviation)	14.25% (4%)

where r_0 is the radius of a tumour calculated from the first MRI scan considered in the study, d is the detection threshold and h_0 is the mean cell density. Parameters h_0, ρ_L, D_L and D_H were considered to be patient-specific, and thus, fitted for each patient. The remaining parameters were chosen as described in Section 3.3.1. The error between measured tumour sizes and model outputs for each patient was based on the relative least squares method. The fitted parameters were obtained as a result of the sum of squared relative residuals minimalisation performed through particle swarm optimisation algorithm, *cf.* Section 1.7. For the purpose of fitting LGGs evolution, 100 iterations of this algorithm were computed for each patient and the size of a swarm in each iteration step was set to be 100. For each patient, the set of fitted parameters (h_0, ρ_L, D_L, D_H) were fitted at once with starting point chosen visually.

For each patient included in the study, we show in Figure 3.1 both the real tumour diameter longitudinal data obtained from the MRI scans and the results of fitting to system (3.1). Parameters values obtained by model fitting to patients data together with errors of fit are listed in Table 3.4. The model dynamics shows a very good agreement with the real dynamics despite the use of a minimal number of parameters.

Table 3.4: **Model parameters fitted for each patient and errors of fits**

patient id	h_0/K	ρ_L (/day)	D_L (mm^2/day)	D_H (mm^2/day)	error
60	0.3404	0.001223	0.001227	0.004056	0.38%
61	0.3005	0.000253	0.000306	0.894292	0.21%
65	0.5435	0.000447	0.000858	0.745564	0.14%
66	0.5371	0.000243	0.000550	0.008817	0.08%
141	0.4613	0.001789	0.003597	0.015512	0.19%
165	0.5692	0.000553	0.0007558	0.001919	0.83%
195	0.4602	0.000764	0.007971	0.173277	0.45%
211	0.4144	0.002387	0.007383	0.087882	0.02%
mean (virtual patient)	0.4533	0.0009	0.0028	0.2414	0.2875%
st. deviation	0.0973	0.0008	0.0031	0.3639	0.2622%

3.3.3 Evolution of virtual patients' tumours

The typical evolution of a virtual tumour governed by system (3.1) is presented in Figures 3.2 and 3.3. Parameters h_0, ρ_L, D_L, D_H of the virtual patient were fixed to the mean values of parameters fitted to patients data, see Table 3.4. The initial condition for

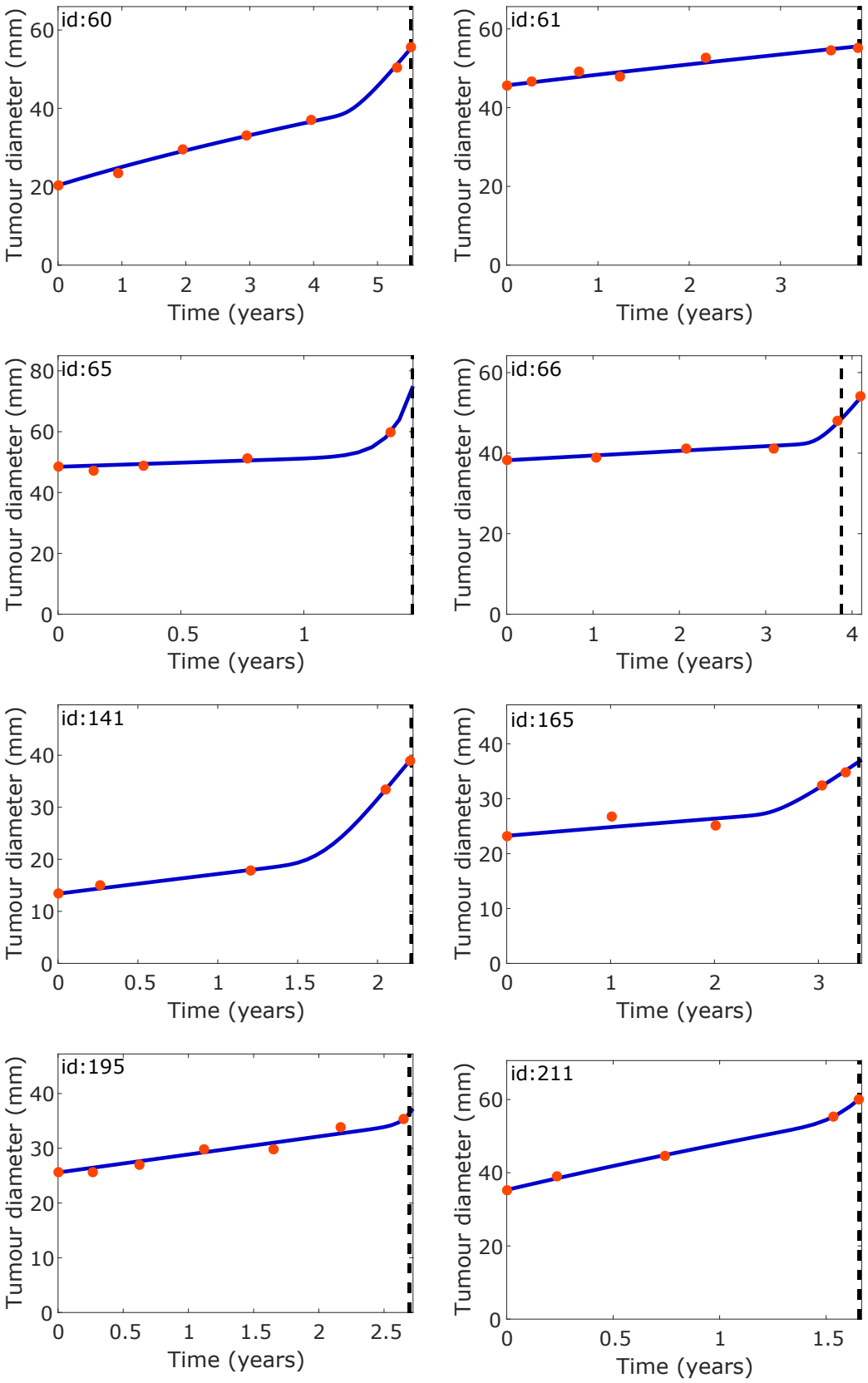

Figure 3.1: Tumour diameter evolution for patients with confirmed malignant transformation of LGG. The diameters calculated from MRI scans (red circles) and from the fitted mathematical model (3.1) (solid blue lines) are shown. The vertical black dashed lines mark the times when malignant transformation was confirmed histopathologically. The values of parameters σ, h_0, ρ_L, D_L, D_H were different for each patient (see Table 3.4). The parameter σ was calculated using Eq. (3.8). Other parameters values are listed in Table 3.1.

the simulation is

$$L(0,x) = h_0 \exp\left(-x^2/235.012\right), \quad H(0,x) = 0$$

with x measured in mm, what gives an initial tumour diameter of 31.278 mm, being the mean value of initial tumour diameters of patients selected for model fitting. The remaining parameters used in the simulations are fixed as listed in Table 3.1 and in penultimate row of Table 3.4.

When the cell density of LGG cells (Figures 3.2(a) and 3.3(a)) reaches the critical level (Figure 3.3(b)) HGG cells appear and start growing (Figure 3.3(c)) until they completely dominate the dynamics (Figure 3.2(b) and Figure 3.3(d)). This change in a cellular density is observed in patients as an appearance or a significant increment in contrast-enhancing areas in post-contrast T1+Gd MRI scans in the areas where the malignant transformation occurs. It also causes a considerable increase in the total tumour mass that is reflected in solutions of our model, see Figure 3.3 and also visible in diffusion-weighted imaging in the form of a restriction of the water mobility in the corresponding tumour areas [201]. Moreover, after some time the tumour is almost completely composed of the high-grade tumour cells as observed in clinical practice and also reflected by our model.

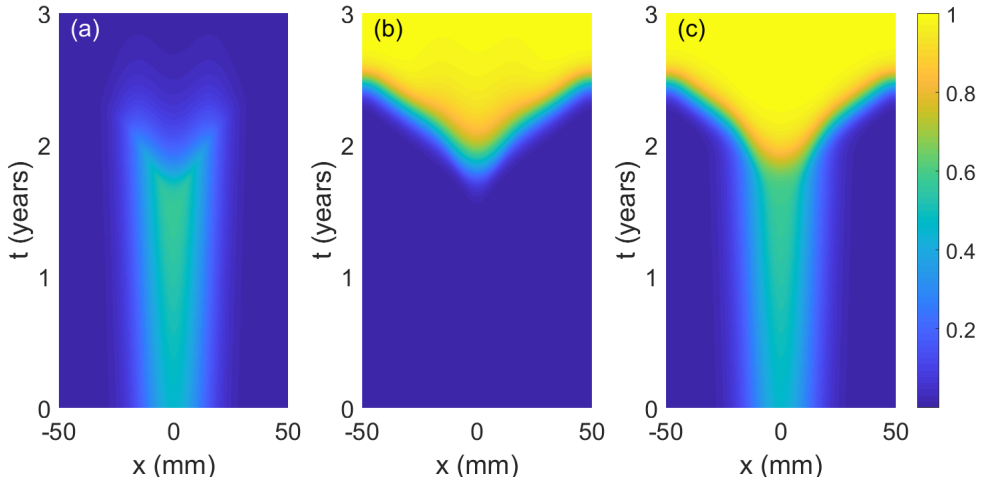

Figure 3.2: Spatiotemporal simulations of the malignant transformation of LGGs. Pseudocolour plots represent densities of (a) LGG cells, (b) HGG cells and (c) total (LGG + HGG) population with maximal density rescaled to 1. The vertical and horizontal axes correspond to the time in years and space in mm, respectively. A virtual tumour evolves according to system (3.1) with initial condition and the values of parameters as in Section 3.3.3.

3.3.4 LGG proliferation rate determines prognosis

To correlate the numerical simulations with the patient prognosis we assume that a tumour of a certain size is not compatible with life as stated, among others, in [108, 102]. This critical size is usually referred to as "fatal tumour burden". In this chapter, we fix the value of the fatal tumour burden to be equal to the tumour of 8 cm in diameter. Although this is critically dependent on tumour location, in general, this is believed to be a reasonable approximation. The assumed value of fatal tumour burden is larger than the value suggested in previous studies of HGG growth with the use of mathematical models [108, 102] due to the fact that in our database there were reported tumours of diameter even greater than 7.5 cm. Moreover, the slow evolution of LGGs allows the brain to remap neurological functions to other brain areas enabling these tumours to grow to larger sizes in comparison to HGGs. In our mathematical

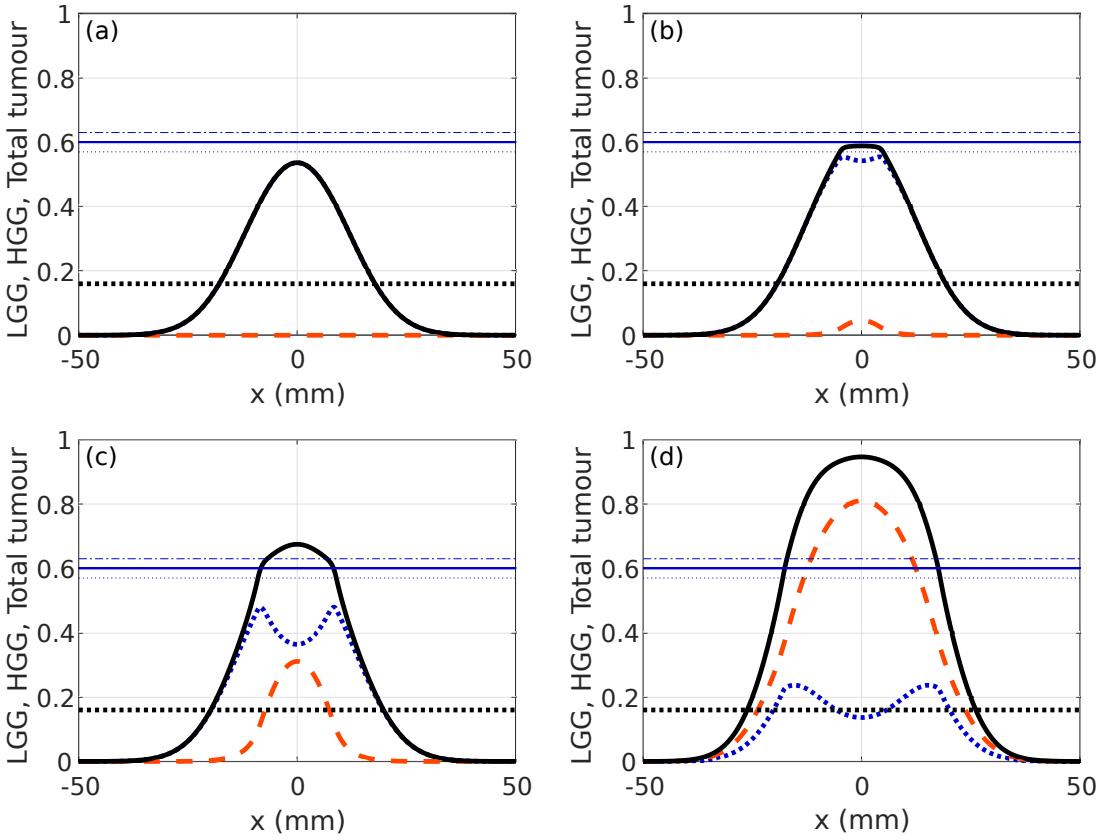

Figure 3.3: Snapshots of the evolution of the LGG and HGG cells densities solving system (3.1) for the parameter values and initial conditions as described in Section 3.3.3. The densities of LGG cells $L(x,t)$ (red dashed lines), HGG cells $H(x,t)$ (blue dotted lines) and the total tumour (black solid line) are shown. The horizontal blue lines correspond to the value L_{crit} (solid line), $L_{\text{crit}} - \Delta_{\text{crit}}$ (blue dotted line) and $L_{\text{crit}} + \Delta_{\text{crit}}$ (blue dashed-dotted line). The value of the detection threshold is marked with dashed horizontal lines. Results are shown for time t equal (a) 12, (b) 20, (c) 22 and (d) 25 months.

framework, we treat the time ranging from the virtual tumour detection to the time when it reaches the fatal tumour burden size as the estimate of overall survival, *cf.* Section 2.3.3.

Based on numerical simulations of system (3.1) we conclude that the parameter ρ_L has a large influence on the overall survival of virtual patients, estimated as described in Section 2.3.3. Figure 3.4 presents overall survival as a function of both proliferation rates for LGG and HGG in the absence of any treatment and the remaining parameters fixed to the mean values obtained from fit to real patients data (in the penultimate row of Table 3.4). We observe that changes in ρ_H have a minor effect on survival. However, a modification of ρ_L, the proliferation rate in the slowly growing stage of the disease, affects very significantly the virtual patient survival. For the mean value of proliferation rate $\rho_L = 0.0009$/day, overall survival for virtual patients varies from 3.7222 years (for $\rho_H = 0.008$/day) to 2.1944 years (for $\rho_H = 0.08$/day). For the typical value of $\rho_H = 0.042$/day (see Table 3.1) virtual patient survival varies from 22.2778 years (for $\rho_L = 0.001$/day) to 1.0556 year (for $\rho_L = 0.008$/day). This is an expected outcome of the model since in previous works [115, 116, 118, 124] it has been shown that the velocity of LGG growth is a prognostic factor for malignant transformation-free survival and overall survival. It is also reflected in our model.

This is an interesting result which can have an influence on treatment planning as nowadays in many cases more intensive therapies such as radiotherapy or even significantly less

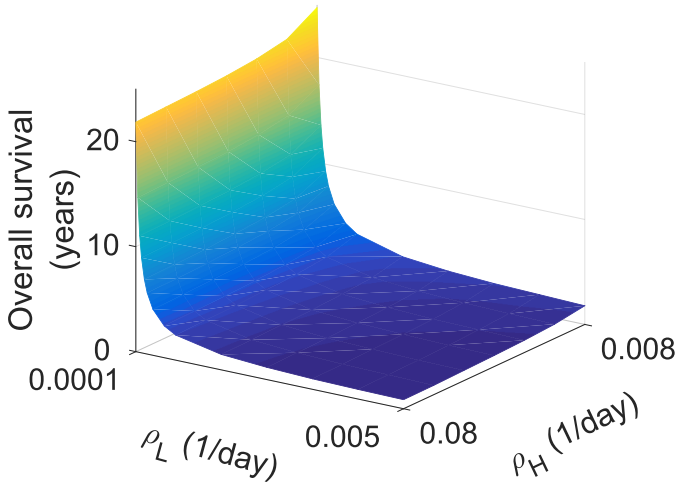

Figure 3.4: Overall survival for virtual patients with different proliferation rates of LGG and HGG cells evolving as indicated by system (3.1). The initial tumour cell densities and parameters for virtual patients were taken as in Section 3.3.3.

toxic chemotherapy are still reserved until there are signs of radiological progression to HGG (*e.g.* spots of contrast enhancement on T1+Gd MRI scans), *cf.* Section 1.5.

Although an inclusion of treatment into the model and further analysis are needed, our results indicate that preventing or delaying malignant transformation should be the main objective of LGGs care. Thus, it may be better to use more aggressive interventions earlier than to wait and treat already transformed and fast-growing tumours. One can base the treatment decisions on the estimates of the tumour aggressiveness and predicted time to malignant transformation which can be obtained from imaging [1, 2], taking into account also the levels of cytotoxicity induced. This is in line with recent results suggesting that one may get a substantial therapeutical benefit by the use of protracted therapies instead of waiting for the malignant transformation to occur [26, 134].

3.3.5 The role of the rate of phenotypic change

Intuitively, time τ gives an order of magnitude of the time to complete malignant transformation once the density reaches the critical level. Figure 3.5 shows the dependence of the virtual patient survival on the parameter τ for our standard set of parameters described in Section 3.3.3. In our simulations, the choice of this parameter does not essentially influence survival which differs within the range of 3 months, which is not significant when compared to the average survival of LGGs, being of the order of years [10]. Since the major component of survival time is given by the survival before the malignant transformation, this time adds only weeks or at most a few months to the total survival. For the other sets of parameters, the results are very similar.

3.3.6 Sensitivity analysis

To study the effects of parameter value uncertainties for system (3.1) we perform sensitivity analysis, described in Section 1.7. We allow variation in the following parameters: $\rho_L, \rho_H, D_L, D_H, r_0, h_0$. Each of these parameters' values is sampled from a uniformly distributed random variable within the respective range. Ranges of parameters h_0, ρ_L, D_L, D_h considered for sensitivity analysis are taken as in Table 3.2. The range of parameter r_0 is given by the

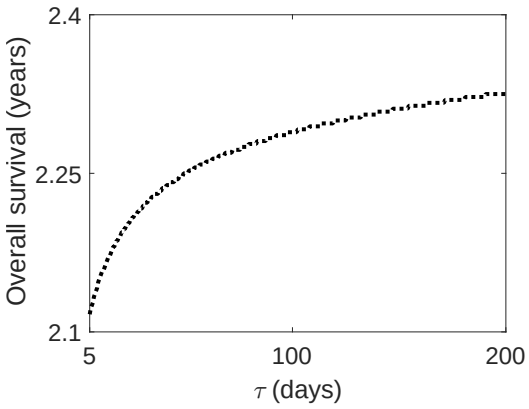

Figure 3.5: Relation between the characteristic time of phenotypic change τ and overall survival for virtual patients. The initial tumour cell densities and parameters' values are taken as in Figure 3.2.

minimal and maximal value of initial tumour radius of patients described in Section 3.3.2, thus, $r_0 \in [6, 25]$mm, whilst the range of ρ_H is fixed to be [0.008, 0.08]/day as observed in the study of HGGs [29]. The remaining parameters' values are taken as in Table 3.1.

In order to perform sensitivity analysis first we generate 1000 samples using Latin Hypercube Sampling algorithm. To measure the linear associations between the result and each parameter we compute Spearman's partial rank correlation coefficients.

Firstly, we focus on the sensitivity of the onset of malignant transformation, thus, we neglect the tumour evolution after the appearance of the HGG phenotype. As a consequence, we take into account the following parameters: ρ_L, D_L, h_0, r_0.

Secondly, we consider the sensitivity of the overall survival calculated for virtual tumours as described in Section 3.3.4. We study the influence of parameters $\rho_L, \rho_H, D_L, D_H, r_0, h_0$.

Main sensitivity analysis results are shown in Figure 3.6 and Table 3.5. As far as the onset of malignant transformation is considered, it correlates negatively with proliferation rate ρ_L and the initial mean LGG cell density h_0. There are no strong relations between diffusion rate D_L or initial tumour radius r_0 with the independent variable (onset of malignant transformation). Overall survival is observed to have a strong correlation only with ρ_L and h_0, both of them are negative. All of the computed correlation coefficients were statistically significant at the significance level 0.005.

Table 3.5: **Correlation rates between overall survival and onset of malignant transformation and model parameters**

model parameter	overall survival	onset of malignant transformation
ρ_L	-0.877	-0.905
h_0	-0.823	-0.908
ρ_H	-0.526	—
D_H	-0.47	—
r_0	-0.211	-0.212
D_L	0.096	0.172

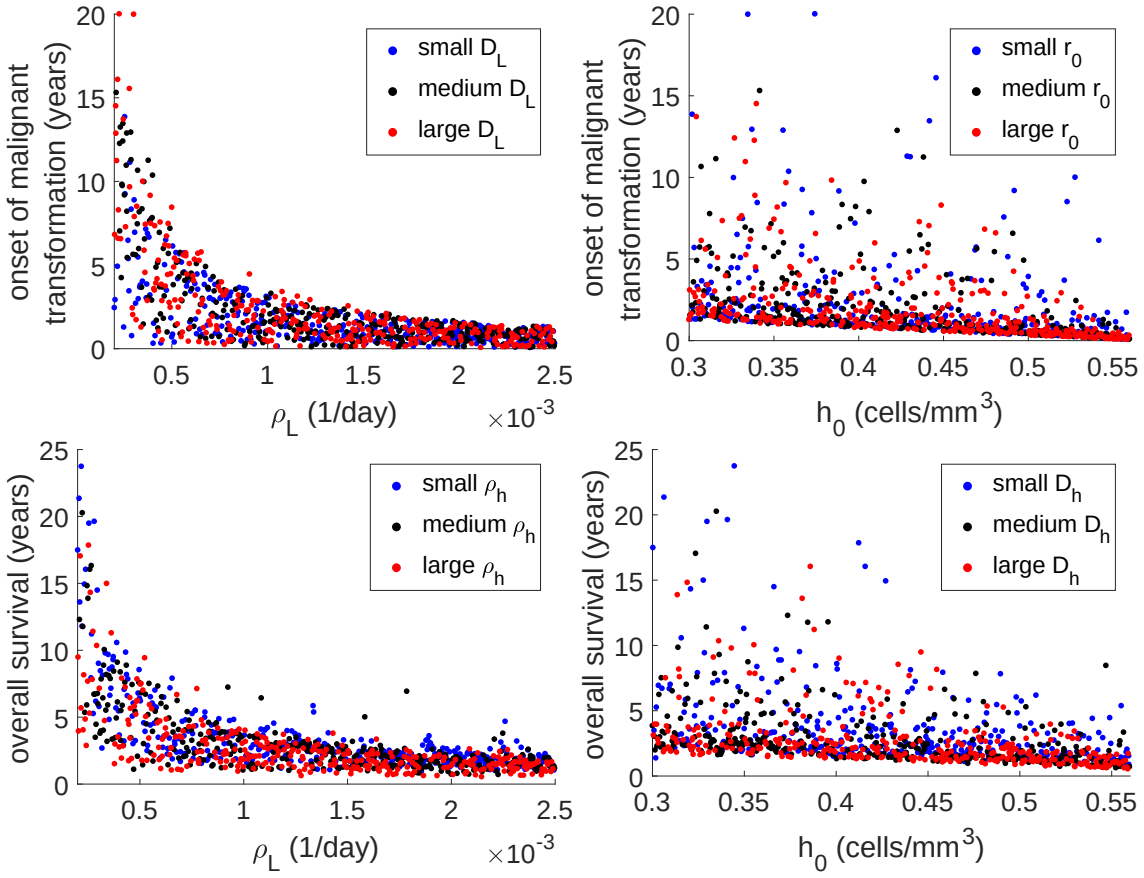

Figure 3.6: The results of sensitivity analysis. We show the dependence between LGG cells' proliferation rate ρ_L and the onset of malignant transformation (top left), initial mean tumour density h_0 and onset of malignant transformation (top right) for 1000 virtual patients with different values of diffusion rates D_L and initial tumour diameters r_0. The dependences between LGG cells' proliferation rate ρ_L and overall survival (bottom left), initial mean tumour density h_0 and overall survival (bottom right) were plotted for 1000 virtual patients with different values of HGG cells' proliferation rate ρ_H and diffusion rates D_H.

3.4 Analytical estimates of LGG growth and malignant transformation

3.4.1 Estimates of LGG growth

We assume that initially, until the onset of malignant transformation, the tumour is composed of LGG cells, and thus, its evolution is described by a single FKE:

$$\frac{\partial L}{\partial t} = \rho_L L \left(1 - \frac{L}{K}\right) + D_L \Delta L \tag{3.9a}$$

with initial condition:

$$L(0, x) = L_0(x), \tag{3.9b}$$

where the function L_0 is given by Eq. (3.7), that is

$$L_0(x) = h_0 \exp\left(-\frac{x^2}{\sigma}\right).$$

We consider Eq. (3.9a) with no-flux boundary condition:

$$\left.\frac{\partial L}{\partial n}\right|_{\partial\Omega} = 0, \tag{3.9c}$$

see also system (3.1). For convenience throughout this section, we use ρ and D instead of ρ_L and D_L.

We assume that until malignant transformation, glioma total density is smaller than the maximal cellular density in the brain. Therefore, in Eq. (3.9a) we neglect the non-linear term and approximate the solution L to system (3.9) by a solution u to the following equation referred to as Skellam equation [100]:

$$u_t = \rho u + D\Delta u \tag{3.10}$$

together with free boundary condition and the initial condition

$$u(0, x) = L_0(x),$$

cf. Eq. (3.9b).

Let us denote by $\delta(x)$ the Dirac distribution centered at $x = 0$. Note that function L_0 given by Eq. (3.7) is a solution of Eq. (3.10) with initial condition

$$u(-\bar{t}, x) = \ell_0 \delta(x)$$

and free boundary condition at time $t = -\bar{t}$.
If $\bar{t}$ is the initial time for Eq. (3.10), then the solution in one spatial dimension is given by:

$$u(\bar{t} + t, x) = \frac{\ell_0}{2\sqrt{\pi D(\bar{t} + t)}} e^{\rho(\bar{t}+t)} e^{-\frac{x^2}{4D(\bar{t}+t)}}. \tag{3.11}$$

We calculate the values of parameters ℓ_0 and $\bar{t}$ by comparing Eq. (3.11) with Eq. (3.7) describing glioma distribution at the time of first MRI scan. Then the measure of the dispersion σ and the mean tumour density h_0 at time $\bar{t}$ are given by:

$$h_0 = \frac{\ell_0}{2\sqrt{\pi D\bar{t}}} e^{\rho\bar{t}}, \quad \sigma = 4D\bar{t}. \tag{3.12}$$

Using (3.12) we eliminate $\bar{t}$ and ℓ_0 from (3.11), obtaining

$$u(\bar{t} + t, x) = \frac{\ell_0 e^{\rho\bar{t}}}{2\sqrt{\pi D\bar{t}}} \sqrt{\frac{\bar{t}}{\bar{t} + t}}\, e^{\rho t} e^{-\frac{x^2}{4D\bar{t}} \cdot \frac{\bar{t}}{\bar{t}+t}} = h_0 e^{\rho t} \sqrt{\frac{\sigma}{\sigma + 4Dt}}\, e^{-\frac{x^2}{\sigma+4Dt}}. \tag{3.13}$$

One should bear in mind that $\bar{t}$, ℓ_0 and Dirac delta are only mathematical tools used here to estimate the onset of malignant transformation. Due to the limitations of continuous macroscopic models, time $\bar{t}$ cannot be directly interpreted as a time from the "tumour birth" till the first MRI. Possibly some stochastic model would be a more realistic method to describe a tumour growth in its initial stage (when it is impossible to diagnose and detect through imaging techniques). However, the study of tumour growth when there are very few mutated cells is out of the scope of this thesis and here we use a simplification outlined above.

Hence, we approximate the tumour cell density after diagnosis by the explicit solution of Eq. (3.10):

$$u(t, x) = h_0 e^{\rho t} \sqrt{\frac{\sigma}{\sigma + 4Dt}}\, e^{-\frac{x^2}{\sigma+4Dt}}. \tag{3.14}$$

The virtual tumour is detectable at time t if $\max_x u(t, x) \geq d$. Clearly it is detectable for all positive times if

$$\min_{t\geq 0} \max_x u(t, x) = \min_{t\geq 0} u(t, 0) = \frac{\partial}{\partial t} u(t, 0) \geq d.$$

For

$$\sigma\rho > 2D \tag{3.15}$$

the function $u(t,0)$ is increasing and the tumour starts growing for time greater than $\frac{2D-\sigma\rho}{4D\rho}$. Finally when the condition

$$u(t,0) = h_0 e^{\frac{2D-\sigma\rho}{4D}} \sqrt{\frac{\sigma\rho}{2D}} \geq d$$

holds we can calculate the evolution of tumour radius by finding such r that

$$u(t, r(t)) = d.$$

Consequently, the analytical formula for the tumour radius reads

$$\begin{aligned} r(t) =& 2t\sqrt{D\rho}\left(1 - \frac{\ln(\sigma+4Dt)}{2\rho t} + \frac{1}{t}\left(\frac{\sigma}{4D} + \frac{1}{\rho}\ln\left(\frac{h_0}{d}\sqrt{\sigma}\right)\right) + \right. \\ & \left. - \frac{\sigma\ln(\sigma+4Dt)}{8D\rho t^2} + \frac{\sigma}{4D\rho t^2}\ln\left(\frac{h_0}{d}\sqrt{\sigma}\right)\right)^{1/2}. \end{aligned} \tag{3.16}$$

Next, calculating the first derivative of r with respect to time we obtain the tumour growth velocity:

$$r'(t) = \frac{2\sqrt{D\rho}\left(1 - \frac{\ln(\sigma+4Dt)}{4\rho t} + \frac{1}{2t}\left(\frac{\sigma}{4D} + \frac{1}{\rho}\ln\left(\frac{h_0}{d}\sqrt{\sigma}\right) - \frac{1}{2\rho}\right)\right)}{\sqrt{1 - \frac{\ln(\sigma+4Dt)}{2\rho t} + \frac{1}{t}\left(\frac{\sigma}{4D} + \frac{1}{\rho}\ln\left(\frac{h_0}{d}\sqrt{\sigma}\right)\right) - \frac{\sigma\ln(\sigma+4Dt)}{8D\rho t^2} + \frac{\sigma\ln\left(\frac{h_0}{d}\sqrt{\sigma}\right)}{4D\rho t^2}}}. \tag{3.17}$$

Clearly, the formulae for the tumour radius and tumour growth velocity are rather complex. Thus, we now derive approximations of these formulae for the cases when $t \ll 1$ and $t \gg 1$. First, we investigate the long-time behaviour of Eqs. (3.16) and (3.17). In this case, using Taylor expansion, we have

$$\begin{aligned} \ln(\sigma+4Dt) &= \ln\left(4Dt\left(1+\frac{\sigma}{4Dt}\right)\right) = \ln t + \ln(4D) + \ln\left(1+\frac{\sigma}{4Dt}\right) \\ &= \ln t + \ln(4D) + \frac{\sigma}{4Dt} + o\left(\frac{1}{t}\right). \end{aligned} \tag{3.18}$$

Plugging Eq. (3.18) into Eq. (3.16), using asymptotic approximation and keeping only terms of order equal or higher than $1/t$ we obtain

$$r(t) = 2t\sqrt{D\rho}\left(1 - \frac{\ln t}{4\rho t} + \frac{1}{2\rho t}\left(\frac{\sigma\rho}{4D} + \ln\left(\frac{h_0}{d}\sqrt{\sigma}\right) - \frac{\ln 4D}{2}\right) + o\left(\frac{1}{t}\right)\right).$$

The use of similar methods leads to the formula for the velocity:

$$r'(t) = 2\sqrt{D\rho}\left(1 - \frac{1}{4\rho}\cdot\frac{1}{t} + o\left(\frac{1}{t}\right)\right).$$

This result shows that tumour radius asymptotically grows with a speed slower than the asymptotic velocity of FKE, where the first correction term is equal to $1/(4\rho t)$. This means that for large times the lack of restriction on the density leads to slower tumour growth. This might seem a surprising result, but in fact, it not so. In the regions of elevated tumour cells' density, cell division is slower due to the competition. On the other hand, high cell density also

forces tumour cells to move to the area with a lower density which leads to a faster increase of tumour radius.

The behaviour of the tumour radius and velocity for small times is also relevant. Since in that regime the maximal tumour density is relatively small, we expect better agreement of the results with those of the full model. In order to obtain an asymptotic approximation of the tumour radius for $t \ll 1$ we expand the right-hand side of Eq. (3.16) in Taylor series around $t = 0$, obtaining

$$\ln(\sigma + 4Dt) = \ln\left(\sigma\left(1 + \frac{4D}{\sigma}t\right)\right) = \ln\sigma + \ln\left(1 + \frac{4D}{\sigma}t\right) = \ln\sigma + \frac{4D}{\sigma}t + o(t), \quad \text{as} \quad t \to 0.$$

Neglecting the terms of order higher than t and using Eq. (3.8) to eliminate $\ln(h_0/d)$ we arrive at

$$r(t) = r_0\left(1 + \frac{1}{2}\left(\frac{4D}{\sigma} + \frac{\sigma\rho - 2D}{r_0^2}\right)t + o(t)\right). \tag{3.19}$$

Finally using the same techniques as before for approximation of tumour radius, we derive the approximation of the velocity of the tumour growth as $t \to 0$:

$$r'(t) = \frac{2D}{\sigma}r_0 + \frac{\sigma\rho - 2D}{2r_0} + t\left(\frac{4D}{\sigma}\cdot\frac{\sigma\rho - D}{r_0} - \frac{r_0}{4}\left(\frac{4D}{\sigma} + \frac{\sigma\rho - 2D}{r_0^2}\right)^2\right) + o(t).$$

It is interesting to note that the tumour growth velocity depends on r_0, *i.e.* on the term $\ln(h_0/d)$. In particular, for $\sigma\rho > D$ there exists a ratio h_0/d for which this velocity is minimal and equals $\frac{2D}{\sigma}r_0 + \frac{\sigma\rho - 2D}{2r_0}$. It is easily seen that for $t \to 0$ the value of tumour radius and tumour growth velocity tend to r_0 and $\frac{2D}{\sigma}r_0 + \frac{\sigma\rho - 2D}{2r_0}$, respectively. In Figure 3.7 we compare the results obtained using FKE, Skellam model and the asymptotic formula (3.19) for the parameters values estimated for patients indicated in Section 3.3.2.

3.4.2 Estimates of malignant transformation

Here we intend to provide some analytical estimates for the onset of malignant transformation. The onset of malignant transformation can be estimated directly from numerical simulations of Eq. (3.9a), let us denote it as t_{OMT}. On the other hand, instead of considering partial differential equations, we would like to obtain a simple algebraic formula.

Based on Eq. (3.14) we can estimate the time $t_{\mathrm{OMT,S}}$ of the onset of malignant transformation as the time when the LGG cell density hits the value $L_{\mathrm{crit}} - \Delta_{\mathrm{crit}}$. Let us recall that $h_0 < L_{\mathrm{crit}} - \Delta_{\mathrm{crit}}$, see Section 3.3.1. As the function u attains its maximum at $x = 0$, we calculate $t_{\mathrm{OMT,S}}$ in the following way:

$$\begin{aligned} L_{\mathrm{crit}} - \Delta_{\mathrm{crit}} &= h_0 e^{\rho t_{\mathrm{OMT,S}}}\sqrt{\frac{\sigma}{\sigma + 4Dt_{\mathrm{OMT,S}}}}, \\ 2\rho t_{\mathrm{OMT,S}} &= \ln\left(\left(\frac{L_{\mathrm{crit}} - \Delta_{\mathrm{crit}}}{h_0}\right)^2\left(1 + \frac{4D}{\sigma}t_{\mathrm{OMT,S}}\right)\right). \end{aligned} \tag{3.20}$$

The right-hand side of Eq. (3.20) is a convex function of $t_{\mathrm{OMT,S}}$, thus, it have unique solutions. The solution of Eq. (3.20) exists when the condition

$$\sigma\rho \geq 2D$$

holds, compare condition (3.15).

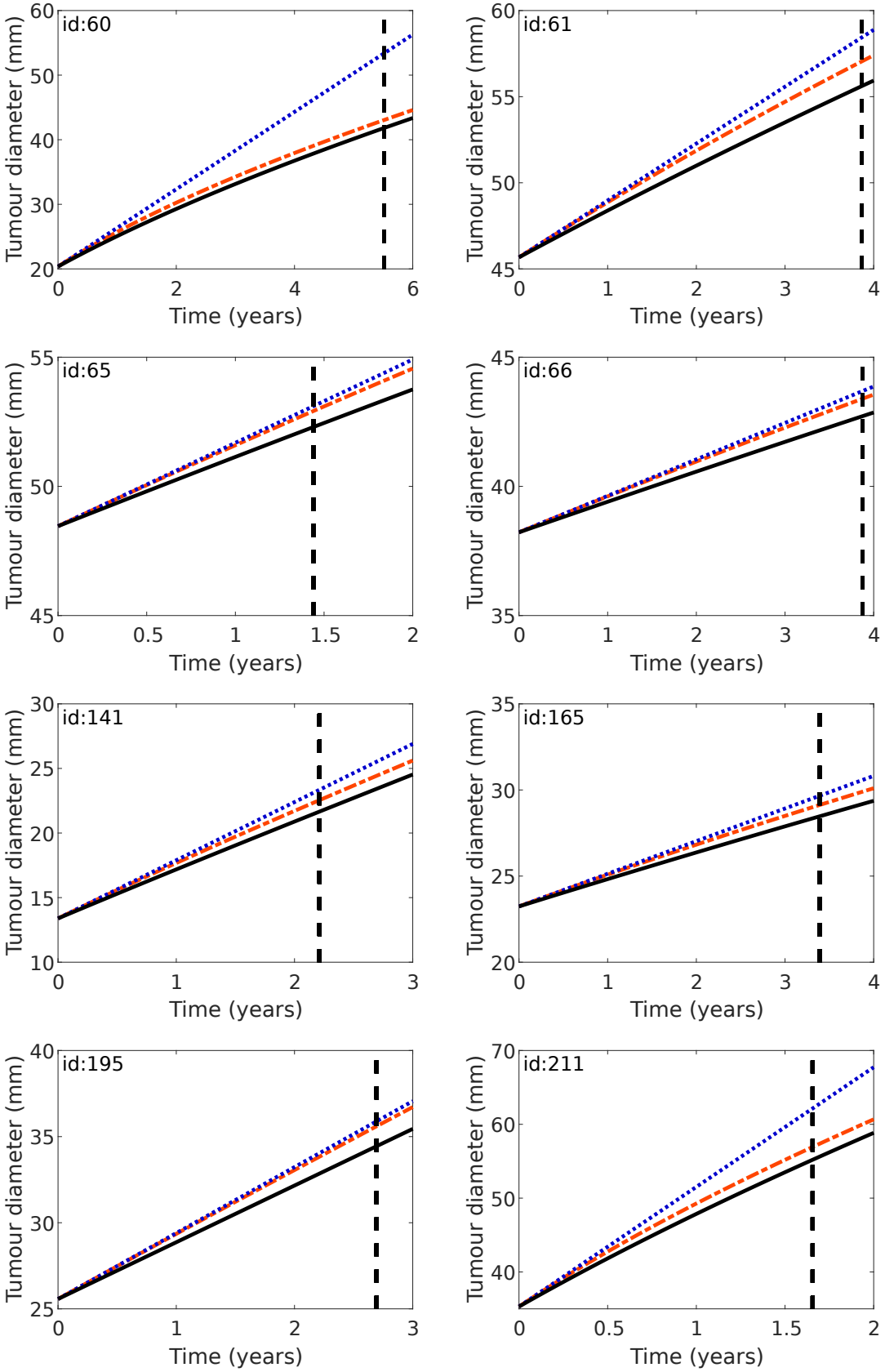

Figure 3.7: Evolution of LGGs diameter – results based on the simulations of FKE (3.9a) (black solid line), analytical equation of radius evolution (3.16) (red dashed-dotted line) according to Skellam model (3.10) and asymptotic behaviour of radius as $t \to 0$ (3.19) (blue dotted line). The vertical dashed line denotes the time when malignant transformation was confirmed histopathologically. The model parameters and initial conditions are the same as in Figure 3.1 for patients indicated in Section 3.3.2.

We observe that $t_{\mathrm{OMT,S}}$ strongly depends on tumour density at the point where the cellular density is the highest. For sufficiently small LGG cell diffusion coefficient we can approximate the evolution of tumour density at $x = 0$ by the logistic equation. Thus, we consider $L(0,t) \leq u(t)$, where u is a solution to

$$u_t = \rho u \left(1 - \frac{u}{K}\right) \tag{3.21a}$$

with initial condition given by the density in the centre of the tumour:

$$u(0) = h_0. \tag{3.21b}$$

Solving system (3.21), we obtain the lower estimate of onset of malignant transformation:

$$t_{\mathrm{OMT,L}} = \frac{1}{\rho} \ln \left(\frac{(L_{\mathrm{crit}} - \Delta_{\mathrm{crit}})(1 - h_0)}{h_0 (1 - (L_{\mathrm{crit}} - \Delta_{\mathrm{crit}}))} \right). \tag{3.22}$$

This estimate is expected to be good for small diffusion rates of LGG cells. For larger diffusion rates estimation given by Eq. (3.20) is a better one for considered ranges of parameters, compare Figure 3.8. Thus, we propose to estimate t_{OMT} analytically as

$$t_{\mathrm{OMT}} \approx \max\left\{ t_{\mathrm{OMT,S}}, t_{\mathrm{OMT,L}} \right\}. \tag{3.23}$$

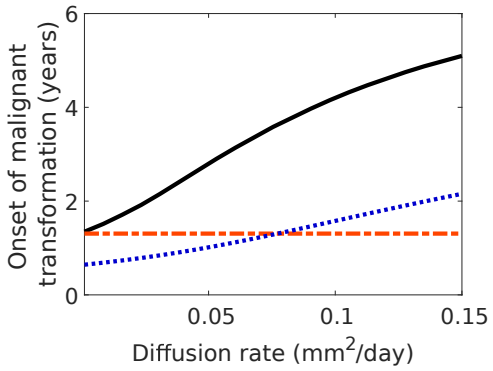

Figure 3.8: Estimates of the onsets of malignant transformation: t_{OMT} (black solid line), $t_{\mathrm{OMT,S}}$ (blue dotted line) and $t_{\mathrm{OMT,L}}$ (red dashed-dotted line) for virtual patients with different values of diffusion rate D. The initial tumour cell densities and other parameters' values are taken as in Figure 3.2.

We have computed the estimates of the onset of malignant transformation for six patients for which the occurrence of malignant transformation was observable radiologically in tumour size, see Figure 3.9. Our work shows that all estimated onsets of malignant transformation appear in a medically viable time period. We can observe a significant delay from the onset of malignant transformation to the visible change in the velocity of tumour radius growth. A natural explanation is that there is a visible increase in the detectable tumour size when the significant part of a tumour is formed by already transformed cells.

3.5 Discussion

In this chapter, we addressed the process of malignant transformation of low-grade gliomas, which is the main reason for the disease lethality. The early detection of malignant transformation could improve the therapeutical management and prevent the misdiagnosis of tumour

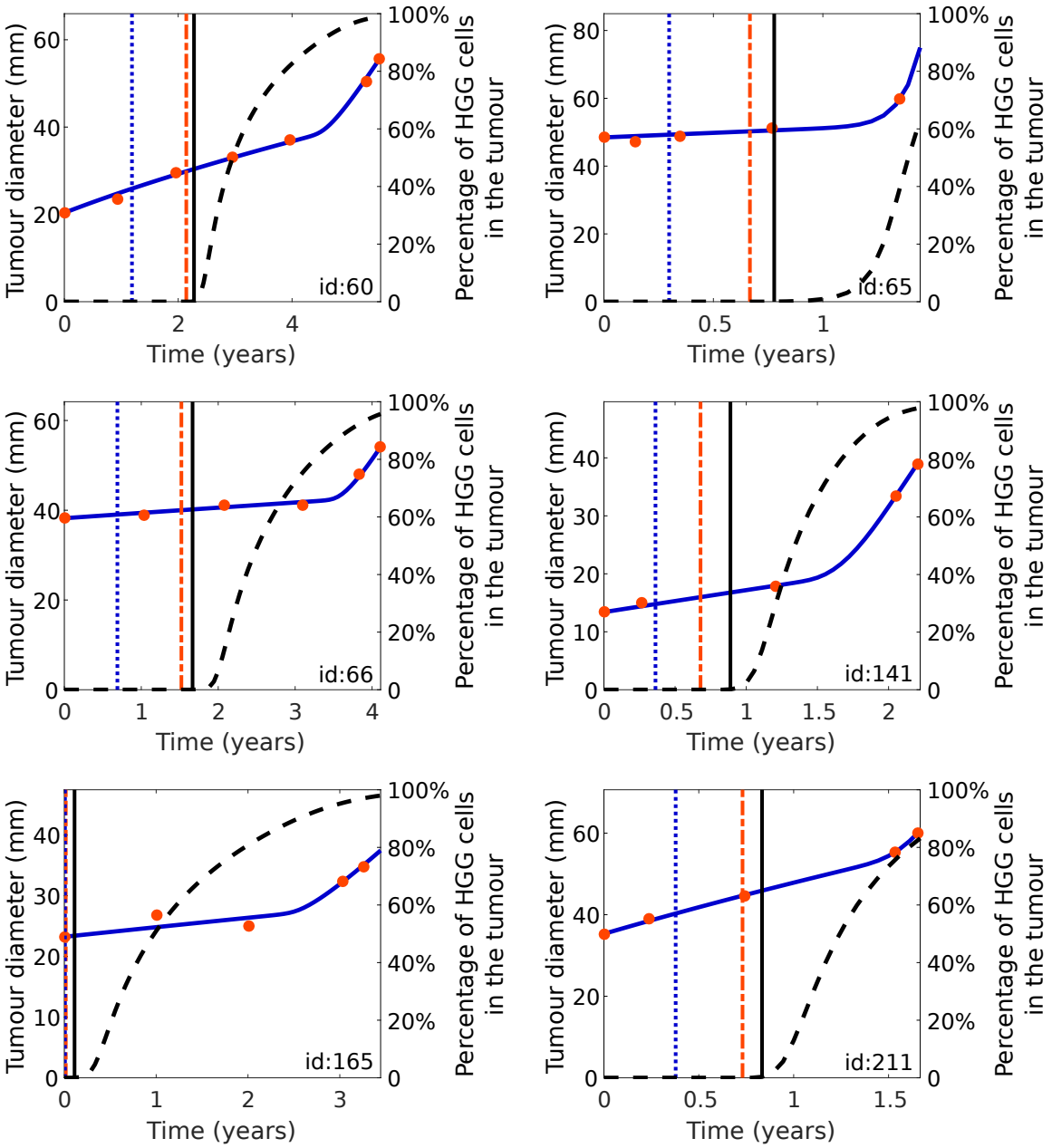

Figure 3.9: Evolution of tumour diameter due to system (3.1) together with the clinical data as in Figure 3.1, the estimation of the onset of malignant transformation calculated using simulations of Eq. (3.9a) (vertical black solid lines), Eq. (3.22) (red dashed-dotted lines) and Eq. (3.20) (blue dotted lines). We also show the percentages of HGG cells in total tumour mass calculated based on the results of simulations. The time scale of simulation ends when malignant transformation was confirmed histopathologically. Model parameters and initial conditions were the same as in Figure 3.1 for the first six patients in this study (dashed lines).

grade. It can have major therapeutic implications, namely the tumour with undetected malignant transformation would be treated less aggressively than necessary.

Recently it has been hypothesised that malignant transformation may be triggered by the change of the tumour microenvironment due to the elevation of the cell density in specific tumour areas [150, 1, 26, 121]. Here for the first time, we try to use this concept in a quantitative way to describe the full process of the malignant transformation from a LGG to a HGG. We describe this process in a minimal way using a model of two coupled FKEs in which total tumour density is a driving force of phenotypic change. Interestingly, the model is able to

reproduce the main features of the transition from low-grade into high-grade glioma. We presume that in our mathematical framework we can treat a tumour consisting of both LGG and HGG cells (see Figure 3.7) as WHO grade III glioma, which is an intermediate tumour stage between LGG (grade II) and secondary glioblastoma (grade IV) both histologically and at the molecular levels [202, 203]. Grade III gliomas, compared to grade II tumours, are more cellular, demonstrate more atypia, and mitoses are seen. However, unlike glioblastomas, they lack vascular proliferation and necrosis on pathologic evaluation. The difference between grade III and grade IV gliomas is also reflected in the patients' overall survival [204, 205] and prognosis.

We have also studied the analytical properties of the proposed model. We proved the global existence, non-negativity and uniqueness of solutions. As observed *in vivo* the model suggests that asymptotically all tumour cells transform into more aggressive HGG phenotype. We also showed that the diffusion-driven instability does not appear in the model. We believe that it is a biologically viable situation as spatial patterns and heterogeneity in glioma density should be a result of brain anisotropy rather than the processes of tumour growth and transformation.

We were also able to fit the model to the retrospective volumetric data of LGG patients who had undergone malignant transformation and obtained a very good agreement. Based on this results we can treat our new model as a first step in the investigation of malignant transformation as a function of patient-specific coefficients. From the practical point of view, the most interesting application of the model is to study its dynamics before malignant transformation as its early detection could improve prognosis. We believe that the knowledge of the approximated time of this transformation and its early detection could improve prognosis and help in making clinical decisions [204, 5].

We suggest combining the use of early imaging and the results of mathematical modelling. To be specific, first we simplified our model of evolution of LGGs and obtained analytical equations for tumour radius and velocity before the onset of malignant transformation. As a result, we were able to provide an early approximation of the onset of malignant transformation based on the patient-specific parameters. Although Eq. (3.23) looks complex, this formula is a significant simplification as instead of considering, in fact, a system of partial differential equations, we deal with an algebraic equation. Based on this formula and retrospective volumetric patients data, we have been able to compute *post-hoc* estimates of the onset of malignant transformation using the values of fitted parameters for individual patients. All estimated onsets of malignant transformation appear in a medically viable time period. However, there has been a significant delay from these times to times when the visible change in the velocity of tumour radius growth could be observed. It suggests that there is a visible increase in detectable tumour size when the already transformed cells form the substantial part of a tumour. Importantly, the obtained values do not overestimate medically confirmed malignant transformation time. Thus, we can interpret the estimated values as the earliest times when malignant transformation could occur.

Let us note that the estimated time of onset of malignant transformation depends crucially on three biologically relevant parameters: proliferation rate, motility rate and mean initial density. The last one is essential to estimate in an unambiguous way the time of malignant transformation before it occurs. In general, we would like to provide predictions of time to malignant transformation for individual patients using data of only a few medical examinations (MRI scans). However, our research shows that in order to do so, we would need imaging data from which an initial tumour density could be estimated. Clearly, the proliferation and diffusion rates for LGG cells could be estimated from a few MRI scans (possibly three) using *e.g.* a standard linear regression method. Subsequently, having parameters describing initial

LGG density and tumour growth rates, the estimate of malignant transformation time can be computed very easily from Eq. (3.23). In such a way, combining the modelling approach and imaging, one would be possibly able to predict non-invasively the malignant transformation. Interestingly, Hathout *et al.* in [124] using the methodology from the previous works, *e.g.* [29], estimated mean proliferation and motility rate based on results of two MRI scans for contrast-enhancing grade II astrocytoma and found out that those kinetics rates were significantly higher in the tumours that transformed to grade III or IV gliomas. It has been discussed recently that using different MRI modalities it may be possible to identify tumours undergoing malignant transformation [206] and predict if the risk of rapid malignant transformation is large [207, 85, 86]. The use of perfusion-weighted and diffusion-weighted MRI should be considered for broader use due to its potential [207, 85, 86, 208]. We believe that by continuing the research on both advances in the analysis of imaging data and mathematical modelling we would also be able to predict successfully malignant transformation.

Using such an approach, the results obtained from imaging data and the proposed model may open avenues for the treatment personalisation. In particular, fast-growing tumours or those which initial density was found to be significant should be followed with imaging thoroughly and early treatments strategies should be taken into account. One could consider planning treatments in advance for the time of predicted malignant transformation. By eradicating glioma cells either by surgery or chemotherapy, the tumour cells density will be reduced resulting in prolonged malignant transformation-free survival and as a consequence overall survival, as well.

We also believe that further understanding of the dynamics of the malignant transformation of LGGs may enable the development of more effective treatment strategies aimed at prolonging recurrence and delaying the arising of malignancy. Thus, further studies aimed at improving the understanding of the evolution of the malignant transformation, coupling multimodal imaging with mathematical models and studying the impact of optimised therapeutical schedules on the time to malignant transformation are necessary.

Chapter 4

Model of LGG growth with diffusion and response to chemotherapy. Alternative chemotherapy fractionations

In Chapter 2 we have studied a system of ODEs describing the evolution of LGGs' volumes and response to chemotherapy. However, in the course of this research, we have identified malignant transformation as the key process leading to major symptoms and subsequent patient death, *cf.* Chapters 1 and 3. It is believed that treatment of LGGs patients should be personalised according to the risk of malignant transformation. In Chapter 3 we have constructed a simple model relating the onset of malignant transformation with the increased local density of tumour cells. As a consequence of those results, we note that possibly a more effective treatment could be the one which delays the onset of malignant transformation the most. To study the evolution of LGGs local density, we consider the model of LGGs growth with motility term and response to chemotherapy. We intend to study a model of continuous chemotherapy (thus, different from the one proposed earlier in Chapter 2) administered to tumours that evolve not only due to proliferation, but also diffusion (that was not included there). We study the obtained model analytically and investigate the existence of travelling waves. Due to practical motivations, we also study whether the onset of malignant transformation could be deferred using some specific chemotherapy treatment schedules.

4.1 Travelling waves in the model of LGG growth with diffusion and response to chemotherapy

We modify system (2.2) with function f as in Eq. (2.1) by including a term describing motility of tumour cells with a constant rate δ. Thus, we consider the system:

$$\begin{aligned} \frac{\partial P}{\partial t} &= \delta \Delta P + \rho P \left(1 - \frac{P+D}{K}\right) - \alpha C P, \\ \frac{\partial D}{\partial t} &= \delta \Delta D - \frac{\rho}{k} D \left(1 - \frac{P+D}{K}\right) + \alpha C P, \end{aligned} \tag{4.1}$$

where $P(t,x)$ denotes the local density of proliferating tumour cells, $D(t,x)$ — local density of irreversibly damaged tumour cells for $(t,x) \in [0,+\infty) \times \Omega$ and $\Delta = \sum_{j=1}^{n} \partial^2/\partial x_j^2$. In general, Ω is assumed to be an open subset of $\mathbb{R}^n$ with a smooth boundary. System (4.1) is complemented by non-negative initial conditions and homogeneous von Neumann boundary conditions. We assume here the constant concentration C of chemotherapy drug acting on a tumour.

At the outset, for the purpose of the mathematical analysis, we rescale system (4.1) by taking $\widetilde{P} = P/K$, $\widetilde{D} = D/K$, $\widetilde{t} = \rho t$, $\widetilde{x} = \sqrt{\frac{\rho}{\delta}} \cdot x$. Omitting the tildes for simplicity we arrive at the non-dimensional system:

$$\begin{aligned} \frac{\partial P}{\partial t} &= \Delta P + P(1-P-D) - zP, \\ \frac{\partial D}{\partial t} &= \Delta D - \frac{1}{k} D(1-P-D) + zP, \end{aligned} \tag{4.2}$$

where $z = \alpha C/\rho$ with von Neumann boundary conditions

$$\left.\frac{\partial P}{\partial \vec{n}}\right|_{\partial\Omega} = \left.\frac{\partial D}{\partial \vec{n}}\right|_{\partial\Omega} = 0 \tag{4.3}$$

and initial conditions

$$P(0,x) \in [0,1], \quad D(0,x) = 0. \tag{4.4}$$

We postulate that initial function is of class C^2 on $\bar{\Omega}$.

Theorem 4.1. *There exists local unique classical solution to system (4.2)–(4.4).*

Proof. The reaction term of system (4.2)–(4.4) and initial conditions are C^2 functions, thus, solution to system (4.2)–(4.4) exists locally and is unique due to general properties of reaction-diffusion systems, see *e.g.*Theorem 3.3.3. in [193]. □

In Chapter 2, among others, we have studied the dynamics of system (2.11), which for f given by Eq. (2.1) is an equivalent of system (4.2) without diffusion, *i.e.* a system of the form:

$$\begin{aligned} \frac{\mathrm{d}P}{\mathrm{d}t} &= P(1-P-D) - zP, \\ \frac{\mathrm{d}D}{\mathrm{d}t} &= -\frac{1}{k} D(1-P-D) + zP. \end{aligned} \tag{4.5}$$

We recall that system (4.5) has at most three steady states:

- $(0,0)$ which is either a stable node for $z > 1$ or a saddle for $z < 1$,
- $(0,1)$ which is a saddle,
- $(\widetilde{x}, k\widetilde{x})$ which exists for $z < 1$ and is either a stable node or stable focus,

see Section 2.2 for details. Thus, for system (4.2) there exists a heteroclinic orbit connecting steady states $(0,1)$ and $(0,0)$ provided that $z < 1$. This heteroclinic orbit is $\{P = 0\} \times [0,1]$, see also Figure 2.4.

Now, we verify whether for system (4.2) with $z < 1$ there exist travelling waves which connect the two uniform steady state solutions $(0,1)$ and $(0,0)$. From now on, for simplicity, we assume that $\Omega \subset \mathbb{R}$.

By travelling wave we mean a wave which propagates with constant speed ϑ without changing the shape [112], *i.e.* we look for the solutions $P(t,x)$, $D(t,x)$ of system (4.2) corresponding to the front

$$P(t,x) = U(x+\vartheta t), \quad D(t,x) = V(x+\vartheta t),$$

and satisfying boundary conditions:

$$\begin{aligned} P(t,-\infty) &= 0, \qquad D(t,-\infty) = 1, \\ P(t,+\infty) &= 0, \qquad D(t,+\infty) = 0. \end{aligned}$$

In short, we use geometric singular perturbation theory (to be specific the Fenichel invariant manifold theory [209, 210]) to prove that such waves exist for sufficiently large speed ϑ. First, we show the existence of an invariant manifold for the ODE system describing the desired front [210]. Next, we study the dynamics of the new perturbed system in this invariant manifold. Finally, we employ Fredholm alternative to prove the existence of the front in this invariant manifold [211]. A similar method has been used to prove the existence of travelling wave solutions in [212, 211, 210], to cite a few.

We introduce a new variable $w = x + \vartheta t$, $\vartheta \in \mathbb{R}$ denoting wave speed and postulate

$$P(t,x) = U(w), \quad D(t,x) = V(w).$$

Thus, based on system (4.2) we derive an ODE system describing dynamics of $U(w)$ and $V(w)$:

$$\begin{aligned} U'' - \vartheta U' + U(1-U-V-z) &= 0, \\ V'' - \vartheta V' - \frac{1}{k} V(1-U-V) + zU &= 0 \end{aligned} \tag{4.6}$$

with boundary conditions:

$$\begin{aligned} U(-\infty) &= 0, \qquad V(-\infty) = 1, \\ U(+\infty) &= 0, \qquad V(+\infty) = 0. \end{aligned}$$

Note that partial differential equations in x and t in system (4.2) become ordinary differential equations (4.6) in w. We consider a small perturbation, thus, we assume that $\vartheta^2 \gg 1$ and denote $\epsilon := \frac{1}{\vartheta^2} \ll 1, \xi = \frac{w}{\vartheta} = w\sqrt{\epsilon}$. Then system (4.6) for $U(\xi)$ and $V(\xi)$ reads:

$$\begin{aligned} \epsilon U_{\xi\xi} - U_\xi + U(1-U-V-z) &= 0, \\ \epsilon V_{\xi\xi} - V_\xi - \frac{1}{k} V(1-U-V) + zU &= 0 \end{aligned} \tag{4.7}$$

with conditions:

$$U(-\infty) = 0, \quad V(-\infty) = 1, \quad U(+\infty) = 0, \quad V(+\infty) = 0,$$

where U_ξ and V_ξ denote derivative of U and V with respect to the variable ξ. Defining $M = U_\xi$, $N = V_\xi$ we recast system (4.7) into a so-called "slow system":

$$U_\xi = M, \tag{4.8a}$$

$$\epsilon M_\xi = M - U(1-U-V-z), \tag{4.8b}$$

$$V_\xi = N, \tag{4.8c}$$

$$\epsilon N_\xi = N + \frac{1}{k} V(1-U-V) - zU. \tag{4.8d}$$

Let $\zeta = \xi/\epsilon = \vartheta w$, then $U_\zeta = \epsilon U_\xi$, $M_\zeta = \epsilon M_\xi$ and we obtain a system:

$$\begin{aligned} U_\zeta &= \epsilon M, \\ M_\zeta &= M - U(1-U-V-z), \\ V_\zeta &= \epsilon N, \\ N_\zeta &= N + \frac{1}{k} V(1-U-V) - zU, \end{aligned} \tag{4.9}$$

which is called "dual fast system" associated to the slow system (4.8), *cf.* [211].

For $\epsilon = 0$ from Eqs. (4.8b) and (4.8d) we have

$$M = U(1 - U - V - z),$$
$$N = -\frac{1}{k}V(1 - U - V) + zU,$$

thus, the evolution of U and V is described by a system of two ODEs:

$$\begin{aligned} U_\xi &= U(1 - U - V - z), \\ V_\xi &= -\frac{1}{k}V(1 - U - V) + zU. \end{aligned} \tag{4.10}$$

Clearly, system (4.10) has the same dynamic properties as system (4.5). For $\epsilon = 0$ we define a set:

$$\mathcal{M}^0 = \left\{(U, M, V, N):\ M = U(1 - U - V - z),\ N = -\frac{1}{k}V(1 - U - V) + zU\right\},$$

which is a two-dimensional submanifold on $\mathbb{R}^4$. Subsequently we study a perturbation $\mathcal{M}^\epsilon$ of manifold $\mathcal{M}^0$, which is invariant for the flow of system (4.9). Its existence for sufficiently small $\epsilon > 0$ is guaranteed by Fenichel first theorem [210].

Definition 4.1. *We say that $\mathcal{M}^0$ is a normally hyperbolic manifold if the linearisation of system (4.9) at each point in $\mathcal{M}^0$ restricted to $\mathcal{M}^0$ (i.e. for $\epsilon = 0$) has exactly* $\dim \mathcal{M}^0$ *eigenvalues on the imaginary axis.*

Theorem 4.2 (Fenichel first theorem). *Let $\mathcal{M}^0$ be a normally hyperbolic manifold. There exists sufficiently small $\epsilon > 0$ for which there exists a manifold $\mathcal{M}^\epsilon$ which is within distance ϵ of $\mathcal{M}^0$ and is diffeomorphic to $\mathcal{M}^0$. Furthermore, $\mathcal{M}^\epsilon$ is locally invariant under the flow of system (4.9) and of class C^p for any $p < +\infty$.*

In order to use Theorem 4.2, we prove that $\mathcal{M}^0$ is a normally hyperbolic manifold. Jacobi matrix of the linearisation of system (4.9) for $\epsilon = 0$ has the following form:

$$J(U, V) = \begin{bmatrix} 0 & 0 & 0 & 0 \\ 2U + V + z - 1 & 1 & U & 0 \\ 0 & 0 & 0 & 0 \\ -\frac{V}{k}z & 0 & \frac{1}{k}(1 - U - 2V) & 1 \end{bmatrix}. \tag{4.11}$$

Matrix (4.11) has two double eigenvalues: $\lambda_1 = 0$ and $\lambda_2 = 1$. As a consequence, $\mathcal{M}^0$ is normally hyperbolic. Thus, for sufficiently small $\epsilon > 0$ there exists a perturbation $\mathcal{M}^\epsilon$ of manifold $\mathcal{M}^0$ with properties given above.

Now we study the model dynamics on manifold $\mathcal{M}^\epsilon$. As U, V are slow variables and M, N are fast variables, the manifold $\mathcal{M}^\epsilon$ can be represented in the following way:

$$\begin{aligned} \mathcal{M}^\epsilon = \{(U, M, V, N) \in \mathbb{R}^4 \colon\ & M = U(1 - U - V - z) + g^\epsilon(U, V), \\ & N = -\frac{1}{k}V(1 - U - V) + zU + h^\epsilon(U, V)\}, \end{aligned} \tag{4.12}$$

for some functions $g^\epsilon(U, V), h^\epsilon(U, V) \in C^p, p < +\infty$ such that

$$g^0(U, V) = h^0(U, V) = 0 \tag{4.13}$$

and the equations describing the evolution of U and V in $\mathcal{M}^\epsilon$ are given by:

$$\begin{aligned} U_\xi =& U(1-U-V-z)+g^\epsilon(U,V),\\ V_\xi =& -\frac{1}{k}V(1-U-V)+zU+h^\epsilon(U,V). \end{aligned} \tag{4.14}$$

We differentiate equations in (4.12) describing M and N and obtain

$$\begin{aligned} M_\xi &= (1-U-V-z)\cdot U_\xi - U\,(U_\xi+V_\xi)+\frac{\partial g^\epsilon(U,V)}{\partial U}U_\xi+\frac{\partial g^\epsilon(U,V)}{\partial V}V_\xi\\ &= U_\xi(1-2U-V-z)-UV_\xi+\frac{\partial g^\epsilon(U,V)}{\partial U}U_\xi+\frac{\partial g^\epsilon(U,V)}{\partial V}V_\xi,\\ N_\xi &= -\frac{1}{k}V_\xi(1-U-V)+\frac{1}{k}V(U_\xi+V_\xi)+zU_\xi++\frac{\partial h^\epsilon(U,V)}{\partial U}U_\xi+\frac{\partial h^\epsilon(U,V)}{\partial V}V_\xi. \end{aligned}$$

Now, taking into account Eqs. (4.14) and the fact that $U_\xi = M,\ V_\xi = N$ (see Eqs. (4.8a) and (4.8c)), we have:

$$\begin{aligned} M_\xi &= (U(1-U-V-z)+g^\epsilon(U,V))\,(1-2U-V-z)\\ &\quad + U\left(\frac{1}{k}V(1-U-V)-zU-h^\epsilon(U,V)\right)+\frac{\partial g^\epsilon(U,V)}{\partial U}M+\frac{\partial g^\epsilon(U,V)}{\partial V}N\\ &= (1-U-V-z)\,((1-2U-V-z)U+g^\epsilon(U,V))\\ &\quad + U\left(\frac{1}{k}V(1-U-V)-zU-g^\epsilon(U,V)-h^\epsilon(U,V)\right)+\frac{\partial g^\epsilon(U,V)}{\partial U}M+\frac{\partial g^\epsilon(U,V)}{\partial V}N,\\ N_\xi &= -\frac{1}{k}(1-U-V)\left(-\frac{1}{k}V(1-U-V)+zU+h^\epsilon(U,V)\right)\\ &\quad + \frac{1}{k}V\left(U(1-U-V-z)+g^\epsilon(U,V)-\frac{1}{k}V(1-U-V)+zU+h^\epsilon(U,V)\right)\\ &\quad + z\,(U(1-U-V-z)+g^\epsilon(U,V))+\frac{\partial h^\epsilon(U,V)}{\partial U}U_\xi+\frac{\partial h^\epsilon(U,V)}{\partial V}V_\xi\\ &= \frac{1}{k}(1-U-V)\left(\frac{1}{k}(1-U-2V)+U(V-z)-h^\epsilon(U,V)\right)\\ &\quad + z\,(U(1-U-V-z)+g^\epsilon(U,V))+\frac{1}{k}V(g^\epsilon(U,V)+h^\epsilon(U,V))\\ &\quad + \frac{\partial h^\epsilon(U,V)}{\partial U}M+\frac{\partial h^\epsilon(U,V)}{\partial V}N. \end{aligned}$$

We substitute the obtained equations on M_ξ and N_ξ to Eqs. (4.8b) and (4.8d) and compute that g^ϵ and h^ϵ satisfy the following partial differential equations:

$$\begin{aligned} g^\epsilon(U,V) &= \epsilon\Big[(1-U-V-z)\,((1-2U-V-z)U+g^\epsilon(U,V))\\ &\qquad + U\left(\frac{1}{k}V(1-U-V)-zU-g^\epsilon(U,V)-h^\epsilon(U,V)\right)\\ &\qquad + \frac{\partial g^\epsilon(U,V)}{\partial U}M+\frac{\partial g^\epsilon(U,V)}{\partial V}N\Big],\\ h^\epsilon(U,V) &= \epsilon\Big[\frac{1}{k}(1-U-V)\left(\frac{1}{k}(1-U-2V)+U(V-z)-h^\epsilon(U,V)\right)\\ &\qquad + z\,(U(1-U-V-z)+g^\epsilon(U,V))+\frac{1}{k}V\,(g^\epsilon(U,V)+h^\epsilon(U,V))\\ &\qquad + \frac{\partial h^\epsilon(U,V)}{\partial U}M+\frac{\partial h^\epsilon(U,V)}{\partial V}N\Big]. \end{aligned} \tag{4.15}$$

We expand h^ϵ and g^ϵ in Taylor series around $\epsilon = 0$, obtaining

$$\begin{aligned} g^\epsilon(U,V) =& g^0(U,V) + \epsilon\frac{\partial g^0(U,V)}{\partial\epsilon} + \ldots + \frac{\epsilon^{n-1}}{(n-1)!}\frac{\partial^{n-1} g^0(U,V)}{\partial\epsilon^{n-1}} + \epsilon^n R_n^g(\epsilon), \\ h^\epsilon(U,V) =& h^0(U,V) + \epsilon\frac{\partial h^0(U,V)}{\partial\epsilon} + \ldots + \frac{\epsilon^{n-1}}{(n-1)!}\frac{\partial^{n-1} h^0(U,V)}{\partial\epsilon^{n-1}} + \epsilon^n R_n^h(\epsilon), \end{aligned}$$

where R_n^g, R_n^h are such that $\lim_{\epsilon\to 0} R_n^g(\epsilon) = 0$ and $\lim_{\epsilon\to 0} R_n^h(\epsilon) = 0$. Clearly, due to (4.13) we have $g^0(U,V) = h^0(U,V) = 0$. Now, using Eqs. (4.15), we calculate partial derivatives of g^ϵ and h^ϵ with respect to ϵ, arriving at:

$$\begin{aligned} \frac{\partial g^0(U,V)}{\partial\epsilon} =& U\left[(1-U-V)\left(1-2U-\frac{k-1}{k}V-2z\right)+z^2\right], \\ \frac{\partial h^0(U,V)}{\partial\epsilon} =& \frac{1}{k}(1-U-V)\left(\frac{1}{k}(1-U-2V)+U(V-z)\right)+zU(1-U-V-z). \end{aligned}$$

Hence, Taylor series of g^ϵ and h^ϵ have the following forms:

$$\begin{aligned} g^\epsilon(U,V) =& U\left[(1-U-V)\left(1-2U-\frac{k-1}{k}V-2z\right)+z^2\right]\epsilon + O\left(\epsilon^2\right), \\ h^\epsilon(U,V) =& \left[\frac{1}{k}(1-U-V)\left(\frac{1}{k}(1-U-2V)+U(V-z)\right)+zU(1-U-V-z)\right]\epsilon \\ &+ O\left(\epsilon^2\right). \end{aligned} \tag{4.16}$$

We substitute Eqs. (4.16) omitting terms of the order of ϵ^2 to system (4.14) to obtain the approximate equations:

$$\begin{aligned} U_\xi =& U(1-U-V-z) + U\left[(1-U-V)\left(1-2U-\frac{k-1}{k}V-2z\right)+z^2\right]\epsilon, \\ V_\xi =& -\frac{1}{k}V(1-U-V) + zU \\ &+ \left[\frac{1}{k}(1-U-V)\left(\frac{1}{k}(1-U-2V)+U(V-z)\right)+zU(1-U-V-z)\right]\epsilon, \end{aligned} \tag{4.17}$$

which approximate the dynamics on the manifold $\mathcal{M}^\epsilon$ for sufficiently small ϵ.

Now, let us denote by (U_0, V_0) the solution of system (4.17) for $\epsilon = 0$, that is

$$\begin{aligned} \frac{\mathrm{d}}{\mathrm{d}\xi}U_0 &= U_0(1-U_0-V_0-z), \\ \frac{\mathrm{d}}{\mathrm{d}\xi}V_0 &= -\frac{1}{k}V_0(1-U_0-V_0)+zU_0. \end{aligned} \tag{4.18}$$

Clearly, system (4.18) is equivalent to system (4.5). Consequently, there exists a heteroclinic orbit connecting the steady state $(0,1)$ and $(0,0)$. For $\epsilon > 0$ system (4.17) has steady states

$$P_1 = (0,1) \quad \text{and} \quad P_2 = \left(0, \frac{\epsilon}{k+2\epsilon}\right).$$

Note that $\epsilon/(k+2\epsilon) \to 0$ for $\epsilon \to 0$. Thus, it is sufficient to show that for a sufficiently small $\epsilon > 0$ there exist a heteroclinic orbit connecting the steady states P_1 and P_2 of system (4.17). This orbit corresponds to a travelling wave solution of system (4.2). To find such a connection we write:

$$\begin{aligned} U &= U_0 + \epsilon U_1, \\ V &= V_0 + \epsilon V_1. \end{aligned} \tag{4.19}$$

In what follows, we determine the dynamics of U_1 and V_1. Substituting new variables (4.19) to system (4.17) we get

$$\begin{aligned}
U_\xi =& U_0(1-U_0-V_0-z)+\epsilon U_1(1-2U_0-V_0-z)-\epsilon U_0V_1\\
&+\epsilon U_0\left[(1-U_0-V_0)\left(1-2U_0-\frac{k-1}{k}V_0-2z\right)+z^2\right]+O(\epsilon^2),\\
V_\xi =& -\frac{1}{k}V_0(1-U_0-V_0)+zU_0-\epsilon\frac{1}{k}\left(V_1(1-U_0-2V_0)-U_1V_0\right)+\epsilon zU_1\\
&+\epsilon\left[\frac{1}{k}(1-U_0-V_0)\left(\frac{1}{k}(1-U_0-2V_0)+U_0(V_0-z)\right)+zU_0(1-U_0-V_0-z)\right]+O(\epsilon^2).
\end{aligned}$$

Clearly, $U_\xi=\frac{\mathrm{d}}{\mathrm{d}\xi}U_0+\epsilon\frac{\mathrm{d}}{\mathrm{d}\xi}U_1$ and $V_\xi=\frac{d}{d\xi}V_0+\epsilon\frac{d}{d\xi}V_1$. Moreover, as (U_0,V_0) satisfy the system (4.18), omitting terms of the order of ϵ^2, we have:

$$\begin{aligned}
\frac{d}{d\xi}U_1 =& U_1(1-2U_0-V_0-z)-V_1U_0+U_0\left[(1-U_0-V_0)\left(1-2U_0-\frac{k-1}{k}V_0-2z\right)+z^2\right]\\
\frac{d}{d\xi}V_1 =& U_1\left(\frac{1}{k}V_0+z\right)-\frac{1}{k}V_1(1-U_0-2V_0)+zU_0(1-U_0-V_0-z)\\
&+\frac{1}{k}(1-U_0-V_0)\left(\frac{1}{k}(1-U_0-2V_0)+U_0(V_0-z)\right).
\end{aligned}$$

We rewrite the system of equations governing U_1 and V_1 in the following way:

$$\frac{d}{d\xi}\begin{bmatrix}U_1\\V_1\end{bmatrix}-\begin{bmatrix}1-2U_0-V_0-z & -U_0\\ \frac{1}{k}V_0+z & -\frac{1}{k}(1-U_0-2V_0)\end{bmatrix}\begin{bmatrix}U_1\\V_1\end{bmatrix}=\begin{bmatrix}f_1(U_0,V_0)\\f_2(U_0,V_0)\end{bmatrix},\tag{4.20}$$

where

$$\begin{aligned}
f_1(U_0,V_0) =& U_0\left[(1-U_0-V_0)\left(1-2U_0-\frac{k-1}{k}V_0-2z\right)+z^2,\right]\\
f_2(U_0,V_0) =& zU_0(1-U_0-V_0-z)+\frac{1}{k}(1-U_0-V_0)\left(\frac{1}{k}(1-U_0-2V_0)+U_0(V_0-z)\right).
\end{aligned}$$

Transforming steady states P_1 and P_2 using Eqs. (4.19) we get:

$$P_1=(0,1)+\epsilon\cdot(0,0),\qquad P_2=(0,0)+\epsilon\cdot\left(0,\frac{1}{k+2\epsilon}\right).$$

Thus, our aim is to prove that system (4.20) has a solution satisfying the conditions:

$$\lim_{\xi\to\pm\infty}U_1(\xi)=\lim_{\xi\to-\infty}V_1(\xi)=0,\qquad \lim_{\xi\to+\infty}V_1(\xi)=\frac{1}{k+2\epsilon}.$$

Note that function

$$F(\xi)=\frac{1}{k+2\epsilon}\cdot\frac{1}{1+\mathrm{e}^{-\xi}}$$

satisfies conditions

$$\lim_{\xi\to-\infty}F(\xi)=0,\qquad \lim_{\xi\to+\infty}F(\xi)=\frac{1}{k+2\epsilon}.$$

Thus, we make the change of variables $V_1=W_1+F$. System (4.20) now reads

$$\frac{d}{d\xi}\begin{bmatrix}U_1\\W_1\end{bmatrix}-\begin{bmatrix}1-2U_0-V_0-z & -U_0\\ \frac{1}{k}V_0+z & -\frac{1}{k}(1-U_0-2V_0)\end{bmatrix}\begin{bmatrix}U_1\\W_1\end{bmatrix}=\begin{bmatrix}h_1(U_0,V_0,\xi)\\h_2(U_0,V_0,\xi)\end{bmatrix},\tag{4.21}$$

where

$$h_1(U_0, V_0, \xi) = f_1(U_0, V_0) - \frac{1}{k + 2\epsilon} \cdot \frac{1}{1 + e^{-\xi}} U_0$$
$$h_1(U_0, V_0, \xi) = f_2(U_0, V_0) + \frac{1}{k + 2\epsilon} \cdot \frac{1}{1 + e^{-\xi}} \left[-\frac{1}{k}(1 - U_0 - 2V_0) - \frac{e^{-\xi}}{1 + e^{-\xi}} \right].$$

As a consequence, we verify the existence of solution of system (4.21) with homogeneous boundary conditions:

$$\lim_{\xi \to \pm\infty} U_1(\xi) = \lim_{\xi \to \pm\infty} W_1(\xi) = 0.$$

As previously said, in order to do so, we use the Fredholm alternative as formulated in [213]. Suppose that $\mathbb{L}$ is a linear differential operator acting on a subspace of $L^2(\mathbb{R}^2)$ of square-integrable functions. Given the standard inner product $\langle \cdot, \cdot \rangle$ on $L^2(\mathbb{R}^2)$:

$$\langle f, g \rangle = \int_{-\infty}^{+\infty} (f(\xi), g(\xi))\, d\xi,$$

where $(\cdot, \cdot)$ is the Euclidean inner product on $\mathbb{R}^2$, the adjoint linear operator $\mathbb{L}^*$ is defined as:

$$\langle f, \mathbb{L}g \rangle = \langle \mathbb{L}^* f, g \rangle.$$

Fredholm alternative theorem states that the inhomogeneous equation

$$\mathbb{L}f = h$$

has a solution if and only if condition

$$\langle \nu, h \rangle = 0$$

is fulfiled for all ν satisfying the homogeneous equation:

$$\mathbb{L}^* \nu = 0.$$

In our case, the linear operator $\mathbb{L}$ is defined by the left-hand side of system (4.21). We claim that system (4.21) has a solution if and only if equation

$$\int_{-\infty}^{+\infty} \Big(s_1(\xi) h_1(U_0, V_0, \xi) + s_2(\xi) h_2(U_0, V_0, \xi) \Big) d\xi = 0 \tag{4.22}$$

holds for all solutions (s_1, s_2) of the adjoint problem:

$$\frac{d}{d\xi} \begin{bmatrix} s_1 \\ s_2 \end{bmatrix} = \begin{bmatrix} -1 + 2U_0 + V_0 + z & -\frac{1}{k} V_0 - z \\ U_0 & \frac{1}{k}(1 - U_0 - 2V_0) \end{bmatrix} \begin{bmatrix} s_1 \\ s_2 \end{bmatrix} \tag{4.23}$$

with boundary conditions:

$$\lim_{\xi \to \pm\infty} s_1(\xi) = \lim_{\xi \to \pm\infty} s_2(\xi) = 0.$$

Recall that (U_0, V_0) corresponds to the heteroclinic solution of system (4.18). Letting $\xi \to -\infty$ we have that $(U_0, V_0) \to (0, 0)$, then the matrix in system (4.23) is a constant one with eigenvalues equal:

$$\lambda_1 = z - 1, \quad \lambda_2 = \frac{1}{k}.$$

Eigenvalue λ_1 is negative due to our assumption that $z < 1$, while λ_2 is positive. Thus, when $\xi \to -\infty$ any solution of system (4.23), other than the zero solution, is a sum of two exponentially increasing and decreasing functions. Therefore, the only solution of the adjoint problem (4.23) in space $L^2(\mathbb{R}^2)$ is $(s_1, s_2) \equiv (0, 0)$. Thus, condition (4.22) holds and we arrive at the following result:

Theorem 4.3. *If $z < 1$ and $\vartheta \gg 1$, there exists a sufficiently small $\varepsilon > 0$ such that for every $\epsilon \in (0, \varepsilon]$, system (4.2) admits a travelling wave solution $P(t,x) = U(x + \vartheta t)$, $D(t,x) = V(x+\vartheta t)$ satisfying boundary conditions: $U(-\infty) = 0$, $V(-\infty) = 0$, $U(+\infty) = 0$, $V(+\infty) = 1$.*

4.2 Estimate of malignant transformation for LGGs treated with chemotherapy

Now, we assume that concentration of chemotherapeutic drug C in system (4.1) is not a constant, but it is a function of time, representing more realistically the decay of chemotherapeutic drug concentration after each of its administrations, to be described in details later on. We would like to verify if it is possible to get any suggestion on improving chemotherapy fractionations protocols based on our mathematical modelling approach. If an objective of the treatment is to delay the onset of malignant transformation for as long as possible, then we would like to be able to estimate onset of malignant transformation as a function of some parameters describing tumour growth and the chemotherapy fractionation scheme. Like in Chapter 3, we want to estimate t_{OMT} as the time when the LGG cell density hits the critical value L_{crit} triggering malignant transformation. However, such a goal is very difficult to achieve on a basis of system (4.1) with arbitrary non-constant function C. Thus, we simplify this system. To this end, firstly we neglect the evolution of damaged cells in time assuming that their death is faster than the proliferation of undamaged cells. Hence, system (4.1) reduces to an equation:

$$\frac{\partial P}{\partial t} = \delta \Delta P + \rho P \left(1 - \frac{P}{K}\right) - \alpha C P \tag{4.24a}$$

complemented with initial condition:

$$P(0,x) = P_0(x) \geq 0 \tag{4.24b}$$

and homogeneous von Neumann boundary condition.

Secondly, recall our assumption that malignant transformation is directly related to LGG density at the centre of a tumour, *cf.* Chapters 1 and 3. Thus, in our problem, we focus only on the evolution of tumour cell density P at the centre of a tumour (for $x = 0$). We would like to derive a reasonably good estimation $L(t)$ of this density $P(t,0)$ for each time t. Note that if L is the solution of an ODE of a form:

$$\frac{\mathrm{d}L}{\mathrm{d}t} = \rho L \left(1 - \frac{L}{K}\right) - \alpha C L \tag{4.25a}$$

with initial condition:

$$L(0) = \max_{x \in \Omega} P_0(x), \tag{4.25b}$$

then the solution of system (4.24) fulfils the inequality $0 \leq P(t,x) \leq L(t)$ for all t and x. It follows from the simple fact that for $t = 0$ we take $\max_{x\in\Omega} P_0(x)$. Consequently, L is a reasonably good upper bound of tumour cell density P. In particular, it is an upper bound for the density at the centre of a tumour. Subsequently instead of Eq. (4.24a) we use Eq. (4.25a) to describe the local density of LGG cells in its centre. We complement Eq. (4.25a) with an equation describing the local concentration of chemotherapy drug. As in Chapter 2, we assume that the drug is distributed homogeneously within a tumour and concentration of the drug

decays exponentially. We consider chemotherapy consisting of n equal doses administered at times $0 \leq t_1 < t_2 < \ldots < t_n$. Without loss of generality, we assume that the drug administration starts at time $t_1 = 0$. Moreover, we assume that drug is administered in equal time intervals r, thus

$$t_i = (i-1)r \quad \text{for } i \in \{1, \ldots, n\}. \tag{4.26}$$

By C_0 we denote the effective part of dose acting on a tumour and L_1 denotes LGG cell density at the centre of the tumour at the time of the first dose administration t_1 measured in the units of the maximal cell density K. Then, taking $\widetilde{L} = L/K$ and omitting tildes for simplicity, the model to be considered here is of the following form:

$$\begin{aligned} \frac{\mathrm{d}L}{\mathrm{d}t} &= \rho L\,(1-L) - \alpha C L, \\ \frac{\mathrm{d}C}{\mathrm{d}t} &= -\lambda C \end{aligned} \tag{4.27a}$$

with initial conditions

$$L(t_1) = L_1 > 0, \quad C(t_1) = C_0 > 0 \tag{4.27b}$$

and function C satisfying

$$C(t_i) = C(t_i^-) + C_0 \quad \text{for } i \in \{2, \ldots, n\}. \tag{4.27c}$$

As previously, all model parameters and initial conditions are assumed to be positive.

Remark. Note that if we solve an ODE of the following general form:

$$\frac{\mathrm{d}L}{\mathrm{d}t} = \rho L(1-L) - F(t)L,$$

with initial condition $L(0) = L_1 > 0$, where a function F describes chemotherapy drug concentration and action on tumour cells, we obtain

$$L(t) = \left\{ \exp\left(\int_0^t (F(s) - \rho)\mathrm{d}s \right) \cdot \left[\frac{1}{L_1} - \int_0^t \frac{\rho}{\exp\left(\int_{t_0}^s (F(\xi) - \rho)\mathrm{d}\xi \right)} \mathrm{d}s \right] \right\}^{-1}.$$

Therefore, we simplify the description of chemotherapy. We take into account that the standard dose of the chemotherapeutic drug is almost completely absorbed within less than a day from the time of its administration, see *e.g.* [163]. Thus, we divide the period between subsequent doses in two parts in such a way that in the first one (of the length ϵ) drug concentration decays to zero and in the second – equals zero. Then we approximate the function C in the following way:

$$C(t) \approx \begin{cases} C_0 \mathrm{e}^{-\lambda(t - t_i)} & t \in [t_i, t_i + \epsilon), \\ 0 & \text{for other } t, \end{cases}$$

for $i \in \{1, ..., n\}$. Furthermore, in order to obtain a possibly simple form of the solution of system (4.27), instead of describing the drug concentration by exponential decay function, we use the mean value $\bar{C}$ of function C in each time interval $[t_i, t_i + \epsilon)$, that is

$$\bar{C} = \frac{1}{\epsilon} \int_{t_i}^{t_i+\epsilon} C(s)\mathrm{d}s = \frac{1}{\epsilon} \int_{t_i}^{t_i+\epsilon} C_0 \mathrm{e}^{-\lambda(s-s_i)} \mathrm{d}s = \frac{1}{\epsilon} \int_0^{\epsilon} C_0 \mathrm{e}^{-\lambda s} \mathrm{d}s = \frac{C_0}{\lambda\epsilon} \left(1 - \mathrm{e}^{-\lambda\epsilon}\right).$$

Thus, we arrive at the following form of the model describing the temporal evolution of tumour density at the centre of a tumour:

$$\frac{\mathrm{d}L}{\mathrm{d}t} = \begin{cases} \rho L(1-L) - \alpha\bar{C}L & \text{for } t \in [t_i, t_i+\epsilon), \\ \rho L(1-L) & \text{for } t \in [t_i+\epsilon, t_{i+1}) \text{ and } t \geq t_n+\epsilon \end{cases} \tag{4.28a}$$

with initial condition

$$L(t_1) = L_1, \tag{4.28b}$$

where times t_i are given by Eq. (4.26).

System (4.28) can be solved analytically.

For $i \in \{2, \ldots, n\}$ we denote the solution of system (4.28) at time t_i by L_i. We also introduce the following notation

$$\begin{aligned} \zeta &= e^{\rho r - \alpha\bar{C}\epsilon}, \\ \eta &= \frac{1}{\rho - \alpha\bar{C}} \left(\alpha\bar{C} \mathrm{e}^{(\rho-\alpha\bar{C})\epsilon} - \rho \right). \end{aligned} \tag{4.29}$$

Note that ζ is positive. On the other hand, the sign of η is not fixed.

Theorem 4.4. *Solution of system (4.28) is of a form:*

$$L(t) = \begin{cases} \dfrac{\rho - \alpha\bar{C}}{\rho\left[1 + \left(\frac{\rho-\alpha\bar{C}}{\rho L_i} - 1\right)\mathrm{e}^{(\alpha\bar{C}-\rho)(t-t_i)}\right]} & \text{for } t \in [t_i, t_i+\epsilon), \quad (4.30a) \\ \dfrac{1}{1 + \left(\frac{1}{L(t_j+\epsilon)} - 1\right)\mathrm{e}^{-\rho(t-(t_j+\epsilon))}} & \text{for } t \in [t_j+\epsilon, t_{j+1}) \text{ and } t \geq t_n+\epsilon, \quad (4.30b) \end{cases}$$

where $i \in \{1, \ldots, n\}$, $j \in \{1, \ldots, n-1\}$ and L_i satisfies the following relation:

$$L_{i+1} = \frac{\zeta L_i}{1 + (\zeta + \eta) L_i}. \tag{4.31}$$

Proof. Solving system (4.28) for time $t \in [t_i, t_i+\epsilon]$ we have:

$$L(t) = \frac{\rho - \alpha\bar{C}}{\rho\left[1 + \left(\frac{\rho-\alpha\bar{C}}{\rho L_i} - 1\right)\mathrm{e}^{(\alpha\bar{C}-\rho)(t-t_i)}\right]}$$

and

$$L(t_i+\epsilon) = \frac{\rho - \alpha\bar{C}}{\rho\left[1 + \left(\frac{\rho-\alpha\bar{C}}{\rho L_i} - 1\right)\mathrm{e}^{(\alpha\bar{C}-\rho)\epsilon}\right]}.$$

The solution for time $t \in [t_i+\epsilon, t_{i+1}]$ and $t \geq t_n+\epsilon$ is of a form:

$$L(t) = \frac{1}{1 + \left(\frac{1}{L(t_i+\epsilon)} - 1\right)\mathrm{e}^{-\rho(t-(t_i+\epsilon))}}$$

and consequently we have

$$\begin{aligned} L_{i+1} &= \frac{1}{1 + \left(\frac{1}{L(t_i+\epsilon)} - 1\right)\mathrm{e}^{-\rho(r-\epsilon)}} = \frac{1}{1 + \left[\frac{\rho}{\rho-\alpha\bar{C}}\left(1 + \left(\frac{\rho-\alpha\bar{C}}{\rho L_i} - 1\right)\mathrm{e}^{(\alpha\bar{C}-\rho)\epsilon}\right) - 1\right]\mathrm{e}^{\rho(\epsilon-r)}} \\ &= \frac{1}{1 + \frac{1}{L_i}\mathrm{e}^{\alpha\bar{C}\epsilon - r\rho} + \left(\frac{\rho}{\rho-\alpha\bar{C}}\left(1 - \mathrm{e}^{(\alpha\bar{C}-\rho)\epsilon}\right) - 1\right)\mathrm{e}^{\rho(\epsilon-r)}} \\ &= \frac{\mathrm{e}^{r\rho-\alpha\bar{C}\epsilon} L_i}{1 + \left[\mathrm{e}^{r\rho-\alpha\bar{C}\epsilon} + \frac{1}{\rho-\alpha\bar{C}}\left(\alpha\bar{C}\mathrm{e}^{(\rho-\alpha\bar{C})\epsilon} - \rho\right)\right] L_i}. \end{aligned}$$

Using the definition of ζ and η, see Eqs. (4.29), we arrive at Eq. (4.31), which finishes the proof. □

Now let us study the dynamics of the discrete system defined by Eq. (4.31). There exist two fixed points of Eq. (4.31):

$$\bar{L}_1 = 0, \quad \bar{L}_2 = \frac{\zeta - 1}{\zeta + \eta}. \tag{4.32}$$

As the dynamics of Eq. (4.31) depends on the sign of $\zeta + \eta$, we state the following

Lemma 4.5. *If $\rho < \alpha\bar{C}$, then*

$$\eta > 0 \iff \epsilon > \frac{1}{\rho - \alpha\bar{C}} \ln\left(\frac{\rho}{\alpha\bar{C}}\right)$$

and

$$\zeta + \eta > 0 \quad \iff \left(\eta > 0 \quad \vee \quad r > \frac{1}{\rho}\left[\alpha\bar{C}\epsilon + \ln\left(\frac{\rho - \alpha\bar{C}e^{(\rho-\alpha\bar{C})\epsilon}}{\rho - \alpha\bar{C}}\right)\right]\right).$$

Proof. The assertion follows from the direct computations and positiveness of ζ. □

As we are studying the tumour growth in the rescaled variables, we are interested in solutions in $[0, 1]$.

Theorem 4.6. *Let $L_1 \in (0, 1)$. A solution of Eq. (4.31)*

- *converges to $\bar{L}_1$ if $\zeta < 1$ and*
  - *$\zeta + \eta > 0$ or*
  - *$\bar{L}_2 > 1$,*
- *converges to $\bar{L}_2$ if $\zeta > 1$ and $\bar{L}_2 < 1$,*
- *increases and there exists $i_0 \geq 2$ such that $L_{i_0} > 1$ or $L_{i_0} < 0$ if*
  - *$\zeta > 1$ and $\bar{L}_2 > 1$ or:*
  - *$\zeta < 1$ and $L_1 > \bar{L}_2$.*

The solution of Eq. (4.31) is the following:

$$L_i = \frac{\zeta^{i-1} L_1}{1 + \frac{1-\zeta^{i-1}}{1-\zeta}(\zeta + \eta) L_1} \tag{4.33}$$

for $i \geq 2$.

Proof. Difference equation Eq. (4.31) have at most two non-negative fixed points: $\bar{L}_1 = 0$ and $\bar{L}_2 = (\zeta - 1)/(\zeta + \eta)$. Recall that ζ is positive. Thus, steady state $\bar{L}_2$ is positive if either $\zeta > 1$ and $\zeta + \eta > 0$ or $0 < \zeta < 1$ and $\zeta + \eta < 0$.

Let us study the asymptotic behaviour of Eq. (4.31). In order to do that, we investigate the right-hand side of Eq. (4.31), that is a function:

$$g(L) = \frac{\zeta L}{1 + (\zeta + \eta) L}. \tag{4.34}$$

Clearly, the derivative of g:

$$g'(L) = \frac{\zeta}{(1 + (\zeta + \eta) L)^2}.$$

is positive and $g'(0) = \zeta$ as well.

First consider the case $\zeta < 1$ and $\zeta + \eta > 0$. It is easy to see that for such parameters values we have $\bar{L}_2 < 0$ and $L_i > 0$ (from the assumption that $L_1 > 0$). As the derivative

of g is a decreasing function, the graph of g (see Figure 4.1a) lies below the line $y = L$, thus, $L_{i+1} < L_i$ for all $i > 0$. The sequence $(L_i)_{i\in\mathbb{N}}$ is decreasing and bounded from below by 0, thus, it has a limit. Fixed point $\bar{L}_2 \notin [0, 1]$, thus, $L_i \to \bar{L}_1 = 0$.

Second, we study the case $\zeta < 1$ and $\zeta + \eta < 0$. Now, the derivative of g is an increasing function and the graph of g lies below the line $y = L$ for $L < \bar{L}_2$, see Figure 4.1b. Thus, if $L_1 < \bar{L}_2$, then the sequence (L_i) is decreasing and converges to 0. On the other hand, if $L_1 > \bar{L}_2$, the sequence (L_i) is increasing taking values greater than $\frac{-1}{\zeta+\eta}$ and later – negative values.

Third, we investigate the dynamics of Eq. (4.31) for $\zeta > 1$ and $\zeta + \eta > 0$. For such parameters values the derivative of g is an increasing function and the graph of function g lies above the line $y = L$ for $L < \bar{L}_2$ and below this line for $L > \bar{L}_2$. Moreover, we have $g(L) < \bar{L}_2$ for $L < \bar{L}_2$ and $g(L) > \bar{L}_2$ for $L > \bar{L}_2$, see Figure 4.1c. As a consequence, if $L_i < \bar{L}_2$, then $L_i < L_{i+1} < \bar{L}_2$, while condition $\bar{L}_2 < L_{i+1} < L_i$ holds if $L_i > L_2$. This proves that sequence (L_i) converges to $\bar{L}_2$. However if $\bar{L}_2 > 1$ (*i.e.* $1 + \eta < 0$), then $\bar{L}_2$ cannot be attained from above (as $L_1 < 1$).

Finally, we consider the case $\zeta > 1$ and $\zeta + \eta < 0$. In that case $\bar{L}_2 < 0$. The derivative of g is increasing and the graph of g lies above the line $y = L$, see Figure 4.1d. Consequently, the sequence (L_i) is increasing, and thus, divergent.

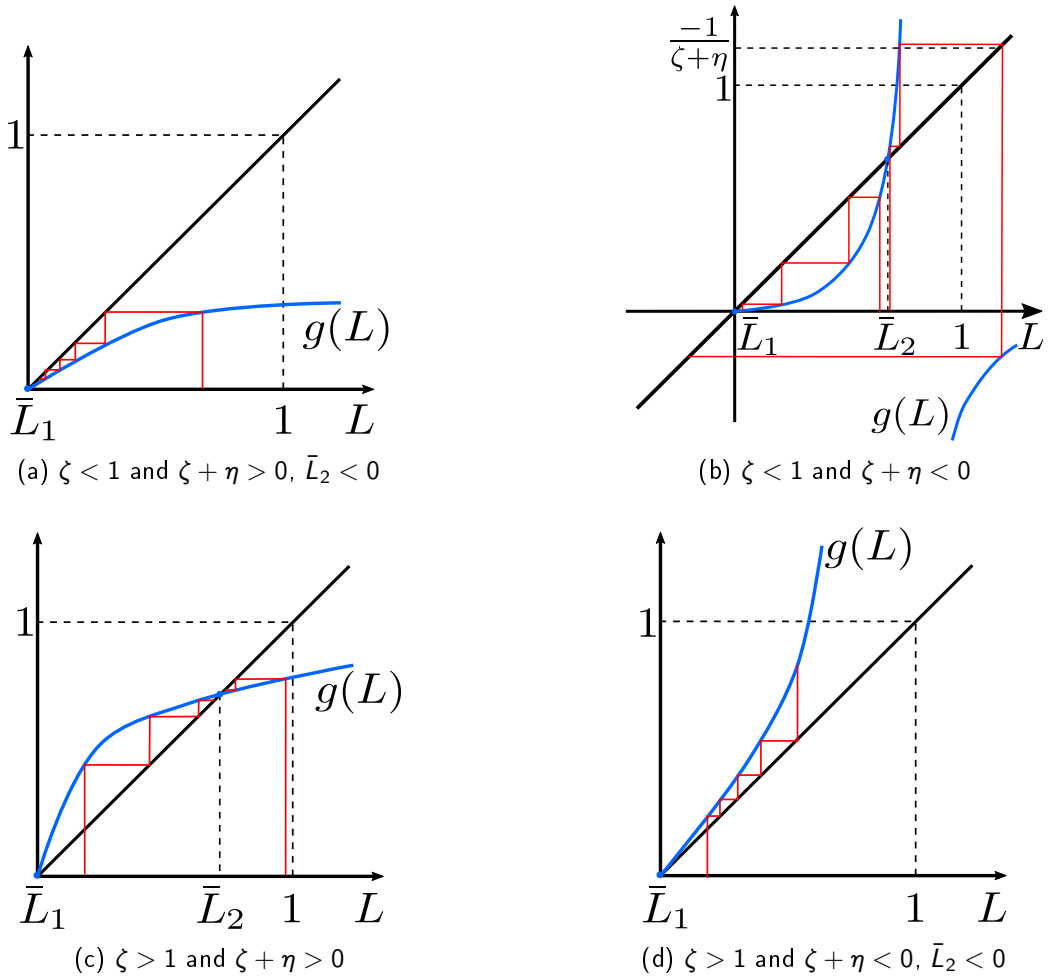

(a) $\zeta < 1$ and $\zeta + \eta > 0$, $\bar{L}_2 < 0$

(b) $\zeta < 1$ and $\zeta + \eta < 0$

(c) $\zeta > 1$ and $\zeta + \eta > 0$

(d) $\zeta > 1$ and $\zeta + \eta < 0$, $\bar{L}_2 < 0$

Figure 4.1: Graph of function g defined by Eq. (4.34) together with line $y = L$ and auxiliary lines.

Now, let us prove the form of solution of Eq. (4.31). Firstly, formula (4.33) is easily seen to be a solution of Eq. (4.31) for $i = 2$. Secondly, let us assume that it is a solution of Eq. (4.31)

for some $m \geq 2$. As a consequence, we have:

$$L_{m+1} = \frac{\zeta L_m}{1+(\zeta+\eta)L_m} = \frac{\zeta^m L_1}{1+\frac{1-\zeta^{m-1}}{1-\zeta}(\zeta+\eta)L_1} \cdot \left(1+(\zeta+\eta)\cdot\frac{\zeta^{m-1}L_1}{1+\frac{1-\zeta^{m-1}}{1-\zeta}(\zeta+\eta)L_1}\right)^{-1}$$
$$= \frac{\zeta^m L_1}{1+(\zeta+\eta)L_1\left(\frac{1-\zeta^{m-1}}{1-\zeta}+\zeta^{m-1}\right)} = \frac{\zeta^m L_1}{1+\frac{1-\zeta^m}{1-\zeta}(\zeta+\eta)L_1}.$$

Thus, by mathematical induction the formula (4.33) is a solution of Eq. (4.31) for $i \geq 2$. □

Now, based on the obtained solution L, we derive estimation for time t_{OMT} of the onset of malignant transformation. Clearly, we assume that at the beginning of treatment $L_1 < L_{\mathrm{crit}}$, otherwise, we would deal with already-transformed virtual HGG. Moreover, from now on, unless stated otherwise, we assume that

$$\rho - \alpha\bar{C} < 0,$$

that is one can observe a tumour mass decrease as long as there is some concentration of chemotherapeutic drug present in the tumour tissue. As a consequence of this assumption, the onset of malignant transformation occurs either when chemotherapy is finished and all the drug is cleared from the body, *i.e.* $t_{\mathrm{OMT}} \geq t_n + \epsilon$, or it occurs in the time interval $[t_k+\epsilon, t_{k+1})$ with

$$k = \max\left\{i : 1 \leq i < n, L_i < L_{\mathrm{crit}}\right\}.$$

To estimate t_{OMT} we need to know whether value L_{crit} would be attained during treatment or after its end. From Theorem 4.6 we know that value L_{crit} could be attained before the end of chemotherapy in any of the following cases:
(C1) $\zeta > 1$ and $\zeta + \eta < 0$,
(C2) $\zeta > 1$, $\zeta + \eta > 0$ and $\bar{L}_2 > L_{\mathrm{crit}}$,
(C3) $0 < \zeta < 1$, $\zeta + \eta < 0$ and $0 < \bar{L}_2 < L_1 < L_{\mathrm{crit}}$,
see also Figure 4.1. In the remaining cases value L_{crit} would be attained after the last dose administration. Thus, we need to focus on cases (C1)–(C3) and compute index k of the last chemotherapy dose before the onset of malignant transformation. In order to do so, we solve inequality $L_i < L_{\mathrm{crit}}$ using Eq. (4.33), arriving at

$$\zeta^{i-1}L_1\left(1+\frac{\zeta+\eta}{1-\zeta}L_{\mathrm{crit}}\right) < L_{\mathrm{crit}}\left(1+\frac{\zeta+\eta}{1-\zeta}L_1\right). \tag{4.35}$$

Note that, because of the form of $\bar{L}_2$, Eq. (4.35) is equivalent to:

$$\zeta^{i-1}L_1\left(1-\frac{L_{\mathrm{crit}}}{\bar{L}_2}\right) < L_{\mathrm{crit}}\left(1-\frac{L_1}{\bar{L}_2}\right).$$

As we consider cases (C1)-(C3), we arrive at

$$i < 1 + \frac{1}{\rho r - \alpha\bar{C}\epsilon}\ln\left(\frac{L_{\mathrm{crit}}\left(1-\frac{L_1}{\bar{L}_2}\right)}{L_1\left(1-\frac{L_{\mathrm{crit}}}{\bar{L}_2}\right)}\right).$$

Finally, we estimate t_{OMT} to occur after k-th dose administration with

$$k = \begin{cases} \min\left\{\left\lfloor 1 + \frac{1}{\rho r - \alpha\bar{C}\epsilon}\ln\left(\frac{L_{\mathrm{crit}}\left(1-\frac{L_1}{\bar{L}_2}\right)}{L_1\left(1-\frac{L_{\mathrm{crit}}}{\bar{L}_2}\right)}\right)\right\rfloor, n\right\} & \text{for cases (C1)-(C3),} \\ n & \text{otherwise.} \end{cases} \tag{4.36}$$

Now, solving $L(t_{\mathrm{OMT}}) = L_{\mathrm{crit}}$ for t_{OMT}, from Eq. (4.30b) we obtain the following relation:

$$1 + \left(\frac{1 - L(t_k + \epsilon)}{L(t_k + \epsilon)} \right) \mathrm{e}^{-\rho(t_{\mathrm{OMT}} - t_k - \epsilon)} = \frac{1}{L_{\mathrm{crit}}}$$

and consequently:

$$t_{\mathrm{OMT}} = t_k + \epsilon - \frac{1}{\rho} \ln \left(\frac{1 - L_{\mathrm{crit}}}{1 - L(t_k + \epsilon)} \frac{L(t_k + \epsilon)}{L_{\mathrm{crit}}} \right).$$

Finally, from assumption (4.26), the time of the onset of malignant transformation can be estimated by the following formula:

$$t_{\mathrm{OMT}} = (k-1)r + \epsilon - \frac{1}{\rho} \ln \left(\frac{1 - L_{\mathrm{crit}}}{1 - L(t_k + \epsilon)} \frac{L(t_k + \epsilon)}{L_{\mathrm{crit}}} \right), \tag{4.37}$$

with k defined by Eq. (4.36).

We study the estimate of t_{OMT} given by Eq. (4.37) for the realistic set of parameters values. To be specific, we take values of LGG proliferation rates ρ, TMZ-cell kill strength α, initial LGG density at the centre of the tumour L_1 and critical LGG density triggering malignant transformation L_{crit} used in Section 3.3.1, *cf.* [3]. Recall that due to rescaling L is dimensionless variable, consequently L_1 and L_{crit} as well. We assume that parameters C_0 and λ have the same values as provided in Section 2.3.1. We also take into account that the drug is acting on the tumour during 12h as for that time we obtained a reasonably good agreement with the results of system (4.27). The possible number of doses is within the range 10–150 indicated by clinical reports, see *e.g.* [69, 22, 70]. The values and ranges of parameters are summarised in Table 4.1.

Table 4.1: **Values and ranges of biological and clinical parameters used in the mathematical model of LGG evolution and response to chemotherapy**

Parameter	Value	Description
ρ	0.0001–0.008/day	proliferation rate of LGG cells
L_1	0.3–0.57	initial mean LGG cell density
L_{crit}	0.6	LGG cell density causing malignant transformation
α	0.1–1.5ml/μg/day	TMZ-cell kill strength
C_0	0.6μg/ml	initial TMZ concentration in brain interstitium
λ	0.3466/h	rate of decay of TMZ
ϵ	12h	time of whole dose elimination
n	10–150	total number of administered drug doses

First, we verify the goodness of our estimation. To do so, we compare the results from simulations of system (4.27) and Eq. (4.37) for different values of model parameters, see Figure 4.2. We would like to underline that sharp increases in difference in t_{OMT} estimations appeared only for such parameters values that t_{OMT} occurs before the end of the treatment. In other words, the resulting treatments are not optimal for such parameters ranges, and thus, should not be taken into account while attempting to select the best treatment scenario.

In Figure 4.3 we show how estimated onset of malignant transformation depends on patient-specific parameters, *i.e.* tumour proliferation rate ρ and TMZ-cell kill strength α. For fixed ρ, it seems that t_{OMT} is smaller for smaller α rates, that is malignant transformation occurs sooner for virtual tumours which are less sensitive to chemotherapy. On the other hand, for

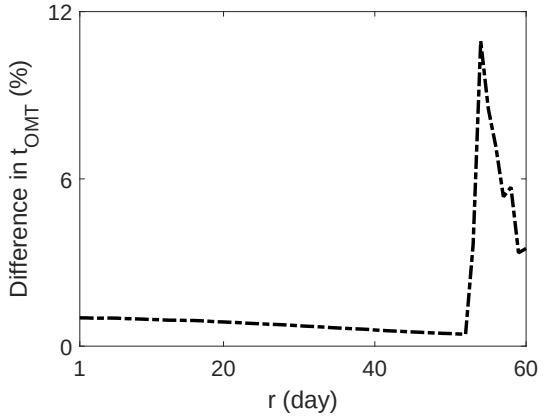

(a) $\rho = 0.002$/day, $\alpha = 0.6$ml/μg/day

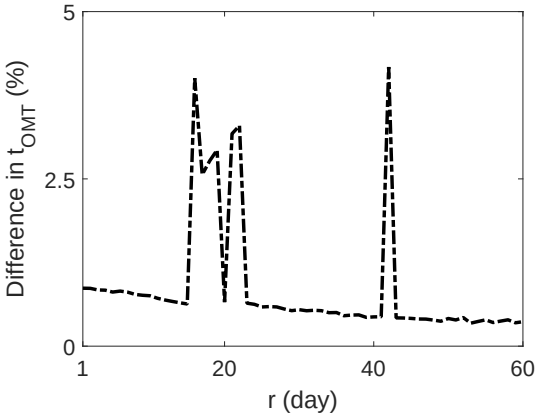

(b) $\rho = 0.004$/day, $\alpha = 0.3$ml/μg/day

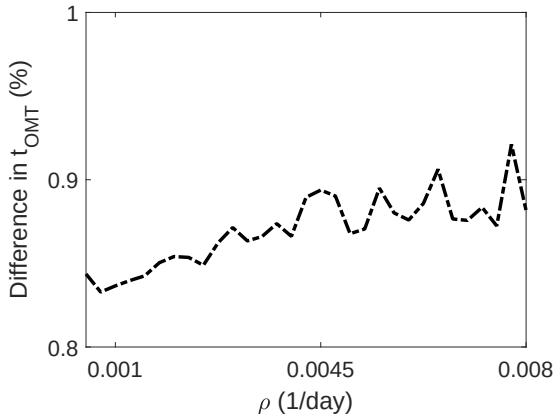

(c) $\alpha = 0.3$ml/μg/day, $r = 1$

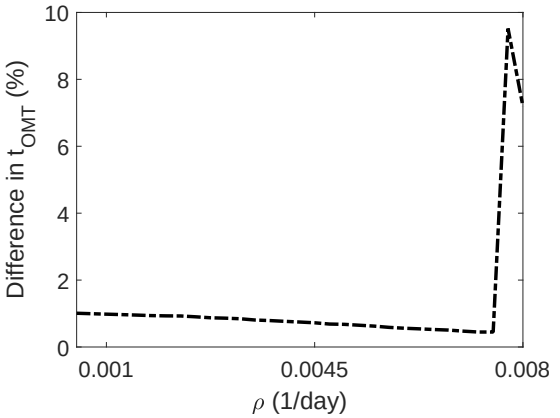

(d) $\alpha = 0.6$ml/μg/day, $r = 14$

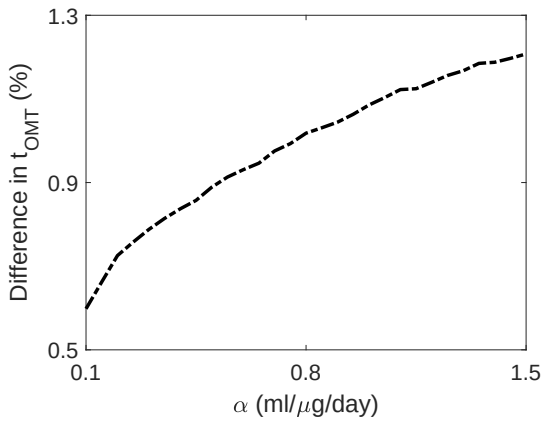

(e) $\rho = 0.002$/day, $r = 14$

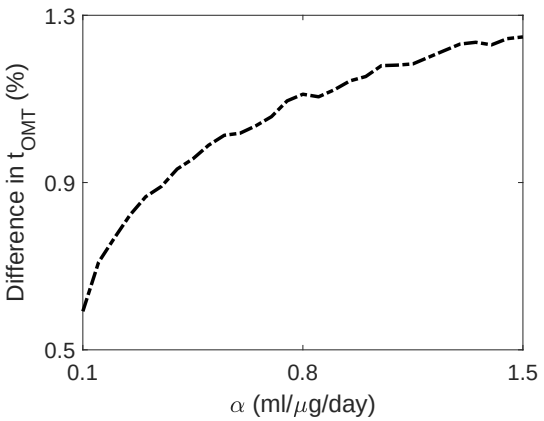

(f) $\rho = 0.004$/day, $r = 1$

Figure 4.2: Relative percentage differences between t_{OMT} calculated from Eq. (4.37) and from simulations of system (4.27). We considered 60 doses of TMZ and assumed that $L_1 = 0.35$.

fixed α, greater proliferation rates imply shorter time to malignant transformation, *i.e.* greater velocity of tumour growth is associated with malignant transformation occurring earlier. These results of our model seem to be self-evident and they are in a full agreement with biological observations. Yet, to our knowledge, they have been not considered in a treatment planning of LGGs.

In clinical practice, it could be difficult to control value of α, however, proliferation rate ρ can be predicted on the basis of few initial post-surgical MRI scans, as discussed previously in Section 3.5. Thus, for fixed unit dose and a total number of doses we can study if there is any better possible chemotherapy fractionation scheme if different velocities of tumour

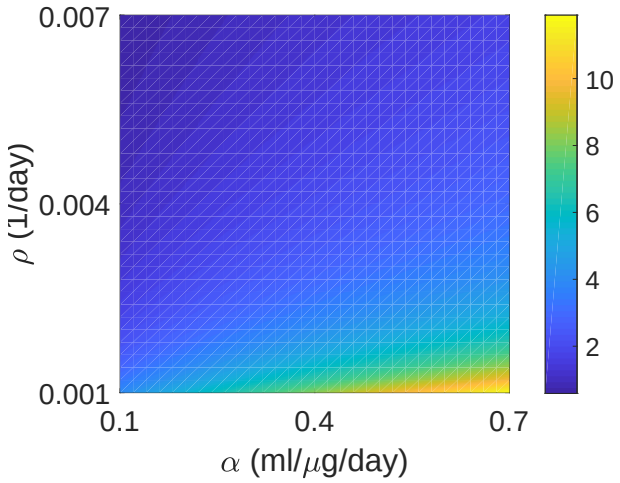

Figure 4.3: Pseudocolour plot representing onset of malignant transformation (t_{OMT}) estimated from Eq. (4.37) for different proliferation rates ρ and TMZ-cell kill strength α for the case when $L_1 = 0.4$, $r = 1$ and number of doses equals 60.

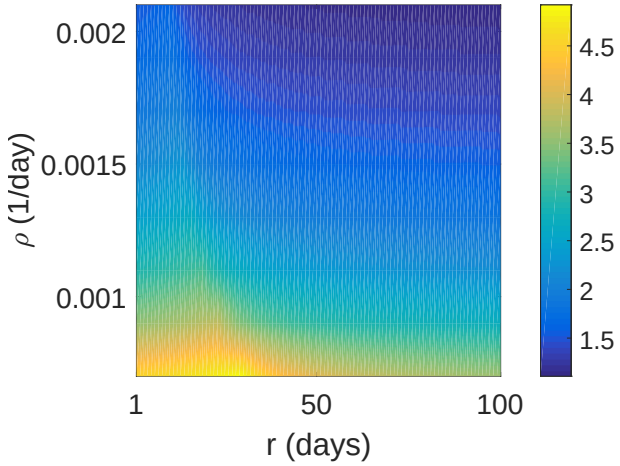

Figure 4.4: Pseudocolour plot representing onset of malignant transformation (t_{OMT}) estimated from Eq. (4.37) for different proliferation rates ρ and breaks r between subsequent doses for the case when $L_1 = 0.4$, $\alpha = 0.1$ and number of doses equals 60.

growth are considered. We present in Figures 4.4 and 4.5 the exemplary results, which show the general relation between t_{OMT} and r for different values of ρ. It seems that the current standard break between subsequent doses (*i.e.* one day) may be the best one only for relatively big proliferation rates. In fact to treat HGGs with higher proliferation rates chemotherapy doses have been originally administered every day. Historically, a rule "maximum tolerated doses in minimal time" has been widely applied for malignant tumours. However, LGG is usually not a fast-growing tumour, for which this rule has been established. Figures 4.4 and 4.5 suggest that for slowly growing tumours with small proliferation rates possibly a fractionation scheme with larger breaks between doses should be considered. Such a chemotherapy with prolonged time between subsequent doses is called a "protracted chemotherapy", *cf. e.g.* [26]. In Figure 4.5 we see that if chemotherapy is applied in a protracted manner a potential increase in time when malignant transformation starts could be around a year. Such an idea is breaking well-established concept. However, it becomes easier to understand if we notice that in the case of a very slow growing tumour, applying drug doses every day may simply mean attacking

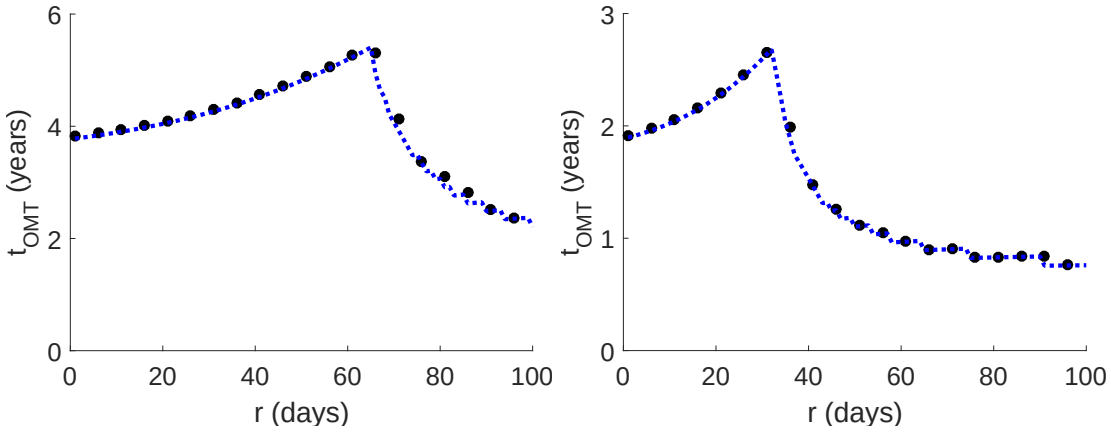

Figure 4.5: Onset of malignant transformation estimated from Eq. (4.37) (dotted lines) and from simulations of system (4.27) (black circles) for different breaks r between subsequent doses for $\rho = 0.002$ (left) and $\rho = 0.004$ (right). The remaining parameters were: $\alpha = 0.7, L_1 = 0.4$, and number of doses equals 30.

the same tumour cells many times.

On the other hand, the break between subsequent doses cannot be too large, see Figure 4.5, as in such situations malignant transformation may already begin during the total treatment time. It is due to the fact that in such cases the break between doses r is so large that a tumour starts regrowing when there is no drug in tumour tissue, that is in times of length $r - \epsilon$. Thus, taking a too large break between doses leads to a sharp drop of the time of malignant transformation onset and even a worse outcome than for treatment with doses given every day. Hence, the choice of proper spacing between doses needs to be cautiously and carefully studied.

4.3 Discussion

In this chapter, we considered first a reaction-diffusion system (4.1) describing LGG growth and response to constant chemotherapy. Of our interest was especially the question of the existence of travelling wave solutions. We proved the existence of such front using singular geometric perturbation theory [209, 210].

Later on, in Section 4.2 we have modified system (4.1) in such a way that chemotherapy is described more realistically by some function of time. Motivated by results of Chapter 3, the model was simplified in order to obtain an analytical estimate of the onset of malignant transformation for patients treated with chemotherapy. We obtained an explicit formula and verified its goodness, see Figure 4.2. We also performed a study on how does estimated t_{OMT} depends on the model parameters and break between subsequent doses.

We believe that such outcomes could have a potential application in selecting better chemotherapy schedules for different patients in the future. Our results indicate that the treatment fractionation scheme could be optimised by changing the duration of the treatment or the break between subsequent doses. We propose to consider increasing the break between doses administered to LGG patients. The predicted increase in t_{OMT} obtained by this simple modification depends on the tumour proliferation rate and can be around one year which may be significant especially for faster-growing LGGs.

On the basis of current clinical studies, we presume that such a prolongation of chemotherapy would remain safe for LGG patients. Khasraw *et al.* report cases of LGGs patients

for which chemotherapy treatment administered for even 5-8 years did not cause serious side effects [174]. Moreover, Mannas *et al.* conclude that long-term chemotherapy with TMZ could be considered a therapeutic option as long as appropriate monitoring is assured [175].

We hope that in the next few years it will be possible to verify the effectiveness of such schedules *in vivo*, leading to next clinical steps. Some studies on prolonged chemotherapies with increased breaks between subsequent cycles like [61, 214] give us promising results to follow in this direction. Our results are also in line with research presented in [134], where authors study previously designed mathematical model of response to PCV, another chemotherapeutic drug for gliomas see Section 1.5. Mazzocco *et al.* conclude that only prolonging the break between subsequent cycles of drug administration can lead to improvement in virtual patients overall survival of around a year.

In this chapter, we have considered administration of a fixed number of doses equal to the standard dose of 150mg/m^2. However, the obtained formulation of the simplified model allows also to consider different doses of chemotherapy. Unfortunately, in order to do so, we would need, currently unavailable, reliable information about different TMZ doses distributions obtained from brain tissue, just as is in the case of the standard dose, *cf.* [78, 157]. Thus, we hope that the presented results will lead to further research on optimised chemotherapy fractionations for individual LGG patients.

Chapter 5

Summary

In this dissertation, we developed macroscopic mathematical models describing several aspects of the growth dynamics of low-grade gliomas and their response to chemotherapy. As explained in **Chapter 1**, low-grade gliomas (abbreviated as LGGs) are brain tumours having a poor prognosis and causing a premature death for almost all patients. The clinical course of this disease is usually very difficult to predict. Some of these tumours remain stable for years, while others progress rapidly into their more malignant counterparts known as high-grade gliomas, which induce the appearance of major neurological deficits and, eventually, death.

Up to now only few studies have been intended to describe LGG growth and its response to therapies using a mathematical framework, for details see Section 1.6. Some of the mathematical models presented so far take into account a large number of quantities which are very difficult, or impossible, to measure or estimate. Models proposed in this thesis are based on biological and clinical studies concerning LGGs and all models' parameters have a clear biological meaning. Most of them were estimated from the appropriate data or literature and at most four parameters were considered to be patient-specific. Such a "minimalistic approach" enabled to fit the models' solutions to reflect the growth kinetics of individual patients, obtaining very good results. We validated our models using LGGs patients' data provided by our collaborators from Bern University Hospital, for details see Section 1.7. Importantly, we performed mathematical analysis of our models and studied various quantities of potential practical interest.

In **Chapter 2** we formulated a mathematical model describing LGGs growth and their response to temozolomide, a specific chemotherapeutic drug currently used to treat these tumours. The model was developed in the form of two ODEs describing the evolution of two populations of LGG cells: proliferating and damaged by chemotherapy. Such an approach was chosen to characterise the prolonged response of LGGs to cytotoxic treatments, which lasts months or sometimes even years after the end of therapy. A drug dynamics was modelled directly by an impulsive ODE, allowing to realistically model the way chemotherapy drugs are administered in the clinical practice. Recall that other mathematical models for glioma response to chemotherapy did not focus on a very realistic description of chemotherapy drug administration, see Section 1.6.

We investigated the mathematical properties of the proposed model with a general form of tumour growth function. In particular, we proved the existence and uniqueness of solutions. We showed that there exists a compact set invariant with respect to the evolution of the model

in a case when initial conditions and model parameters fulfil given conditions. We showed that the long-term behaviour of the model is similar for different choices of the specific growth function. To be specific, we showed that in the case of constant treatment, the conditions for stability of existing steady states are the same for Gompertz type and logistic type of tumour growth function, *cf.* Theorem 2.8. In addition, we also considered drug concentration to be described by an asymptotically periodic function, which is a generalisation of the previously proposed one [2]. In Theorem 2.12 we indicated the condition under which the trivial steady state is asymptotically stable in the case of asymptotically periodic treatment. Based on this result, we provided estimations of suggested minimal effective doses for individual LGG patients. Finally, we showed that in some cases of periodic treatment there exist periodic solutions.

We used numerical analysis methods, see Appendix B, to solve our system and analyse the dependence of the model dynamics on parameters values. It turned out that our ODE model with logistic growth function not only reflected the fundamental phenomena on LGGs growth and response to chemotherapy but also fitted well to volumetric data of LGG patients treated with chemotherapy. We also studied various quantities of practical meaning, among others the time to radiological progression, defined as the time when a tumour attains its minimum volume after the chemotherapy and subsequently starts regrowing. Investigating a wide range of possible values of parameters, we concluded that virtual tumours having a shorter time to radiological progression after chemotherapy may be more aggressive. Such a behaviour was also noticeable in LGGs patients data and has been previously observed likewise for LGGs treated with radiotherapy [1, 116]. We suggested that estimated time to radiological progression can be useful as a measure of tumour aggressiveness and a possible indicator of tumour prognosis.

Through simplifications made to the original model, we managed to estimate the time to radiological progression as a function of the relevant biological and therapeutic parameters. The obtained formula given by Eq. (2.46) may be helpful in designing improved personalised treatment schedules, due to its dependence on tumour-specific parameters.

On the basis of our mathematical model, we also proposed a probing procedure which could be considered in clinical practice. We suggested applying a small number of chemotherapeutic drug doses and monitoring the tumour response to verify tumour's characteristics. The latter treatment decisions would depend on the observed time of maximal response. Tumours attaining their minimal volume early after a short course of chemotherapy treatment may be more aggressive, thus the remaining drug doses should be finished as soon as possible and other therapeutic options (further surgery if feasible or radiotherapy) should be considered. In the opposite case of slowly-responding tumours, it seems that after such a probing procedure the rest of treatment might be delayed (as these tumours seem to be less aggressive).

In **Chapter 3** we described mathematically the process of malignant transformation, *i.e.* the switch of low-grade gliomas to high-grade gliomas. Based on biological observations, we raised the hypothesis that malignant transformation may be induced by changes in tumour microenvironment happening as a result of increased tumoural density. Such assumption led us to a formulation of a system of two reaction-diffusion equations coupled by a switch function describing the transition from low-grade glioma phenotype to a more malignant one, characterised by larger both proliferation and motility rates. We showed the existence, uniqueness and non-negativity of solutions of the proposed model. We demonstrated the local stability of homogeneous steady states of the system in the case of zero and non-zero diffusion coefficient. We also investigated the stability of space homogeneous steady states and showed in Theorem 3.5 that no diffusion-driven instabilities occur in the system, which is a biologically

viable result.

As the model was developed with a minimal number of adjustable parameters, we were able to successfully fit its solutions to data describing the evolution of tumours which underwent malignant transformation. Subsequently, using numerical simulations and performing sensitivity analysis, we studied how the patient-specific parameters influence the long-term prognosis. We found out that the initial cell density at the centre of a tumour and rate of LGG cells growth are the parameters which have the biggest influence on both time to malignant transformation and overall survival.

These results suggest that the main goal of LGGs care should be the possible prevention or delay in appearing malignant transformation. Thus, we focused on studying analytically the tumour dynamics in the time horizon before the onset of malignant transformation. We discussed a possible model simplification in this period of time. Using a solution of Skellam equation we derived explicit formulae for the evolution of radius of the detectable part of a tumour and the velocity of its growth. Due to practical motivations, we also determined an analytic formula for the time of malignant transformation onset as a function of patient-specific parameters. Finally, we discussed the possible ways to apply some of these results in clinical oncology practice. We believe that by coupling detailed radiological imaging information with mathematical estimation derived in Chapter 3, malignant transformation could be predicted in a non-invasive way. Such a prediction could have a huge impact on treatment planning for low-grade glioma patients.

Motivated by the above results, in **Chapter 4** we studied a reaction-diffusion system capable of describing both the process of malignant transformation and the tumour response to chemotherapy. It was based on both models presented in Chapters 2 and 3. We studied the system analytically proving the existence and uniqueness of solutions. In the case of constant chemotherapy, using Fredholm alternative theorem, among others, we also showed that travelling wave solutions exist for some parameters values, see Theorem 4.3.

Afterwards, we used that model to investigate possibly improved chemotherapy fractionations. Usually, while studying theoretically the possible more effective treatment schedules, researchers aim at minimising the total tumour size or the total number of cells. However, in the case of LGGs, the total tumour size does not have to be related with the tumour aggressiveness or responsiveness to treatments. There have been reported cases of large tumours that remain stable for long periods of time and small tumours growing very fast. However, it seems unquestionable that after the malignant transformation onset the mean velocity of tumour growth increases significantly. Thus, it appears that the possible delaying of malignant transformation is an alternative goal potentially applicable in selecting treatment schemes for LGGs patients.

We proceeded to estimate the time of malignant transformation onset for virtual patients treated with a fixed number of chemotherapeutic drug doses. In order to do so, we considered the evolution of local tumour density at the centre of a tumour. In Theorem 4.4 we derived the solution of the resulting ODE system. We also studied the long-term dynamics of the obtained difference equation describing the density of tumour cells at the centre of a tumour at times of the drug administration, see Theorem 4.6. Afterwards, we proposed an estimate of the onset of malignant transformation for virtual patients treated with a fixed number of chemotherapeutic drug doses. We investigated the dependence of obtained estimate on model parameters and treatment scheme. Based on numerical simulations, we suggested that a better treatment outcome could be possibly attained only by increasing the break between subsequent doses. We also discussed the feasibility of such a solution.

We conclude that therapy schemes designed on the basis of tumour-specific characteristics may lead to significant improvements (even of the order of a year) in therapy effectiveness. We hope that optimised cancer treatment protocols on the basis of mathematical models, such as the ones presented in this dissertation, may become in the future a standard element of personalised medicine.

In each chapter, we presented results suggesting some novel strategies for LGG care. However, they require meticulous verification in an experimental setting. Both *in vitro* and *in vivo* experiments are being planned to verify the outcomes of this thesis and study their possible use in practice. In the future, having more specific experimental or clinical data would enable to include in our mathematical models more phenomena (such as acquiring drug resistance or toxicity) and address other clinically-driven questions, see *e.g.* discussion in Section 2.5.

The results of this dissertation were published in four scientific articles in peer-reviewed high-ranked international journals and in a number of proceedings of national and international conferences (*e.g.* in AIMS Conference on Dynamical Systems, Differential Equations and Applications, Quadrennial Meeting of the World Federation of Neuro-Oncology Societies, International Seminar on Statistics and Clinical Practice, BIOMAT International Symposium on Mathematical and Computational Biology). In the nearest future, the results presented in Chapter 4 will be submitted to other peer-reviewed journals. Additionally, in Appendix A we included the first publication of the thesis author presenting the model of low-grade gliomas growth and response to radiotherapy, which actually led to the following study of mathematical models for LGGs presented in this dissertation.

Bibliography

[1] V. Pérez-García, M. Bogdańska, A. Martínez-González, J. Belmonte-Beitia, P. Schucht, and L. Pérez-Romasanta, "Delay effects in the response of low-grade gliomas to radiotherapy: a mathematical model and its therapeutical implications," *Math. Med. Biol.*, vol. 32, pp. 307–29, 2015. [cited at p. 1, 3, 4, 5, 15, 17, 18, 24, 41, 55, 58, 63, 69, 77, 100]

[2] M. U. Bogdańska, M. Bodnar, J. Belmonte-Beitia, M. Murek, P. Schucht, J. Beck, and V. M. Pérez-García, "A mathematical model of low grade gliomas treated with temozolomide and its therapeutical implications," *Math. Biosci.*, vol. 288, pp. 1–13, 2017. [cited at p. 4, 9, 17, 69, 100]

[3] M. U. Bogdańska, M. Bodnar, M. J. Piotrowska, M. Murek, P. Schucht, J. Beck, A. Martínez-González, and V. M. Pérez-García, "A mathematical model describes the malignant transformation of low grade gliomas: Prognostic implications," *PLOS ONE*, vol. 12, no. 8, p. e0179999, 2017. [cited at p. 4, 18, 63, 94]

[4] M. Bodnar, M. J. Piotrowska, and M. U. Bogdańska, "Mathematical analysis of generalised model of chemotherapy for low grade gliomas," *DCDS-B*, 2018 (accepted). [cited at p. 4]

[5] M. U. Bogdańska, M. Bodnar, M. J. Piotrowska, M. Murek, P. Schucht, J. Beck, A. Martínez-González, and V. M. Pérez-García, "Malignant transformation of low-grade gliomas. Prognostic implications from mathematical model," *Neuro-Oncol*, vol. 19, no. suppl_3, p. iii85, 2018. [cited at p. 78]

[6] M. Weller, M. van den Bent, J. C. Tonn, R. Stupp, M. Preusser, E. Cohen-Jonathan-Moyal, *et al.*, "European association for neuro-oncology (eano) guideline on the diagnosis and treatment of adult astrocytic and oligodendroglial gliomas.," *Lancet Oncol.*, vol. 18, no. 6, pp. e315–e329, 2017. [cited at p. 1, 8]

[7] N. Burnet, S. Jefferies, R. Bensona, D. Hunt, and F. Treasure, "Years of life lost (yll) from cancer is an important measure of population burden–and should be considered when allocating research funds," *Br J Cancer.*, vol. 92, no. 2, pp. 241–245, 2005. [cited at p. 1]

[8] F. Pignatti, M. Van den Bent, D. Curran, C. Debruyne, R. Sylvester, P. Therasse, D. Afra, P. Cornu, M. Bolla, C. Vecht, and A. Karim, "Prognostic factors for survival in adult patients with cerebral low-grade glioma," *J. Clin. Oncol.*, vol. 20, pp. 2076–2084, 2002. [cited at p. 1]

[9] N. Pouratian and D. Schiff, "Management of low-grade glioma," *Curr Neurol Neurosci Rep*, vol. 10, no. 3, pp. 224–31, 2010. [cited at p. 1, 9]

[10] G. Keles, K. Lamborn, and M. Berger, "Low-grade hemispheric gliomas in adults: a critical review of extent of resection as a factor influencing outcome," *J Neurosurg*, vol. 95, no. 5, pp. 735–45, 2011. [cited at p. 1, 9, 69]

[11] A. Mangional, C. Anile, A. Pompucci, G. Capone, L. Rigante, and P. De Bonis, "Glioblastoma therapy: Going beyond hercules columns," *Expert Rev Neurother*, vol. 10, no. 4, pp. 507–514, 2010. [cited at p. 1]

[12] D. N. Louis, H. Ohgaki, O. D. Wiestler, W. K. Cavenee, P. C. Burger, A. Jouvet, B. W. Scheithauer, and P. Kleihues, "The 2007 WHO classification of tumours of the central nervous system," *Acta Neuropathol*, vol. 114, no. 2, pp. 97–109, 2007. [cited at p. 1, 7]

[13] M. J. van den Bent, D. Afra, O. de Witte, M. Ben Hassel, S. Schraub, K. Hoang-Xuan, *et al.*, "Long-term efficacy of early versus delayed radiotherapy for low-grade astrocytoma and oligodendroglioma in adults: the EORTC 22845 randomised trial," *Lancet*, vol. 366, pp. 985–90, 2005. [cited at p. 1]

[14] H. Byrne, "Dissecting cancer through mathematics: from the cell to the animal model.," *Nat Rev Cancer.*, vol. 10, no. 3, pp. 221–30, 2010. [cited at p. 1, 2]

[15] J. Clairambault, "Can theorems help treat cancer?," *J.Math.Biol.*, vol. 66, pp. 1555–8, 2013. [cited at p. 2, 3, 17]

[16] T. Jackson, N. Komarova, and K. Swanson, "Mathematical oncology: Using mathematics to enable cancer discoveries," *Amer. Math. Monthly*, vol. 121, pp. 840–56, 2014. [cited at p. 2, 3]

[17] A. L. Baldock, K. Yagle, D. E. Born, S. Ahn, A. D. Trister, M. Neal, *et al.*, "Invasion and proliferation kinetics in enhancing gliomas predict IDH1 mutation status," *Neuro Oncol*, vol. 16, no. 6, pp. 779–86, 2014. [cited at p. 2, 14]

[18] T. S. Deisboeck, L. Zhang, J. Yoon, and J. Costa, "*In silico* cancer modeling: is it ready for primetime?," *Nat Clin Pract Oncol.*, vol. 6, no. 1, pp. 34–42, 2009. [cited at p. 2, 3]

[19] L. E. Friberg, A. Henningsson, H. Maas, L. Nguyen, and M. O. Karlsson, "Model of chemotherapy-induced myelosuppression with parameter consistency across drugs," *J. Clin. Oncol.*, vol. 20, no. 24, pp. 4713–4721, 2002. [cited at p. 2]

[20] J. E. Cohen, "Mathematics is biology's next microscope, only better; biology is mathematics' next physics, only better," *PLoS Biol*, vol. 2, no. 12, pp. 2017–22, 2004. [cited at p. 2]

[21] V. M. Pérez-García, S. Fitzpatrick, L. A. Pérez-Romasanta, M. Pesic, P. Schucht, E. Arana, and P. Sánchez-Gómez, "Applied mathematics and nonlinear sciences in the war on cancer," *AMNS*, vol. 1, no. 2, pp. 423–36, 2016. [cited at p. 3]

[22] B. Ribba, G. Kaloshi, M. Peyre, D. Ricard, V. Calvez, M. Tod, B. Cajavec-Bernard, A. Idbaih, D. Psimaras, L. Dainese, J. Pallud, S. Cartalat-Carel, J. Delattre, J. Honnorat, E. Grenier, and F. Ducray, "A tumor growth inhibition model for low-grade glioma treated with chemotherapy or radiotherapy," *Clin Can Res*, vol. 18, pp. 5071–80, 2012. [cited at p. 3, 10, 17, 18, 25, 56, 94]

[23] K. R. Swanson, R. C. Rockne, J. Claridge, M. A. Chaplain, E. C. Alvord Jr, and A. A. Anderson, "Quantifying the role of angiogenesis in malignant progression of gliomas: In silico modeling integrates imaging and histology," *Cancer Res*, vol. 71, pp. 7366–7375, 2011. [cited at p. 3, 15, 18, 58, 63, 64]

[24] P. Y. Bondiau, M. Frenay, and N. Ayache, "Biocomputing: numerical simulation of glioblastoma growth using diffusion tensor imaging," *Phys.Med.Biol.*, vol. 53, pp. 879–893, 2008. [cited at p. 3]

[25] C. Gerin, J. Pallud, B. Grammaticos, E. Mandonnet, C. Deroulers, P. Varlet, *et al.*, "Improving the time-machine: estimating the date of birth of grade II gliomas," *Cell Prolif*, vol. 45, no. 1, pp. 76–90, 2012. [cited at p. 3, 15, 16, 41, 62, 63, 64]

[26] V. M. Pérez-García and L. A. Pérez-Romasanta, "Extreme protraction for low-grade gliomas: Theoretical proof of concept of a novel therapeutical strategy," *Math. Med. Biol.*, vol. 33, no. 3, pp. 253–271, 2015. [cited at p. 3, 41, 63, 64, 69, 77, 96]

[27] A. Dufour, E. Gontran, C. Deroulers, P. Varlet, J. Pallud, B. Grammaticos, and et al., "Modeling the dynamics of oligodendrocyte precursor cells and the genesis of gliomas," *PLoS Comput Biol*, vol. 14, no. 3, p. e1005977, 2018. [cited at p. 3]

[28] K. R. Swanson, R. C. Rostomily, and E. C. Alvord Jr, "A mathematical modelling tool for predicting survival of individual patients following resection of glioblastoma: a proof of principle," *Br J Cancer*, vol. 98, pp. 113–9, 2008. [cited at p. 3, 13, 15]

[29] C. H. Wang, J. K. Rockhill, M. Mrugala, *et al.*, "Prognostic significance of growth kinetics in newly diagnosed glioblastomas revealed by combining serial imaging with a novel biomathematical model," *Cancer Res*, vol. 69, no. 23, pp. 9133–40, 2009. [cited at p. 3, 14, 58, 63, 64, 70, 79]

[30] D. Hanahan and R. A. Weinberg, "Hallmarks of cancer: the next generation," *Cell*, vol. 144, no. 5, pp. 646–74, 2011. [cited at p. 5]

[31] Q. T. Ostrom, H. Gittleman, P. Liao, C. Rouse, Y. Chen, J. Dowling, Y. Wolinsky, C. Kruchko, and J. Barnholtz-Sloan, "CBTRUS statistical report: primary brain and central nervous system tumors diagnosed in the United States in 2007–2011," *Neuro Oncol*, vol. 16, no. suppl 4, pp. iv1–iv63., 2014. [cited at p. 6]

[32] S. Bauer, R. Wiest, L. P. Nolte, and M. Reyes, "A survey of MRI-based medical image analysis for brain tumor studies," *Phys Med Biol*, vol. 58, no. 13, pp. R97–129, 2013. [cited at p. 6]

[33] P. H. Wessels, W. E. J. Weber, G. Raven, F. C. S. Ramaekers, A. H. N. Hopman, and A. Twijnstra, "Supratentorial grade II astrocytoma: biological features and clinical course," *Lancet Neurol*, vol. 2, pp. 395–403, 2003. [cited at p. 6, 8, 10]

[34] N. A. Oberheim Bush and S. Chang, "Treatment strategies for low-grade glioma in adults," *J Oncol Pract*, vol. 12, no. 12, pp. 1235–41, 2016. [cited at p. 7, 8]

[35] D. N. Louis, A. Perry, G. Reifenberger, A. von Deimling, D. Figarella-Branger, W. K. Cavenee, and et al., "The 2016 world health organization classification of tumors of the central nervous system: a summary," *Acta Neuropathol.*, vol. 131, pp. 803–20, 2016. [cited at p. 7, 8]

[36] W. J. Chen, D. S. He, R. X. Tang, F. H. Ren, and G. Chen, "Ki-67 is a valuable prognostic factor in gliomas: evidence from a systematic review and meta-analysis," *Asian Pac J Cancer Prev*, vol. 16, no. 2, pp. 411–20, 2015. [cited at p. 7]

[37] N. V. Shivaprasad, S. Satish, S. Ravishankar, and M. G. Vimalambike, "Ki-67 immunostaining in astrocytomas: Association with histopathological grade - A South Indian study," *J Neurosci Rural Pract*, vol. 7, no. 4, pp. 510–4, 2016. [cited at p. 7, 12]

[38] S. Everhard, G. Kaloshi, E. Crinière, *et al.*, "MGMT Methylation: A Marker of Response to Temozolomide in Low-Grade Gliomas," *Ann Neurol*, vol. 60, no. 6, pp. 740–43, 2006. [cited at p. 8, 10]

[39] J. T. Grier and T. Batchelor, "Low-grade gliomas in adults," *Oncologist*, vol. 11, pp. 681–693, 2006. [cited at p. 8, 9]

[40] H. Duffau and L. Taillandier, "New concepts in the management of diffuse low-grade glioma: Proposal of a multistage and individualized therapeutic approach," *Neuro-Oncology*, vol. 17, no. 3, pp. 332–42, 2015. [cited at p. 8]

[41] A. M. Sonabend and M. S. Lesniak, "Oligodendrogliomas: clinical significance of 1p and 19q chromosomal deletions," *Expert Rev Neurother.*, vol. 5, no. 6 Suppl, pp. S25–32, 2005. [cited at p. 8]

[42] A. A. Kanner, S. M. Staugaitis, E. A. Castilla, O. Chernova, R. A. Prayson, M. A. Vogelbaum, G. Stevens, D. Peereboom, J. Suh, S. Lee, R. R. Tubbs, and G. H. Barnett, "The impact of genotype on outcome in oligodendroglioma: validation of the loss of chromosome arm 1p as an important factor in clinical decision making," *J. Neurosurg.*, vol. 104, no. 4, pp. 542–50, 2006. [cited at p. 8]

[43] J. Smith, E. Chang, K. Lamborn, S. Chang, M. Prados, S. Cha, T. Tihan, S. Vandenberg, M. McDermott, and M. Berger, "Role of extent of resection in the long-term outcome of low-grade hemispheric gliomas," *J Clin Oncol*, vol. 26, no. 8, pp. 1338–45, 2008. [cited at p. 9]

[44] A. S. Jakola, K. S. Myrmel, R. Kloster, S. H. Torp, S. Lindal, G. Unsgard, and O. Solheim, "Comparison of a strategy favoring early surgical resection vs a strategy favoring watchful waiting in low-grade gliomas," *JAMA*, vol. 308, no. 18, pp. 1881–8, 2012. [cited at p. 9]

[45] L. Capelle, D. Fontaine, E. Mandonnet, L. Taillandier, J. L. Golmard, L. Bauchet, *et al.*, "Spontaneous and therapeutic prognostic factors in adult hemispheric World Health Organization Grade II gliomas: a series of 1097 cases: clinical article," *J Neurosurg*, vol. 118, no. 1157–68, 2013. [cited at p. 9]

[46] R. Soffietti, B. G. Baumert, L. Bello, A. von Deimling, H. Duffau, M. Frénay, *et al.*, "Guidelines on management of low-grade gliomas: report of an EFNS-EANO Task Force," *Eur J Neurol*, vol. 17, no. 1124–33, 2010. [cited at p. 9]

[47] A. Karim, B. Maat, R. Hatlevoll, J. Menten, E. Rutten, D. Thomas, *et al.*, "A randomized trial on dose-response in radiation therapy of low-grade cerebral glioma: European Organization for Research and Treatment of Cancer (EORTC) study 22844," *Int J Radiat Oncol Biol Phys*, vol. 36, no. 3, pp. 549–56, 1996. [cited at p. 9]

[48] A. Karim, D. Afra, P. Cornu, N. Bleehan, S. Schraub, O. De Witte, *et al.*, "Randomized trial on the efficacy of radiotherapy for cerebral low-grade glioma in the adult: European Organization for Research and Treatment of Cancer Study 22845 with the Medical Research Council study BRO4: an interim analysis," *Int J Radiat Oncol Biol Phys*, vol. 52, no. 2, pp. 316–24, 2002. [cited at p. 9]

[49] E. Shaw, R. Arusell, B. Scheithauer, J. O'Fallon, B. O'Neill, R. Dinapoli, D. Nelson, J. Earle, C. Jones, T. Cascino, *et al.*, "Prospective randomized trial of low- versus high-dose radiation therapy in adults with supratentorial low-grade glioma: initial report of a North Central Cancer Treatment Group/Radiation Therapy Oncology Group/Eastern Cooperative Oncology Group study," *J Clin Oncol*, vol. 20, no. 9, pp. 2267–76, 2002. [cited at p. 9]

[50] G. Cairncross, M. Wang, E. Shaw, *et al.*, "Phase III trial of chemoradiotherapy for anaplastic oligodendroglioma: long-term results of RTOG 9402," *J Clin Oncol*, vol. 31, no. 3, pp. 337–43, 2012. [cited at p. 9]

[51] M. van den Bent, A. Brandes, M. Taphoorn, J. Kros, M. Kouwenhoven, J. Delattre, H. Bernsen, M. Frenay, C. Tijssen, W. Grisold, L. Sipos, R. Enting, P. French, W. Dinjens, C. Vecht, A. Allgeier, D. Lacombe, T. Gorlia, and K. Hoang-Xuan, "Adjuvant procarbazine,lomustine, and vincristine chemotherapy in newly diagnosed anaplastic oligodendroglioma: Long-term follow-up of EORTC Brain Tumor Group Study 26951," *J. Clin. Oncol.*, vol. 31, no. 3, pp. 344–50, 2012. [cited at p. 9]

[52] W. Mason, G. Krol, and L. DeAngelis, "Low-grade oligodendroglioma responds to chemotherapy," *Neurology*, vol. 46, no. 1, pp. 203–7, 1996. [cited at p. 9]

[53] J. Buckner, D. J. Gesme, J. O'Fallon, *et al.*, "Phase II trial of procarbazine, lomustine, and vincristine as initial therapy for patients with low-grade oligodendroglioma or oligoastrocytoma: Efficacy and associations with chromosomal abnormalities," *J Clin Oncol*, vol. 21, no. 2, pp. 251–5, 2003. [cited at p. 9]

[54] R. Liu, K. Solheim, M. Polley, K. Lamborn, M. Page, A. Fedoroff, *et al.*, "Quality of life in low-grade glioma patients receiving temozolomide," *Neuro Oncol*, vol. 11, no. 1, pp. 59–68, 2009. [cited at p. 9]

[55] A. Pace, A. Vidiri, E. Galiè, M. Carosi, S. Telera, A. Cianciulli, P. Canalini, D. Giannarelli, B. Jandolo, and C. Carapella, "Temozolomide chemotherapy for progressive low-grade glioma: clinical benefits and radiological response," *Ann. Oncol.*, vol. 14, no. 12, pp. 1722–26, 2003. [cited at p. 9]

[56] N. Pouratian, J. Gasco, J. Sherman, M. Shaffrey, and D. Schiff, "Toxicity and efficacy of protracted low dose temozolomide for the treatment of low grade gliomas," *J Neurooncol*, vol. 82, no. 3, pp. 281–8, 2007. [cited at p. 9, 57]

[57] E. Newlands, M. Stevens, S. Wedge, R. Wheelhouse, and C. Brock, "Temozolomide: a review of its discovery, chemical properties, pre-clinical development and clinical trials," *Cancer Treat Reviews*, vol. 23, no. 1, pp. 35–61, 1997. [cited at p. 9, 25]

[58] F. Marchesi, M. Turriziani, G. Tortorelli, G. Avvisati, F. Torino, and L. De Vecchis, "Triazene compounds: Mechanism of action and related DNA repair systems," *Pharmacol. Res.*, vol. 56, pp. 275–87, 2007. [cited at p. 9, 24, 52]

[59] A.-M. Barciszewska, D. Gurda, P. Głodowicz, S. Nowak, and M. Z. Naskręt-Barciszewska, "A new epigenetic mechanism of temozolomide action in glioma cells," *PLoS ONE*, vol. 10, no. 8, pp. 1–12, 2015. [cited at p. 9, 52]

[60] R. Stupp, W. Mason, and M. van den Bent et al., "Radiotherapy plus concomitant and adjuvant temozolomide for glioblastoma," *N Engl J Med*, vol. 352, pp. 987–96, 2005. [cited at p. 9, 10]

[61] S. Kesari, D. Schiff, J. Drappatz, D. LaFrankie, L. Doherty, E. Macklin, *et al.*, "Phase II study of protracted daily temozolomide for low-grade gliomas in adults," *Clin Cancer Res*, vol. 15, no. 1, pp. 330–7, 2009. [cited at p. 9, 10, 47, 56, 98]

[62] G. Kaloshi, A. Benouaich-Amiel, F. Diakite, *et al.*, "Temozolomide for low-grade gliomas: predictive impact of 1p/19q loss on response and outcome," *Neurology*, vol. 68, no. 21, pp. 1831–6, 2007. [cited at p. 9, 10]

[63] M. Blonski, J. Pallud, C. Gozé, *et al.*, "Neoadjuvant chemotherapy may optimize the extent of resection of World Health Organization grade II gliomas: a case series of 17 patients," *J Neurooncol*, vol. 113, no. 2, pp. 267–75, 2013. [cited at p. 9]

[64] J. Jo, B. Williams, M. Smolkin, M. Wintermark, M. Shaffrey, M. Lopes, and D. Schiff, "Effect of neoadjuvant temozolomide upon volume reduction and resection of diffuse low-grade glioma," *J. Neuro-Oncol.*, vol. 120, no. 1, pp. 155–61, 2014. [cited at p. 9]

[65] J. Koekkoek, L. Dirven, J. Heimans, T. Postma, M. Vos, J. Reijneveld, and M. Taphoorn, "Seizure reduction in a low-grade glioma: more than a beneficial side effect of temozolomide," *J Neurol Neurosurg Psychiatry*, vol. 86, no. 4, pp. 366–73, 2015. [cited at p. 10]

[66] M. Wyss, S. Hofer, M. Bruehlmeier, *et al.*, "Early metabolic responses in temozolomide treated low-grade glioma patients," *Curr Opin Oncol*, vol. 95, no. 1, pp. 87–93, 2009. [cited at p. 10]

[67] R. Guillevin, C. Menuel, S. Taillibert, L. Capelle, R. Costalat, L. Abud, *et al.*, "Predicting the outcome of grade II glioma treated with temozolomide using proton magnetic resonance spectroscopy," *Br J Cancer*, vol. 104, no. 12, pp. 1854–61, 2011. [cited at p. 10]

[68] M. Peyre, S. Cartalat-Carel, D. Meyronet, D. Ricard, A. Jouvet, J. Pallud, K. Mokhtari, J. Guyotat, E. Jouanneau, M. Sunyach, D. Frappaz, J. Honnorat, and D. F., "Prolonged response without prolonged chemotherapy: a lesson from PCV chemotherapy in low-grade gliomas," *Neuro-Oncology*, vol. 12, no. 10, pp. 1078–82, 2010. [cited at p. 10, 24]

[69] D. Ricard, G. Kaloshi, A. Amiel-Benouaich, J. Lejeune, Y. Marie, E. Mandonnet, M. Kujas, K. Mokhtari, S. Taillibert, F. Laigle-Donadey, A. Carpentier, A. Omuro, L. Capelle, H. Duffau, P. Cornu, R. Guillevin, M. Sanson, K. Hoang-Xuan, and J. Delattre, "Dynamic history of low-grade gliomas before and after temozolomide treatment," *Ann. Neurol.*, vol. 61, no. 5, pp. 484–90, 2007. [cited at p. 10, 15, 24, 39, 53, 94]

[70] M. Chamberlain, "Temozolomide for recurrent low-grade spinal cord gliomas in adults," *Cancer*, vol. 113, no. 5, pp. 1019–24, 2008. [cited at p. 10, 24, 53, 94]

[71] K. Hoang-Xuan, L. Capelle, M. Kujas, S. Taillibert, H. Duffau, J. Lejeune, *et al.*, "Temozolomide as initial treatment for adults with low-grade oligodendrogliomas or oligoastrocytomas and correlation with chromosome 1p deletions," *J Clin Oncol*, vol. 22, no. 15, pp. 3133–38, 2004. [cited at p. 10]

[72] S. Ohba, J. Mukherjee, W. Mukherjee, and R. Pieper, "Mutant IDH1-driven cellular transformation increases RAD51-mediated homologous recombination and temozolomide resistance," *Cancer Res.*, vol. 74, no. 17, pp. 4836–44, 2014. [cited at p. 10]

[73] S. Sevinc, U. A. Sanli, and E. Goker, "Algorithms for scheduling of chemotherapy plans," *Comput Biol Med*, vol. 43, no. 12, pp. 2103–9, 2013. [cited at p. 10]

[74] W. Wick, M. Platten, and W. Weller, "New (alternative) temozolomide regimens for the treatment of gliomas," *Neuro Oncol*, vol. 11, no. 1, pp. 69–79, 2009. [cited at p. 10, 56]

[75] W. Taal, J. M. Segers-van Rijn, J. M. Kros, *et al.*, "Dose dense 1 week on/1 week off temozolomide in recurrent glioma: a retrospective study," *J Neurooncol*, vol. 108, no. 1, pp. 195–200, 2012. [cited at p. 10]

[76] A. Viaccoz, A. Lekoubou, and F. Ducray, "Chemotherapy in low-grade gliomas," *J Neurooncol*, vol. 24, no. 6, pp. 694–701, 2012. [cited at p. 10]

[77] M. Hegi, A. Diserens, T. Gorlia, M. Hamou, N. de Tribolet, M. Weller, *et al.*, "MGMT gene silencing and benefit from temozolomide in glioblastoma," *N Engl J Med*, vol. 352, no. 10, pp. 997–1003, 2005. [cited at p. 10]

[78] L. Hammond, J. Eckardt, S. Baker, S. Eckhardt, M. Dugan, K. Forral, *et al.*, "Phase I and pharmacokinetic study of temozolomide on a daily for 5 days schedule in patients with advanced solid malignancies," *J Clin Oncol*, vol. 17, no. 8, pp. 2604–13, 1999. [cited at p. 10, 25, 39, 40, 52, 98]

[79] D. E. Gannett, W. M. Wisbeck, D. L. Silbergeld, and M. S. Berger, "The role of postoperative irradiation in the treatment of oligodendroglioma.," *Int J Radiat Oncol Biol Phys*, vol. 30, no. 3, pp. 567–73, 1994. [cited at p. 10]

[80] C. Leighton, B. Fisher, G. Bauman, S. Depiero, L. Stitt, D. MacDonald, and G. Cairncross, "Supratentorial low-grade glioma in adults: an analysis of prognostic factors and timing of radiation.," *J Clin Oncol*, vol. 15, no. 4, pp. 1294–301, 1997. [cited at p. 10]

[81] J. M. Piepmeier, "Observations on the current treatment of low-grade astrocytic tumors of the cerebral hemispheres.," *J Neurosurg*, vol. 67, no. 2, pp. 177–81, 1987. [cited at p. 10]

[82] K. Chaichana, M. J. McGirt, J. Laterra, A. Oliv, and A. Quiñones-Hinojosa, "Recurrence and malignant degeneration after resection of adult hemispheric low-grade gliomas," *J Neurosurg*, vol. 112, no. 1, pp. 10–7, 2010. [cited at p. 10, 11]

[83] I. Sakarunchai, R. Sangthong, N. Phuenpathom, and M. Phukaoloun, "Free survival time of recurrence and malignant transformation and associated factors in patients with supratentorial low-grade gliomas," *J Med Assoc Thai*, vol. 96, no. 12, pp. 1542–9., 2013. [cited at p. 10]

[84] C. A. J. Romanowski, N. Hoggard, D. Jellinek, D. Levy, S. Wharton, C. Kotsarini, R. Batty, and I. Wilkinson, "Low grade gliomas. Can we predict tumour behaviour from imaging features?," *Neuroradiol. J.*, vol. 21, pp. 41–66, 2008. [cited at p. 10]

[85] B. Bobek-Billewicz, G. Stasik-Pres, A. Hebda, K. Majchrzak, W. Kaspera, and M. Jurkowski, "Anaplastic transformation of low-grade gliomas (WHO II) on magnetic resonance imaging," *Folia Neuropathol*, vol. 52, no. 2, pp. 128–140, 2014. [cited at p. 11, 79]

[86] M. Law, S. Oh, J. S. Babb, E. Wang, M. Inglese, D. Zagzag, E. A. Knopp, and G. Johnson, "Low-grade gliomas: Dynamic susceptibility-weighted contrast enhanced perfusion MR imaging— prediction of patient clinical response," *Radiology*, vol. 238, no. 2, pp. 658–67, 2006. [cited at p. 11, 79]

[87] T. Y. Jung, S. Jung, J. H. Moon, I. Y. Kim, K. S. Moon, and W. Y. Jang, "Early prognostic factors related to progression and malignant transformation of low-grade gliomas," *Clin Neurol Neurosurg*, vol. 113, no. 9, pp. 752–7, 2011. [cited at p. 11]

[88] J. L. Frazier, M. W. Johnson, P. C. Burger, J. D. Weingart, and A. Quinones-Hinojosa, "Rapid malignant transformation of low-grade astrocytomas: report of 2 cases and review of the literature," *World Neurosurg*, vol. 73, no. 1, pp. 53–62, 2010. [cited at p. 11]

[89] G. W. Swan, *Cancer Modeling*, ch. Tumour growth models and cancer therapy, pp. 91–104. New York: Marcel Dekker, 1987. [cited at p. 11]

[90] V. P. Collins, R. K. Loeffler, and H. Tivey, "Observations on growth rates of human tumors," *Amer J Roentgenol*, vol. 76, pp. 988–1000, 1956. [cited at p. 12]

[91] R. P. Araujo and D. L. McElwain, "A history of the study of solid tumour growth: the contribution of mathematical modelling," *Bull Math Biol.*, vol. 66, pp. 1039–91, 2004. [cited at p. 12]

[92] T. Malthus, *An Essay on the Principle of Population*. 1798. [cited at p. 12]

[93] G. Gompertz, "On the nature of the function expressive of the law of human mortality, and on the new mode of determining the value of life contingencies," *Philos. Trans. R. Soc. London*, vol. 115, pp. 513–585, 1825. [cited at p. 12, 24]

[94] P. Verhulst, "Notice sur la loi que population suit dans son accroissement," *Corr. Math. Et Phys.*, vol. 10, pp. 113–121, 1838. [cited at p. 12, 23]

[95] A. Laird, "Dynamics of tumour growth," *Br. J. Cancer*, vol. 18, pp. 490–502, 1964. [cited at p. 12]

[96] A. Laird, "Dynamics of tumour growth: comparison of growth rates and extrapolation of growth curve to one cell," *Br. J. Cancer*, vol. 19, pp. 278–291, 1965. [cited at p. 12]

[97] V. G. Vaidya and F. J. Alexandro Jr., "Evaluation of some mathematical models for tumor growth," *Int. J. Biomed. Comput.*, vol. 13, pp. 19–35, 1982. International Journal of Bio-Medical Computing. [cited at p. 12]

[98] J. D. Murray, *Mathematical biology II*. Springer-Verlag, 2002. [cited at p. 12, 22, 58, 61, 62]

[99] P. Tracqui, G. C. Cruywagen, D. E. Woodward, G. T. Bartoo, J. D. Murray, and E. C. J. Alvord, "A mathematical model of glioma growth: the effect of chemotherapy on spatio-temporal growth," *Cell Proliferat*, vol. 28, pp. 17–31, 1995. [cited at p. 12, 14]

[100] J. G. Skellam, "Random dispersal in theoretical populations," *Biometrika*, vol. 38, no. 1/2, pp. 196–218, 1951. [cited at p. 13, 72]

[101] D. L. Silbergeld and M. R. Chicoine, "Isolation and characterization of human malignant glioma cells from histologically normal brain," *J Neurosurg*, vol. 86, no. 3, pp. 525–31, 1997. [cited at p. 13]

[102] D. Woodward, J. Cook, P. Tracqui, G. Cruywagen, J. Murray, and E. J. Alvord, "A mathematical model of glioma growth: the effect of extent of surgical resection," *Cell Proliferat*, vol. 29, no. 6, pp. 269–88, 1996. [cited at p. 13, 16, 39, 64, 67]

[103] K. R. Swanson, E. C. Alvord Jr, and J. D. Murray, "A quantitative model for differential motility of gliomas in grey and white matter," *Cell Proliferat*, vol. 33, no. 5, pp. 317–30, 2000. [cited at p. 13]

[104] S. Jbabdi, E. Mandonnet, H. Duffau, L. Capelle, M. Swanson, K. R andPélégrini-Issac, R. Guillevin, and H. Benali, "Simulation of anisotropic growth of low-grade gliomas using Diffusion Tensor Imaging," *Magn. Reson. Med.*, vol. 54, no. 3, pp. 616–24, 2005. [cited at p. 13]

[105] O. Clatz, M.Sermersant, P.Y.Bondiau, H.Delingette, S. Warfield, G. Malandain, and N.Ayache, "Realistic simulation of the 3-D growth of brain tumors in MR images coupling diffusion with biomechanical deformation," *IEEE Trans Med Imaging*, vol. 24, pp. 1334–1346, 2005. [cited at p. 13]

[106] E. Mandonnet, J. Pallud, O. Clatz, L. Taillandier, E. Konukoglu, H. Duffau, and L. Capelle, "Computational modeling of the WHO grade II glioma dynamics: principles and applications to management paradigm," *Neurosurgical Review*, vol. 31, pp. 263–269, 2008. [cited at p. 13, 14, 15, 16, 20]

[107] K. R. Swanson, E. C. Alvord Jr, and J. D. Murray, "Virtual brain tumours (gliomas) enhance the reality of medical imaging and highlight inadequacies of current therapy," *Br. J. Cancer*, vol. 86, pp. 14–18, 2002. [cited at p. 13, 22]

[108] K. Swanson, H. Harpold, D. Peacock, R. Rockne, C. Pennington, L. Kilbride, *et al.*, "Velocity of radial expansion of contrast-enhancing gliomas and the effectiveness of radiotherapy in individual patients: a proof of principle," *Clin Oncol*, vol. 20, no. 4, pp. 301–8, 2008. [cited at p. 13, 39, 63, 64, 67]

[109] R. Fisher, "The wave of advance of advantageous genes," *Ann Eugen*, vol. 7, pp. 355–69, 1937. [cited at p. 14]

[110] A. Kolmogorov, I. Petrovsky, and N. Piscounov, "Study of the diffusion equation with growth of the quantity of matter and its application to a biological problem," *Bull. State Univ. Mos.*, pp. 1–25, 1937. [cited at p. 14]

[111] M. Shakeel, "Travelling wave solution of the Fisher-Kolmogorov equation with non-linear diffusion," *Applied Mathematics*, vol. 4, no. 8A, 2013. [cited at p. 14]

[112] J. D. Murray, *Mathematical Biology*. Springer-Verlag, 1989. [cited at p. 14, 81]

[113] M. J. Ablowitz and A. Zeppetella, "Explicit solutions of Fisher's equation for a special wave speed," *Bull. Math. Biol*, vol. 41, p. 835, 1979. [cited at p. 14]

[114] H. McKean, "Application of brownian motion to the equation of Kolmogorov-Petrovskii-Piskunov," *Communications on Pure and Applied Mathematics*, vol. 28, no. 3, pp. 323–331, 1975. [cited at p. 14]

[115] J. Pallud, E. Mandonnet, and H. Duffau, "Prognostic value of initial magnetic resonance imaging growth rates for World Health Organization grade II gliomas," *Annals of Neurology*, vol. 60, no. 3, pp. 380–3, 2006. [cited at p. 14, 16, 19, 68]

[116] J. Pallud, L. Taillandier, L. Capelle, D. Fontaine, M. Peyre, F. Ducray, H. Duffau, and E. Mandonnet, "Quantitative morphological magnetic resonance imaging follow-up of low-grade glioma: A plea for systematic measurement of growth rates," *Neurosurg*, vol. 71, no. 3, pp. 729–740, 2012. [cited at p. 15, 68, 100]

[117] E. Mandonnet, J. Delattre, M. Tanguy, K. Swanson, A. Carpentier, H. Duffau, *et al.*, "Continuous growth of mean tumor diameter in a subset of grade II gliomas," *Ann Neurol*, vol. 53, no. 4, pp. 524–8, 2003. [cited at p. 15, 16]

[118] J. Pallud, M. Blonski, E. Mandonnet, E. Audureau, D. Fontaine, N. Sanai, L. Bauchet, P. Peruzzi, M. Frenay, P. Colin, R. Guillevin, V. Bernier, M. H. Baron, J. Guyotat, H. Duffau, L. Taillandier, and L. Capelle, "Velocity of tumor spontaneous expansion predicts long-term outcomes for diffuse low-grade gliomas. velocity of tumor spontaneous expansion predicts long-term outcomes for diffuse low-grade gliomas.," *Neuro-oncol*, vol. 15, no. 5, pp. 595–606, 2013. [cited at p. 15, 68]

[119] A. Martínez-González, G. F. Calvo, L. A. Pérez Romasanta, and V. M. Pérez-García, "Hypoxic cell waves around necrotic cores in glioblastoma: A biomathematical model and its therapeutic implications," *Bull Math Biol*, vol. 74, no. 12, pp. 2875–96, 2012. [cited at p. 15, 58, 62]

[120] A. Martínez-González, M. Durán-Prado, G. F. Calvo, F. J. Alcaín, L. A. Pérez Romasanta, and V. M. Pérez-García, "Combined therapies of antithrombotics and antioxidants delay in silico brain tumour progression," *Mathematical Medicine and Biology*, vol. 32, no. 3, pp. 239–62, 2015. [cited at p. 15, 58]

[121] A. Martínez-González, G. F. Calvo, J. M. Ayuso, I. Ochoa, L. J. Fernández, and V. M. Pérez-García, *Systems Biology of Tumor Microenvironment: Quantitative Modeling and Simulations*, ch. Hypoxia in Gliomas: Opening Therapeutical Opportunities Using a Mathematical-Based Approach, pp. 11–31. Springer, 2016. [cited at p. 15, 58, 77]

[122] H. Gomez, "Quantitative analysis of the proliferative-to-invasive transition of hypoxic glioma cells," *Integr. Biol.*, vol. 9, pp. 257–62, 2017. [cited at p. 15]

[123] M. Badoual, C. Gerin, C. Deroulers, B. Grammaticos, J.-F. Llitjos, C. Oppenheim, P. Varlet, and J. Pallud, "Oedema-based model for diffuse low-grade gliomas: application to clinical cases under radiotherapy," *Cell Prolif.*, vol. 47, no. 4, pp. 369–80, 2014. [cited at p. 15, 16]

[124] L. Hathout, W. B. Pope, A. Lai, P. L. Nghiemphu, T. F. Cloughesy, and B. M. Ellingson, "Radial expansion rates and tumor growth kinetics predict malignant transformation in contrast-enhancing low-grade diffuse astrocytoma," *CNS Oncol*, vol. 4, no. 4, pp. 247–56, 2015. [cited at p. 15, 58, 63, 68, 79]

[125] H. L. P. Harpold, E. C. Alvord Jr., and K. R. Swanson, "The evolution of mathematical modeling of glioma proliferation and invasion," *J Neuropathol Exp Neurol.*, vol. 66, no. 1, pp. 1–9, 2007. [cited at p. 16, 64]

[126] K. R. Swanson, C. Bridge, J. D. Murray, and E. C. Alvord Jr, "Virtual and real brain tumors: using mathematical modeling to quantify glioma growth and invasion," *J Neurol Sci*, vol. 216, 2003. [cited at p. 16, 21, 22]

[127] J. L. S. Au, S. H. Jang, J. Zheng, C. T. Chen, S. Song, L. Hu, and M. G. Wientjes, "Determinants of drug delivery and transport to solid tumors," *J. Control. Release*, vol. 74, no. 1-3, pp. 31–46, 2001. [cited at p. 17]

[128] T. Jackson, "Intracellular accumulation and mechanism of action of doxorubicin in a spatio-temporal tumor model," *J Theor Biol*, vol. 220, no. 2, pp. 201–13, 2003. [cited at p. 17]

[129] A. Tzafriri, E. Lerner, M. Flashner-Barak, M. Hinchcliffe, E. Ratner, and H. Parnas, "Mathematical modeling and optimization of drug delivery from intratumorally injected microspheres," *Clin Can Res*, vol. 11, pp. 826–34, 2005. [cited at p. 17]

[130] A. Swierniak, M. Kimmmel, and J. Smieja, "Mathematical modeling as a tool for planning anticancer therapy," *Eur J Pharmacol*, vol. 625, pp. 108–21, 2009. [cited at p. 17]

[131] S. Gardner and M. Fernandes, "New tools for cancer chemotherapy: computational assistance for tailoring treatments," *Mol Cancer Ther*, vol. 2, no. 10, pp. 1079–84, 2003. [cited at p. 17]

[132] M. C. Joiner and A. van der Kogel, "Basic clinical radiobiology fourth edition," Mar 2009. [cited at p. 18, 46]

[133] P. Mazzocco, C. Barthelemy, G. Kaloshi, M. Lavielle, D. Ricard, A. Idbaih, D. Psimaras, M.-A. Renard, A. Alentorn, J. Honnorat, J.-Y. Delattre, F. Ducray, and B. Ribba, "Prediction of response to temozolomide in low-grade glioma patients based on tumor size dynamics and genetic characteristics," *CPT Pharmacometrics Syst Pharmacol*, vol. 4, pp. 728–37, 2015. [cited at p. 18]

[134] P. Mazzocco, J. Honorat, F. Ducray, and B. Ribba, "Increasing the time interval between PCV chemotherapy cycles as a strategy to improve duration of response in low-grade gliomas: Results from a model-based clinical trial simulation," *Comput Math Methods Med*, vol. 2015, p. 297903, 2015. [cited at p. 18, 69, 98]

[135] G. Teschl, *Ordinary Differential Equations and Dynamical Systems*, vol. 140 of *Graduate Studies in Mathematics*. Amer Math Soc, 2012. [cited at p. 19, 35]

[136] D. V. Anosov, S. K. Aranson, V. I. Arnold, I. U. Bronshtein, V. Z. Grines, and Y. S. Ilyashenko, *Dynamical Systems I: Ordinary Differential Equations and Smooth Dynamical Systems*. Encyclopaedia of Mathematical Sciences, Springer-Verlag Berlin Heidelberg, 1988. [cited at p. 19]

[137] L. E. J. Brouwer, "Über abbildungen von mannigfaltigkeiten," *Math Ann*, vol. 71, pp. 97–115, 1911. [cited at p. 19, 37]

[138] J. Pallud, J. Llitjos, F. Dhermain, P. Varlet, E. Dezamis, B. Devaux, R. Souillard-Scémama, N. Sanai, M. Koziak, P. Page, M. Schlienger, C. Daumas-Duport, J. Meder, C. Oppenheim, and F. Roux, "Dynamic imaging response following radiation therapy predicts long-term outcomes for diffuse low-grade gliomas," *Neuro-Oncology*, vol. 14, no. 4, pp. 496–505, 2012. [cited at p. 20]

[139] S. M. Stigler, "Gauss and the invention of least squares," *Ann. Stat.*, vol. 9, no. 3, pp. 465–74, 1981. [cited at p. 20]

[140] [cited at p. 21, 41]

[141] J. Kennedy and R. Eberhart, "Particle swarm optimization," *Proceedings of IEEE International Conference on Neural Networks*, vol. 4, pp. 1942–8, 1995. [cited at p. 21]

[142] Y. Shi and R. C. Eberhart, "A modified particle swarm optimizer," *IEEE Trans Evol Comput*, pp. 69–73, 1998. [cited at p. 21]

[143] M. Clerc and J. Kennedy, "The particle swarm–explosion, stability, and convergence in a multidimensional complex space," *IEEE Trans Evol Comput*, pp. 58–73, 2002. [cited at p. 21]

[144] R. Poli, "Analysis of the publications on the applications of Particle Swarm Optimisation," *J. Artif. Evol. App.*, pp. 4:1–4:10, 2008. Journal of Artificial Evolution and Applications. [cited at p. 21]

[145] [cited at p. 21]

[146] [cited at p. 21]

[147] A. Hoare, D. G. Regan, and D. P. Wilson, "Sampling and sensitivity analyses tools (SaSAT) for computational modelling," *Theor. Biol. Med. Model.*, vol. 5, no. 4, 2008. [cited at p. 21]

[148] P. R. Jackson, J. Juliano, A. Hawkins-Daarud, R. C. Rockne, and K. R. Swanson, "Patient-specific mathematical neuro-oncology: Using a simple proliferation and invasion tumor model to inform clinical practice," *Bull Math Biol*, vol. 77, no. 5, pp. 846–856, 2015. [cited at p. 21]

[149] S. E. Eikenberry, T. Sankar, M. C. Preul, E. J. Kostelich, C. J. Thalhauser, and Y. Kuang, "Virtual glioblastoma: growth, migration and treatment in a three-dimensional mathematical model," *Cell Prolif*, vol. 42, pp. 511–528, 2009. [cited at p. 22]

[150] T. Galochkina, A. Bratus, and V. M. Pérez-García, "Optimal radiation fractionation for low-grade gliomas: Insights from a mathematical models," *Math Biosci*, vol. 267, pp. 1–9, 2015. [cited at p. 24, 77]

[151] M. van den Bent, T. Snijders, and J. Bromberg, "Current treatment of low grade gliomas," *J. Clin. Oncol.*, vol. 5, pp. 223–7, 2012. [cited at p. 24, 53]

[152] W. P. Roos, L. F. Z. Batista, S. C. Naumann, W. Wick, M. Weller, C. F. M. Menck, and B. Kaina, "Apoptosis in malignant glioma cells triggered by the temozolomide-induced DNA lesion O^6-methylguanine," *Oncogene*, vol. 26, pp. 186–197, 2007. [cited at p. 24, 52, 55]

[153] S. D. Baker, M. Wirth, P. Statkevich, *et al.*, "Absorption, metabolism, and excretion of ^{14}C-Temozolomide following oral administration to patients with advanced cancer," *Clin Cancer Res*, vol. 5, pp. 309–17, 1999. [cited at p. 24, 25, 52]

[154] S. Ostermann, C. Csajka, T. Buclin, S. Leyvraz, F. Lejeune, L. A. Decosterd, and R. Stupp, "Plasma and cerebrospinal fluid population pharmacokinetics of temozolomide in malignant glioma patients," *Clinical Cancer Research*, vol. 10, pp. 3728–36, 2004. [cited at p. 24, 52]

[155] R. J. Shannon, K. L. H. Carpenter, M. R. Guilfoyle, A. Helmy, and P. J. Hutchinson, "Cerebral microdialysis in clinical studies of drugs: pharmacokinetic applications," *J Pharmacokinet Pharmacodyn*, vol. 40, pp. 343–58, 2013. [cited at p. 24]

[156] J. Blakeley and J. Portnow, "Microdialysis for assessing intratumoral drug disposition in brain cancers: a tool for rational drug development," *Expert Opin Drug Metab Toxicol*, vol. 6, no. 12, pp. 1477–1491, 2010. [cited at p. 24]

[157] J. Portnow, B. Badie, M. Chen, A. Liu, S. Blanchard, and T. Synold, "The neuropharmacokinetics of temozolomide in patients with resectable brain tumors: potential implications for the current approach to chemoradiation," *Clin Can Res*, vol. 15, no. 22, pp. 7092–8, 2009. [cited at p. 24, 25, 39, 40, 52, 53, 98]

[158] P. Jacqmin, E. Snoeck, E. van Schaick, R. Gieschke, P. Pillai, J. Steimer, and P. Girard, "Modelling response time profiles in the absence of drug concentrations: definition and performance evaluation of the K-PD model," *Journal of Pharmacokinetics and Pharmacodynamics*, vol. 34, no. 1, pp. 57–85, 2007. [cited at p. 25]

[159] M. Bodnar, U. Foryś, and M. J. Piotrowska, "Logistic type equations with discrete delay and quasi-periodic suppression rate," *Appl Math Lett*, vol. 26, no. 6, pp. 607–11, 2013. [cited at p. 26]

[160] H. Dulac, "Recherche des cycles limites," *C.R, Acad. Sci. Paris*, vol. 204, pp. 1703–6, 1937. [cited at p. 35]

[161] M. Mosteller, "Simplified calculation of body-surface area," *The New England Journal of Medicine*, vol. 317, no. 17, p. 1098, 1987. [cited at p. 39]

[162] A. Sparreboom and J. Verweij, "Paclitaxel pharmacokinetics, threshold models, and dosing strategies," *J Clin Oncol*, vol. 21, no. 14, pp. 2083–4, 2003. [cited at p. 39]

[163] S. S. Agarwala and J. M. Kirkwood, "Temozolomide, a novel alkylating agent with activity in the central nervous system, may improve the treatment of advanced metastatic melanoma," *Oncologist*, vol. 5, pp. 144–151, 2000. [cited at p. 46, 53, 57, 89]

[164] P. Schmitt, E. Mandonnet, A. Perdreau, and E. D. Angelini, "Effects of slice thickness and head rotation when measuring glioma sizes on MRI: in support of volume segmentation versus two largest diameters methods," *J Neurooncol*, vol. 112, pp. 165–72, 2013. [cited at p. 51]

[165] N. Porz, S. Bauer, A. Pica, P. Schucht, J. Beck, and et al., "Multi-modal glioblastoma segmentation: Man versus machine," *PLoS ONE*, vol. 9, no. 5, p. e96873, 2014. [cited at p. 51]

[166] Q. Zhou, P. Guo, G. D. Kruh, P. Vicini, X. Wang, and J. M. Gallo, "Predicting human tumor drug concentrations from a preclinical pharmacokinetic model of temozolomide brain disposition," *Clin Cancer Res*, vol. 13, no. 14, pp. 4271–9, 2007. [cited at p. 53]

[167] L. Rosso, C. S. Brock, J. M. Gallo, A. Saleem, P. M. Price, F. E. Turkheimer, and E. O. Aboagye, "A new model for prediction of drug distribution in tumor and normal tissues: Pharmacokinetics of temozolomide in glioma patients," *Cancer Res*, vol. 69, no. 1, pp. 120–7, 2009. [cited at p. 53]

[168] A. Ballesta, Q. Zhou, X. Zhang, H. Lv, and J. M. Gallo, "Multiscale design of cell-type–specific pharmacokinetic/ pharmacodynamic models for personalized medicine: Application to temozolomide in brain tumors," *CPT Pharmacometrics Syst Pharmacol*, vol. 3, no. 4, p. e112, 2014. [cited at p. 53]

[169] J. Pallud, J. Llitjos, F. Dhermain, P. Varlet, E. Dezamis, B. Devaux, R. Souillard-Scémama, N. Sanai, M. Koziak, P. Page, M. Schlienger, C. Daumas-Duport, J. Meder, C. Oppenheim, and F. Roux, "Dynamic imaging response following radiation therapy predicts long-term outcomes for diffuse low-grade gliomas," *Neuro-Oncology*, vol. 14, no. 4, pp. 496–505, 2012. [cited at p. 54]

[170] F. Ducray, G. Kaloshi, C. Houillier, *et al.*, "Ongoing and prolonged response in adult low-grade gliomas treated with radiotherapy," *J Neurooncol*, vol. 115, no. 2, pp. 261–5, 2013. [cited at p. 54]

[171] B. Neyns, A. Tosoni, W.-J. Hwu, and D. A. Reardon, "Dose-dense temozolomide regimens: antitumor activity, toxicity, and immunomodulatory effects," *Cancer*, vol. 116, no. 12, pp. 2868–77, 2010. [cited at p. 56]

[172] H. P. Lashkari, S. Saso, L. Moreno, T. Athanasiou, and S. Zacharoulis, "Using different schedules of Temozolomide to treat low grade gliomas: systematic review of their efficacy and toxicity," *J Neurooncol*, vol. 105, pp. 135–47, 2011. [cited at p. 56]

[173] C. Rojas, J. Belmonte-Beitia, V. M. Pérez-García, and H. Maurer, "Dynamics and optimal control of chemotherapy for low grade gliomas: Insights from a mathematical model," *Discrete & Continuous Dynamical Systems - B*, vol. 21, no. 6, pp. 1895–915, 2016. [cited at p. 56]

[174] M. Khasraw, D. Bell, and H. Wheeler, "Long-term use of temozolomide: Could you use temozolomide safely for life in gliomas?," *J Clin Neurosci*, vol. 16, pp. 854–5, 2009. [cited at p. 56, 98]

[175] J. P. Mannas, D. D. Lightner, S. R. DeFrates, T. Pittman, and J. L. Villano, "Long-term treatment with temozolomide in malignant glioma," *Journal of Clinical Neuroscience*, vol. 21, pp. 121–3, 2014. [cited at p. 56, 98]

[176] S. Benzekry and P. Hahnfeldt, "Maximum tolerated dose versus metronomic scheduling in the treatment of metastatic cancers," *Journal of Theoretical Biology*, vol. 335, pp. 235–44, 2013. [cited at p. 56]

[177] N. Andre, D. Barbolosi, F. Billy, G. Chapuisat, F. Hubert, E. Grenier, and A. Rovini, "Mathematical model of cancer growth controled by metronomic chemotherapies," *CANUM 2012, 41e Congrês National d'Analyse Numérique*, vol. 41, pp. 77–94, 2012. [cited at p. 56]

[178] E. T. Wong, J. Timmons, A. Callahan, L. O'Loughlin, B. Giarusso, and D. C. Alsop, "Phase I study of low-dose metronomic temozolomide for recurrent malignant gliomas," *BMC Cancer*, vol. 16, p. 914, 2016. [cited at p. 56]

[179] D.-S. Kong, J.-I. Lee, J. H. Kim, S. T. Kim, W. S. Kim, and Y.-L. Suh, "Phase II trial of low-dose continuous (metronomic) treatment of temozolomide for recurrent glioblastoma," *Neuro-Oncology*, vol. 12, no. 3, pp. 289–96, 2010. [cited at p. 56]

[180] M. Heng, L. Padovani, P. Dory-Lautrec, *et al.*, "Can metronomic maintenance with weekly vinblastine prevent early relapse/progression after bevacizumab-irinotecan in children with low-grade glioma?," *Cancer Med*, vol. 5, pp. 1542–5, 2016. [cited at p. 57]

[181] J. L. Villano, C. A. Collins, E. E. Manasanch, C. Ramaprasad, and K. van Besien, "Aplastic anaemia in patient with glioblastoma multiforme treated with temozolomide," *Lancet Oncol*, vol. 7, pp. 436–8, 2006. [cited at p. 57]

[182] Y. B. Su, S. Sohn, S. E. Krown, P. O. Livingston, J. D. Wolchok, C. Quinn, and et al, "Selective CD4+ lymphopenia in melanoma patients treated with temozolomide: a toxicity with therapeutic implications," *J Clin Oncol*, vol. 22, pp. 610–6, 2004. [cited at p. 57]

[183] J. T. Kim, J. Kim, K. W. Ko, D. Kong, C. Kang, M. H. Kim, and et al., "Metronomic treatment of temozolomide inhibits tumor cell growth through reduction of angiogenesis and augmentation of apoptosis in orthotopic models of gliomas," *Oncol Rep*, vol. .16, no. 1, pp. 33–9, 2006. [cited at p. 57]

[184] K.-K. Ko, E.-S. Lee, Y.-A. Joe, and Y.-K. Hong, "Metronomic treatment of temozolomide increases antiangiogenicity accompanied by down-regulated O6-methylguanine-DNA methyltransferase expression in endothelial cells," *Exp Ther Med*, vol. 2, no. 2, pp. 343–8, 2011. [cited at p. 57]

[185] R. H. Chisholm, T. Lorenzi, and J. Clairambault, "Cell population heterogeneity and evolution towards drug resistance in cancer: Biological and mathematical assessment, theoretical treatment optimisation," *Biochim Biophys Acta*, vol. 1860, no. 11 Pt B, pp. 2627–45, 2016. [cited at p. 57]

[186] M. I. S. Costa, J. L. Boldrini, and R. C. Bassanezi, "Drug kinetics and drug resistance in optimal chemotherapy," *Math Biosci*, vol. 125, pp. 191–209, 1995. [cited at p. 57]

[187] J. C. Panetta, "A mathematical model of drug resistance: heterogeneous tumors," *Math Biosci*, vol. 147, no. 1, pp. 41–61, 1998. [cited at p. 57]

[188] U. Ledzewicz and H. M. Schättler, "Drug resistance in cancer chemotherapy as an optimal control problem," *DCDS-B*, vol. 6, no. 1, pp. 129–50, 2006. [cited at p. 57]

[189] C. Gerin, J. Pallud, C. Deroulers, P. Varlet, C. Oppenheim, F. X. Roux, *et al.*, "Quantitative characterization of the imaging limits of diffuse low-grade oligodendrogliomas," *Neuro Oncol*, vol. 15, no. 10, pp. 1379–88, 2013. [cited at p. 58, 63, 64]

[190] G. L. Semenza, "Targeting HIF-1 for cancer therapy," *Nat Rev Cancer*, vol. 10, pp. 721–32, 2003. [cited at p. 58]

[191] E. Poon, A. L. Harris, and M. Ashcroft, "Targeting the hypoxia-inducible factor (HIF) pathway in cancer," *Expert Rev Mol Med*, vol. 11, 2009. [cited at p. 58]

[192] R. Pardo, A. Martínez-González, and V. M. Pérez-García, "Nonlinear ghost waves accelerate the progression of high-grade brain tumors," *Comm Nonlin Sci Numer Simul*, vol. 39, pp. 360–380, 2016. [cited at p. 58, 62]

[193] D. Henry, *Geometric theory of semilinear parabolic equations*. Springer-Verlag, 1981. [cited at p. 60, 81]

[194] P. C. Fife, *Lecture Notes in Biomathematics*. Springer-Verlag, 1979. [cited at p. 60]

[195] A. M. Turing, "The chemical basis of morphogenesis," *Philos Trans Roy Soc London B*, vol. 237, pp. 37–72, 1952. [cited at p. 61]

[196] A. Marciniak-Czochra, *Lecture Notes in Mathematics*, vol. 2126, ch. Reaction-Diffusion-ODE Models of Pattern Formation, pp. 387–438. Springer-Verlag, 2015. [cited at p. 62]

[197] R. Rockne, J. K. Rockhill, M. Mrugala, A. M. Spence, I. Kalet, K. Hendrickson, A. Lai, T. Cloughesy, E. C. J. Alvord, and K. R. Swanson, "Predicting the efficacy of radiotherapy in individual glioblastoma patients in vivo: a mathematical modeling approach," *Phys.Med.Biol.*, vol. 55, pp. 3271–3285, 2010. [cited at p. 63, 64]

[198] L. Barazzoul, N. Burnet, R. Jena, B. Jones, S. Jefferies, and N. Kirkby, "A mathematical model of brain tumour response to radiotherapy and chemotherapy considering radiobiological aspects," *J Theor Biol*, vol. 262, no. 3, pp. 553–65, 2010. [cited at p. 63, 64]

[199] M. Tovi, M. Hartman, A. Lilja, and A. Ericsson, "MR imaging in cerebral gliomas. Tissue component analysis in correlation with histopathology of whole-brain specimens," *Acta Radiol*, vol. 35, no. 5, pp. 495–505, 1994. [cited at p. 63]

[200] V. M. Pérez-García, G. F. Calvo, J. Belmonte-Beitia, D. Diego, and L. A. Pérez Romasanta, "Bright solitons in malignant gliomas," *Phys Rev E*, vol. 84, p. 021921, 2011. [cited at p. 63]

[201] B. M. Ellingson, M. G. Malkin, S. D. Rand, J. M. Connelly, C. Quinsey, P. S. LaViolette, *et al.*, "Validation of functional diffusion maps (fDMs) as a biomarker for human glioma cellularity," *J Magn Reson Imaging*, vol. 31, no. 3, pp. 538–48, 2010. [cited at p. 67]

[202] R. J. Macaulay, "Impending impact of molecular pathology on classifying adult diffuse gliomas," *Cancer Control*, vol. 22, no. 2, pp. 200–5, 2015. [cited at p. 78]

[203] P. Y. Wen and S. Kesari, "Malignant gliomas in adults," *N Engl J Med*, vol. 359, pp. 492–507, 2008. [cited at p. 78]

[204] H. Ohgaki and P. Kleihues, "The definition of primary and secondary glioblastoma," *Clin Cancer Res*, vol. 19, no. 4, pp. 764–72, 2013. [cited at p. 78]

[205] X. Dong, A. Noorbakhsh, B. R. Hirshman, *et al.*, "Survival trends of grade I, II, and III astrocytoma patients and associated clinical practice patterns between 1999 and 2010: A SEER-based analysis.," *Neurooncol Pract*, vol. 3, no. 1, pp. 29–38, 2016. [cited at p. 78]

[206] L. E. Jalbert, E. Neill, J. J. Phillips, *et al.*, "Magnetic resonance analysis of malignant transformation in recurrent glioma," *Neuro Oncol*, vol. 18, no. 8, pp. 1169–79, 2016. [cited at p. 79]

[207] N. Danchaivijitr, A. D. Waldman, D. J. Tozer, *et al.*, "Low-grade gliomas: Do changes in rCBV measurements at longitudinal perfusion-weighted MR imaging predict malignant transformation?," *Radiology*, vol. 247, no. 1, pp. 170–8, 2008. [cited at p. 79]

[208] M. T. Freitag, K. H. Maier-Hein, F. Binczyk, F. B. Laun, C. Weber, D. Bonekamp, *et al.*, "Early detection of malignant transformation in resected who ii low-grade glioma using diffusion tensor-derived quantitative measures," *PLoS ONE*, vol. 11, no. 10, p. e0164679, 2016. [cited at p. 79]

[209] N. Fenichel, "Geometric singular perturbations theory for ordinary differential equations," *J. Diff. Eqs.*, vol. 31, pp. 53–98, 1979. [cited at p. 82, 97]

[210] C. K. R. T. Jones, *Dynamical Systems*, ch. Geometric Singular Perturbation Theory. Springer-Verlag, 1995. [cited at p. 82, 83, 97]

[211] S. A. Gourley and M. V. Bartuccelli, "Existence and construction of travelling wavefront solutions of Fisher equations with fourth-order perturbations," *Dyn. Stab. Syst.*, vol. 15, pp. 253–62, 2000. [cited at p. 82, 83]

[212] J. Belmonte-Beitia, "Existence of travelling wave solutions for a Fisher-Kolmogorov system with biomedical applications," *Commun Nonlinear Sci Numer Simul*, vol. 36, pp. 14–20, 2016. [cited at p. 82]

[213] P. C. Bressloff, *Waves in Neural Media: From Single Neurons to Neural Fields*. Springer Science & Business Media, 2013. [cited at p. 87]

[214] A. W. Tolcher, S. L. Gerson, D. L, and et al., "Marked inactivation of O6-alkylguanine-DNA alkyltransferase activity with protracted temozolomide schedules," *Br J Cancer*, vol. 88, no. 7, pp. 1004–11, 2003. [cited at p. 98]

Appendices

Appendix A

Mathematical model of response to radiotherapy

Mathematical Medicine and Biology (2015) **32**, 307–329
doi:10.1093/imammb/dqu009
Advance Access publication on May 24, 2014

Delay effects in the response of low-grade gliomas to radiotherapy: a mathematical model and its therapeutical implications

Víctor M. Pérez-García*
Departamento de Matemáticas, Universidad de Castilla-La Mancha, ETSI Industriales, Avda. Camilo José Cela 3, 13071 Ciudad Real, Spain
*Corresponding author. Email: victor.perezgarcia@uclm.es

Magdalena Bogdanska
Mathematics Department, Technical University of Lodz, Lodz, Wolczanska 214 Street, Lodz, Poland

Alicia Martínez-González, Juan Belmonte-Beitia
Departamento de Matemáticas, Universidad de Castilla-La Mancha, ETSI Industriales, Avda. Camilo José Cela 3, 13071 Ciudad Real, Spain

Philippe Schucht
Universitätsklinik für Neurochirurgie, Bern University Hospital, CH-3010 Bern, Switzerland

and

Luis A. Pérez-Romasanta
Radiotherapy Unit, University Hospital of Salamanca, Salamanca, Spain

[Received on 7 January 2013; revised on 10 January 2014; accepted on 20 April 2014]

Low-grade gliomas (LGGs) are a group of primary brain tumours usually encountered in young patient populations. These tumours represent a difficult challenge because many patients survive a decade or more and may be at a higher risk for treatment-related complications. Specifically, radiation therapy is known to have a relevant effect on survival but in many cases it can be deferred to avoid side effects while maintaining its beneficial effect. However, a subset of LGGs manifests more aggressive clinical behaviour and requires earlier intervention. Moreover, the effectiveness of radiotherapy depends on the tumour characteristics. Recently Pallud *et al.* (2012. *Neuro-Oncology*, **14**, 1–10) studied patients with LGGs treated with radiation therapy as a first-line therapy and obtained the counterintuitive result that tumours with a fast response to the therapy had a worse prognosis than those responding late. In this paper, we construct a mathematical model describing the basic facts of glioma progression and response to radiotherapy. The model provides also an explanation to the observations of Pallud *et al.* Using the model, we propose radiation fractionation schemes that might be therapeutically useful by helping to evaluate tumour malignancy while at the same time reducing the toxicity associated to the treatment.

Keywords: low-grade gliomas; radiotherapy; mathematical model of tumour response.

1. Introduction

Low-grade glioma (LGG) is a term used to describe WHO grade II primary brain tumours of astrocytic and/or oligodendroglial origin. These tumours are highly infiltrative and generally incurable but have a median survival time (ST) of >5 years because of low proliferation (Pignatti *et al.*, 2002; Pouratian

© The authors 2014. Published by Oxford University Press on behalf of the Institute of Mathematics and its Applications. All rights reserved.

& Schiff, 2010). While most patients remain clinically asymptomatic besides seizures, tumour transformation to aggressive high-grade glioma is eventually seen in most patients.

Management of LGG has historically been controversial because these patients are typically young, with few, if any, neurological symptoms. Historically, a wait and see approach was often favoured in most cases of LGG due to the lack of symptoms in these mostly young and otherwise healthy adults. The support for this practice came from several retrospective studies showing no difference in outcome (survival, quality of life) if therapy was deferred (Olson *et al.*, 2000; Grier & Batchelor, 2006). Other investigations have suggested a prolonged survival through surgery (Smith *et al.*, 2008). In this absence of a randomized controlled trial, recently published studies may provide the most convincing evidence in support of an early surgery strategy (Jakola *et al.*, 2012) and waiting for the use of other therapeutical options such as radiotherapy and chemotherapy. However, the decision on the individual treatment strategy is based on a number of factors including patient preference, age, performance status and location of tumour (Ruiz & Lesser, 2009; Pouratian & Schiff, 2010).

As to radiation therapy the clinical trial by Garcia *et al.* (2004) showed the advantage of using radiotherapy in addition to surgery. However, the timing of radiotherapy after biopsy or debulking is debated. It is now well known that immediate radiotherapy after surgery increases the time of response (progression-free survival), but does not seem to improve overall survival while at the same time inducing serious neurological deficits as a result of normal brain damage (Van den Bent, 2005). Overall survival depends more on patient- and tumour-related characteristics such as age, tumour grade, histology and neurological function than the details of the plan of radiotherapy treatment. Radiotherapy is usually offered for patients with a combination of poor risk factors such as age, sub-total resection and diffuse astrocytoma pathology (Higuchi *et al.*, 2004).

Mathematical modelling has the potential to select patients who may benefit from early radiotherapy. Also it may help in developing specific optimal fractionation schemes for selected patient subgroups. However, despite its enormous potential, mathematical modelling has had a limited use with strong focus on some aspects of radiation therapy (RT) for high-grade gliomas (Barazzuol *et al.*, 2010; Konukoglu *et al.*, 2010; Rockne *et al.*, 2010; Bondiau *et al.*, 2011). Up to now, no ideas coming from mathematical modelling have been found useful for clinical application.

There is thus a need for models accounting for the fundamental features of LGG dynamics and their response to radiation therapy without involving excessive details on the -often unknown- specific processes but allowing the qualitative understanding of the phenomena involved. The availability of systematic and quantitative measurements of LGG growth rates provides key information for the development and validation of such models (Pallud *et al.*, 2012a,b).

In this paper, we present a simple mathematical model capturing the key features seen in the response of LGGs to radiation. Our model incorporates the basic elements of tumour dynamics: infiltration and invasion of the normal brain by the tumour cells, proliferation and tumour cell death in response to therapy. Radiation therapy is included in an almost parameter-free way that captures the essentials of the dynamics and explains the relationship between proliferation, response to the therapy and prognosis as recently reported by Pallud *et al.* (2012b).

In addition to explaining the counterintuitive observations of Pallud *et al.* (2012b) the model presented in this paper can be used to explore different radiation regimes. The analysis to be presented in this paper suggests the possibility of using radiation therapy with palliative intent and also to test what the tumour response is and help the oncologists in making the best possible decisions on when and how to act on the tumour.

Our plan in this paper is as follows. First, in Section 2 we present our model accounting for tumour cell dynamics and the response of the tumour cells to radiation. Next in Section 3, we present the results

of the numerical simulations of the model in different scenarios and study the dependence of the model on the different parameters. In Section 4, we display some analytical estimates of the typical dynamics of the tumour response to radiation. In Section 5, we discuss some hypothesis suggested from the model that may be useful for therapy. Finally, in Section 6 we summarize our conclusions.

2. Mathematical model for the response of LGGs to radiotherapy

2.1 *Tumour cell compartment*

In the last years there has been a lot of activity on mathematical models of glioma progression (Stamatakos *et al.*, 2006a,b; Frieboes *et al.*, 2007; Murray, 2007; Swanson *et al.*, 2008; Bondiau *et al.*, 2008; Eikenberry *et al.*, 2009; Tanaka *et al.*, 2009; Wang *et al.*, 2009; Konukoglu *et al.*, 2010; Rockne *et al.*, 2010; Pérez-García *et al.*, 2011; Badoual *et al.*, 2012; Gu *et al.*, 2012; Hatzkirou *et al.*, 2012; Martínez-González *et al.*, 2012; Pérez-García & Martínez-González, 2012; Painter and Hillen, 2013). In this paper, we will consider a model for the compartment of tumour cells of the simplest possible type: a Fisher–Kolmogorov (FK) type equation (Murray, 2007). More complicated models such as single-cell-based models would allow one, in principle, to follow the individual movement of the transformed astrocytes through the brain parenchyma. However, considering that the basic rules behind a model are more important than the model details, we have discarded both the use of on-lattice models, which are not realistic when cell motion is considered, and off-lattice models, which assume fixed cell geometries and/or incorporate unknown cell–cell interactions. Besides, these models often require the estimation of a large number of unknown parameters and the determination of initial cell configurations, which are extremely difficult to validate in *in vivo experiments* and/or using clinical data. Thus, to keep our description as simple as possible, we have opted for a continuous model as follows:

$$\frac{\partial C}{\partial t} = D\Delta C + \rho(1 - C)C, \tag{2.1a}$$

$$C(x, 0) = C_0(x), \tag{2.1b}$$

where $C(x, t)$ is the tumour cell density as a function of time t and the spatial position x and it is measured in units of the maximal cell density allowed in the tissue C_* (typically around 10^3 cell/cm); $\Delta = \sum_{j=1}^{n} \partial^2/\partial x_j^2$ is the n-dimensional Laplacian operator.

By D, we denote the diffusion coefficient accounting for the average cellular motility measured in mm^2/day assumed in this paper to be constant and spatially uniform. Migration in gliomas is not simple and in fact many authors have proposed that the highly infiltrative nature of human gliomas recapitulates the migratory behaviour of glial progenitors (Dirks, 2001; Suzuki *et al.*, 2002). Here we assume, as in most models, that glioma cell invasion throughout the brain is basically governed by a standard Fickian diffusion process. More realistic and complicated diffusion terms in gliomas should probably be governed by fractional (anomalous) diffusion (Fedotov *et al.*, 2011) or other more elaborate terms (Deroulers *et al.*, 2009) to account for the high infiltration observed in this type of tumours (Onishi *et al.*, 2011) and the fact that cells do not behave like purely random walkers and may actually remain immobile for long time periods before being compelled to migrate to a more favourable place. In addition, in real brain there are spatial inhomogeneities expected in the parameter values such as different propagation speeds in white and gray matter, and anisotropies (e.g. on the diffusion tensor with preferential propagation directions along white matter tracts). Many papers have incorporated these details (Clatz, 2005; Jbadi *et al.*, 2005; Bondiau *et al.*, 2008; Konukoglu *et al.*, 2010; Painter and Hillen, 2013) mostly with the intention to make patient-specific progression predictions. However, the main limitation

is the lack of information on the (many) patient-specific unknown details, which has limited progress in that direction. Thus, in order to simplify the analysis and focus on the essentials of the phenomena, we have chosen to study the model in one spatial dimension and in isotropic media. It is interesting that up to now only the simplest models such as those given by Equations (2.1) have been used to extract conclusions useful for clinicians (Swanson *et al.*, 2008; Wang *et al.*, 2009).

The choice of 1D diffusion intends to incorporate qualitatively diffusion phenomena in the simplest possible way. Front solutions of the 1D FK equation have been extensively studied and are known to propagate with a minimal speed $c = 2\sqrt{\rho D}$ when starting from still initial data (Murray, 2007). It is interesting that the 1D model recapitulates the most relevant -for us-phenomenology observed in higher-dimensional scenarios. First, it is obvious and well known that front (invasion wave) solutions of the 1D FK equation also solve higher-dimensional version of the equation (Brazhnik and Tyson, 2000; Xin, 2000). Moreover, those solutions are asymptotically stable (Sattinger, 1976; Xin, 2000), which means that, unlike other more complicated non-symmetrical solutions (Brazhnik and Tyson, 2000), they do arise as limits of non-symmetric initial data. It is also well known that radially symmetric (in 2D) or spherically symmetric (in 3D) travelling wave solutions of FK do not exist in high dimensions but that symmetric fronts also develop in those scenarios with a non-constant speed that depends on the local curvature R (Brazhnik and Tyson, 2000; Volpert & Petrovskii, 2009). As the front grows with time, the now radius-dependent front speed is given by $c(R) = c - D/R(t)$. Thus, growing symmetric multidimensional solutions with large curvature radii ($R \to \infty$) grow with the same speed as 1D fronts (Volpert & Petrovskii, 2009; Gerlee and Nelander, 2012).

In this paper, we are interested on the description of LGGs that typically are very extended when diagnosed, thus the initial data radius is large and fronts are well developed by then. Although during the initial stages of tumour development the dimensionality may play a relevant role, for spatially extended tumours the effect of using higher-dimensional operators is not expected to be substantial.

Moreover, some of the phenomena to be described later in this paper are found to be essentially independent of diffusion and a very good qualitative agreement will be found between our simplified analysis and the growth dynamics of the mean tumour diameter. Taking into account all these evidences, we will keep the system 1D, since our intention is not to provide a detailed quantitative description of the processes -that in any way would be beyond the reach of a simple model such as FK- but instead to provide a qualitative description of the dynamics in the simplest possible way. As we will discuss in detail later, this approach will lead to a simple yet qualitatively correct description of the response of LGGs to radiotherapy.

The parameter ρ in Equation (2.1) is the proliferation rate (1/day), its inverse giving an estimate of the typical cell doubling times. We have chosen a logistic type of proliferation leading to a maximum cell density $C(x,t) = 1$. Finally, the tumour evolves from an initial cell density given by the function $C_0(x)$ in an unbounded domain, so we implicitly assume it to be located initially sufficiently far from the grey matter.

A very interesting feature of model Equations (2.1) is the well-known fact that a tumour front arises propagating at the asymptotic (constant) speed of $v_* = 2\sqrt{D\rho}$, which is in very good agreement with the observed fact that the tumour mean diameter grows at an approximately constant speed (Pallud *et al.*, 2012a).

While many other mathematical models of gliomas incorporate different cell phenotypes, e.g. normoxic (proliferative) and hypoxic (migratory) phenotypes, such as in Martínez-González *et al.* (2012), Hatzkirou *et al.* (2012) and Pérez-García & Martínez-González (2012), here we focus our attention on LGGs and as such will consider a single (dominant) tumour cell phenotype. In our model, we do not include the possible existence of different tumour cell populations with different sensitivities to therapy

such as stem cells, since the function and mechanisms of stem cells in glioblastoma are yet under debate (Barrett *et al.*, 2012; Chen *et al.*, 2012).

2.2 *Response to radiation*

Radiation therapy has been incorporated in different forms to mathematical models of high-grade glioma progression (Barazzuol *et al.*, 2010; Konukoglu *et al.*, 2010; Rockne *et al.*, 2010; Bondiau *et al.*, 2011). In this paper, we want to focus our attention on LGGs whose response to radiation is very different from the one observed in HGGs. Radiation therapy in LGGs typically induces a response that prolongs for several years after therapy.

Very interesting quantitative data on the response of LGGs to radiation have been reported in a retrospective study by Pallud *et al.* (2012a). The authors studied patients diagnosed with grade II LGGs treated with first-line radiotherapy before evidence of malignant transformation. Patients with a post-RT velocity of diametric expansion (VDE) (Pallud *et al.*, 2012a) slower than -10 mm/year were taken as a subgroup of slowly growing LGGs. Patients with a post-RT VDE of -10 mm/year or faster were included in the group of fast-growing LGGs. The authors concluded that the post-RT VDE was significantly faster in the group with high proliferation. Also, in the patients with an available pre-RT VDE, the low pre-RT VDE subgroup presented a slower VDE at imaging progression. With regard to the ST, post-radiotherapy VDE carried a prognostic significance on ST, as the fast post-radiotherapy tumour volume decrease (VDE at -10 mm/year or faster) was associated with a significantly shorter survival than slow post-radiotherapy tumour volume decrease (VDE slower than -10 mm/year).

The very slow response to radiotherapy, leading to tumour regression lasting for several years is difficult to understand in the context of the standard linear quadratic model in which damage is instantaneous and leads to cell death early after radiation therapy. However, a key aspect of the cell response to radiation is that irradiated cells usually die because of the so-called mitotic catastrophe after completing one or several mitosis cycles (Van der Kogel & Joiner, 2009). This means that slowly proliferating tumours, as in the case of LGGs with typical low proliferation indexes between 1% and 5% in pathological analyses, need a very long time to manifest the accumulated cell damage that cannot be repaired.

Thus, in order to capture in a minimal way the response of the tumour to radiation, we will complement Equation (2.1) for the density of functionally alive tumour cells $C(x,t)$ with an equation for the evolution of the density of irreversibly damaged cells after irradiation $C_d(x,t)$. Our model for the evolution of both tumour cell densities will be given by the equations

$$\frac{\partial C}{\partial t} = D\Delta C + \rho(1 - C - C_d)C, \tag{2.2a}$$

$$\frac{\partial C_d}{\partial t} = D\Delta C_d - \frac{\rho}{k}(1 - C - C_d)C_d. \tag{2.2b}$$

The first equation is a Fisher–Kolmogorov-type equation describing the evolution of tumour cells $C(x,t)$. The saturation term includes the total tumour cell density, i.e. both the functional tumour cells and those damaged by radiation $C_d(x,t)$. The evolution of cells irreversibly damaged by radiation is given by Equation (2.2b). As is well described in the literature (Van der Kogel & Joiner, 2009), most of these cells behave normally until a certain number of mitosis cycles; thus we will consider that, after an average of k mitosis cycles, these cells die resulting in a negative proliferation. The longer ST $k\tau$, with $\tau = 1/\rho$ being the tumour population doubling time, results in a reduced proliferation potential ρ/k, which is the coefficient used for the negative proliferation term. Thus, the parameter k in Equation (2.2b) has the meaning of the average number of mitosis cycles that damaged cells are able to

complete before dying. As with the normal population, the number of cells entering mitosis depends in a non-linear way on both tumour cell populations (cf. last term in Equation (2.2b)).

We will assume a series of radiation doses $d_1, d_2, \ldots, d_n$ given at times $t_1, t_2, \ldots, t_n$. The initial data for the first subinterval will be given by the equations

$$C(x, t_0) = C_0(x), \tag{2.3a}$$

$$C_d(x, t_0) = 0. \tag{2.3b}$$

The evolution of the tumour follows then Equations (2.2) until the first radiation dose d_1, given at time t_1. The irradiation results in a fraction of the cells (surviving fraction) able to repair the radiation-induced damage given by $S_f(d_1)$ and a fraction $1 - S_f(d_1)$ of cells unable to repair the accumulated damage, thus feeding the compartment of irreversibly damaged cells. The subsequent evolution of the populations is again given by Equations (2.2) until the next RT dose is given. In general, after each irradiation event we obtain

$$C(x, t_j^+) = S_f(d_j) C(x, t_j^-), \tag{2.3c}$$

$$C_d(x, t_j^+) = C_d(x, t_j^-) + [1 - S_f(d_j)] C(x, t_j^-), \tag{2.3d}$$

where $S_f(d_j)$ is the survival fraction after a dose of radiation d_j, i.e. the fraction of damaged tumour cells after irradiation that are not able to repair lethal damage and are incorporated to the compartment of damaged cells. For the doses to be considered independent, the interval between doses (typically 1 day) has to be larger than the typical damage repair times (of the order of hours). The evolution of both cell densities between irradiation events is given by the partial differential equations (PDEs) (2.2).

2.3 *Parameter estimation*

Equations (2.2) together with the initial conditions for each subproblem (2.3) define completely the dynamics of an LGG in the framework of our simplified theoretical approach.

We have chosen the parameters to describe the typical growth patterns of LGG. For the proliferation rate we have chosen typical values to be small and around $\rho = 0.003$ day^{-1} (see e.g. Badoual *et al.*, 2012), which give doubling times of the order of a year. Specifically, we have considered values ranging from $\rho = 0.001$ day^{-1} for very slowly growing LGGs to $\rho = 0.01$ day^{-1}. For the cell diffusion coefficient we have taken values around $D = 0.0075$ mm^2/day (Jbadi *et al.*, 2005). This choice, together with the previously chosen ρ, leads to asymptotic tumour diameter growth speeds given by $v = 4\sqrt{D\rho}$ of the order of several millimetres per year, in agreement with typical diametric growth speeds of LGGs (Pallud *et al.*, 2012a). However, the fact that the asymptotic speed is only reached when the tumour cell density is around 1 may require taking larger values of D to match the real growth speeds.

With regards to the radiobiological parameters, gliomas being very resistant to radiation, we have taken values in the range $S_f(1.8\,\text{Gy}) \equiv \text{SF}_{1.8} \sim 0.9$ considering the median survival fraction value 0.83 after one dose of 2 Gy given by Barazzuol *et al.* (2010) .

Finally, the average number of mitosis cycles completed before the mitotic catastrophe occurs is difficult to estimate. This parameter intends to summarize in a single number a complex process in which a cell hit by radiation and its progeny die after some more mitosis cycles leading to a final extinction after a variable time. Death by mitotic catastrophe implies a minimal value of $k = 1$ and, to allow for some more time, we may choose values in the range $k = 1 - 3$ (Van der Kogel & Joiner, 2009). We will show later that the choice of this parameter has a limited effect on the model dynamics and that, in standard fractionation schemes, there may be biological reasons to take it as $k = 1$.

TABLE 1 *Typical values of the biological parameters in the model of LGG evolution*

Variable	Description	Value (Units)	References
C_*	Maximum tumour cell density	10^6 cell/cm^2	Swanson *et al.* (2008)
D	Diffusion coefficient for tumour cells	0.01 mm^2/day	Jbadi *et al.* (2005)
ρ	Proliferation rate	0.00356 day^{-1}	Badoual *et al.* (2012)
$SF_{1.8}$	Survival fraction for 1.8 Gy	$\sim$0.9	Barazzuol *et al.* (2010)
k	Average number of mitosis cycles completed before the mitotic catastrophe	1–3	Van der Kogel & Joiner (2009)

Our typical choices for the full set of model parameters is summarized in Table 1.

In this paper, we will fix the dose per fraction in agreement with the standard fractionation schemes for LGGs to be 1.8 Gy; the only relevant parameter is the survival fraction $SF_{1.8}$, which will be taken to be around $SF_{1.8} \sim 0.9$, as discussed above. In many examples, we will choose the radiotherapy scheme as the standard fractionation of a total of 54 Gy in 30 fractions of 1.8 Gy over a time range of 6 weeks (5 sessions per week from Monday to Friday).

3. Results

3.1 *Computational details*

We have studied the evolution of the tumour diameter using our model Equations (2.2) and (2.3). To solve the PDEs we have used standard second order finite differences both in time and space. Since the tumour diameter in the framework of this model tends to grow linearly in any spatial dimension we have focused on the simplest 1D version of the model. We have checked with simulations in higher dimensions that the dynamics is essentially the same and thus have sticked to the simplest possible model. To avoid boundary effects and focus on the bulk dynamics, we have assumed our computational domain to be much larger than the tumour size.

In each simulation, we have computed the tumour diameter as the distance between the points for which the density reaches a critical detection value C_{th} that provides a signal in the T2 (or FLAIR) MRI sequence. Although which is that precise value is a debated question and in fact depends on the thresholds used in the images, we have assumed that $C_{\text{th}} \sim 0.05 - 0.07$. This is in agreement with the reported value of cellular density about 0.16 for detection (Swanson *et al.*, 2008) and a normal tissue density of about 0.1. In agreement with previous studies we take a fatal tumour burden (FTB) size of 6 cm in diameter (Swanson *et al.*, 2008; Wang *et al.*, 2009). As parameters containing useful information we have computed: the time in which the tumour starts regrowing after the therapy, usually called in clinical practice time to tumour progression (TTP), the time for which the tumour size equals its initial size -denoted as growth delay (GD)- and the time for which the tumour size equals the FTB or ST.

We have studied a broad range of parameter values corresponding to the possible range of realistic values in the framework of our simple description of the tumour dynamics and its response to radiotherapy. We have also taken different types of initial data ranging from more localized (such as gaussian initial profiles) to more infiltrative (such as sech-type functions). In what follows, we summarize our results.

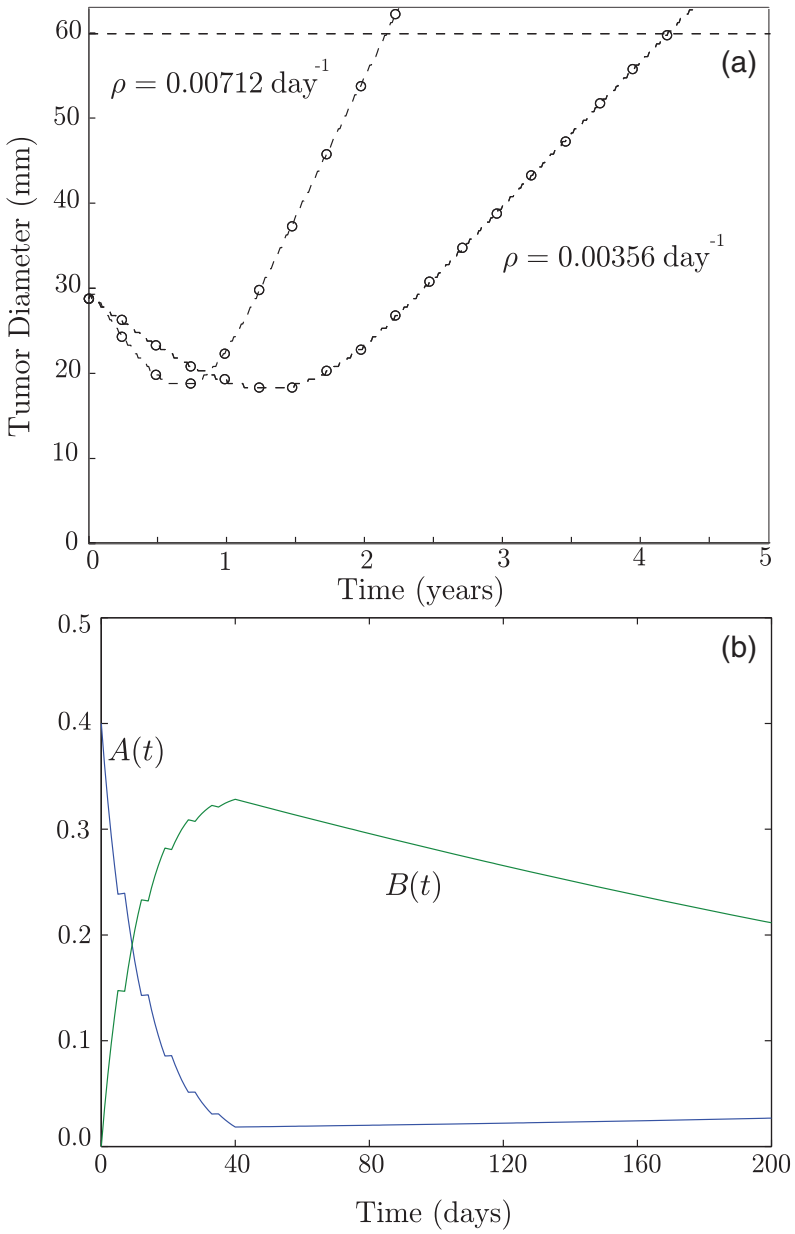

FIG. 1. (a) Tumour diameter evolution for two different values of the proliferation: $\rho = 0.00356$ day^{-1}, $\rho = 0.00712$ day^{-1}. Other parameter values are: $D = 0.0075$ mm^2/day, critical detection value $C_{\text{th}} = 0.07$, $\text{SF}_{1.8} = 0.90$ and $k = 1$. The initial tumour cell densities are taken as $C_d(x, 0) = 0, C(x, 0) = 0.4\,\text{sech}(x/6)$, with x measured in millimetres, which gives an initial tumour diameter of 28.8 mm. Radiotherapy follows the standard scheme (6 weeks with 1.8 Gy doses from Monday to Friday) and starts at time $t = 0$. Circles denote measurements every three months that would correspond to a close follow-up of the patient. The upper dashed line (horizontal) shows the FTB size taken through this paper to be 6 cm, as discussed in the text. (b) Evolution of the tumour cell amplitudes $A(t) = \max_x |C(x, t)|$ and $B(t) = \max_x |C_d(x, t)|$ during the first 200 days showing the early response to the therapy for $\rho = 0.00356$ day^{-1}.

3.2 *Tumour proliferation rate determines the response to radiotherapy*

In a first series of simulations, we have studied the dependence of the evolution of the tumour diameter on the proliferation rate. Figure 1(a) shows the evolution of the tumour diameter for two different

proliferation rates $\rho = 0.00356$ day^{-1} and $\rho = 0.00712$ day^{-1} (Fig. 1). In the first case of low proliferation, the tumour responds more slowly to therapy as measured by the speed of tumour regression (decrease in size) but the total response time is significantly longer, the TTP being 16.9 months against 8.2 months in the later case. Also the GDs is 14.7 months for the faster proliferating tumour against 29.9 months for the less proliferative one. Finally the 'virtual patient' with the slowly proliferating tumour survives much longer than that with the more proliferative one. This is just an example of a tendency shown in all of our simulations where 'more aggressive tumours respond earlier to the therapy'.

It is remarkable that this fact is in full agreement with the results from Pallud *et al.* (2012b). Our model based on reasonable biological assumptions leads to a long remission time (e.g. in Fig. 1 of about 3 years), much larger than the treatment duration (6 weeks) and negatively correlated with the tumour proliferation rate. As a second relevant finding, also seen in the results shown by Pallud *et al.* (2012b), we observe that tumours responding faster have also shorter re-growth time.

Figure 1(b) shows the dynamics of the maximum density of tumour cells ($A(t) = \max_x C(x,t)$) and damaged tumour cells ($B(t) = \max_x C_d(x,t)$). As could be expected, the amplitude of functionally alive tumour cells decreases during the therapy with the exception of the breaks in the weekends when a small increase is seen and correspondingly the amplitude of damaged tumour cells grows after every irradiation and for the full treatment period (6 weeks = 42 days). After $t = 42$ days the population of tumour cells starts a slow recovery, while the population of damaged cells declines in a much longer time scale. However, the width of the total tumour population evolves only in the slow time scale and does not display any effects during the treatment period.

It is important to emphasize that this behaviour is not the result of a fortunate choice of the parameters but a generic behaviour as we have confirmed through a large number of simulations covering the full clinically relevant parameter space. As an example, in Fig. 2 we show how the variation of ρ over a broad range of values leads to the same conclusion. Larger proliferation values accelerate the response but lead to earlier re-growth and, as such, shorter GDs and STs (Fig. 2(a)). Our simulations also point out that the maximum volume reduction is only weakly dependent on the proliferation rate ρ (Fig. 2(b)), the smaller the proliferation rates the larger being the maximum reduction in diameter. This fact is also in very good agreement with the results of Pallud *et al.* (2012b) (see e.g. Fig. 2 bottom of their paper).

3.3 *The role of the number of mitosis cycles before clonogenic cell death*

It is well known that most cells die after irradiation through the so-called mitotic catastrophe, i.e. due to incomplete mitosis, after completing one or several mitosis cycles. However, the specific choice of the parameter k is not a priori obvious although a number between one and three is to be expected a priori from previous experience in vitro (Van der Kogel & Joiner, 2009). To get some information on how our model's results depend on this parameter, we have explored numerically the range $k = 1$–3.

Our results are summarized in Fig. 3. First, in Fig. 3(a) we show typical evolutions of the tumour diameter for three different values of $k = 1$ (triangles), $k = 2$ (squares) and $k = 3$ (circles) for $\rho = 0.00712$ day^{-1}. It is clear that although the diameter reduction depends on k (Fig. 3(b)), the specific choice of this parameter does not affect the more relevant parameters such as the GD and the total survival (see Fig. 3(a,c)). From this and other simulations, we think the specific choice of this parameter does not have a crucial role on the dynamics of clinically relevant features.

In addition, although in vitro irradiation of cells with a single dose allows cells to complete a few mitosis cycles, the accumulation of many doses in real treatment schedules implies that a typical cell receives a lot of DNA damage. This will probably make it very difficult for cells in vivo to progress after the first mitosis, thus making it reasonable to take $k = 1$. This fact, together with the previous result

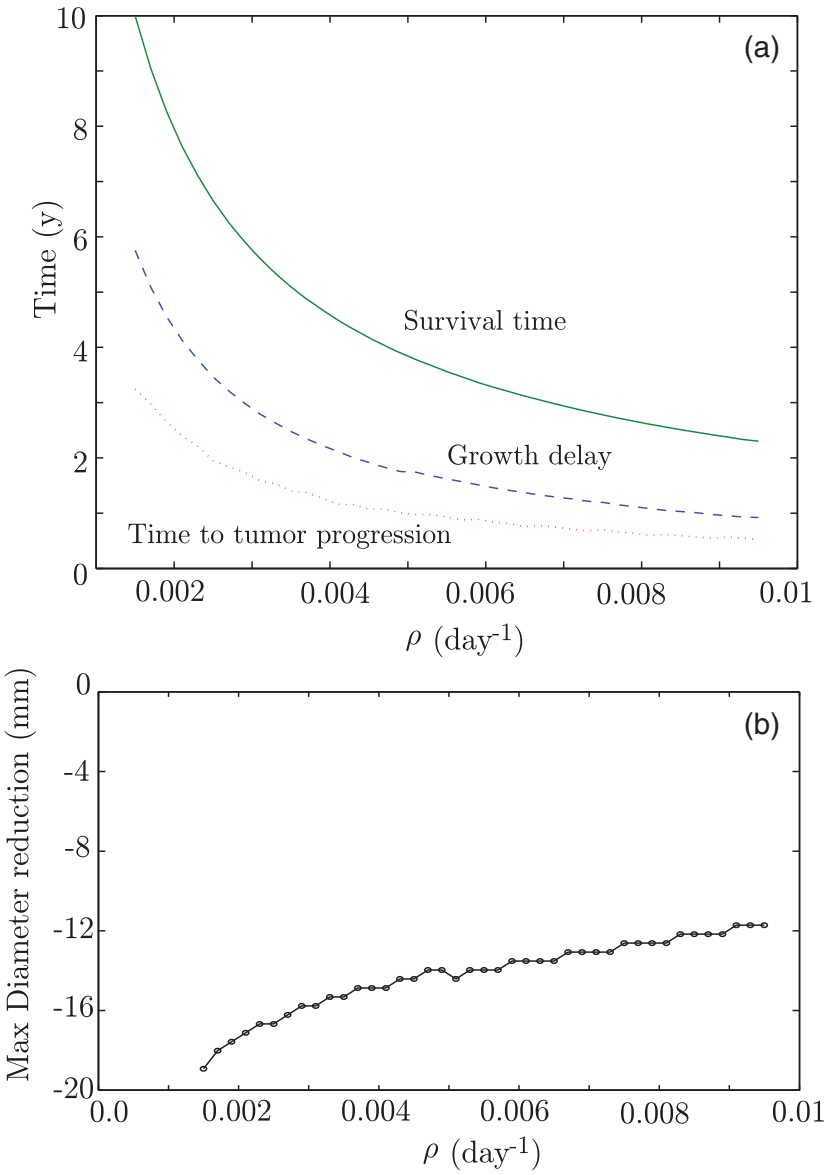

FIG. 2. Dependence of the (a) ST (solid line), GD (dashed line), TTP (dotted line) and (b) maximal reduction in diameter as a function of ρ. The curves summarize the outcome of many individual simulations with initial data $C_d(x,0) = 0, C(x,0) = 0.2\exp(-x^4/81920)$, with x measured in millimetres, which gives an initial tumour diameter of 33.80 mm. Radiotherapy follows the standard scheme (6 weeks with 1.8 Gy doses from Monday to Friday) and starts at time $t = 0$. Other parameters used in the simulations are as in Fig. 1.

on the independence of the clinically relevant endpoints on k makes the choice of $k = 1$ a reasonable assumption not expected to have a relevant impact on the final results.

3.4 *The role of cell motility*

We have also analysed the role of the variation of the cell motility (invasion) parameter D. The typical outcome of several simulations for different values of this parameter is shown in Fig. 4. It is clear from Fig. 4(a) that cell motility does not affect too much the dynamics of the response to the therapy except

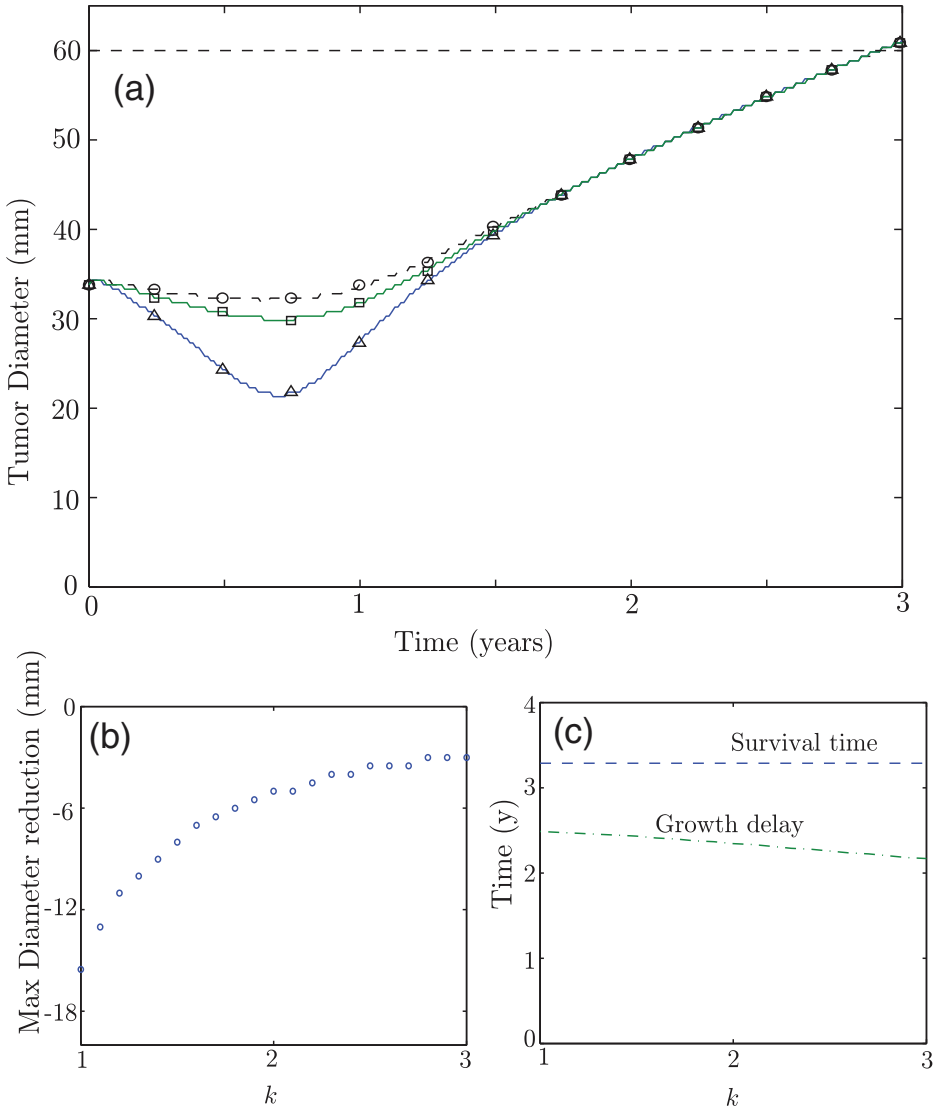

FIG. 3. (a) Tumour diameter evolution for three different values of $k = 1$ (triangles), $k = 2$ (squares) and $k = 3$ (circles) for $\rho = 0.00712\ \text{day}^{-1}$. Other parameters are as in Fig. 2. The upper dashed line (horizontal) corresponds to the FTB size. Radiotherapy follows the standard scheme (6 weeks with 1.8 Gy doses from Monday to Friday) and starts at time $t = 0$. It is clear that, for this set of parameters, the ST does not depend on k despite the differences in the maximum diameter reduction achieved by the therapy. (b) Maximum diameter reduction for different values of the mean number of mitosis cycles completed before cell death with k between 1 and 3. (c) ST and GD as a function of k.

for long times because of the effect of the mobility on the asymptotic VDE $v = 4\sqrt{\rho D}$. This manifests in the independence of the TTP and GD on D and the relevant impact of this parameter on the ST (Fig 4(b)).

3.5 *Deferring radiotherapy does not affect ST*

One clinical fact on radiotherapy of LGGs that has been proved in the last years is that deferring radiotherapy has no significant impact on the ST (Bauman *et al.*, 1999; Van den Bent, 2005). To test if our

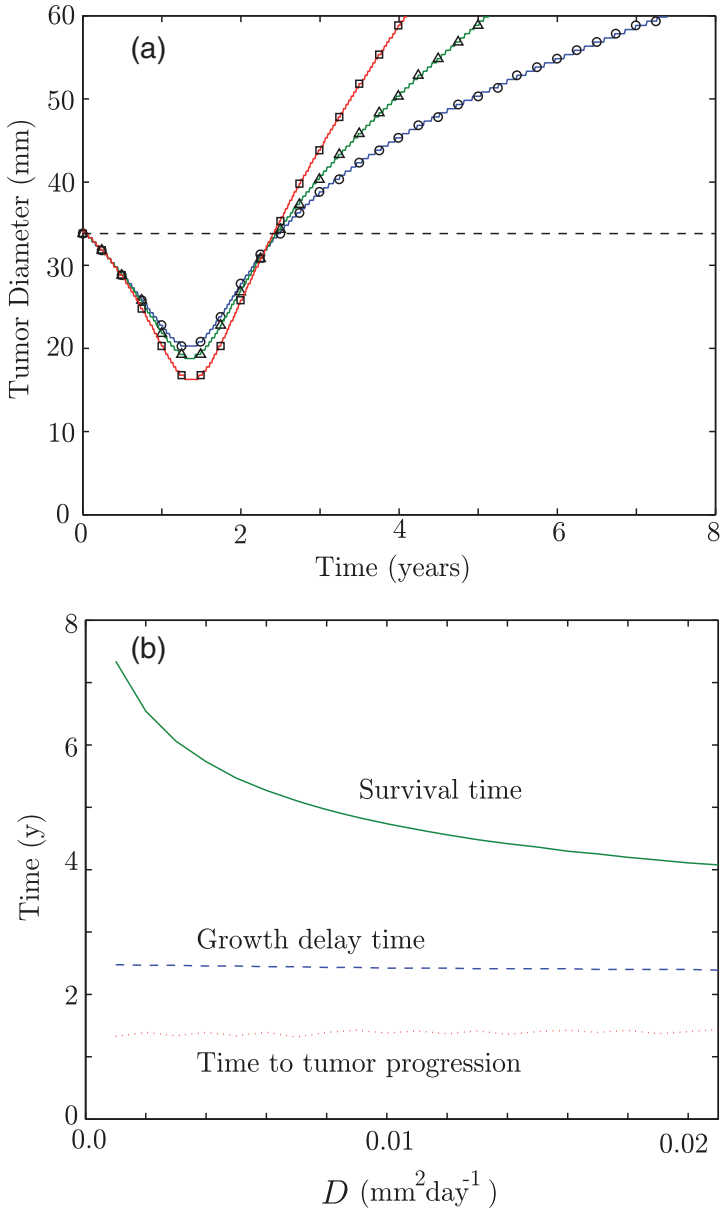

FIG. 4. (a) Tumour diameter evolution for three different values of $D = 0.001\ \mathrm{mm^2 day^{-1}}$ (circles), $D = 0.007\ \mathrm{mm^2 day^{-1}}$ (triangles) and $D = 0.021\ \mathrm{mm^2 day^{-1}}$ (squares) for $\rho = 0.00356\ \mathrm{day^{-1}}$. Other parameters and initial data are as in Fig. 2. Radiotherapy follows the standard scheme (6 weeks with 1.8 Gy doses from Monday to Friday) and starts at time $t = 0$. It is clear that, for this set of parameters, the early response to the therapy does not depend on D, while the asymptotic growth does (b) ST, GD and TTP as a function of D. Only the ST depends substantially on the cell motility D.

model presents this behaviour, we have run several series of simulations with different delays in the start of the radiotherapy and compared the outcome. Typical results are shown in Fig. 5. The results of the model fully agree with this very well-known fact, which gives us more confidence in the model's predictive power, despite its simplicity.

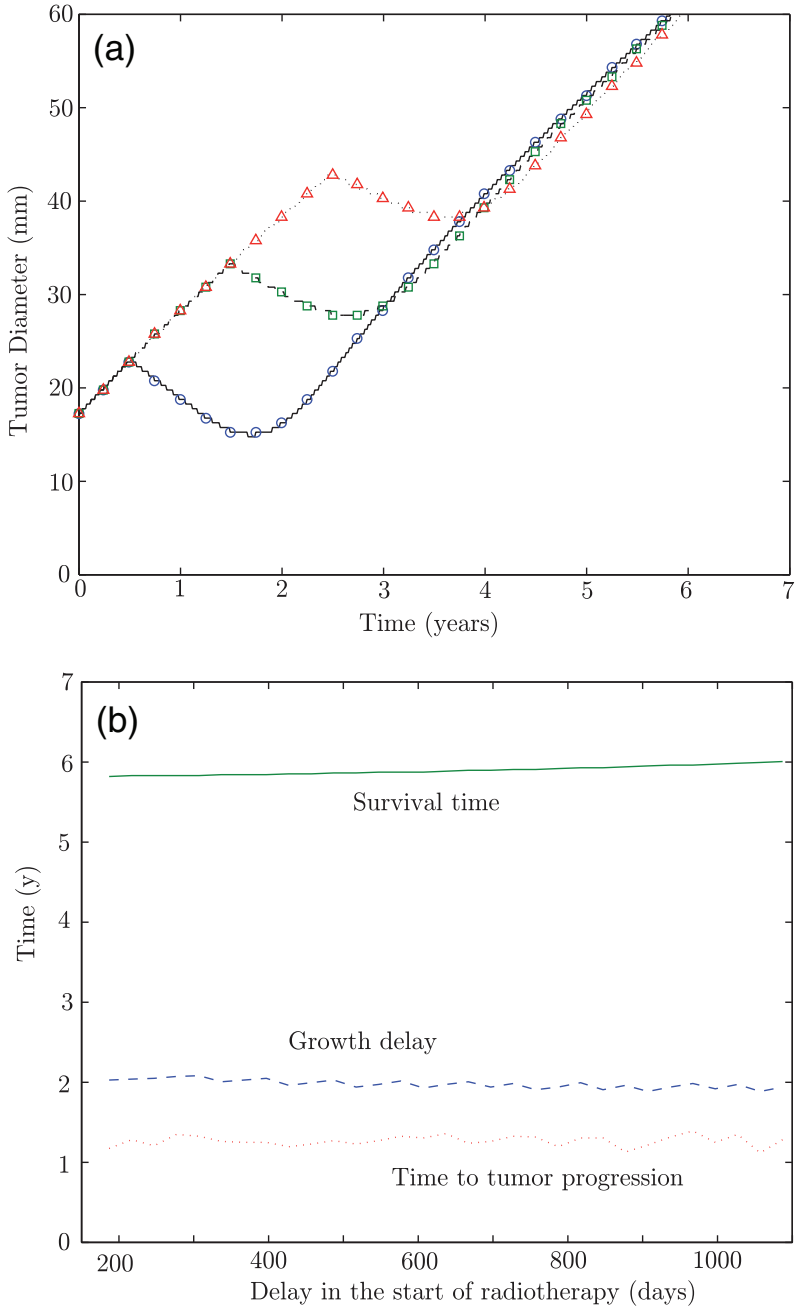

FIG. 5. Evolution of an initial tumour density given by $C(x,0) = 0.2\exp(-x^2/(2w^2))$, $C_d(x,0) = 0$ for $w = 6$, with (x, w) being measured in millimetres, and parameter values $D = 0.01\ \text{mm}^2/\text{day}$, $\rho = 0.004\ \text{day}^{-1}$, $\text{SF}_{1.8} = 0.9$ and $k = 1$. Radiotherapy follows the standard scheme (6 weeks with 1.8 Gy doses from Monday to Friday) and starts at a given time T_{RT} after the beginning of the simulation for $t = 0$. Shown are (a) Tumour diameter evolution for three different values of $T_{\text{RT}} = 6$ months (solid line, circles), $T_{\text{RT}} = 18$ months (dashed line, squares), $T_{\text{RT}} = 30$ months (dotted line, triangles). (b) ST (solid line), GD (dashed line) and TTP (dotted line) as a function of the delay T_{RT} in the start of radiotherapy.

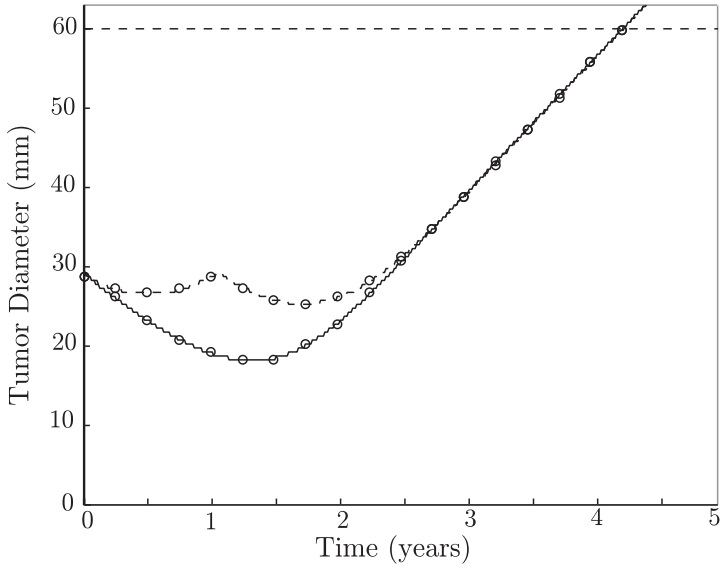

FIG. 6. Tumour diameter evolution for parameter values $D = 0.007\ \text{mm}^2/\text{day}$, $\rho = 0.00356\ \text{day}^{-1}$, initial data as in Fig. 1 and two different fractionations of the total dose. The solid line corresponds to the tumour evolution under 30 doses of 1.8 Gy given from Monday to Friday for six consecutive weeks starting 1 week after $t = 0$. The dashed line corresponds to the tumour diameter evolution under the same fractionation scheme for the first three weeks and then deferring the remaining 15 doses for 1 year. Despite the time of response being shorter, the final ST is the same in both fractionation schemes.

3.6 *Splitting doses does not affect ST*

We have studied the response of the tumour to radiotherapy under many different fractionation schemes, maintaining the dose per fraction to be 1.8 Gy. Surprisingly, all of the studied fractionations lead to very similar results for the virtual patient's ST. A typical example is shown in Fig. 6.

Although we have not tried every possible combination, this fact points out the difficulty of constructing specific fractionation schemes leading to a better outcome than those currently in use. However, the results of Fig. 6 have interesting potential practical applications as will be discussed in Section 5.

4. Some analytical estimates

The model equations given by Equations (2.2), though simple, do not have known analytical solutions allowing for the direct calculation of the clinically relevant quantities, i. e. the TTP (t_{TTP}), the GD (t_{GD}) and the time to FTB. Even for the simplest version of the Fisher–Kolmogorov equations only a limited number of solutions are known for specific parameter values (Ablowitz & Zeppetella, 1979; Murray, 2007).

Here, we present some back-of-the-envelope calculations that may help in getting a qualitative idea of the typical dynamics of the tumour response to radiation. The basic idea behind our estimates is that, during some time after irradiation, the dominant component of the dynamics is the refilling of the compartment of the proliferating tumour cells, and diffusion acts on a longer time scale, being responsible for the asymptotic front speed (see e.g. Fig. 4(a)) but having only a negligible influence both on the TTP and the GD (Fig. 4(b)).

We will assume the tumour densities shortly after irradiation to be small enough to allow for the non-linear terms to be neglected (it is in agreement with the low cellularity characteristic in LGG histologic samples). This is obviously true for the tumour compartment whose typical cell densities after irradiation are small until the tumour refills the space. With regard to the damaged tumour cell compartment its maximal density is of the order of the maximal initial tumour cell density (about 0.3–0.4) but decays in space to smaller cell densities and will be assumed to contribute only through the leading linear terms.

As a final assumption, we will assume the total treatment time to be short in comparison with the typical proliferation times so that the effect of the radiotherapy will be incorporated through a modification of the pretreatment tumour cell density $C_0(x)$. Thus, for our rough estimates we will take

$$C(x,0) = S_f^n C_0(x), \tag{4.1a}$$

$$C_d(x,0) = (1 - S_f^n) C_0(x). \tag{4.1b}$$

Our set of hypothesis leads to a very simple evolution law for the total densities, valid for short times:

$$C(x,t) \approx S_f^n C_0(x)\, \mathrm{e}^{\rho t}, \tag{4.2a}$$

$$C_d(x,t) \approx (1 - S_f^n) C_0(x)\, \mathrm{e}^{-\rho t/k}, \tag{4.2b}$$

so that, for some time after the therapy, the total tumour cell density $C_T(x,t)$ can be roughly approximated by

$$C_T(x,t) \approx [S_f^n\, \mathrm{e}^{\rho t} + (1 - S_f^n)\, \mathrm{e}^{-\rho t/k}] C_0(x), \tag{4.3}$$

where $A(t) \equiv S_f^n\, \mathrm{e}^{\rho t} + (1 - S_f^n)\, \mathrm{e}^{-\rho t/k}$ provides an estimate of the tumour maximum density as a function of time. From this simple formula, we can estimate the GD time since it would correspond to the time $t_{\mathrm{GD}} > 0$ such that

$$S_f^n\, \mathrm{e}^{\rho t_{\mathrm{GD}}} + (1 - S_f^n)\, \mathrm{e}^{-\rho t_{\mathrm{GD}}/k} \approx 1. \tag{4.4}$$

Although Equation (4.4) is an algebraic equation with no simple explicit solutions by the time re-growth occurs, we can expect the first term to have a very small contribution, while the second one would dominate, which gives

$$t_{\mathrm{GD}} \approx \frac{1}{\rho} \log\left(\frac{1}{S_f^n}\right) \approx \frac{n(1 - S_f)}{\rho}. \tag{4.5}$$

This equation incorporates the fact that the GD time does not depend much on the diffusion parameter D (see e.g. Fig. 4(b)), nor on the number of mitosis cycles before cell death for damaged cells (see e.g. Fig. 3(c)), and points out a direct simple dependence of this time on the survival fraction, number of doses and proliferation parameter. Moreover, the dependence of t_{GD} on ρ is $\sim 1/\rho$, which resembles closely the dependence depicted in Fig. 2. We can also get estimates for the TTP since it corresponds to the point of minimum amplitude, corresponding to the time t_{TTP} such that $A'(t_{\mathrm{TTP}}) = 0$,

$$\frac{\mathrm{d}}{\mathrm{d}t}[S_f^n\, \mathrm{e}^{\rho t} + (1 - S_f^n)\, \mathrm{e}^{-\rho t/k}] = 0, \tag{4.6}$$

which leads to

$$t_{\mathrm{TTP}} = \frac{1}{\rho(1 + 1/k)} \log\left(\frac{1 - S_f^n}{S_f^n}\right) \simeq \frac{n(1 - S_f)}{\rho(1 + 1/k)} \tag{4.7}$$

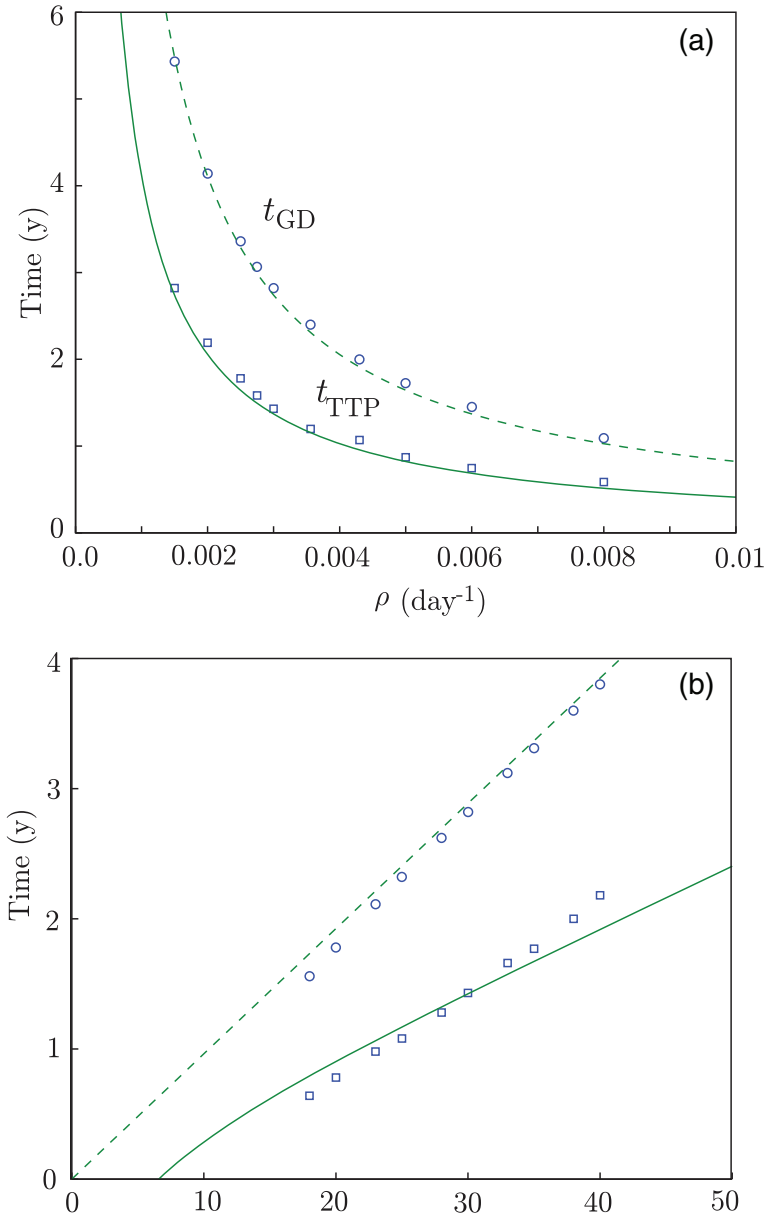

FIG. 7. Comparison of the estimates for t_{GD} (circles) and t_{TTP} (squares) obtained from Equations (4.5) and (4.7) and their exact values (lines) obtained from numerical simulations of Equations (2.2) in different scenarios. In all cases $D = 0.007\,\text{mm}^2/\text{day}$, $S_f = 0.9$ and $k = 1$ and initial data are as in Fig. 1. (a) Dependence on the proliferation parameter ρ for a fixed number of doses $n = 30$ following the standard fractionation scheme. (b) Dependence on the number of doses n for fixed $\rho = 0.002\,\text{day}^{-1}$.

While these estimates are obtained as rough approximations for the response to radiation, they provide a very reasonable agreement with the results of direct numerical simulations of Equations (2.2). For instance, in Fig. 7(a), we compare the results for the GD and TTP provided by Equations (4.5) and (4.7) with the results from Equations (2.2) for a typical set of parameters and varying the proliferation parameter ρ. In Fig. 7(b), we compare the predictions for t_{TTP} and t_{GD} given by Equations (4.5) and (4.7) for different values of the number of radiation fractions n, with the simulations of the full PDEs.

In addition to these quantities, it is possible to use Equation (4.3) to get estimates for the conditions of response to therapy ($A'(0) < 0$), i.e.

$$A'(0) = \rho S_f^n - \rho(1 - S_f^n)/k < 0. \tag{4.8}$$

This leads to the result that an estimate for the minimal number of doses leading to a response is about

$$n > -\frac{\log(1+k)}{\log S_f}. \tag{4.9}$$

Interestingly, this number is independent of ρ and, for the typical values of S_f used in our simulations, we get a minimal number of sessions around 7 and 9. We have compared this estimate with the results of direct simulations of Equations (2.2) and found a very good agreement. For instance, taking typical initial data and parameter values $C(x,0) = 0.4\,\mathrm{sech}(x/11)$, $\rho = 0.00356\,\mathrm{day}^{-1}$, $k = 1$, $D = 0.0075\,\mathrm{mm}^2/\mathrm{day}$ and $S_f = 0.92$, we get a response for $n \geqslant 10$ that is very close to the theoretical estimate computed from Equation (4.9), which is $n \geqslant 9$. The same happens for other parameter choices.

Finally, neither the GD as given by Equation (4.5) nor the TTP (4.7) depends on the initial amplitude or time t_0. This means that radiation can be deferred with no effect on these quantities, which matches very well the behaviour observed in Fig. 5(b).

5. Discussion and therapeutical implications

The intention of this paper is to propose a simple mathematical model adding radiation therapy in a minimal way to the simplest model of tumour progression. Despite its simplicity, the model reproduces many of the well-known facts of RT of LGGs as well as the recent results by Pallud *et al.* (2012b). The fact that the model reproduces so well what is known makes us wonder if it can be used to obtain any new information and/or to propose novel ideas with the potential of translational application. In this section we make several proposals based on the mathematical model.

The first one is based on the fact, discussed in Section 3.6, that deferring part of the treatment does not affect ST. This concept opens the door to dose fractionation approaches where part of the radiation is given right after surgery as an adjuvant therapy and the remaining radiation is given on progression (or later), thus controlling early the tumour while deferring in time the appearance of side effects. A specific way of implementing this idea would be to complete the radiation therapy exactly when the tumour size is minimal so that the irradiated volume is substantially smaller than initially and the side effects due to the so-called volume effect would be reduced. Thus, instead of waiting till the tumour has extended substantially, the first dose would be given right after resection and the second one on minimal volume. The fact that the tumour volume irradiated would be smaller might allow for the consideration of dose escalation protocols while maintaining the side effects under control.

A second implication of our model is that delivery of a reduced radiation dose larger than the minimal response dose (e.g. 30 Gy) should have a verifiable effect on tumour size. Monitoring the response of the tumour to radiation, one could get an idea of its malignancy due to the relation between response time and proliferation, and correlate the finding with the proliferation index obtained through immunohistochemistry when available. The toxicity of this approach for the normal brain is low since 30 Gy is about the same level of the prescriptions for even full-brain irradiation under metastatic spreading, a dose that is very well tolerated by the brain.

Having an early estimate of the tumour aggressiveness is a potentially interesting information since, in addition to making survival estimates (from the tumour parameters ρ, D), it would allow to discriminate tumours that are not as benign as initially thought. A first reason is that the tumour may have transformed to some degree into a more malignant one. This happens sometimes when the histological analysis is old, and by the time RT starts the tumour has become malignant. A different relevant source of error on diagnosis is sampling error if the histology was obtained through biopsy. In fact, biopsy is known to underestimate glioma grade in roughly 30% of cases (Muragaki *et al.*, 2008) due to localized malignant transformation outside the biopsy location. Those tumours with high proliferation values obtained from the mathematical modelling should be expected to have early (radiological) malignant transformation and then MRIs should be taken at shorter intervals, as suggested e.g. by Pallud *et al.* (2012b) for fast-growing tumours. A final therapeutic option for those tumours with fast growth and/or expected early malignant transformation should be to consider another surgery (if feasible) or to start chemotherapy.

Thus, taking together our two ideas, we could make specific recommendations: for tumours with a high risk of malignant transformation, i.e. short re-growth time, our suggestion would be to complete the full radiation dosing, while for those growing slowly one could wait either until the malignant transformation or to the point where the tumour starts re-growing.

6. Conclusions

In conclusion, in this paper we have constructed a mathematical model combining the standard Fisher–Kolmogorov dynamics for tumour cells with a model for the response to radiation based on radiobiological facts. Our equations provide a theoretical link between proliferation and response to therapy, which is one of the main results of this paper. The model predicts that tumours with high proliferation will respond faster to RT than those with slower proliferation values. However, this regression would only be transient and a regrowth is expected early in those tumours responding faster. This fact, despite being somewhat counterintuitive, has been confirmed in very recent retrospective studies by Pallud *et al.* (2012b). The model also displays the observed behaviour that deferring RT does not affect ST.

The equations allow one to obtain analytical estimations for the GD time, TTP and conditions of response to therapy such as the minimal number of doses leading to a response.

In addition to describing the known features of the response of LGGs to radiotherapy, the model allows one to get interesting predictions that may be amenable to further research. One of them is to follow a split-dose approach with a fraction of the total amount of radiation being given after surgery and the remaining on progression. This methodology would allow one to get information on the tumour growth parameters that may lead to estimates of the expected time to malignant transformation, survival, etc., while at the same time reducing toxicity.

We hope that our results will stimulate further collaborative studies directed to improve the quality of life of patients suffering from this devastating disease.

Funding

This work has been supported by grant MTM2012-31073 (Ministerio de Economía y Competitividad, Spain) and the James S. McDonnell Foundation (USA) through the 21st Century Science Initiative in Mathematical & Complex Systems Approaches for Brain Cancer-Pilot Award 220020351.

References

Ablowitz, M. J. & Zeppetella, A. (1979) Explicit solutions of Fisher's equation for a special wave speed. *Bull. Math. Biol.*, **41**, 835.

Barazzuol, L., Burnet, N. G., Jena, R., Jones, B., Jefferies, S. J. & Kirkby, N. F. (2010) A mathematical model of brain tumour response to radiotherapy and chemotherapy considering radiobiological aspects. *J. Theor. Biol.*, **262**, 553–565.

Barrett, L. E., Granot, Z., Coker, C., Iavarone, A., Hambardzumyan, D., Holland, E. C., Nam, H. S. & Benezra, R. (2012) Self-renewal does not predict tumor growth potential in mouse models of high-grade glioma. *Cancer Cell*, **21**, 11–24.

Bauman, G., Pahapill, P., Macdonald, D., Fisher, B., Leighton, C. & Cairncross, G. (1999) Low grade glioma: a measuring radiographic response to radiotherapy. *Can. J. Neurol. Sci.*, **26**, 18–22.

Bondiau, P. Y., Frenay, M. & Ayache, N. (2008) Biocomputing: numerical simulation of glioblastoma growth using diffusion tensor imaging. *Phys. Med. Biol.*, **53**, 879–893.

Bondiau, P. Y., Konukoglu, E., Clatz, O., Delingette, H., Frenay, M. & Paquis, P. (2010) Biocomputing: numerical simulation of glioblastoma growth and comparison with conventional irradiation margins. *Phys. Med.*, **27**, 103–108.

Braznhnik, P. K. & Tyson, J. J. (2000) On traveling wave solutions of Fisher's equation in two spatial dimensions. *SIAM J. Appl. Math.*, **60**, 371–391.

Chen, J., Li, Y., Yu, T. S., McKay, R. M., Burns, D. K., Kernie, S. G. & Parada, L. F. (2012) A restricted cell population propagates glioblastoma growth after chemotherapy. *Nature*, **488**, 522–526.

Clatz, O., Sermesant, M., Bondiau, P. Y., Delingette, H., Warfield, S. K., Malandain, G. & Ayache, N. (2005) Realistic simulation of the 3-D growth of brain tumors in MR images coupling diffusion with biomechanical deformation. *IEEE Trans. Med. Imaging*, **24**, 1334–1346.

Deroulers, C., Aubert, M., Badoual, M. & Grammaticos, B. (2009) Modeling tumor cell migration: From microscopic to macroscopic models. *Phys. Rev. E*, **79**, 031917.

Dirks, P. B. (2001). Glioma migration: clues from the biology of neural progenitor cells and embryonic CNS cell migration. *J. Neurooncol.*, **53**, 203–212.

Eikenberry, S. E. & Kuang, Y. (2009). Virtual glioblastoma: growth, migration and treatment in a three-dimensional mathematical model. *Cell Prolif.*, **42**, 511–528.

Fedotov, S., Iomin, A. & Ryashko, L. (2011) Non-Markovian models for migration-proliferation dichotomy of cancer cells: Anomalous switching and spreading rate. *Phys. Rev. E*, **84**, 061131.

Frieboes, H. B., Bearer, E. & Cristini, V. (2007). Computer simulation of glioma growth and morphology. *Neuroimage*, **37**, S59–S70.

Garcia, D. M., Fulling, K. H. & Marks, J. E. (1985) The value of radiation therapy in addition to surgery for astrocytomas of the adult cerebrum. *Cancer*, **55**, 919–927.

Gerin, C., Pallud, J., Grammaticos, B., Mandonnet, E., Deroulers, C., Varlet, P., Capelle, L., Taillandier, L., Bauchet, L., Duffau, H. & Badoual, M. (2012) Improving the time-machine: estimating date of birth of grade II gliomas. *Cell Prolif.*, **45**, 76–90.

Gerlee, P. & Nelander, S. (2012) The impact of phenotypic switching on glioblastoma growth and invasion. *PLOS Comp. Biol.*, **8**, e1002556.

Grier, J. T. & Batchelor, T. (2006) Low-grade gliomas in adults. *Oncologist*, **11**, 681–693.

Gu, S., Chakraborty, G., Champley, K., Alessio, A. M., Claridge, J., Rockne, R., Muzi, M., Krohn, K. A., Spence, A. M., Alvord, Jr, E. C., Anderson, A. R., Kinahan, P. E. & Swanson, K. R. (2012) Applying a patient-specific bio-mathematical model of glioma growth to develop virtual [18F]-FMISO-PET images. *Math. Med. Biol.*, **29**, 31–48.

Hatzikirou, H., Basanta, D., Simon, M., Schaller, K. & Deutsch, A. (2012) 'Go or grow': the key to the emergence of invasion in tumour progression? *Math. Med. Biol.*, **29**, 49–65.

Higuchi, Y., Iwadate, Y. & Yamaura, A. (2004) Treatment of low-grade oligodendroglial tumors without radiotherapy. *Neurology*, **63**, 2384–2386.

Jakola, A. S., Myrmel, K. S., Kloster, R., Torp, S. H., Lindal, S., Unsgard, G. & Solheim, O. (2012) Comparison of a strategy favoring early surgical resection vs a strategy favoring watchful waiting in low-grade gliomas. *J. Am. Med. Assoc.*, **308**, 1881–1888.

Jbabdi, S., Mandonnet, E., Duffau, H., Capelle, L., Swanson K. R., Pelegrini-Issac, M., Guillevin, R. & Benali, H. (2005) Simulation of anisotropic growth of low-grade gliomas using diffusion tensor imaging. *Magn. Reson. Med.*, **54**, 616–624.

Konukoglu, E., Clatz, O., Bondiau, P. Y., Delingette, H. & Ayache, N. (2010). Extrapolating glioma invasion margin in brain magnetic resonance images: suggesting new irradiation margins. *Med. Image Anal.*, **14**, 111–125.

Martínez-González, A., Calvo, G. F., Pérez-Romasanta, L. A. & Pérez-García, V. M. (2012) Hypoxic cell waves around necrotic cores in glioblastoma: a biomathematical model and its therapeutic implications. *Bull. Math. Biol.*, **74**, 2875–2896.

Muragaki, Y., Chernov, M., Maruyama, T., Ochiai, T., Taira, T., Kubo, O., Nakamura, R., Iseki, H., Hori, T. & Takakura, K. (2008) Low-grade glioma on stereotactic biopsy: how often is the diagnosis accurate? *Minim. Invasive Neurosurg.*, **51**, 275–279.

Murray, J. D. (2007) *Mathematical Biology: I. An Introduction*. Berlin: Springer.

Olson, J. D., Riedel, E. & DeAngelis, L. M. (2000) Long-term outcome of low-grade oligodendroglioma and mixed glioma. *Neurology*, **54**, 1442–1448.

Onishi, M., Ichikawa, T., Kurozumi, K. & Date, I. (2011) Angiogenesis and invasion in glioma. *Brain Tumor Pathol.*, **28**, 13–24.

Painter, K. J. & Hillen, T. (2013) Mathematical modelling of glioma growth: the use of Diffusion Tensor Imaging (DTI) data to predict the anisotropic pathways of cancer invasion. *J. Theoretical Biol.*, **323**, 25–39.

Pallud, J., Llitjos, J. F., Dhermain, F., Varlet, P., Dezamis, E., Devaux, B., Souillard-Scemama, R., Sanai N, Koziak, M., Page, P., Schlienger, M., Daumas-Duport, C., Meder, J. F., Oppenheim, C. & Roux F. X. (2012b) Dynamic imaging response following radiation therapy predicts long-term outcomes for diffuse low-grade gliomas. *Neuro-Oncology*, **14**, 496–505.

Pallud, J., Taillandier, L., Capelle, L., Fontaine, D., Peyre, M., Ducray, F., Duffau, H. & Mandonnet, E. (2012a) Quantitative morphological MRI follow-up of low-grade glioma: a plead for systematic measurement of growth rates. *Neurosurgery*, **71**, 729–740.

Pérez-García, V. M., Calvo, G. F., Belmonte-Beitia, J., Diego, D. & Pérez-Romasanta, L. (2011). Bright solitary waves in malignant gliomas. *Phys. Rev. E*, **84**, 021921.

Pérez-García, V. M. & Martínez-González, A. (2012) Hypoxic ghost waves accelerate the progression of high-grade gliomas. *J. Theor. Biol.* (2013).

Pignatti, F., Van den Bent, M., Curran, D., Debruyne, C., Sylvester, R., Therasse, P., Afra, D., Cornu, P., Bolla, M., Vecht, C. & Karim, A. B. (2002) Prognostic factors for survival in adult patients with cerebral low- grade glioma. *J. Clin. Oncol.*, **20**, 2076–2084.

Pouratian, N. & Schiff, D. (2010) Management of low-grade glioma. *Curr. Neurol. Neurosci. Rep.*, **10**, 224–231.

Rockne, R., Hendrickson, K., Lai, A., Cloughesy, T., Alvord, Jr, E. C. & Swanson, K. R. (2010). Predicting the efficacy of radiotherapy in individual glioblastoma patients in vivo: a mathematical modeling approach. *Phys. Med. Biol.*, **55**, 3271–3285.

Ruiz, J. & Lesser, G. J. (2009) Low-grade gliomas. *Curr. Treat. Opt. Oncol.*, **10**, 231–242.

Sattinger, D. H. (1976) On the stability of waves of nonlinear parabolic systems. *Adv. Math.*, **22**, 312–355.

Smith, J. S., Chang, E. F., Lamborn, K. R., Chang, S. M., Prados, M. D., Cha, S., Tihan, T., Vandenberg, S., McDermott, M. W. & Berger, M. S. (2008) Role of extent of resection in the long-term outcome of low-grade hemispheric gliomas. *J. Clin. Oncol.*, **26**, 1338–1345.

Stamatakos, G. S., Antipas, V. P. & Uzunoglu, N. K. (2006a) A spatiotemporal patient individualized simulation model of solid tumor response to chemotherapy in vivo: the paradigm of glioblastoma multiforme treated by temozolomide. *IEEE Trans. Biomed. Eng.*, **53**, 1467–1477.

Stamatakos, G. S., Antipas, V. P. & Uzunoglu, N. K. (2006b) Simulating chemotherapeutic schemes in the individualized treatment context: the paradigm of glioblastoma multiforme treated by temozolomide in vivo. *Comp. Biol. Med.*, **36**, 1216–1234.

Suzuki, S. O., Kitai, R., Llena, J., Lee, S. C., Goldman, J. E. & Shafit-Zagardo, B. (2002). MAP-2e, a novel MAP-2 isoform, is expressed in gliomas and delineates tumor architecture and patterns of infiltration. *J. Neuropathol. Exp. Neurol.*, **61**, 403–412.

Swanson, K. R., Rostomily, R. C. & Alvord, Jr, E. C. (2008). A mathematical modelling tool for predicting survival of individual patients following resection of glioblastoma: a proof of principle. *Br. J. Cancer*, **98**, 113–119.

Tanaka, M. L., Debinski, W. & Puri, I. K. (2009) Hybrid Mathematical model of glioma progression. *Cell. Prolif.*, **42**, 637–646.

Van den Bent, M. J., Afra, D., de Witte, O., Ben Hassel, M., Schraub, S., Hoang-Xuan, K., Malmström, P. O., Collette, L., Piérart, M., Mirimanoff, R. & Karim, A. B. (2005) Long-term efficacy of early versus delayed radiotherapy for low-grade astrocytoma and oligodendroglioma in adults: the EORTC 22845 randomised trial. *Lancet*, **366**, 985–990.

Van der Kogel, A. & Joiner, M. (2009) *Basic Clinical Radiobiology*. Oxford: Oxford University Press.

Volpert, V. & Petrovskii, S. (2009) Reaction-diffusion waves in biology. *Phys. Life Rev.*, **6**, 267–310.

Wang, C. H., Rockhill, J. K., Mrugala, M., Peacock, D. L., Lai, A., Jusenius, K., Wardlaw, J. M., Cloughesy, T., Spence, A. M., Rockne, R., Alvord, Jr, E. C. & Swanson, K. R. (2009). Prognostic significance of growth kinetics in newly diagnosed glioblastomas revealed by combining serial imaging with a novel biomathematical model. *Cancer Res.*, **69**, 9133–9140.

Xin, J. (2000) Front propagation in heterogeneous media. *SIAM Rev.*, **42**, 161–230.

Appendix. Study of the system without diffusion

A.1 *Motivation and simplified model*

The main focus of the paper is the obtention of results on LGG progression that is related to the tumour size if the transition to malignancy is not taken into account. However, it is interesting to note that a lot of information on the kinetic part of equations (2.2) can be obtained. Thus, in this appendix, we will study the pair of ordinary differential equations

$$\frac{\mathrm{d}A}{\mathrm{d}t} = \rho(1 - A - B)A, \tag{A.1a}$$

$$\frac{\mathrm{d}B}{\mathrm{d}t} = -\frac{\rho}{k}(1 - A - B)B, \tag{A.1b}$$

where now both $A(t)$ and $B(t)$ are positive functions depending only on time and describing the evolution of both tumour cell populations in systems without spatial inhomogeneities. The effect of radiotherapy given at times $(t_1, \ldots, t_n)$ with doses $(d_1, \ldots, d_n)$ and survival fractions $(S_f(d_1), \ldots, S_f(d_n))$ in this simplified model is given by the equations

$$A(t_j^+) = S_f(d_j)A(t_j^-), \tag{A.2a}$$

$$B(t_j^+) = B(t_j^-) + [1 - S_f(d_j)]A(t_j^-). \tag{A.2b}$$

A.2 *Analysis of equations* (A.1)

Since Equations (A.1) correspond to an autonomous planar dynamical system, the possible dynamics in the phase space can be completely understood. First of all, note that there are two families of equilibria. First, the equilibrium point with $(A, B) = (0, 0)$ and then the line of points $\mathcal{R}$ satisfying $A + B = 1$, with $A, B > 0$. The first one is a saddle point, thus unstable and means that tumour cells tend to regrow no matter how small is their density. With regards to those in $\mathcal{R} = \{(a, 1 - a),\ 0 < a < 1\}$, the Jacobian

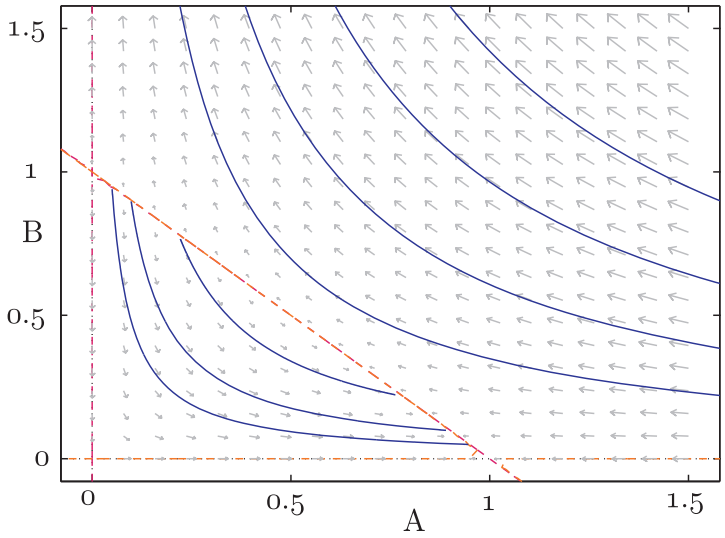

FIG. A1. Phase portrait of the dynamical system (A.1). Shown are the velocity field (arrows) and some orbits (blue) including some heteroclinic orbits connecting unstable equilibrium points on $\mathcal{R}$ with stable equilibria on the same set (blue). Also in red are shown the stable and unstable manifold of the point (0,0) (located on the axes), and the manifold of equilibria $\mathcal{R}$. The red lines determine the limits of the invariant region $\mathcal{S}$.

matrix reads

$$J(\mathcal{R}) = \rho \begin{pmatrix} -a & -a \\ (1-a)/k & (1-a)/k \end{pmatrix}. \tag{A.3}$$

The eigenvalues of this Jacobian matrix are given by

$$\lambda_1 = 0, \quad \lambda_2 = \frac{\rho}{k}(1-a) - \rho a,$$

and the corresponding eigenvectors are $(1,-1)$ and $(1,-(1-a)/ka)$, respectively (for $\lambda_2 \neq 0$). The equilibrium points on $\mathcal{R}$ are non-hyperbolic points. If $a < 1/(k+1)$, then the fixed point $(a, 1-a)$ possesses a local unstable manifold and a local centre manifold. Otherwise, $(a, 1-a)$ has a local stable manifold and a local centre manifold. Thus, to get a heteroclinic orbit joining two points, say $(a_1, 1-a_1)$ and $(a_2, 1-a_2)$, with $a_2 > a_1$, it is a necessary condition that $a_2 > 1/(k+1)$ and $a_1 < 1/(k+1)$.

A straightforward application of the centre manifold theory shows that the centre manifold of $\mathcal{R}$ is the same set, i.e. $W^c(\mathcal{R}) = \mathcal{R}$. Moreover, the points of $\mathcal{R}$ satisfying $a < 1/(k+1)$ are unstable, while the points over the centre manifold satisfying $a > 1/(k+1)$ are stable.

The explicit form of the equation of the orbits can be obtained from Equations (A.1)

$$\frac{\mathrm{d}A}{\mathrm{d}B} = -k\frac{A}{B} \tag{A.4}$$

which leads to

$$AB^k = C, \tag{A.5}$$

with $C = A_0 B_0^k$, where $A(0) = A_0 > 0, B(0) = B_0 > 0$. Thus, the orbits correspond to hyperbolas. Some orbits together with the velocity field are shown in Fig. A1. We want to note that the centre manifold is given by the red line joining the points $(1,0)$ and $(0,1)$.

The feasible region of our model is the set

$$\mathcal{S} = \{(A, B) : A, B > 0,\ A + B \leqslant 1\}.$$

Since the set $\mathcal{S}$ is bounded by the centre manifold and by the line orbits of the saddle point $A = 0$ and $B = 0$, it is straightforward to see that the region $\mathcal{S}$ is an invariant region, that is, all the orbits inside $\mathcal{S}$ belong to $\mathcal{S}$ for all times $t \in \mathbb{R}$. Therefore, all the orbits inside $\mathcal{S}$ start and end in the centre manifold (except for the line orbits asymptotically approaching the saddle point $(0, 0)$ for $t = \pm\infty$).

A.3 *Exact solutions*

It is interesting to note that in special cases it is possible to compute some explicit solutions for equations (A.1). One of the most relevant cases corresponds to $k = 1$, which, as has been discussed through the paper, is the biologically most relevant situation. In that case, substituting the orbits equation, $AB = C$, in (A.1b), we obtain

$$\int \frac{\mathrm{d}B}{(B - 1/2)^2 + C - 1/4} = \rho(t - t_0). \tag{A.6}$$

It is interesting to note that, for solutions starting in the feasible region $A + B \leqslant 1$, a simple calculation shows that $0 < C < \frac{1}{4}$. Let us define $Q_+ = \sqrt{\frac{1}{4} - C} < \frac{1}{2}$. In that case, we can compute explicitly the integrals in Equation (A.6) to obtain

$$B(t) = \frac{1}{2} - Q_+ \tanh[Q_+\rho(t - t_0)], \tag{A.7a}$$

$$A(t) = \frac{C}{1/2 - Q_+ \tanh[Q_+\rho(t - t_0)]}. \tag{A.7b}$$

In the phase space, these solutions correspond to hyperbolas inside the region $\mathcal{S}$.

For the limit case $C = \frac{1}{4}$, Equations (A.6) can also be solved explicitly to obtain

$$B(t) = \frac{1}{2} - \frac{1}{\rho(t - t_0)}, \tag{A.8a}$$

$$A(t) = \frac{1}{2 - 4/\rho(t - t_0)}. \tag{A.8b}$$

This is a special case, since the solutions correspond to hyperbolas through the point $(\frac{1}{2}, \frac{1}{2})$, which is a point of the centre manifold and for which $\lambda_2 = 0$.

For completeness, we also present the solutions for the case $C > \frac{1}{4}$. In that case the solutions correspond to hyperbolas outside the region $\mathcal{S}$. Defining $Q_- = \sqrt{C - \frac{1}{4}}$, we obtain

$$B(t) = \frac{1}{2} + Q_- \tan[Q_-\rho(t - t_0)], \tag{A.9a}$$

$$A(t) = \frac{C}{1/2 + Q_- \tan[Q_-\rho(t - t_0)]}. \tag{A.9b}$$

Appendix B

Numerical procedures

B.1 Numerical procedures for model of response to chemotherapy

We present functions used to solve model given by system (2.2) with function f as in Eq. (2.1) and fit its parameters.

main

```
function main
% Estimating model parameters based on data of LGGs treated with chemotherapy

[time_beforeCT, vol_beforeCT, vol_afterCT, time_afterCT, time_med, n_cycles, ...
    t_beforeCT, time, out_per_day, delay, index0, time_to_CTend] = data_159();
[K,lambda,dose_eff,rho0,alpha0,k0] = parameters_man();

%%
% estimation of tumour growth before the onset of chemotherapy treatment
% that is till index0 defined from patients data

resultP=zeros(size(time));
P0=vol_beforeCT(1);

tic
[rho,err_rho]= estim_rho(time_beforeCT,vol_beforeCT,rho0,K);
toc
fprintf('Estimation before chemotherapy onset: rho = %f, error: %f\n', rho, err_rho)

resultP(1:index0)=calculateP(t_beforeCT,P0,rho,K);
P1=resultP(index0);
params0=[alpha0,k0];
params2=[rho,K,lambda,dose_eff];

%%
% initial guess of parameters alpha and k
[~,~,Total0]=calculateP_D(time,n_cycles,index0,out_per_day,params0,params2,P1);

Total0(1:index0)=resultP(1:index0);
diff=(vol_afterCT-Total0(time_afterCT.*out_per_day))./vol_afterCT;
err0=sum(sum(diff.^2));
fprintf('Starting values: alpha = %f, k = %f, error: %f\n', alpha0, k0,err0);
```

```
tic
[params,err1] = estim_alpha_k(vol_afterCT, time_afterCT, time, n_cycles, index0, ...
    out_per_day, params0, params2, P1);
toc
alpha=params(1);
k=params(2);
fprintf('Results of fit: alpha = %f, k = %f, error: %f\n', alpha, k, err1);

% compute solution for estimated parameters
[~,~,Total]=calculateP_D(time,n_cycles,index0,out_per_day,params,params2,P1);
Total(1:index0)=resultP(1:index0);

end
```

calculateP

```
function solP=calculateP(t,P0,rho,K)
% calculating solution of logistic equation
% describing tumour growth before the onset of chemotherapy treatment
    solP=P0*exp(rho*t)./(1+P0/K*(exp(rho*t)-1));
end
```

calculateP_D

```
function [solP,solD,Total] = ...
    calculateP_D(time,n_cycles,index0,out_per_day,params,params2,P1)
% calculating solution of system
% describing tumour growth from the onset of chemotherapy treatment

    alpha=params(1);
    k=params(2);
    rho=params2(1);
    K=params2(2);
    lambda=params2(3);
    dose_eff=params2(4);

    function f=F(~,y)
        f=zeros(size(y));
        C=y(1);     P=y(2);         D=y(3);
        % right-hand side of the system
        f(1)=-lambda*C;
        f(2)= (1-(P+D)/K).*P*rho-alpha*P.*C;
        f(3)= -(1-(P+D)/K).*D*rho/k + alpha*P.*C;
    end

resultC=zeros(size(time));
resultD=zeros(size(time));
resultP=zeros(size(time));
resultP(index0)=P1;

for cycle=1:n_cycles
    % first solve system for the first 4 days of drug administration
    % 28 is the length of the cycle
    % out_per_day - number of outputs per day
    for j=1:4
```

```
        index=(index0-1)+28*out_per_day*(cycle-1)+(j-1)*out_per_day+1;
        if index<length(time)
        C0=resultC(index)+dose_eff;
        P0=resultP(index);
        D0=resultD(index);

        sol=ode45(@F, [time(index), time(index+out_per_day)], [C0,P0,D0]);
        result=deval(sol, time(index:index+out_per_day));
        resultC(index:index+out_per_day)=result(1,:);
        resultP(index:index+out_per_day)=result(2,:);
        resultD(index: index+out_per_day)=result(3,:);
        end
    end

    index1=index0-1+28*out_per_day*(cycle-1)+4*out_per_day;
    if index<length(time)

    if cycle<n_cycles
        indeks2=index0+28*out_per_day*cycle+1;
        % solve for the time from the last dose till the next cycle
    else
        indeks2=time(end)*out_per_day+1;
        % solve for the time from the last dose till the end of the time of
        % observation
    end
    C0=resultC(index1)+dose_eff;
    P0=resultP(index1);
    D0=resultD(index1);

    sol=ode45(@F, [time(index1), time(indeks2)], [C0,P0,D0]);
    result=deval(sol,time(index1:indeks2));
    resultC(index1:indeks2)=result(1,:);
    resultP(index1:indeks2)=result(2,:);
    resultD(index1:indeks2)=result(3,:);
    end
end

solP=resultP(index0:(time(end)*out_per_day+1));
solD=resultD(index0:(time(end)*out_per_day+1));
Total=resultP+resultD;

end
```

estim_rho

```
function [rho,err_rho]=estim_rho(time_beforeCT,vol_beforeCT,rho0,K)
% Finding best value of parameter rho using relative least squares method
% based on initial guess - value rho0

P0=vol_beforeCT(1);

    function y=diff_volumes(rho)
        y=(vol_beforeCT-calculateP(time_beforeCT,P0,rho,K))./vol_beforeCT;
    end

options=optimset('TolX',1e-13,'MaxFunEvals',8000);
[rho,err_rho]=lsqnonlin(@diff_volumes,rho0,0.0001, 0.008, options);
```

```
end
```

estim_alpha_k

```
function [params,err] = estim_alpha_k(vol_afterCT, time_afterCT, time, n_cycles, ...
    indeks0, out_per_day, params0, params2, P1)
% Finding best value of parameters alpha and k using relative least squares method
% based on initial guesses stored in params0

t=time_afterCT.*out_per_day;

function z=estim(params)

    [~,~,Total]=calculateP_D(time,n_cycles,indeks0,out_per_day,params,params2,P1);
    Total_afterTMZ=Total(t);
    z=(Total_afterTMZ-vol_afterCT)./Total_afterTMZ;
end

options=optimset('TolX',1e-10,'MaxFunEvals',8000,'TolFun',1e-15);
[params, err]=lsqnonlin(@estim,params0,[0.0001, 0.0005],[3, 1],options);

end
```

B.2 Numerical procedures for model of malignant transformation

We present functions used to solve system (3.1) and fit its parameters.

EstimationPSO_malignant_transf_main

```
function EstimationPSO_malignant_transf_main
% Fitting values of h_0,rho_l,D_l, D_h to patients data with PSO algorithm

%% PATIENT DATA
id=165;
[time_med,time_total,diams_med,date_transform,r0]= patients_data(id);

%% FIXED PARAMETERS
d_thres=0.16;
tau_lh=100;
Lcrit=0.6;
Delta_crit=0.05*Lcrit;
rhoh= 0.042;
params_fixed=[d_thres,tau_lh, Lcrit, Delta_crit, rhoh];

%% SIMULATION SPACE DOMAIN (mm)
L = 50;                             % Tissue size 100 mm=10cm
Nx = 1000;
x = linspace(-L,L,Nx);              % Simulation domain (mm)

%% TIME MESH
dt = 10;                            % Time step (days) - for visualisation
t=(0:dt:time_total(end)+dt);

%% PARAMETERS TO ESTIMATE - INITIAL VALUES
```

```
h0= 0.56;
Dl= 0.0004;
rhol= 0.0005;
Dh=0.08;
params0=[h0,rhol,Dl,Dh];

%% INITIAL SOLUTION
sol=LH_sol(t,x,params_fixed,params0,r0);
diams= diameter(x,sol,d_thres);
visualisation_diam(t,diams,diams_med,time_med,date_transform,1);

%% INITIAL ERROR
err0 = error_h0_rhol_Dl_Dh(params0, params_fixed, diams_med,time_med, x, r0);
%%%%%%%%%%%%%%%%%%%%%%%%%%%%%%%%%%%%%%%%%%%%%%%%%%%%%%%%%%%%%%%%%%%%%%%%%%%%

%% FITTING h0, rhol, Dl, Dh
% we will save results of fitting to a file every
n_iter=100;
step_size=5;
n_steps = floor(n_iter/step_size);
if (n_steps*step_size == n_iter)
    steps = step_size*ones(1,n_steps);
else
    steps = step_size*ones(1,n_steps+1);
    steps(end) = n_iter-n_steps*step_size;
end

filename = sprintf('id_%d.txt',id);
fileID = fopen(filename,'a');

fprintf(fileID,'Before: error: %2.10f%%,\nh_{0}=%1.5e, rho_{l} = %1.5e, D_{l} = ...
    %1.5e, D_{h} = %1.5e.\n', 100*err0,h0,rhol,Dl,Dh);
fclose(fileID);

addpath('../../PSO');
for i=1:length(steps);
    tic
    [paramsF,errF] = estimPSO_h0_rhol_Dl_Dh(params_fixed,params0, ...
        diams_med,time_med, x, r0, steps(i));
    toc
    h0=paramsF(1);
    rhol=paramsF(2);
    Dl=paramsF(3);
    Dh=paramsF(4);

    krok = i*step_size;
    fileID = fopen(filename,'a');
    fprintf(fileID,'\nIteration: %4.d, h_0 = %1.10e, rho_{l} = %1.10e, ...
        D_{l}=%1.10e, D_{h}=%1.10e, error: %2.10f%%\n', 30+krok, h0, rhol, Dl, ...
        Dh, 100*errF);
    fclose(fileID);
    params0=[h0, rhol, Dl, Dh];
end
fprintf('Fit: h_0 = %.10f, rho_{l} = %.10f, D_{l}=%10f, D_{h}=%10f, error: ...
    %f%%\n', h0, rhol, Dl,  Dh,100*errF);
fileID = fopen(filename,'a');
fprintf(fileID,'\nAfter fit: h_{0} = %1.10e, rho_{l} = %1.10e, D_{l}=%1.10e, ...
    D_{h}=%10f, error: %2.10f%%\n', h0, rhol, Dl,  Dh, 100*errF);
fclose(fileID);

%% solve model with selected parameters
```

```
sol=LH_sol(t,x,params_fixed,paramsF,r0);
diams= diameter(x,sol,d_thres);

end
```

LH_solve

```
function solution=LH_solve(time,x,params_fixed,params_estim,r0)
% Calculating the solution of system describing malignant transformation of LGGs

    d_thres=params_fixed(1);
    tau_lh=params_fixed(2);
    Lcrit=params_fixed(3);
    Delta_crit=params_fixed(4);
    rhoh=params_fixed(5);
    h0=params_estim(1);
    rhol=params_estim(2);
    Dl=params_estim(3);
    Dh=params_estim(4);

    invDelta_crit = 1/Delta_crit;
    sigma=-r0^2/log(d_thres/h0);

    Slhp = @(T) 0.5*(1+tanh((T-Lcrit)*invDelta_crit));
    cr1 = Slhp(Lcrit-Delta_crit);
    cr2 = Slhp(Lcrit+Delta_crit);
    crwsp = 1/(cr2-cr1);
    Slh=@(T) min([max([(Slhp(T)-cr1)*crwsp,0]),1]);

    options=odeset('RelTol',1e-5,'AbsTol',1e-8);
    solution = pdepe(0, @pdex1pde, @pdex1ic, @pdex1bc, x, time, options);

    %%%%%%%%%%%%%%%%%%%%%%%%%%%
    % system of PDEs to solve %
    %%%%%%%%%%%%%%%%%%%%%%%%%%%
    function [c,f,s] = pdex1pde(~,~,u,DuDx)
    % right-hand side of the system
        c=[1; 1];
        f=[Dl; Dh].*DuDx;
        L=u(1);     H=u(2);
        s1= (1-(L+H)).*L*rhol-Slh(L+H)/tau_lh*L;
        s2= (1-(L+H)).*H*rhoh + Slh(L+H)/tau_lh*L;
        s=[s1; s2];
    end

    % boundary conditions
    function [pl,ql,pr,qr] = pdex1bc(~,~,~,~,~)
        pl = [0;0];
        ql = [1;1];
        pr = [0;0];
        qr = [1;1];
    end

    % initial conditions
    function u0=pdex1ic(y)
        L0=h0*exp(-y.^2/sigma);
        H0=zeros(size(y));
        u0=[L0;H0];
```

```
    end

end
```

diameter

```
function diam = diameter(x,sol,threshold)
% Calculating diameter of visible part of tumour
% (density is above given treshold)
% based on solution of system of PDEs computed with the use of LH_solve
% and stored in variable "sol"

    Nt = length(sol(:,1,1));
    Nx = length(x);
    diam = zeros(size(sol(:,1,1)));
    m=0;
    for j=1:Nt
        layer = sol(j,:,1)+sol(j,:,2);
        if (layer(end)>threshold)
            ind1 = Nx;
        else
            ind1 = find(layer>threshold,1,'last');
        end

        if (layer(1)>threshold)
            ind0 = 1;
        else
            ind0 = find(layer>threshold,1,'first');
        end


        if isempty(ind1)
            x1 = 0;
        elseif ind1<Nx
            x1=x(ind1) + (threshold-layer(ind1))*(x(ind1+1)-x(ind1))/ ...
                (layer(ind1+1)-layer(ind1));
        else
            x1 = x(end);
        end

        if isempty(ind0)
            x0 = 0;
        elseif ind0>1
            x0=x(ind0-1) + (threshold-layer(ind0-1))*(x(ind0)-x(ind0-1))/ ...
                (layer(ind0)-layer(ind0-1));
        else
            x0 = x(1);
        end
        diam(j) = (x1 - x0)*(1+(m>0)); %mm
    end

end
```

error_h0_rho1_D1_Dh

```
function errTotal = error_h0_rhol_Dl_Dh(params_estim, params_fixed, ...
    diams_med,time_med, x, r0)
% Calculating the total difference between model solution and patient data

    threshold=params_fixed(1);
    sol=LH_solve(time_med,x,params_fixed,params_estim,r0);
    diam_model=diameter(x,sol,threshold);

    if (length(diam_model)==length(diams_med))
        errTotal=sum(((diam_model.'-diams_med)./diams_med).^2);
    else
        errTotal = Inf;
    end
```

estimPSO_h0_rhol_Dl_Dh

```
function [pF,errF] = estimPSO_h0_rhol_Dl_Dh(params_fixed,params_estim, ...
    diams_med,time_med, x, r0, niter)
% estimating values of model parameters with PSO

    initial=params_estim;

    h0lower=0.3;        %lower bound for h0
    h0upper=0.57;       %upper bound for h0 equals Lcrit-Deltacrit
    rhollower=0.0001;
    rholupper=0.008;
    Dllower=0.0003;
    Dlupper=0.008;
    Dhlower=0.0008;
    Dhupper=0.9;
    lb=[h0lower, rhollower, Dllower, Dhlower]; %lower bounds for parameters
    ub=[h0upper, rholupper, Dlupper, Dhupper]; %upper bounds for parameters

    if nargin>=6
        opt = PSOSET('Display', 'iter','MAX_ITER', niter, 'TOLFUN', 1e-12);
    else
        opt = PSOSET('Display', 'iter');
    end

    [pF, errF] = PSO('error_h0_rhol_Dl_Dh',initial, lb, ub, opt, ...
        params_fixed,diams_med,time_med,x,r0);
    % pF stores values of h0, rhol, Dl, Dh

end
```